



Departamento de
Electrónica e Sistemas
UNIVERSIDADE DA CORUÑA

Tese de Doutoramento - 2014

Analog Joint Source Channel Coding for Wireless Communications

Autor **Óscar Fresnedo Arias**

Directores **Francisco J. Vázquez Araújo, Luis Castedo Ribas**

D. Francisco J. Vázquez Araújo e D. Luis Castedo Ribas

CERTIFICAN:

Que a memoria titulada “Analog Joint Source Channel Coding for Wireless Communications” foi realizada por D. Óscar Fresnedo Arias baixo a nosa dirección no Departamento de Electrónica e Sistemas da Universidade da Coruña e remata a Tese que presenta para optar ó grao de Doutor.

A Coruña, 02 Maio de 2014.

Asdo.: Dr. Francisco J. Vázquez Araújo
Director da Tese Doutoral
Univ. Prof. Dr.-Ing.
Departamento de
Electrónica e Sistemas
Universidade da Coruña

Asdo.: Dr. Luis Castedo Ribas
Director da Tese Doutoral
Catedrático de Universidade
Departamento de
Electrónica e Sistemas
Universidade da Coruña

Asdo.: Óscar Fresnedo Arias
Autor da Tese Doutoral

Tese Doutoral: Analog Joint Source Channel Coding for Wireless Communications

Autor: D. Óscar Fresnedo Arias

Directores: Dr. Francisco J. Vázquez Araújo e Dr. Luis Castedo Ribas

Data de defesa:

Tribunal

Presidente: Alberto González Salvador

Vogal 1: Javier García Frías

Vogal 2: Pedro Crespo Bofill

Vogal 3: Matilde Sánchez Fernández

Secretario: Adriana Dapena Janeiro

Á memoria da miña nai

Agradecimientos

Son muchas las personas que merecen mi más sincero agradecimiento por haberme ayudado en mayor o menor medida a realizar este trabajo a lo largo de todos estos años. En primer lugar, me gustaría dar las gracias a mis dos directores de tesis, Luis y Fran por su paciencia, esfuerzo y tiempo dedicado para guiarme en este largo viaje que me ha permitido completar mi tesis. Sus valiosos consejos y enseñanzas han servido para orientarme y motivarme en mi trabajo diario en el departamento. Este trabajo nunca habría sido posible sin vuestra inestimable ayuda.

Me gustaría también expresar mi enorme gratitud a Javier Garca Frías por descubrirme una apasionante y novedosa área de conocimiento donde he podido llevar a cabo mi actividad investigadora. Su supervisión y colaboración a la hora de desarrollar distintos aspectos abordados en esta tesis han sido fundamentales para completar este trabajo. Quiero además expresar mi gratitud al profesor Markus Rupp por su valiosa aportación y por complementar nuestra formación con sus populares cursos.

No quiero olvidarme de dar las gracias a todos y cada uno de mis compañeros del Grupo de Tecnología Electrónica y Comunicaciones por contribuir a generar un ambiente de trabajo muy positivo que, sin duda, ha hecho mucho más sencilla y agradable mi labor investigadora todos estos años. En especial, me gustaría destacar a Jose por enseñarme a no odiar a Jacobianos y operadores de Lagrange y a Jose Antonio por aportar su extensa experiencia y conocimiento en los aspectos más prácticos de la tesis. Gracias también a Ángel, Ismael, Paula, Pedro y Xosé por mostrarme que hablar en inglés puede ser muy divertido. Por supuesto, expresar mi reconocimiento al trabajo de Cristina Ribao que nos ha permitido sobrellevar los tediosos trámites burocráticos sin caer en la desesperación.

Mi amor y eterno agradecimiento a María no sólo por su continuo apoyo y por alentarme en los momentos más difíciles para que no decayera en mi empeño de terminar mi doctorado sino por todas esas cosas intangibles que no pueden ser descritas simplemente mediante palabras. Por último, pero en absoluto no menos importante, me gustaría darle las gracias a mi padre por su enorme sacrificio durante tantos años para darme esa oportunidad que él nunca tuvo y por enseñarme que mereza la pena luchar por alcanzar nuestros objetivos.

Gracias a esa persona tan especial que nunca olvidaré. Gracias mamá.

Resumo

En 1948, o traballo de Shannon titulado "A mathematical theory of communication" revolucionou por completo a forma de entender o problema de transmitir información de xeito fiable. Shannon demostrou que un sistema de comunicación é capaz de transmitir cunha probabilidade de erro arbitrariamente baixa sempre que a taxa de transmisión se manteña por debaixo dun certo límite. Ademais, probou que unha separación entre a codificación de fonte e de canle é a estratexia óptima para acadar os límites teóricos. Estas ideas inspiraron o desenrolo de toda unha teoría da comunicación dixital centrada na construción de esquemas de codificación cada vez máis sofisticados. Isto fixo que, dende ese momento, a maior parte dos sistemas de comunicación foran deseñados seguindo unha aproximación dixital e de acordo ao principio de separación, mentres que outras alternativas foron relegadas a un segundo plano.

Sen embargo, nestos derradeiros anos, os sistemas de comunicación baseados nunha optimización conxunta da codificación de fonte e canle despertou de novo o interese dos investigadores, especialmente no caso da transmisión de sinais analóxicos. Esta estratexia – coñecida en inglés como *analog Joint Source Coding (JSCC)*– tamén é capaz de aproximar os límites teóricos mentres proporciona certas vantaxes con respecto aos sistemas dixitais convencionais como, por exemplo, unha alta taxa de transmisión, baixa complexidade, mínimo retardo e capacidade do sistema para adaptarse a entornos variantes en tempo sen necesidade de ter que rediseñalo por completo. Deste xeito, estas atractivas propiedades fan que a estratexia JSCC sexa especialmente axeitada para aplicacións en tempo real con fortes restriccións de complexidade e/ou retardo así como para a transmisión de datos a alta velocidade a través de canles sen fíos.

Ata o de agora, a investigación nesta área centrouse principalmente na avaliación de diferentes sistemas JSCC analóxicos deseñados para a transmisión de fontes Gaussianas sobre canles AWGN. Sen embargo, o comportamento desta estratexia en entornos máis realistas como, por exemplo, implementacións prácticas sobre canles reais sen fíos, aínda non se estudou en profundidade. O obxectivo desta tese é determinar a viabilidade do esquema JSCC analóxico no contexto das comunicacións sen fíos. Para levar a cabo esta tarefa, varios sistemas JSCC analóxicos son especificamente deseñados para permitir a transmisión de símbolos continuos en amplitude e discretos en tempo a través de canles sen fíos, intentando preservar na medida do posible as propiedades descritas anteriormente para o caso de canles AWGN.

A aplicación da estratexia JSCC en canles sen fíos representa unha serie de importantes

desafíos para o deseño destes sistemas analóxicos. Por unha banda, o sistema JSCC analóxico débese adaptar constantemente ás fluctuacións do canle debido aos desvaecementos para conseguir que o seu rendemento se aproxime á solución de compromiso distorsión-custo. Afortunadamente, este proceso non supón redeseñar por completo o sistema xa que chega con actualizar os parámetros do codificador segundo as condicións reais do canle. Por outra banda, as comunicacións sen fíos sufren os efectos nocivos da dispersión do retardo causado pola propagación do multicamiño dos sinais transmitidos. Os actuais estándares de comunicación sen fíos soen empregar unha serie de técnicas de transmisión para combater estes efectos e explotar a ganancia de diversidade que proporciona o canle, como o uso de múltiples antenas tanto no transmisor como no receptor ou dun esquema de modulación ortogonal. A integración da estratexia JSCC e destas técnicas conleva cambios substanciais no esquema inicial –sobre todo no deseño da operación de decodificación– para preservar a baixa complexidade e retardo do modelo de comunicación resultante. Por último, a aplicación desta estratexia en entornos reais tamén conleva ter que afrontar algúns problemas adicionais na práctica que non se atopan nun escenario simulado.

Resumen

En 1948, el trabajo de Shannon titulado "A mathematical theory of communication" revolucionó por completo la manera de entender el problema de transmitir información de forma fiable. Shannon demostró que un sistema de comunicación es capaz de transmitir con probabilidad de error arbitrariamente baja siempre que la tasa de transmisión se mantenga por debajo de un cierto límite. Además, postuló que una separación entre la codificación de fuente y de canal es la estrategia óptima para alcanzar los límites teóricos. Estas ideas inspiraron el desarrollo de toda una teoría de la comunicación digital centrada en la construcción de esquemas de codificación cada vez más sofisticados. Esto provocó que, a partir de ese momento, la mayor parte de los sistemas de comunicación se diseñasen siguiendo una aproximación digital y de acuerdo al principio de separación, mientras que otras alternativas fueron relegadas a un segundo plano.

Sin embargo, en estos últimos años, los sistemas de comunicación basados en la optimización conjunta de la codificación de fuente y canal han despertado de nuevo el interés de los investigadores, especialmente en el caso de transmisión de señales analógicas. Esta estrategia –conocida en inglés como *analog Joint Source Coding (JSCC)*– también es capaz de aproximarse a los límites teóricos, mientras ofrece ciertas ventajas con respecto a los sistemas digitales convencionales como, por ejemplo, una alta tasa de transmisión, baja complejidad, mínimo retardo y capacidad del sistema para adaptarse a entornos variantes en tiempo sin necesidad de rediseñarlo por completo. De esta forma, estas atractivas propiedades hacen que la estrategia JSCC sea especialmente adecuada para aplicaciones en tiempo real con fuertes restricciones de complejidad y/o retardo así como para la transmisión de datos a alta velocidad a través de canales inalámbricos.

Hasta ahora, la investigación en este área se ha centrado principalmente en la evaluación de diferentes sistemas JSCC analógicos diseñados para transmitir fuentes Gaussianas sobre canales AWGN. Sin embargo, el comportamiento de esta estrategia en entornos más realistas como, por ejemplo, su implementación práctica sobre canales inalámbricos reales, aún no se ha estudiado en detalle. El objetivo de esta tesis es determinar la viabilidad del esquema JSCC analógico en el contexto de las comunicaciones inalámbricas. Para llevar a cabo esta tarea, varios sistemas JSCC analógicos son específicamente diseñados para permitir la transmisión de símbolos continuos en amplitud y discretos en tiempo a través de canales inalámbricos, intentando preservar las propiedades descritas anteriormente para el caso de canales AWGN.

La aplicación de la estrategia JSCC en canales inalámbricos representa una serie de importantes desafíos a la hora de diseñar estos sistemas analógicos. Por un lado, el sistema JSCC analógico debe adaptarse constantemente a las fluctuaciones del canal para conseguir que su rendimiento se aproxime a la solución de compromiso distorsión-coste. Afortunadamente, este proceso no supone rediseñar por completo el sistema, pues basta con actualizar los parámetros del codificador según las condiciones del canal en cada instante. Por otro lado, las comunicaciones inalámbricas sufren los efectos adversos de la dispersión del retardo causado por la propagación del multicamino de las señales transmitidas. Los actuales estándares de comunicación inalámbrica utilizan habitualmente una serie de técnicas de transmisión para combatir estos efectos y explotar la ganancia de diversidad proporcionada por el canal, como el uso de múltiples antenas tanto en el transmisor como el receptor o de un esquema de modulación ortogonal. Integrar la estrategia JSCC junto con estas técnicas impone substanciales cambios en el esquema inicial –sobre todo en el diseño de la operación de decodificación– para preservar la baja complejidad y retardo del modelo de comunicación resultante. Por último, la aplicación de esta estrategia en entornos reales también conlleva ciertos problemas en la práctica que no se encuentran en un escenario simulado.

Abstract

In 1948, the Shannon's work titled "A mathematical theory of communication" completely revolutionized the way to understand the problem of the reliable communications. He showed that any communications system is able to transmit with an arbitrarily low error probability as long as the transmission rate is kept below a certain limit. The separation between the source and channel coding was also shown as the optimal strategy to achieve the theoretical limits. Those ideas inspire the development of a whole digital communication theory focused on building more and more sophisticated coding schemes. It leads to most of communication systems were designed according to a digital approach and the separation principle from that moment, whereas other alternatives were set aside.

However, in the last years, communication systems based on a jointly optimization of the source and channel encoder has aroused the interest of the researchers again, specially in the case of the transmission of analog signals. This strategy –referred to as analog Joint Source Channel Coding (JSCC)– has been also shown to approach the theoretical limits and provides certain advantages with respect to the conventional digital systems, such as high transmission rate, low complexity, almost zero delay and the ability of the system to adapt to time-varying environments without a full redesign. Thus, these appealing properties of the JSCC approach make it specially suitable for both real-time applications with severe requirements on the complexity and/or delay and the transmission of data at high rate over wireless channels.

So far, the research on this area mainly focused on the design and evaluation of different analog JSCC systems for the transmission of Gaussian sources over Additive White Gaussian Noise (AWGN) channels. However, the behavior of this strategy on more realistic environments, such as practical implementations over real wireless channels, has not been deeply studied yet. The objective of this thesis is to evaluate the feasibility of the analog JSCC technique in the context of the wireless communications. For that purpose, several analog JSCC systems are specifically designed for the transmission of discrete-time continuous-amplitude samples over wireless channels, with the aim of preserving the desirable properties described for the case of AWGN channels.

The application of the JSCC strategy on wireless channels represents a series of important challenges for the design of these analog systems. On one hand, the analog JSCC scheme must be constantly adapted to the fluctuations of the wireless channel for the performance approaches the optimal distortion-cost tradeoff. Fortunately, this procedure does not involve a full redesign

of the system since it is just enough to update the encoder parameters according to the actual channel conditions. On the other hand, the wireless communications undergo the undesirable effects of the delay spread caused by the multipath propagation of the transmitted signals. In the current wireless standards, different transmission techniques are usually employed in order to combat such effects and exploit the diversity gain provided by the channel, such as the use of multiples antennas both at the transmitter and the receiver as well as of a multicarrier modulation scheme. The integration of the analog JSCC strategy together with these techniques leads to make substantive modifications on the initial configuration –specially in the design of the decoding operation– to preserve the low complexity and delay of the resulting communication model. Finally, the practical implementation of the analog JSCC on real wireless environment also leads to deal with some additional problems that are not encountered in a simulation scenario.

Contents

1	Introduction	1
1.1	Joint Source Channel Coding	3
1.2	Shannon-Kotel'nikov Mappings	4
1.3	Motivation	6
1.4	Thesis Overview	7
2	Analog Joint Source Channel Coding	9
2.1	Transmission of Analog Signals	10
2.1.1	Channel Capacity	11
2.1.2	Rate Distortion Function	13
2.1.3	Optimum Performance Theoretically Attainable (OPTA)	16
2.2	Analog Joint Source Channel Coding	17
2.2.1	Shannon-Kotel'nikov Mappings	19
2.2.2	Bandwidth Compression	20
2.3	System Description	22
2.3.1	Analog Encoder	23
2.3.1.1	N:K Analog Encoder	24
2.3.1.2	Archimedes' Spiral	26
2.3.2	Analog Decoder	28
2.3.3	Proposed Decoding Method	31
2.3.4	Distortion Analysis and Parameter Optimization	33
2.4	Conclusions	37
3	Comparison between Analog JSCC and Digital Systems	39
3.1	Digital BICM Systems	39
3.1.1	Scalar Quantization	41
3.1.2	Source Coding	44
3.1.3	Channel Coding	47
3.1.3.1	A Historical Perspective	49

3.1.3.2 Irregular Repeat-Accumulate Codes	50
3.2 Design of Digital Bit Interleaved Coded Modulation (BICM) Systems	52
3.3 System Comparison	56
3.4 Conclusions	58
4 Experimental Evaluation of Analog JSCC in Indoor Environments	59
4.1 Testbed Description	60
4.2 General Procedure for Data Transmission	62
4.3 Experimental Measurements	65
4.3.1 Closed-Loop Setup	66
4.3.2 A Typical Indoor Environment	66
4.3.3 Quantization of the Transmitted Signals	67
4.3.4 Measurement Procedure	68
4.4 Results	69
4.5 Conclusions	70
5 Analog JSCC over MIMO Channels	73
5.1 Description of a MIMO Communication System	74
5.2 OPTA for Analog MIMO Systems	76
5.2.1 Channel Known at the Receiver	76
5.2.2 Channel Known at the Transmitter and Receiver	78
5.3 Analog JSCC over MIMO Channels	78
5.3.1 MIMO Decoding with MMSE Linear Detection	80
5.3.2 MIMO Decoding with Decision Feedback Detection	81
5.3.3 Linear MMSE Precoding	83
5.4 Experimental Results	85
5.4.1 Symmetrical MIMO Rayleigh Channels	85
5.4.2 Compression Rate 3:2	87
5.4.3 Asymmetrical MIMO Systems	89
5.4.4 Real Indoor Channels	92
5.5 Conclusions	93
6 Analog JSCC for OFDM Systems	97
6.1 Description of OFDM Modulation	98
6.2 Analog JSCC in MIMO-OFDM	101
6.3 Adaptive Analog JSCC	103
6.3.1 Adaptive Analog JSCC with Linear Precoding	104
6.4 Experimental Results	105
6.5 Conclusions	109

7	Analog JSCC for Multiple Access Channels	111
7.1	OPTA for Analog JSCC Systems over MAC	113
7.2	Gaussian MAC	115
7.2.1	Orthogonal CDMA Scheme	116
7.3	Block-Fading MAC	119
7.3.1	Orthogonal CDMA Scheme	120
7.3.2	Linear MMSE Access Coding	122
7.3.3	Opportunistic Access	124
7.4	Results	126
7.5	Conclusions	131
8	Conclusions and Future Work	133
8.1	Conclusions	133
8.2	Future Work	136
8.2.1	Analog JSCC for Bandwidth Expansion	136
8.2.2	Correlated Sources	136
8.2.3	Imperfect CSI in Fading Channels	137
8.2.4	Analog JSCC in Feedback Channels	137
8.2.5	Broadcast Channel	138
A	Estimation of Channel SNR in MIMO Systems with Decision Feedback Receivers	139
B	Explicit Solution for the Design of MMSE MIMO Transceivers	143
C	List of Acronyms	147
	Bibliography	149

List of Figures

1.1	Block diagram of a Separate Source Channel Coding (SSCC) system.	2
1.2	Block diagram of a Joint Source Channel Coding (JSCC) system.	4
2.1	Block diagram of a general communication system.	10
2.2	Mapping suggested by Shannon for 1:2 bandwidth expansion.	20
2.3	Continuous like-spiral curve proposed for 2:1 bandwidth reduction.	22
2.4	Block diagram of a bandwidth reduction N:1 analog JSCC system over AWGN channels.	23
2.5	Block diagram of a bandwidth compression N:K analog JSCC system over AWGN channel.	25
2.6	Analog mapping based on the use of the doubly intertwined Archimedes' spiral.	27
2.7	Example of Maximum Likelihood (ML) and Minimum Mean Square Error (MMSE) decoding for $N = 2$ and Archimedes' spiral.	30
2.8	Block diagram of the proposed two-stage decoding scheme.	31
2.9	Performance of the 2:1 analog JSCC system when using the two-stage decoding for Gaussian sources.	32
2.10	Performance of the 2:1 analog JSCC system when using the two-stage decoding for Laplacian sources.	33
2.11	Distortion components when using the Archimedes' spiral and ML decoding.	34
3.1	Block diagram of Bit Interleaved Coded Modulation (BICM) systems over AWGN channels.	40
3.2	Example of non uniform scalar quantization of a Gaussian source.	42
3.3	Example of a Huffman code for an input alphabet $S = \{A, B, C, D, E\}$ with probability mass function $p(S) = \{0.05, 0.06, 0.12, 0.25, 0.52\}$. The average length of the code is 1.82 and the entropy of the source is 1.8173.	46
3.4	Example of factor graph for a systematic Irregular Repeat Accumulate (IRA) code.	51
3.5	Performance comparison of 2:1 analog JSCC and digital 256-PAM schemes for Gaussian sources.	56

3.6	Performance comparison of 2:1 analog JSCC and digital 256-PAM schemes for Laplacian sources.	57
4.1	Picture of the GTEC MIMO Testbed.	60
4.2	Block diagram of the testbed hardware components	61
4.3	Picture of a transmit node of the GTEC MIMO Testbed.	61
4.4	Block diagram of hardware and software elements at the transmitter.	63
4.5	Block diagram of hardware and software elements at the receiver.	63
4.6	Frame structure used to transmit the source symbols.	64
4.7	Plan of the second floor of the CITIC building and localization of the transmit and receive nodes.	67
4.8	Performance of the 2:1 analog JSCC scheme over the simulated AWGN channel and on the real indoor scenario.	70
4.9	Performance of the 10:6 analog JSCC scheme: simulated SDR with and without power allocation (PA), and measured SDR with and without power allocation (PA).	71
4.10	Performance of the 10:9 analog JSCC scheme: simulated SDR with and without power allocation (PA), and measured SDR with and without power allocation (PA).	72
5.1	Block diagram of a MIMO system with n_T transmit and n_R receive antennas.	74
5.2	Analog MIMO JSCC system with MMSE linear detection.	80
5.3	Analog MIMO JSCC system with Decision Feedback detection.	82
5.4	Performance of 2:1 analog JSCC over 2×2 MIMO Rayleigh channels: Gaussian source.	85
5.5	Performance of 2:1 analog JSCC over 2×2 MIMO Rayleigh channels: Laplacian source.	86
5.6	Performance of 2:1 analog JSCC over 4×4 MIMO Rayleigh channels: Gaussian source.	87
5.7	Performance of 2:1 analog JSCC over 4×4 MIMO Rayleigh channels: Laplacian source.	88
5.8	Performance of 3:2 analog JSCC over 2×2 MIMO Rayleigh channels with Gaussian sources.	89
5.9	Performance of 3:2 analog JSCC over 4×4 MIMO Rayleigh channels with Gaussian sources.	90
5.10	Performance of 2:1 analog JSCC over 4×1 MIMO Rayleigh channels.	91
5.11	Performance of 2:1 analog JSCC over 4×2 MIMO Rayleigh channels.	92
5.12	Picture of the real indoor scenario setup during measurement campaign.	93

5.13	Performance of 2:1 analog JSCC over indoor measured 2×2 MIMO channels: Gaussian source.	94
5.14	Performance of 2:1 analog JSCC over indoor measured 2×2 MIMO channels: Laplacian source.	95
6.1	Example of the frequency spectrum of the orthogonal subcarriers.	98
6.2	Practical implementation of OFDM modulation using FFT/IFFT and the cyclic prefix.	99
6.3	Block diagram of the analog JSCC MIMO-OFDM system.	101
6.4	Performance of 2:1 analog JSCC SISO-OFDM systems over Rayleigh fading channels.	106
6.5	Performance of 2:1 analog JSCC SISO-OFDM systems over fading channels simulated according to the ITU-Pedestrian B specifications.	107
6.6	Performance of analog JSCC 4×4 MIMO-OFDM systems over Rayleigh channels.	108
6.7	Performance of analog JSCC 4×4 MIMO-OFDM systems over an IMETRA-D channel.	109
7.1	Example of orthogonal spreading codes for the proposed CDMA access scheme.	117
7.2	Capacity of the Gaussian MAC model and the proposed CDMA scheme for $P_1 = 8, P_2 = 1$ and a spreading factor $K = 64$	118
7.3	Block diagram of the orthogonal CDMA access scheme proposed for the block- fading MIMO MAC.	121
7.4	Performance of the orthogonal CDMA scheme for the transmission of uncoded samples over the Gaussian MAC.	127
7.5	Performance of the orthogonal CDMA scheme for the transmission of 2:1 compressed samples over the Gaussian MAC.	128
7.6	Performance of the three proposed access scheme for the transmission of Gaussian samples over a SISO MAC using a 2:1 analog JSCC scheme.	129
7.7	Performance of the three proposed access scheme for the transmission of Gaussian samples over a block-fading 2×2 MIMO MAC using a 2:1 analog JSCC scheme.	130

List of Tables

2.1	Optimal values for δ and γ for 2:1 analog JSCC and Gaussian sources.	36
2.2	Optimal values for δ and γ for 2:1 analog JSCC and Laplacian sources.	36
3.1	Parameters of a 2:1 digital BICM system with Gaussian sources, scalar quantization, Huffman source coding, IRA channel coding and 256-Pulse Amplitude Modulation (PAM) modulation.	54
3.2	Parameters of a 2:1 digital BICM system with Laplacian sources, scalar quantization, Huffman source coding, IRA channel coding and 256-PAM modulation.	55
4.1	Transfer rates according to the code rate. Frame overheads are not included. . .	69

Chapter 1

Introduction

The aim of any communication system is to provide a reliable transmission of the relevant information from a source to a destination according to certain power and bandwidth constraints and specific quality parameters. In 1948, Shannon presented an outstanding work [108] where a general information theory is built on the concepts of information entropy and channel capacity. Using this theory, Shannon laid the main foundations for the designing of efficient communication schemes and determined the theoretical limits for a reliable transmission given a certain source-channel pair.

In order to achieve these limits, Shannon designed a transmission strategy based on the separation between source compression and channel coding. This strategy is referred to as the separation principle in the literature and it has been shown to be optimum for both lossless compression [108], and lossy compression of analog sources [12]. Also, the fact that we can perform source coding independently of the channel coding greatly simplifies the design of the communication system since we can optimize both encoders separately.

Figure 1.1 shows the block diagram of a SSCC communication system. In such system, a source encoder generates a minimum representation of the original information by means of entropy coding (bandwidth compression). The lowest rate at which a source can be compressed without loss of information is called the entropy. Next, the channel encoder modifies the rate at the output of the source encoder according to the channel properties and bandwidth constraints (bandwidth expansion). In general, this operation consists in adding redundancy to protect the source information against the distortion introduced by the channel. If the channel capacity, C , is larger than the source entropy, H , a error-free transmission of the source information is possible by using an appropriate capacity-approaching channel coding method such as Turbo codes or Low Density Parity Check (LDPC) codes.

Unfortunately, the optimality of the separation principle is held on the assumption of infinite complexity and infinite delay. The optimal bounds defined by Shannon can be only achieved if the corresponding encoders are designed assuming an infinite block length. In

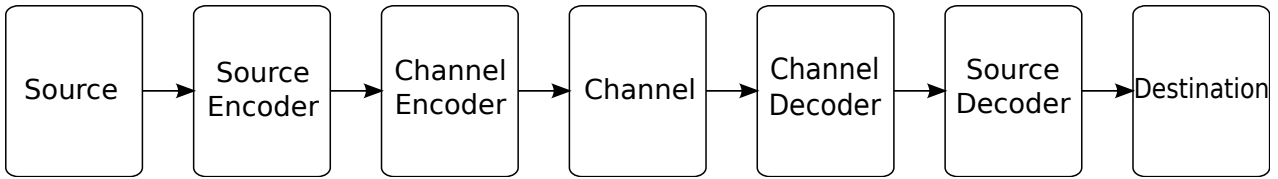


Figure 1.1: Block diagram of a SSCC system.

practice, suboptimal SSCC schemes based on the use of capacity-achieving codes are actually considered. However, these codes approach the theoretical performance closely only if a large block length is employed, incurring long delays and high complexity. Hence, the suitability of the separation principle for the design of practical communication systems with severe constraints on delay and/or complexity is not clear. For example, real-time systems transmitting multimedia contents at high rates or control applications on sensor networks represent a hard challenge when they are addressed from this perspective. Moreover, in the context of sensor networks, where a distributed system must transmit correlated sources over a Multiple Access Channel (MAC), it has been shown that SSCC is not the optimal strategy [71, 82].

The separation principle states a separate design of the source and channel encoders according to source and channel properties such as distortion rate or channel capacity. In the case of digital systems, these codes are specifically optimized to eliminate all transmission errors for a certain Signal-to-Noise Ratio (SNR) value. Nevertheless, when the SNR falls below such threshold value, the channel code is generally unable to correct the transmission errors. It is hence impossible to recover the source information since the source decoder breaks down under the presence of too many erroneous bits. On the other hand, when the SNR is high, less redundant bits are necessary in the channel encoder and more bits could be allocated to the source encoder in order to reduce source distortion.

Thus, the utility of the separation principle is rather questionable when considering the transmission over time-varying channels such as those encountered in wireless communications. Wireless channels suffer from fading caused by multipath propagation which makes the received SNR fluctuate continuously over time. In this case, adaptive tandem systems with separate source and channel coding can be used to cope with time fluctuations of wireless channels. The basic premise is to continuously adapt the source distortion and the channel rate according to the instantaneous channel capacity. Notice, however, the design of an adaptive tandem system based on the separation principle is rather difficult because it is necessary to fully redesign either the source or the channel encoder whenever either the distortion rate or the channel rate change.

Traditional communication systems are generally designed following a digital approach for both discrete and continuous sources. Most of the physical phenomena -such as sound, speech or images- are described by analog signals and, therefore, continuous-time continuous-amplitude sources must be actually sent. However, digital systems require discrete-time discrete-amplitude samples as input, in such a manner that the original analog signals must

be first discretized and later quantized. It is well known that a signal with bandwidth B Hz can be discretized and recovered at the receptor without loss if at least $2B$ samples per second are used [87]-. Nevertheless, quantization is not an invertible operation and, therefore, an analog signal cannot be perfectly recovered after the quantization step since a certain amount of the source information is permanently removed. As a consequence, the quantization operation induces a floor effect on the performance of digital systems since it saturates once the SNR exceeds a certain threshold value directly related to the quantization error. Hence, for digital systems perform close to their theoretical limit, high complexity quantization methods as Vector Quantization (VQ) should be used.

1.1 Joint Source Channel Coding

Recently, a new approach consisting in the analog transmission of discrete-time continuous-amplitude samples has been proposed as an appealing alternative to the traditional design of digital systems, specially when analog sources must be transmitted at high rates and severe delay constraints are imposed.

As mentioned, the separation principle was presented as the optimal strategy for the design of communication systems in order to achieve the theoretical limits predicted by Shannon [108]. Near-optimal high-complexity SSCC schemes are actually employed, attaining a performance quite close to the optimal –but not the optimal–. Hence, other low complexity suboptimal schemes, which do not necessarily follow the separation principle, can be designed to attain a similar or even better performance than of that conventional SSCC systems in certain situations. These schemes merge the source and channel coding into a single operation that directly maps the source space into the corresponding channel space. Thus, the source and channel encoders are jointly optimized in one single step in such a manner that the overall system complexity is drastically reduced. Figure 1.2 shows the block diagram of a Joint Source Channel Coding (JSCC) system.

In the literature, there exists several examples of digital systems that employ some type of JSCC strategy. For example, unequal error protection [89] is used to adjust the encoder parameters of some audio/speech codecs. Another representative example is [24], where a joint source and channel trellis was specifically designed for the encoder operation. Another traditional JSCC approach consists in performing data compression by using a vector quantizer followed by an index assignment where the quantizer outputs are directly mapped to a set of codewords according to a certain ordering criterion. This assignment is usually designed to protect the more sensitive information against the channel noise [28, 112].

Hybrid digital-analog (HDA) schemes has been also considered for both compression and expansion of analog sources [22, 67, 114]. These systems are designed with the aim of



Figure 1.2: Block diagram of a JSCC system.

exploiting the advantages of both the analog and digital schemes. Thus, such systems try to combine the robustness of the digital schemes against the channel interferences with the graceful degradation and low complexity/delay of the analog approach. For that reason, a part of the information is transmitted following the traditional digital approach –quantization, channel encoding and modulation– whereas less sensitive data is normally sent using analog JSCC. An usual strategy employed for this type of systems consists in applying VQ to obtain the sequence of discrete samples that will be sent by mean of the digital subsystem whereas the quantization error is also transmitted using the analog block of the HDA system [22, 98, 113].

A joint optimization of the source-channel encoder pair was first proposed by Farvardin in [29] in order to minimize the overall distortion. The resulting algorithm is commonly referred to as Channel Optimized Vector Quantizer (COVQ). Later, Fuldsheth also addresses this optimization problem including a transmitted power constraint [38, 39]. The resulting discrete mappings –which are called Power Constrained Channel Optimized Vector Quantizer (PCCOVQ)– split the source space into a set of partitions, and determine the correspondence between the source symbols and the associated codewords that minimizes the distortion.

In general, when analog signals are considered to be transmitted, a certain level of distortion is tolerated by the end user. In this case, for a lossy source-channel communication system to be optimal, the source distortion and the channel cost should lie on the optimal distortion-cost tradeoff curve. An example of an optimal system is the direct transmission of discrete-time uncoded Gaussian samples over Additive White Gaussian Noise (AWGN) channels when source and channel have the same bandwidth [44]. In this case, such an optimality is motivated by the fact that the Gaussian sources are probabilistically matched to the AWGN channel. This idea is further explored in [43] where a set of necessary and sufficient conditions for any time memoryless point-to-point communication system to be optimal is provided. These conditions are satisfied not only by digital systems designed according to the separation principle but also by analog JSCC systems for which the complexity and delay can be reduced to the minimum while approaching the optimal distortion-cost tradeoff.

1.2 Shannon-Kotel’nikov Mappings

Analog JSCC is a recent topic in the communication field. However, its origin dates back to the late 1940s when Shannon [109] and Kotel’nikov [66] individually stated a geometrical interpretation of the communication process.

In [109], Shannon presented a geometrical representation of the discrete-time messages to be transmitted and the channel signals on two separated vector spaces, namely message and signal space, whose dimensions are defined by the source entropy and the channel bandwidth, respectively. According to this approach, a message corresponds to a point on the message space and a channel signal is in turn represented by a point on the signal space. Thus, the transmitter must establish a correspondence between the points in the two spaces by using a specific mapping. In a similar way, the receiver has to map the received signal back into the message space. Additionally, Shannon proposed a non-linear mapping based on geometric curves for bandwidth expansion which could be used for bandwidth reduction too. About the same time, Kotel'nikov developed a similar theory for bandwidth expansion in his doctoral dissertation [66] –dating back to 1947, although his work was not translated to English until twelve years later– where he proposed the same type of geometrical structures.

According to the Shannon and Kotel'nikov geometrical interpretation, the source and channel of an analog JSCC system can be represented by a N -dimensional and a K -dimensional space, respectively, and the coding operation consists in directly mapping the elements of the source space into the channel space. Notice that $N < K$ implies bandwidth expansion whereas $N > K$ corresponds to a bandwidth reduction or compression. In [72], an example of linear mapping based on Block Pulse-Amplitude Modulation (BPAM) is presented for both bandwidth reduction and bandwidth expansion, although these systems attain a performance rather far away from the theoretical limits, specially for medium and high SNRs.

Nevertheless, these inspiring ideas were completely eclipsed by the digital communication theory focused on building more and more sophisticated channel coding schemes to achieve the Shannon limits. Fortunately, Chung [20] and Ramstad [94] rediscovered the use of continuous non-linear mappings based on geometric curves for the transmission of discrete-time analog samples using a JSCC strategy. In fact, it was Ramstad in [94] who first proposed the name Shannon mappings referred to such continuous non-linear mappings after discovering Shannon's work. Later, Kotel'nikov's theory was come to light and the name Shannon-Kotel'nikov mappings was commonly agreed for non-linear mappings based on geometric curves.

Several authors [9, 32, 50, 51, 55] have recently delved into the use of Shannon-Kotel'nikov mappings for analog point-to-point communications. In addition, [10, 63] have also applied analog mappings on distributed systems in the context of sensor networks where a low delay is essential for network control applications. In general, these mappings preserve complexity and delay at the minimum and can be used for either bandwidth reduction or bandwidth expansion. However, the performance of analog JSCC systems is closer to the optimal distortion-cost curve as long as such non-linear mappings are used for bandwidth reduction. This is because in the case of bandwidth expansion it is not possible to envisage a mapping that efficiently fills the entire channel space without simultaneously creating multiple neighbors that are far away in

the source space [51]. For bandwidth expansion, alternative non-linear mappings have been considered, such as spherical codes [135], analog codes based on both chaotic systems [19], and orthogonal polynomials [128]. These mappings have obtained promising results although, unfortunately, their performance continues rather far away from the optimal bounds.

Notice that Shannon-Kotel'nikov mappings are closely related to the aforementioned PCCOVQ codes developed by Fuldsheth [39]. In the case of PCCOVQ codes, a discrete representation of the source space is directly mapped into a certain channel codebook that can be interpreted as a discrete set of representation vectors placed on a continuous curve on the source space. Thus, if we consider an enough large number of vectors, PCCOVQ scheme actually approximates a continuous non-linear mapping. However, the PCCOVQ complexity greatly increases as the number of representation vectors becomes larger, whereas Shannon-kotel'nikov mappings always preserve low complexity at the encoding operation.

1.3 Motivation

In the literature, most works focus on the design and evaluation of different analog JSCC systems over AWGN channels. In these works, analog JSCC has been widely proved to achieve a near-optimal performance at high rates with low complexity and an almost negligible delay when it is employed for the compression of Gaussian sources to be transmitted over AWGN channels. In addition, several works [51, 94] have shown that analog JSCC provides a graceful degradation and improvement for imperfect Channel State Information (CSI) at the transmitter. Practical implementations using Shannon-Kotel'nikov mappings have been also developed in [54, 94] but AWGN channels are always assumed.

The behavior of analog JSCC on more realistic environments, such as wireless communications, has not been deeply studied yet. An exception is [23] that considers a two-user single-antenna scenario under simulated flat fading Rayleigh channels. For that reason, an interesting open area of research is the design of more complex analog JSCC systems combined with advanced transmission techniques –such as the use of Multiple Input Multiple Output (MIMO) schemes or Orthogonal Frequency-Division Multiplexing (OFDM)– usually employed in the current wireless transmission models. Notice that MIMO-OFDM is the transmission method commonly adopted by the last generation of broadband wireless communication systems due to its ability to achieve large spectral efficiencies while enabling low-complexity equalization of frequency selective channels. Another potential application of the analog JSCC techniques is the transmission of analog data on a multiuser scenario such as cellular communications or sensor networks, where tight constraints on delay and power consumption are usually imposed, and the information is also required to be simultaneously transmitted at high data rates.

If the analog JSCC strategy based on Shannon-Kotel'nikov mappings is also shown to preserve the appealing properties observed in the case of AWGN channels –near-optimal performance, low complexity, spectral efficiency, robustness–, when it is applied on more real conditions, we will have a powerful tool for multiple applications such as, for example, real-time transmission over wireless communications. An additional benefit of this transmission scheme is that the source information is represented by continuous-amplitude samples, the channel symbols are sent through analog signals and the processing at the transmitter (and the receiver) does not involve an intermediate digital representation. Thus, the proposed JSCC system is purely analog. On the other hand, we think it is essential to prove the feasibility of analog JSCC on real applications and, for that purpose, the performance of the analog JSCC systems need to be assessed on real scenarios using real channels, instead of the traditional synthetically-generated channels employed so far.

In addition, previous work in the literature merely compare the performance of analog JSCC systems with respect to the optimal bounds and/or other similar JSCC schemes. Nevertheless, a more interesting comparison would be between these analog schemes and the traditional digital systems based on the separation principle in order to decide which is more suitable for a given scenario. Notice that such transmission strategies represent completely opposite philosophies and it is not straightforward to accomplish a fair comparison in terms of complexity and transmission rate.

1.4 Thesis Overview

The rest of the thesis is organized as follows. In Chapter 2, we describe a general analog JSCC system that uses a particular Shannon-Kotel'nikov mapping consisting of a doubly intertwined Archimedes' spiral. The basic concepts of the non-linear analog mappings are reviewed and the encoding operation by Archimedes' spiral is explained in detail. The decoding operation at the receiver is also addressed and we present a novel two-step decoding method which achieves a near-optimal performance while maintaining a low complexity. Finally, the relation between the coding parameters at the transmitter and the resulting distortion is analyzed in order to optimize the system performance.

A fair comparison between the analog JSCC scheme described in Chapter 2 and a digital Bit Interleaved Coded Modulation (BICM) system is carried out in Chapter 3. Both schemes are optimally designed for the transmission of discrete-time continuous-amplitude sources over AWGN channels at the same rate. The simulation results obtained for both cases are compared to each other and with respect to the optimal bound.

As already mentioned, the performance of analog JSCC techniques has been only evaluated under simulated conditions. In Chapter 4, we describe a software-defined radio implementation

of an analog JSCC wireless transmission system making use of a wireless testbed developed at the University of A Coruña. We use the developed scheme to assess the actual performance of the proposed analog JSCC system in a real indoor environment.

Chapter 5 is dedicated to study the feasibility of the analog JSCC scheme over Multiple Input Multiple Output (MIMO) fading channels. The design proposed in Chapter 2 is expanded to the MIMO case so that the receiver structure is simplified by splitting the decoding operation in two steps: a linear detector is first used to transform the MIMO channel into several parallel Single Input Single Output (SISO) channels and a bank of conventional Maximum Likelihood (ML) SISO decoders is then used to recover the transmitted source samples. In addition, Decision Feedback (DF) detection rather than linear detection as the first stage of our receiver is considered.

The transmission of analog JSCC samples using Orthogonal Frequency-Division Multiplexing (OFDM) modulation and MIMO systems over frequency selective fading channels is addressed in Chapter 6. In such conditions, the optimization of the encoder parameters significantly impacts on the system performance. Three different alternatives for system optimization are studied: non-adaptive coding, adaptive coding, and adaptive coding using a linear precoder designed according to the Minimum Mean Squared Error (MMSE) criterion.

The application of analog JSCC techniques to multiuser communications is addressed in Chapter 7. There exists a large number of wireless communication that cannot be directly modeled as point-to-point links between transmitters and receivers such as, for instance, cellular communications. In particular, we focus on the transmission of independent analog information over a Multiple Access Channel (MAC) in the context of the uplink of cellular communications. In a MAC scenario, it is necessary to design a channel access scheme to allow multiple users to send their information to the centralized receiver over the same channel, since the signal of one user interferes with the data transmitted by the rest of users. We show that it is possible to approach the optimal performance of MAC systems using the analog JSCC mappings proposed for point- to-point communications if the channel access schemes are properly designed. Finally, Chapter 8 is devoted to the conclusions and future work.

Chapter 2

Analog Joint Source Channel Coding

The transmission of continuous sources using analog Joint Source Channel Coding (JSCC) is addressed in this chapter. Analog JSCC has recently arisen as a zero-delay low complexity alternative to conventional digital systems. This strategy based on the joint optimization of the source and channel encoders has been proved to closely approach the theoretical limits providing high transmission rates with a significant lower complexity and delay than that of the digital systems. In addition, it shows a graceful degradation at low Signal-to-Noise Ratios (SNRs) and removes the floor effect of the digital systems at high SNRs.

At the beginning of this chapter, we derive the theoretical limits for the transmission of discrete-time analog signals using the fundamental concepts of Information Theory. Then, we describe in detail the main ideas of the JSCC techniques employed along this thesis. This novel transmission strategy is based on the use of continuous curves, known as Shannon-Kotel'nikov mappings, which are presented from a geometrical perspective. This approach allows us to explain how their topological properties make them suitable for analog JSCC. Although Shannon-Kotel'nikov mappings can be employed for either bandwidth expansion or compression, we will focus on the 2:1 bandwidth reduction case, where the coding operation is carried out by a doubly intertwined Archimedes' spiral.

Next, we turn our attention to the decoding operation. In the literature, two different methods are usually employed in order to recover the original signal from the symbols corrupted by Gaussian noise: MMSE and ML decoding. The first contribution of this thesis is the design of a two-step receiver structure which achieves a near-optimal performance while a low complexity is preserved. The proposed receiver is based on the separation between the detection and decoding stages and it provides the same performance to that of the quasi-optimal MMSE decoder with a significant lower complexity.

Finally, the overall distortion we can expect after decoding the received signal is analytically determined under certain assumptions. This information can be exploited to determine the encoder parameters that optimize the overall system performance for a specific SNR. We also

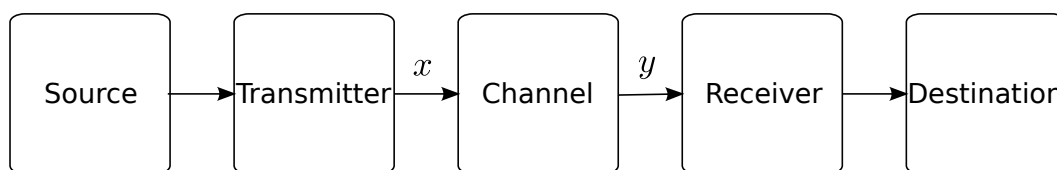


Figure 2.1: Block diagram of a general communication system.

show that the performance of the analog JSCC system can be improved if the initial assumptions are disregarded and the optimal values for the encoder parameters are calculated by computer simulations.

2.1 Transmission of Analog Signals

Most physical phenomena -such as sound, speech or images- are naturally modeled by analog signals. The information transmitted by such signals is usually represented by continuous-time continuous-amplitude functions. It is well known that the Nyquist Theorem [87] proves that any analog signal with bandwidth B Hz can be perfectly recovered (without errors) if sampled at a frequency rate greater than or equal to $2B$ Hz. Therefore, assuming Nyquist frequency and an ideal Nyquist channel, we can disregard the sampling operation and directly consider the transmission of discrete-time continuous-amplitude samples.

A communication system is designed to reliably transmit the information produced by a given source to the destination through a specific medium which can be either a noisy or a noiseless channel. Figure 2.1 shows the general block diagram of a point-to point communication system. Basically, a source generates a sequence of analog samples to be sent to the destination. These source samples are transformed by the transmitter in some way, producing a suitable signal to be sent over the channel. Finally, the received signal is employed by the receiver to recover the transmitted information. From these basic ideas, Shannon developed a complete mathematical theory [108], known as *Information Theory*, where the communication problem is modeled as a statistical process and the information produced by the source can be represented as a random variable measured according to its probability distribution using the concept of entropy.

This theory was brilliantly used by Shannon to prove that splitting source and channel coding is optimum for a lossless transmission over an Additive White Gaussian Noise (AWGN) channel. This strategy is known as the separation principle and is widely used in the design of digital communication systems. In this approach, a source encoder first generates a minimum representation of the original signal. The redundant information is removed and thus the source information is compressed down to its ultimate entropy limit. Next, the channel encoder modifies the data rate at the output of the source encoder according to the channel constraints.

Lossless compression of discrete-time analog sources is generally not feasible since a

continuous-amplitude alphabet normally represents an infinite amount of information and, therefore, the source information needs to be discretized by a quantizer prior to source encoding. The lossy transmission of continuous information was addressed by Shannon in [110], where a theory for source coding according to a certain fidelity criterion was introduced. This theory is referred to as rate distortion theory and is based on compressing the source down to a certain rate given by the rate distortion function $R(D)$. This function determines the minimum rate at which the source data must be transmitted to achieve a given distortion target, D , usually measured in terms of Mean Square Error (MSE). Thus, for continuous sources, the distortion D allowed between the original information and the recovered information determines the rate distortion function, $R(D)$.

In addition, the separation principle was also shown to be optimum by Berger [12] for lossy compression of discrete-time analog sources. Hence, it is necessary to reach a tradeoff between the distortion rate, $R(D)$, at the output of the source encoder and the channel capacity if we want to ensure an error-free transmission of analog sources. We will expand this idea in Section 2.1.3.

2.1.1 Channel Capacity

In Information Theory, the entropy is a measure of the uncertainty in a random variable and can be used to define the quantity of relevant information produced by a source. When considering analog signals, it is helpful to introduce the concept of differential entropy of a continuous random variable X with probability density function $p(x)$, which is given by

$$H(X) = - \int_X p(x) \log_b p(x) dx = -\mathbb{E}\{\log_b p(x)\}, \quad (2.1)$$

where $\mathbb{E}[\cdot]$ denotes mathematical expectation. The logarithm base b determines the entropy measurement unit. If we choose $b = 2$ (the most usual), the entropy is expressed in bits whereas when using natural logarithms the entropy is measured in nats. Unless otherwise specified, we will assume $b = 2$ from now on and, hence, all the entropies will be measured in bits.

Extending the concept of entropy, we can define the joint entropy $H(X, Y)$ for a pair of random variables (X, Y) with a joint probability distribution $p(x, y)$ as

$$H(X, Y) = - \int_X \int_Y p(x, y) \log p(x, y) dx = -\mathbb{E}\{\log p(x, y)\}. \quad (2.2)$$

In similar way, given two random variables (X, Y) , not necessarily dependent, we define the conditional entropy $H(X|Y)$ of X with respect to Y as

$$\begin{aligned} H(X|Y) &= - \int_X p(x) \int_Y p(y|x) \log p(y|x) dx \\ &= - \int_X \int_Y p(x, y) \log p(y|x) dx \end{aligned} \quad (2.3)$$

$$= -\mathbb{E}\{\log p(y|x)\}. \quad (2.4)$$

The conditional entropy measures the average uncertainty in X when Y is known. Notice that, if X and Y are independent, $H(X|Y) = H(X)$ since the knowledge of Y does not reduce any uncertainty in X .

From the conditional entropy $H(X|Y)$, we can determine how much uncertainty in X is reduced due to the knowledge of Y or, equivalently, the amount of information disclosed by Y about X . In Information Theory, this concept is known as the mutual information between two random variables X and Y , and it is mathematically defined as

$$\begin{aligned} I(X; Y) &= \int_X \int_Y p(x, y) \log \left(\frac{p(x, y)}{p(x)p(y)} \right) dx \\ &= \mathbb{E} \left\{ \log \left(\frac{p(x, y)}{p(x)p(y)} \right) \right\}. \end{aligned} \quad (2.5)$$

Notice from Equation (2.5) that the mutual information can be interpreted as the expected logarithm of the likelihood ratio between the joint distribution $p(x, y)$ and the product distribution $p(x)p(y)$.

Logically, $I(X; Y) = H(X) - H(X|Y)$, since the amount of information that Y contains about X is measured as the total uncertainty in X minus the remaining uncertainty in X after Y is known. If the variable Y does not provide any information about X , i.e. $H(X|Y) = H(X)$ and the mutual information $I(X; Y) = H(X) - H(X) = 0$. On the other hand, if X and Y are identical, it can be easily seen that the conditional entropy is zero and the mutual information equals the entropy of X , i.e. $I(X; Y) = H(X)$.

Shannon defined the capacity of a given channel as the maximum amount of information that can be conveyed through it with an arbitrarily low error probability [108]. Let us consider a communication system transmitting a sequence of source symbols over a memoryless noisy channel (see Figure 2.1). If X and Y are a pair of random variables that represent the input and output channel, respectively, and the channel input-output relationship is characterized by the conditional distribution function $p(y|x)$, the capacity of such a channel is given by

$$C = \max_{p(x)} I(X; Y), \quad (2.6)$$

where the maximum is taken over all the possible distributions of the input X . The channel capacity is usually measured in bit per channel use as long as the logarithm base is 2.

In general, it is difficult to find a closed form expression for the capacity of an arbitrary channel. A simple example, usually employed in the literature, is the memoryless Gaussian channel where a sequence of channel symbols, whose average power is σ_c^2 , are corrupted by zero-mean Gaussian noise with variance σ_n^2 . In this case, it can be shown that the input distribution that maximizes the mutual information for this channel is the Gaussian distribution [108], and that the capacity associated to it is given by

$$C = \log \left(1 + \frac{\sigma_c^2}{\sigma_n^2} \right), \quad (2.7)$$

where σ_c^2/σ_n^2 is the Channel Signal-to-Noise Ratio (CSNR) and is usually measured in dB.

2.1.2 Rate Distortion Function

The main concepts corresponding to the rate distortion theory are revisited in this section. A more complete description can be found in [21]. As already commented, analog signals have an infinite information content so a lossless compression of this type of sources is not possible. The continuous-amplitude source samples must be first discretized by using a scalar or a vector quantizer and, next, we can employ some source coding scheme to remove the redundant information of the discrete version.

After revisiting the source-coding problem, Shannon built an elegant theory, referred to as rate distortion theory [110], for lossy transmission of data following a certain fidelity criterion, which is conventionally defined in terms of the distortion between the original and the compressed information. Given a distortion target, Shannon's theory provides a tool to find the minimum rate at which a source should be transmitted (reproduced) to achieve the specified level of distortion after recovering the information. The rate distortion theory can be applied to both discrete and continuous random variables. Notice that the lossless compression case is a special case of the rate distortion theory applied to a discrete source with zero distortion.

Obviously, we first need to define the fidelity criterion, namely a way to assess the distortion between two elements. A distortion measure is a bijective function $d : X^N \times \hat{X}^N \rightarrow \mathbb{R}^+$ from the set of source-compressed signal pairs into the set of non-negative real numbers. The distortion $d(\mathbf{x}, \hat{\mathbf{x}})$ is hence a measure of the cost of representing the symbol vector \mathbf{x} by another vector $\hat{\mathbf{x}}$.

The most commonly used distortion metric is the Mean Squared Error (MSE), in such a manner that the distortion is defined as the expected value of the square of the difference between the source signal \mathbf{x} and the recovered (compressed) signal $\hat{\mathbf{x}}$. Therefore, if the original and reconstructed signals are given by vectors with components x_i and $\hat{x}_i, i = 1, \dots, N$, respectively, the MSE is calculated as

$$d(\mathbf{x}, \hat{\mathbf{x}}) = \mathbb{E} (\|\mathbf{x} - \hat{\mathbf{x}}\|^2) \simeq \frac{1}{N} \sum_{i=1}^N |x_i - \hat{x}_i|^2. \quad (2.8)$$

Notice that the MSE is a simple way to measure the distortion although in some applications is questionable because it does not take into account the human perception of analog signals. Several alternatives have been proposed although, at present, there is no real alternative to using the MSE as the distortion measure.

Let us now address the source coding problem from the traditional point of view of Information Theory. An input signal (source) is disturbed by a noisy channel (source coding) to produce an output signal (compressed) which is a distorted version of the original signal. In

this context, the rate distortion function for a source X can be obtained solving the following minimization problem

$$R(D) = \min_{Q(\hat{X}|X)} I(X; \hat{X}) \quad \text{subject to } d(Q) \leq D, \quad (2.9)$$

where $Q(\hat{X}|X)$, called a test channel or test system, is the conditional probability distribution of the output \hat{X} given the input X ; $d(Q)$ and D represent the average distortion and the desired distortion target (both measured in terms of MSE), respectively; and $I(X; \hat{X})$ is the mutual information between the variables X and \hat{X} . Thus, the rate distortion function can be also interpreted as the minimum channel capacity required to attain a particular level of distortion for a given source.

The rate distortion function measures the average amount of information that each sample must contain when compressing the source X to satisfy the distortion constraint. Thus, we can reformulate the source coding problem with fidelity criterion in the following way: a memoryless source X can be encoded at rate R_c , achieving a distortion not exceeding D as long as $R_c > R(D)$. Conversely, for any code with rate $R_c < R(D)$, the distortion necessarily exceeds D . If the base of the logarithms involved in the calculation of the mutual information is 2, the rate distortion function, $R(D)$ is expressed as number of bits per data sample.

As in the case of channel capacity, it is difficult to find closed form expressions for this bound. However, for a memoryless Gaussian source in which the samples are independent and identically distributed (i.i.d) and, using MSE as distortion measure, the rate distortion function is given by

$$R_G(D) = \max \left[0, \log \left(\frac{\sigma_x^2}{D} \right) \right], \quad (2.10)$$

where σ_x^2 is the source signal power, D is the distortion and the quotient σ_x^2/D is known as Signal-to-Distortion Ratio (SDR). It is important to note that the performance of an analog transmission system is commonly measured in terms of SDR expressed in dB, i.e

$$\text{SDR}_{(\text{dB})} = 10 \log_{10} \left(\frac{\sigma_x^2}{D} \right) = 10 \log_{10} \left(\frac{\sigma_x^2}{\text{MSE}} \right). \quad (2.11)$$

It may not be possible to obtain an analytical solution for the minimization problem given by Equation (2.9). In that case, we can calculate a lower bound for the rate distortion function of a memoryless source as long as the MSE is used as the distortion measure. This lower bound, known also as Shannon bound [110], can be computed as

$$R_S(D) \geq H(X) - H_G(D), \quad (2.12)$$

where $H(X)$ and $H_G(D)$ are the entropy of the source and the entropy of a Gaussian random variable with variance D , respectively. For example, let us consider the case of a Laplacian

source with probability density function

$$f(x) = \frac{1}{2b} \exp\left(-\frac{|x - \mu|}{b}\right),$$

where μ is the mean and b is a scale factor. In this case, it is not possible to obtain a closed form expression for the rate distortion function, but we can calculate the Shannon lower bound. In order to simplify the mathematical operations, natural logarithm is now assumed, and, thus, $H(D)$ and $H(X)$ are actually expressed in nats. The differential entropy for a Gaussian source with variance D is

$$H_G(D) = \log(\sqrt{2\pi e D}),$$

and, in the case of Laplacian sources, it is given by

$$H_L(X) = 1 + \log(2b).$$

Applying the logarithm properties and taking into account that the variance of a Laplacian distribution is $\sigma_x^2 = 2b^2$, this expression can be rewritten as

$$H_L(X) = \frac{1}{2} \log(2\sigma_x^2 e^2).$$

Now, applying directly Equation (2.12) for calculating the Shannon lower bound, we obtain the expression

$$R_L(D) \geq H_L(X) - H_G(D) = \frac{1}{2} \log(2\sigma_x^2 e^2) - \frac{1}{2} \log(2\pi e D).$$

Using again the logarithm properties and simplifying the common factors in the quotient, the lower bound for the rate distortion function of a Laplacian source is finally defined by

$$R_L(D) \geq \frac{1}{2} \log\left(\frac{2\sigma_x^2 e^2}{2\pi e D}\right) = \frac{1}{2} \log\left(\frac{\sigma_x^2 e}{D \pi}\right). \quad (2.13)$$

As observed, the rate distortion function for Laplacian source is given by the Gaussian bound, $R_G(D)$, multiplied by a factor $c = e/\pi$. Since $c < 1$, the number of necessary bits to achieve a given distortion in the case of Laplacian sources is actually lower than for Gaussian sources, i.e. $R_L(D) < R_G(D)$. In general, it is known that coding a Gaussian source requires the greatest number of bits for any given distortion.

The Shannon lower bound is asymptotically tight in the low distortion regime for a wide type of sources. Otherwise, the solution can be found using the Blahut-Arimoto algorithm [11, 15], an elegant iterative method for numerically obtaining rate distortion functions of arbitrary finite alphabet sources.

2.1.3 Optimum Performance Theoretically Attainable (OPTA)

The separation principle devised by Shannon is also optimum for lossy transmission of analog sources [12]. Therefore, the optimal strategy to send an analog source over a noisy channel is to separately perform source and channel coding. According to this result, it is easy to realize that there must exist some relationship between the rate distortion function and the channel capacity since both of them are used to measure the same characteristic -amount of information- in source compression and channel coding, respectively. Remember that the rate distortion function determines the minimum number of bits that must be employed to encode an analog source attaining a certain distortion whereas the channel capacity represents the maximum number of bits that can be transmitted over the channel without errors.

Let us consider an uncorrelated source that is transmitted over a memoryless noisy channel, with capacity C , according to a certain fidelity criterion defined by a distortion level D , which uniquely determines the rate distortion $R(D)$. In this case, the source can be recovered at the receiver with the expected distortion D as long as $R(D) \leq C$. Conversely, distortion D is unattainable if $R(D) > C$ since the channel does not allow an error-free transmission of the information at rate $R(D)$.

Logically, the ideal situation is given when the source encoder generates the information at the same rate as the channel can transmit it, i.e. $R(D) = C$. From this equality we can derive the optimal upper bound for the lossy transmission of analog sources, known as the Optimum Performance Theoretically Attainable (OPTA). Since the performance of analog transmission systems is usually assessed in terms of the distortion between the source and the recovered signals, we can equate the rate distortion function and the channel capacity, and determine the optimal performance of the transmission system as the minimum attainable distortion for a given CSNR.

Let us illustrate the OPTA calculation for the particular case of Gaussian sources and an AWGN channel. In general, the source bandwidth and the channel bandwidth could not be the same, so it is more convenient to consider rate per time unit rather than rate per symbol. Thus, if the bandwidth of a Gaussian source is N , i.e. the source produces N samples per second, its rate is actually given by $NR_G(D)$ bits per second. Likewise, if the bandwidth of the channel is K , we can transmit K symbols per second, which gives us a capacity of KC bits per second. Equating the rate distortion function given by Equation (2.10) and the channel capacity given by Equation (2.7), multiplied by the corresponding bandwidth factors, N and K , respectively, we obtain

$$N \log \left(\frac{\sigma_x^2}{D} \right) = K \log \left(1 + \frac{\sigma_c^2}{\sigma_n^2} \right).$$

Solving this equation with respect to the SDR, the OPTA is given by

$$\frac{\sigma_x^2}{D} = \left(1 + \frac{\sigma_c^2}{\sigma_n^2}\right)^{\frac{K}{N}}, \quad (2.14)$$

where K/N defines the relationship between the source and channel bandwidth. If $K > N$, redundant information can be added for error control. If $K < N$, the bandwidth and thus the source information has to be reduced by some sort of lossy compression before transmission.

Notice that the SDR $= \sigma_x^2/D$ is straightforwardly determined by the inverse of the distortion so it attains its maximum value when the distortion D is minimum. Therefore, the maximum attainable SDR, given by Equation (2.14), is an adequate measure of the optimal upper bound for the transmission of analog sources. In this case, the OPTA in dB can be calculated as

$$\text{OPTA}_{(\text{dB})} = 10 \log_{10}(\{1 + \text{CSNR}\}^{\frac{K}{N}}). \quad (2.15)$$

A similar approach can be followed for the transmission of Laplacian sources over an AWGN channel. Equating the lower bound calculated in the previous section for the rate distortion function of a Laplacian source (see Equation (2.13)) and the capacity of an AWGN channel given by Equation (2.7), we obtain

$$N \log \left(c \frac{\sigma_x^2}{D} \right) \leq K \log \left(1 + \frac{\sigma_c^2}{\sigma_n^2} \right),$$

where $c = e/\pi$. Solving again the equation with respect to the SDR, a lower bound for the OPTA is determined as

$$\frac{\sigma_x^2}{D_t} \leq \left(1 + \frac{\sigma_c^2}{\sigma_n^2} \right)^{c \frac{K}{N}}. \quad (2.16)$$

Notice that this expression is closely related to the bound obtained for Gaussian sources since the only difference between both equations is the constant $c = e/\pi$ multiplying the bandwidth rate in the exponent. Thereby, the OPTA expressed in dB for Laplacian sources is defined by

$$\text{OPTA}_{(\text{dB})} \leq 10 \log_{10}(\{1 + \text{CSNR}\}^{c \frac{K}{N}}). \quad (2.17)$$

The procedure for the OPTA calculation can be extended to other types of sources and channels as we will see, for example, in the case of Multiple Input Multiple Output (MIMO) systems.

2.2 Analog Joint Source Channel Coding

We focus on a point-to-point communication system performing a lossy transmission of uncorrelated continuous sources over a memoryless channel. Henceforth, this system model will be assumed along this thesis unless the opposite is explicitly specified. The optimal

performance (OPTA) of this type of systems can be theoretically attained if source and channel coding are separately tackled. As previously explained, this strategy is known as Separate Source and Channel Coding (SSCC).

Unfortunately, the optimal distortion-cost tradeoff can be only approached closely if sources are compressed using powerful quantization and encoding methods, and the resulting data is transmitted using capacity-approaching channel codes such as Turbo Codes or Low Density Parity Check (LDPC). The utilization of capacity-achieving digital source and channel codes requires significant delay and high computational complexity. Thus, the separation principle does not seem a good choice if we aim to design practical communication systems with severe constraints on delay and/or complexity.

The separation principle allows to separately design the source and channel encoder according to certain properties like distortion rate and CSNR. Nevertheless, if any one of those properties change, it is necessary to completely redesign both encoders. Thus, the utility of the separation principle is rather questionable when considering the transmission over time-varying channels such as those encountered in wireless communications. Moreover, when the information about the channel conditions is not available or is inaccurate at the transmitter, the design of the encoders will not be adequate and hence the system performance completely degrade.

In addition, communication systems are traditionally designed following a digital approach for both discrete and continuous sources. When the system inputs are analog signals, the source information must be discretized and quantized. The quantization is not an invertible operation so a certain quantization error is always generated, inducing a floor effect since the digital system performance saturates as long as the CSNR exceeds a certain threshold value determined by the quantization error.

These drawbacks can be virtually solved if we consider another approach consisting in jointly designing the source and channel encoders. This strategy does not follow the separation principle and is referred to as Joint Source Channel Coding (JSCC). An analog JSCC system directly transforms continuous-amplitude source samples into channel symbols to be transmitted, using some type of continuous mapping. In general, Shannon-Kotel'nikov mappings, based on parametrized geometric curves, are assumed for the encoding operation (see Section 2.2.1).

Analog JSCC systems have been shown to be a low complexity alternative for the transmission of analog sources at high rates with an almost negligible delay. Also, they are characterized by its robustness against varying channel conditions and graceful degradation for imperfect Channel State Information (CSI) at the transmitter. Moreover, the easily-updated structure of a JSCC scheme allows us to continuously adapt the system as the channel conditions change.

At this point, the really interesting question is whether low complexity analog JSCC systems

can closely approach or even improve the performance attained for suboptimal SSCC schemes using finite and affordable block lengths when, for example, tight restrictions on delay are imposed. We try to respond this question for wireless channels along the thesis.

2.2.1 Shannon-Kotel'nikov Mappings

Let N and K be the source and channel bandwidth, respectively. According to the geometrical interpretation proposed by Shannon [109], assuming Nyquist sampling and an ideal Nyquist channel, a source vector of N samples can be spatially represented as a specific point on the N -dimensional source space and, similarly, a vector of K channel symbols corresponds to a point on the K -dimensional channel space. Mathematically, a source vector $\mathbf{x} \in \mathbb{R}^N$ contains N source samples, $\mathbf{x} = \{x_n\}_{n=1}^N$, which represent the coordinate values of the vector on the N -dimensional source space. In the same way, a channel vector $\mathbf{s} \in \mathbb{R}^K$ consists of K channel symbols, $\mathbf{s} = \{s_k\}_{k=1}^K$, which are the coordinates of \mathbf{s} on the K -dimensional channel space. A function $M(\cdot) : \mathbb{R}^N \rightarrow \mathbb{R}^K$ that establishes a correspondence between the points in the source space and the points in the channel space is known as a mapping, i.e. $\mathbf{s} = M(\mathbf{x})$.

When $N \neq K$, this mapping involves either a bandwidth reduction if $N > K$ or a bandwidth expansion if $N < K$. In the first case, the operator M projects the source points onto a lower dimensional subspace and therefore, for practical mappings, it is not invertible and a lossy compression is inevitable. For mappings without dimension change ($N = K$) and mappings with dimension increase, ($N < K$), where the source vectors are mapped onto a higher dimensional space, they can be made invertible so that it is possible to completely recover the source information.

From this geometrical interpretation of a communication system, we can define Shannon-Kotel'nikov¹ mappings as the set of continuous non-linear source-channel mappings based on geometric curves. A first example is the mapping shown in Figure 2.2, which was suggested by Shannon in [109] for a 1:2 dimensional increase but can be employed for a reciprocal dimensional reduction. If used for bandwidth expansion, the length of the rope along the curve from some reference point (origin) to the selected point, represents the source sample amplitude and the two coordinates of the selected point on the bidimensional space correspond to the two channel symbols. Reciprocally, when used for bandwidth reduction, the two coordinates represent the source sample pair that is mapped to the closest point on the curve and the length along the curve to this point will be the channel symbol amplitude.

Nevertheless, according to the topological theory, it is not possible to map a region of

¹Kotel'nikov developed a similar theory for bandwidth expansion systems in his doctoral dissertation [66] employing the same type of geometric structures. This work dates back to 1947, although it was not translated to English until twelve years later. For that reason, the name Shannon-Kotel'nikov mappings is used to designate non-linear mappings based on these type of geometric structures

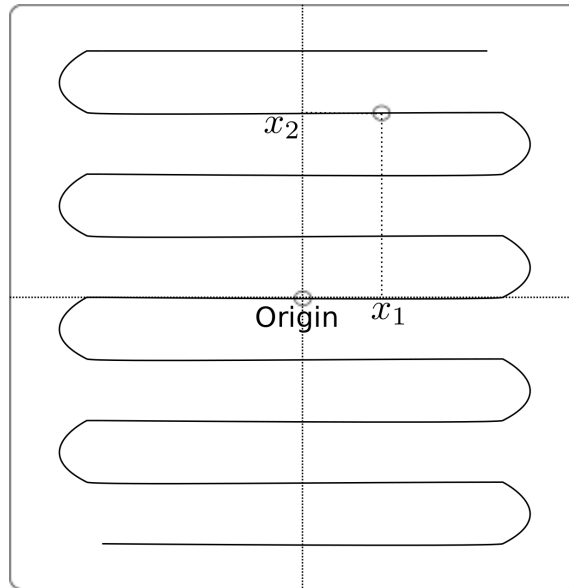


Figure 2.2: Mapping suggested by Shannon for 1:2 bandwidth expansion.

higher dimension into a lower dimension continuously using space filling curves in the presence of noise. Hence, Shannon’s mappings necessarily involve a certain loss in the compression process, which is directly related to the way how the curve fills the bidimensional space. If the rope is very stretched along the source space, the curve can almost completely fill such a region minimizing the loss induced by the mapping operation. Unfortunately, stretching the curve implies that the horizontal lines get closer each other and a side effect, called threshold effect by Shannon [109], can turn up when the channel noise disturbs the channel symbols. When the noise level is below a certain value, the received symbols are only moved along the curve and, therefore, the receiver can recover the transmitted source symbol with a fairly small error. However, if the channel noise reaches a certain level, there is a probability of crossing to a neighbouring line (threshold effect) and the source symbols cannot be recovered because the error is too large. This effect is inherent to all non-linear Shannon-Kotel’nikov mappings.

Notice that Shannon-Kotel’nikov mappings perform a memoryless JSCC where a point on the N -dimensional source space is directly projected onto the K -dimensional channel space by a mapping operation in contrast to the conventional channel coding where long blocks of source samples are used to build the channel signals incurring on long delays and high complexity.

2.2.2 Bandwidth Compression

Shannon-Kotel’nikov mappings closely approach the theoretical limits when employed for bandwidth compression but are not suitable for bandwidth expansion since it is difficult to find non-linear mappings that efficiently fill the channel space without simultaneously creating multiple neighbours that are far away in the source space, hence causing the threshold effect predicted by Shannon. For this reason, in this thesis we will focus on analog JSCC for

dimension reduction by using Shannon-Kotel'nikov mappings. In particular, we will mainly study the 2:1 compression case.

If we aim to represent a 2-D space (a plane) by a one-dimensional continuous curve, the subspace generated by the curve must satisfy certain topological properties in order to ensure an effective representation of the source samples on the channel space [73, 94]:

- The mapping should cover the entire space in such a way that a point on the source space is mapped to the closest point on the channel space.
- The most likely source symbols should be mapped into channel symbols with lower amplitudes to minimize the transmission power.
- If two points are close in the channel space, they should be mapped back into two points that are close in the source space too. The opposite is not necessary, so two source samples that are close can be mapped to completely different regions in the channel space.

According to these requirements, it can be concluded that the non-linear mapping proposed by Shannon (see Figure 2.2) works quite well for 2:1 bandwidth reduction if we have uniformly distributed sources. However, for another types of source distributions which commonly model natural phenomena, such as Gaussian or Laplacian, we must devise other continuous curves whose topological properties fit better.

For example, non-linear mapping for 2:1 compression of Gaussian sources over AWGN channels have been widely studied in several works [20, 50, 94] where it is suggested a particular type of parametrized space-filling continuous curve which consists of a doubly intertwined Archimedes' spiral, as shown in Figure 2.3.

This mapping based on spiral-like curves highly resembles the optimal Power Constrained Channel Optimized Vector Quantizer (PCCOVQ) developed by Fuldsheth [39] for a 2:1 compression rate. Indeed, connecting the adjacent representation vectors in a codebook, we obtain a non-linear continuous curve that, for moderate to high CSNR, is very similar to the spiral-like curve employed for the 2:1 compression case. Also, recently, Akyol et al. [9] have analytically calculated optimal mappings for different bandwidth expansion/compression rates assuming Gaussian sources and Gaussian channels. For a 2:1 compression rate, they have obtained a spiral-like curve that closely approaches the double Archimedes' spiral. Obviously, both arguments support the use of the double Archimedes' spiral for 2:1 analog JSCC since it achieves a performance very close to the optimal one and can be mathematically defined by a closed form, hence simplifying the mapping operation.

This kind of non-linear mappings have been extended for higher compression rates [32] by using more complex structures -called hypersurfaces- as, for example, the ball of yarn for a 3:1 bandwidth compression. These multidimensional structures generally attain a good

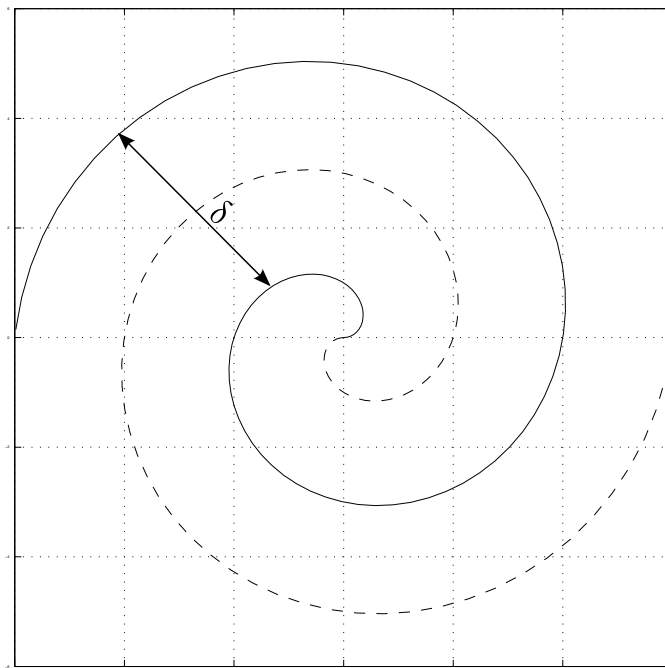


Figure 2.3: Continuous like-spiral curve proposed for 2:1 bandwidth reduction.

performance although they tend to get away from the optimal limits as the compression rate grows.

In addition, a deformed version of the double Archimedes' spiral was proposed in [49] for 2:1 compression of Laplacian sources. Nevertheless, it is shown in [55] that if the encoder parameters are properly chosen, a simple spiral-like curve performs as well as the deformed one.

2.3 System Description

In this section, we describe the basic structure of an analog JSCC system employed for the discrete-time continuous-amplitude transmission of source samples over an AWGN channel. As previously explained, we focus on analog JSCC for bandwidth reduction since these schemes have been shown to closely approach the theoretical limits (specially in the 2:1 case) and they achieve high transmission rates allowing a better usage of the radio spectrum. Figure 2.4 shows the block diagram of an analog JSCC system performing a N :1 bandwidth compression. This system is entirely analog and comprises two main elements:

- An analog encoder that maps a source sample vector into one channel symbol by using a suitable non-linear mapping, namely a one-dimensional parametric space-filling continuous curve.
- An analog decoder that is the device responsible for recovering the transmitted source symbols from the received symbols.

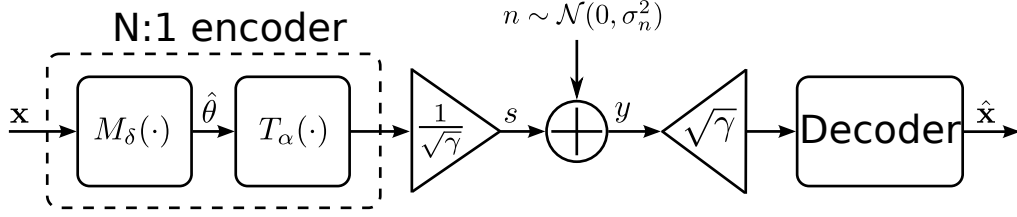


Figure 2.4: Block diagram of a bandwidth reduction $N:1$ analog JSCC system over AWGN channels.

Thus, an $N:1$ analog encoder generates a sequence of channel symbols that is sent over an AWGN channel represented by a zero-mean Gaussian random variable n with variance σ_n^2 , i.e. $n \sim \mathcal{N}(0, \sigma_n^2)$. At the receiver, the analog decoder calculates an estimate of the transmitted source symbols from the received symbols.

2.3.1 Analog Encoder

At the transmitter, an $N:1$ analog encoder performs a lossy compression transforming N independent and identically distributed (i.i.d.) analog source samples into one channel symbol, which is directly transmitted without any explicit error control mechanism. As shown in Figure 2.4, the encoding procedure actually consists of two separated operations: the mapping function $M_\delta(\cdot)$ and an invertible function $T_\alpha(\cdot)$, termed stretching function [51].

The mapping operation is defined as a function $M_\delta(\mathbf{x}) : \mathbb{R}^N \rightarrow \mathbb{R}$, where δ is a parameter that determines how the one-dimensional continuous curve fills the source space. This function implements the dimension reduction, translating the N source samples to a single value in two steps:

- A non-invertible approximation operation where the elements of the N -dimensional source space are restricted to the subspace S_Z generated by the one-dimensional continuous curve. Geometrically, the N source samples are packed into a source vector $\mathbf{x} = (x_1, x_2, \dots, x_N)$, $\mathbf{x} \in \mathbb{R}^N$, whose components represent the coordinates of a specific point on the source space. This point \mathbf{x} is projected onto the closest point -according to Euclidean distance- on the space-filling curve, $\mathbf{z} = (z_1, z_2, \dots, z_N)$, $\mathbf{z} \in S_Z$.
- A dimension changing operation that maps the approximation point \mathbf{z} from the N -dimensional subspace to the one-dimensional channel space. Thus, a lower dimensional representation of the points in S_Z is determined according to a certain curve parameter θ . This parameter defines how the distance from any point on the curve to the origin is measured. We can choose, for example, the rope length along the curve or the angle from the origin (radial distance).

The mapping function can be thus mathematically defined as $M_\delta(\mathbf{x}) = \theta$. Notice that, in this case, the intermediate representation of the source vector \mathbf{x} is a continuous subspace generated

by the employed curve, unlike PCCOVQ mappings where a discrete subset of representation vectors is considered.

The stretching function $T_\alpha(\theta) : \mathbb{R} \rightarrow \mathbb{R}$ is a bijective function operating on the values θ at the mapping operation output, being α the stretching factor. We can change the parameter space distribution to protect the channel symbols against the noise by selecting a proper stretching factor according to the source distribution. For example, choosing $\alpha = 1$, the noise is linearly distributed over the whole parameter space, actually corrupting the lower amplitude channel symbols in a higher proportion. This effect is usually undesirable.

The curve parameter δ and the stretching factor α provide a certain degree of flexibility since they can be jointly optimized at the encoder with the aim of improving the overall system performance.

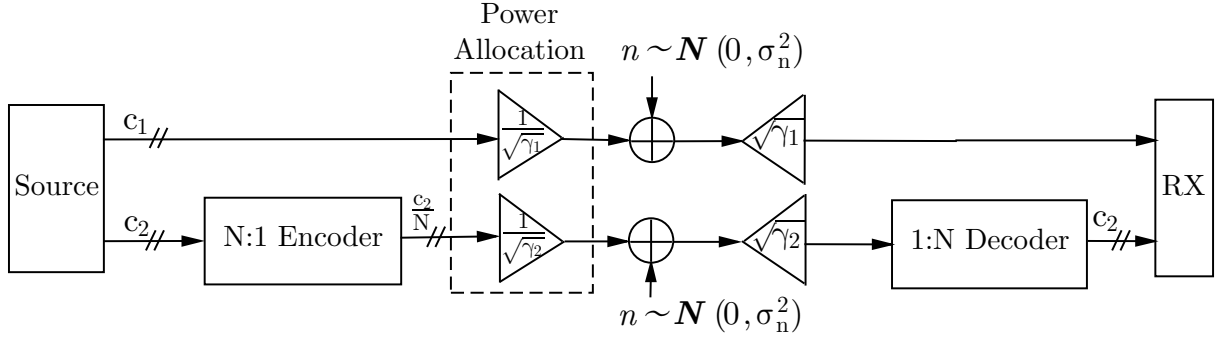
Finally, the channel symbols $s = T_\alpha(\theta)$ are normalized by a factor γ to ensure the average transmitted power satisfies the power constraint, i.e. $\mathbb{E}[|s|^2] \leq P_T$, where $\mathbb{E}[\cdot]$ represents the mathematical expectation and P_T is the total power available at the transmitter .

2.3.1.1 N:K Analog Encoder

In general, we are interested in achieving any compression rate between $N:1$ and $1:1$ with the aim of adapting the transmission rate of analog JSCC systems depending on the channel conditions. However, the analog JSCC scheme introduced in the previous section (see Figure 2.4), which maps N source samples into the closest point of a one-dimensional curve, only provides $N:1$ rates, $N \in \mathbb{N}$. This system is not very flexible but, fortunately, it can be easily extended by combining an $N:1$ compression scheme and a $1:1$ transmission system as shown in [55]. It is worth remembering that, as commented in Chapter 1, the direct transmission of discrete-time uncoded Gaussian samples over an AWGN channel is optimal [44] when the source and the channel have the same bandwidth, i.e. $1:1$.

Figure 2.5 shows the block diagram of an analog JSCC system whose encoder performs a $N:K$ bandwidth compression. For that, c_1 source symbols are directly transmitted by a $1:1$ uncoded system whereas c_2 symbols are encoded into c_2/N channel symbols using an $N:1$ analog encoder. Thus, $c_1 + c_2 = N$ source symbols are transformed into $(c_1 + c_2/N) = K$ channel symbols to be transmitted over the AWGN channel. By properly choosing c_1 and c_2 , any compression ratio between $1:1$ and $N:1$ can be achieved.

Since the average power consumed for transmitting one channel symbol is constrained to P_T , the total available power for transmitting all $c_1 + c_2$ source symbols is $(c_1 + c_2/N)P_T$. However, the transmission power used for each subsystem can be efficiently distributed as long as the total power constraint is satisfied. Therefore, we can add a power allocation module at the encoder that determines how much power should be employed by each subsystem in order to improve the overall system performance.


 Figure 2.5: Block diagram of a bandwidth compression $N:K$ analog JSCC system over AWGN channel.

Let $p \in (0, 1)$ be the fraction of the power spent on sending the uncoded symbols and $1 - p$ the fraction of power for the transmission of the compressed symbols. It is proved in [55] that the optimal value for p , which optimizes the overall performance of the $N:K$ analog JSCC system, can be obtained by solving the following minimization problem

$$p_{\text{opt}} = \arg \min_p \left(\frac{c_1}{1 + \frac{(Nc_1 + c_2)p}{Nc_1\sigma_n^2}} + \frac{c_2}{[1 + \frac{(Nc_1 + c_2)(1-p)}{c_2\sigma_n^2}]^{(1/N)}G} \right), \quad (2.18)$$

where G represents the gap between the real performance and the theoretical limit. Let $a = c_1$, $b = (Nc_1 + c_2)/(Nc_1\sigma_n^2)$, $c = c_2/G$ and $d = (Nc_1 + c_2)/(c_2\sigma_n^2)$. If we define the auxiliary function $F(p)$ as

$$F(p) = \frac{a}{1 + bp} + \frac{c}{1 + d(1 - p)^{1/N}}$$

Equation (2.18) can be rewritten as follows

$$p_{\text{opt}} = \arg \min\{F(p)\}.$$

Calculating the first-order derivative of $F(p)$ with respect to p and equating the result to zero, we obtain

$$\frac{dF(p)}{dp} = \frac{ab}{(1 + bp)^2} + \frac{cd}{N[1 + d(1 - p)]^{N+1/N}} = 0. \quad (2.19)$$

Notice that $\frac{dF(p)}{dp}$ is a continuous and monotone increasing function for all $p \in (0, 1)$. Also, it is easy to check that $\frac{dF(0)}{dp} < 0$ and $\frac{dF(1)}{dp} > 0$, so there must exist a point $p_0 \in (0, 1)$ such that $\frac{dF(p_0)}{dp} = 0$. Taking the second-order derivative of $F(p)$ yields

$$\frac{dF^2(p)}{dp} = \frac{2ab^2}{(1 + bp)^3} + \frac{(N + 1)cd^2}{N^2[1 + d(1 - p)]^{2N+1/N}}. \quad (2.20)$$

Since a , b , c and d are all greater than zero, then for $p_0 \in (0, 1)$, $\frac{dF^2(p_0)}{dp} \geq 0$, which means $F(p)$ achieves a minimum at $p = p_0$, i.e. $p_{\text{opt}} = p_0$. Once p_{opt} has been calculated, it is straightforward to readjust the power allocated to each subsystem.

2.3.1.2 Archimedes' Spiral

In the previous section, a general description for the $N:K$ analog encoder based on Shannon-Kotel'nikov mappings has been given. As mentioned before, the performance of analog JSCC systems closely approaches the OPTA for $N = 2$, but it tends to move away as we increase the compression rate since it is more complicated to find a one-dimensional continuous curve that fills high dimensional spaces efficiently. Hence, we will focus on 2:1 analog JSCC.

At this point, the first and more important question should be what type of Shannon-Kotel'nikov mapping is optimal for the case of a compression with rate 2:1 or, equivalently, what mapping provides the best performance. In Section 2.2.2, we brought forward that several works [20, 50, 94] had suggested the use of a doubly intertwined parametrized Archimedes' spiral for Gaussian sources over AWGN channels. In this case, any point on the Archimedes' spiral can be mathematically defined by

$$\begin{cases} z_1 = \text{sign}(\theta) \frac{\delta}{\pi} \theta \sin \theta \\ z_2 = \frac{\delta}{\pi} \theta \cos \theta \end{cases} \quad \text{for } \theta \in \mathbb{R}, \quad (2.21)$$

where δ is the distance between two neighbouring spiral arms and θ is the angle from the origin to the point on the curve $\mathbf{z} = (z_1, z_2), \mathbf{x} \in \mathbb{R}^2$.

At first glance, the Archimedes' spiral seems a suitable mapping for Gaussian or Laplacian source distributions according to their topological properties. The Archimedes' spiral properly covers the source space on \mathbb{R}^2 and, also, it can be made as dense as we want by decreasing the parameter δ . At the limiting situation $\delta \rightarrow 0$, this like-spiral curve would fill the whole source space continuously. In addition, the most probable samples of a Gaussian or Laplacian distribution are around zero, so they are mapped into points close to the origin, which corresponds to lower amplitude channel symbols. Finally, two neighbouring points in the spiral are mapped back to two points close in the source space. Another important aspect of the double spiral is that it covers the plane in a symmetric fashion for both the negative and positive channel amplitudes, which implies that the channel representation is symmetric.

The use of Archimedes' spiral is also supported by the fact that it can be interpreted as a continuous version of the optimal PCCOVQ developed by Fuldsheth [39] for a 2:1 compression rate. Moreover, a spiral-like curve that quite resembles Archimedes' spirals has been shown in [9] to be the optimal mapping for the 2:1 compression of Gaussian sources. In summary, the mapping based on the doubly intertwined Archimedes' spiral closely approaches the optimal performance for Gaussian sources and it can be also mathematically described in a closed form using Equation (2.21), hence simplifying the encoding operation.

Particularizing for $N = 2$, we can simplify the notation in Section 2.3.1 as follows:

- Two discrete-time continuous-amplitude source symbols correspond to a certain point on

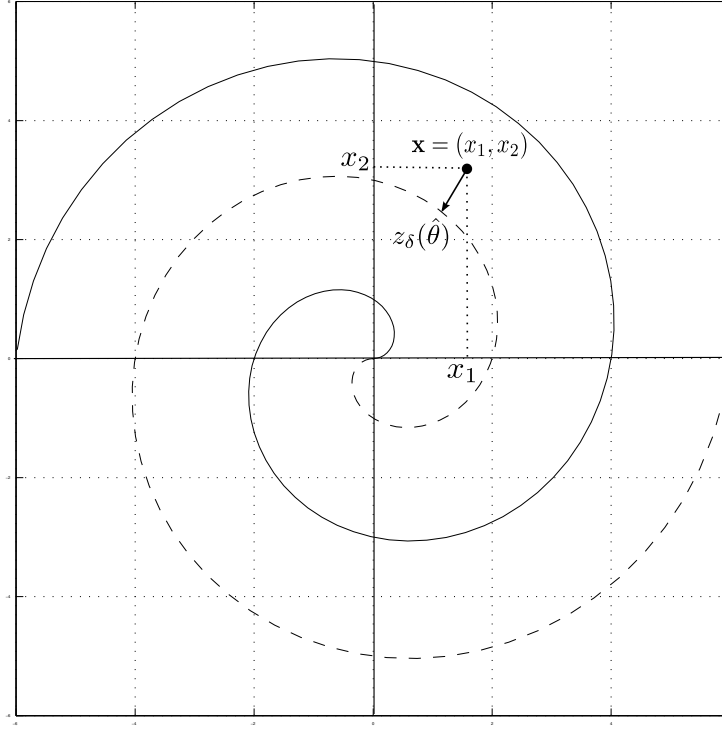


Figure 2.6: Analog mapping based on the use of the doubly intertwined Archimedes' spiral.

the source space, $\mathbf{x} = (x_1, x_2)$, $\mathbf{x} \in \mathbb{R}^2$.

- Any point on the spiral $\mathbf{z} = (z_1, z_2)$, $\mathbf{z} \in S_z$, can be expressed as a function of its angle with respect to the origin by

$$\mathbf{z}_\delta(\theta) = \left(\text{sign}(\theta) \frac{\delta}{\pi} \theta \sin \theta, \frac{\delta}{\pi} \theta \cos \theta \right). \quad (2.22)$$

- The mapping operation, $M_\delta(\mathbf{x}) : \mathbb{R}^2 \rightarrow \mathbb{R}$, provides the angle $\hat{\theta}$ corresponding to the point on the spiral that minimizes the Euclidean distance with respect to the source point \mathbf{x} , i.e.

$$\hat{\theta} = M_\delta(\mathbf{x}) = \arg \min_{\theta} \|\mathbf{x} - \mathbf{z}_\delta(\theta)\|^2. \quad (2.23)$$

Figure 2.6 visualizes this mapping operation graphically. A coarse search is done first to determine which spiral arm the projection falls into, using the position information of the source point $\mathbf{x} = (x_1, x_2)$. Then, \mathbf{x} is projected on the point where the imaginary straight line from the origin to the point \mathbf{x} and the spiral arm intersect. A more refined search can be then made around this coarse point to determine the real closest point, $\mathbf{z}_\delta(\hat{\theta})$. Finally, the dimension reduction operation is carried out by selecting the angle $\hat{\theta}$ from the origin to this point.

After obtaining the compressed samples, the next step is to apply the stretching function $T_\alpha(\cdot)$. In [20, 50, 51], the invertible function

$$T_\alpha(\hat{\theta}) = \text{sign}(\hat{\theta})|\hat{\theta}|^\alpha \quad (2.24)$$

with $\alpha = 2$ was proposed. It is alleged that when using a square function, and if the channel symbol is modified at a constant rate, the corresponding point will be moved on the spiral at constant rate too, providing signal-independent noise [51]. In addition, the channel inputs approximate a Laplacian distribution, thus simplifying the distortion analysis and enabling the analytical calculation of the optimal value for δ . As will see in Section 2.3.4, the system performance can be improved if the optimal values for the parameters δ and α are specifically determined for each CSNR value.

Prior to be transmitted, the channel symbols must be normalized by a factor $\sqrt{\gamma}$ ensuring that the average transmitted power satisfies the power constraint. Thus, the symbol sent over the channel is constructed as

$$s = \frac{T_\alpha(M_\delta(\mathbf{x}))}{\sqrt{\gamma}} = \frac{\tilde{s}}{\sqrt{\gamma}}, \quad (2.25)$$

where \tilde{s} represents the unnormalized channel symbols at the output of the analog encoder.

2.3.2 Analog Decoder

In this section, we will introduce the other important device of the analog system presented in Section 2.3: the analog decoder responsible for recovering the original signal corrupted by a noisy channel. The analog decoder should revert the sequence of the operations performed by the mapping operation, namely the approximation step and the dimension changing operation.

Assuming an AWGN channel, the received symbol is given by

$$y = s + n, \quad (2.26)$$

where $n \sim \mathcal{N}(0, \sigma_n^2)$ is a real-valued zero-mean Gaussian random variable that represents the channel noise. In the noiseless case, the received symbol actually corresponds to a certain point on the source space, $y = (y_1, y_2, \dots, y_N)$ after it is mapped back onto N -dimensional space, undoing the dimension change. Nevertheless, this point does not necessarily belong to the spiral defined by Equation (2.22) when the coded symbol is transmitted over a noisy channel due to the distortion introduced by the channel.

Therefore, the analog decoder has to calculate an estimate \hat{x} of the transmitted source symbol x from the noisy observation y . Since the system performance is maximized as the distortion between source and decoded symbols is minimized, it is sensible to consider an Minimum Mean Square Error (MMSE) strategy as the optimal method for decoding the received symbols.

In [55] it is proposed a quasi-optimal MMSE scheme that, given an observation y , calculates

the point $\hat{\mathbf{x}}$ on the N -dimensional source space that minimizes the MSE with respect to y , i.e.

$$\begin{aligned}\hat{\mathbf{x}}_{\text{MMSE}} &= \mathbb{E}[\mathbf{x}|y] = \int \mathbf{x} p(\mathbf{x}|y) d\mathbf{x} \\ &= \frac{1}{p(y)} \int \mathbf{x} p(y|\mathbf{x}) p(\mathbf{x}) d\mathbf{x}.\end{aligned}\quad (2.27)$$

Unfortunately, calculating $\hat{\mathbf{x}}_{\text{MMSE}}$ is not straightforward. Indeed, since the conditional probability, $p(y|\mathbf{x})$, involves the mapping function $M_\delta(\cdot)$, which is discontinuous and highly non-linear, the integral in Equation (2.27) can only be solved numerically. Therefore, we first need to discretize the set of all possible source values, in such a manner that the N -dimensional source space is represented by a mesh of discrete points. If L discrete-points are selected for each source dimension, the discretized version of the source space is given by $\mathbf{x}_d = \{x_{11}, \dots, x_{1L}; \dots; x_{NL}\}$ and hence we have to calculate L^N values for $p(\mathbf{x})$ and $p(y|\mathbf{x})$ and then compute the integral in Equation (2.27). As the number of discrete points L is reduced, the decoding performance is quickly degraded, so we have to choose large values of L for MMSE decoding to perform close to the theoretical limits.

Notice that $p(\mathbf{x}_d)$ can be directly obtained from the Probability Density Function (PDF) of the source distribution, whereas we need to determine the probability of the received symbol y with respect to the L^N mapped values $T_\alpha(M_\delta(\mathbf{x}_d))$ in order to obtain a discretized version of $p(y|\mathbf{x})$. Since $p(\mathbf{x}_d)$ and $T_\alpha(M_\delta(\mathbf{x}_d))$ do not depend on the received symbol, they can be precalculated once off-line and the results stored at the decoder. Despite that, we have to calculate L^N probabilities and compute a sum of L^N terms for each received symbol, which negatively impacts on the decoding complexity.

A low complexity alternative is Maximum Likelihood (ML) decoding, mostly employed in the literature [20, 51]. This decoding method consists in selecting the symbol on the channel space that maximizes the likelihood function $p(y|\mathbf{x})$. Notice that, unlike the MMSE approach, the set of usable received symbols is just restricted to the channel space. Thus, the ML decoder first projects the N -dimensional point corresponding to the received symbol y on the one-dimensional continuous curve used for the encoding operation, and then the resulting point is mapped back into the source space in order to obtain the ML estimate.

Mathematically, the ML estimate $\hat{\mathbf{x}}_{\text{ML}}$ of the transmitted source symbol \mathbf{x} is calculated as the tuple $(\hat{x}_1, \hat{x}_2, \dots, \hat{x}_N)$ that belongs to the non-linear curve and maximizes the likelihood function $p(y|\mathbf{x})$, i.e.

$$\hat{\mathbf{x}}_{\text{ML}} = \arg \max_{\mathbf{x} \in \text{curve}} p(y|\mathbf{x}) = \{\mathbf{x} | \mathbf{x} \in \text{curve and } \mathbf{x} = M_\delta(T_\alpha(\sqrt{\gamma} y)^{-1})\}.\quad (2.28)$$

As mentioned, the received symbol y is decoded as the point on the curve that minimizes the Euclidean distance with respect to the point obtained after applying the inverse of the stretching function $T_\alpha(\cdot)$ to the denormalized version of y . To compute the closest point \mathbf{x} on the curve, the mapping function $M_\delta(\cdot)$ is conveniently employed.

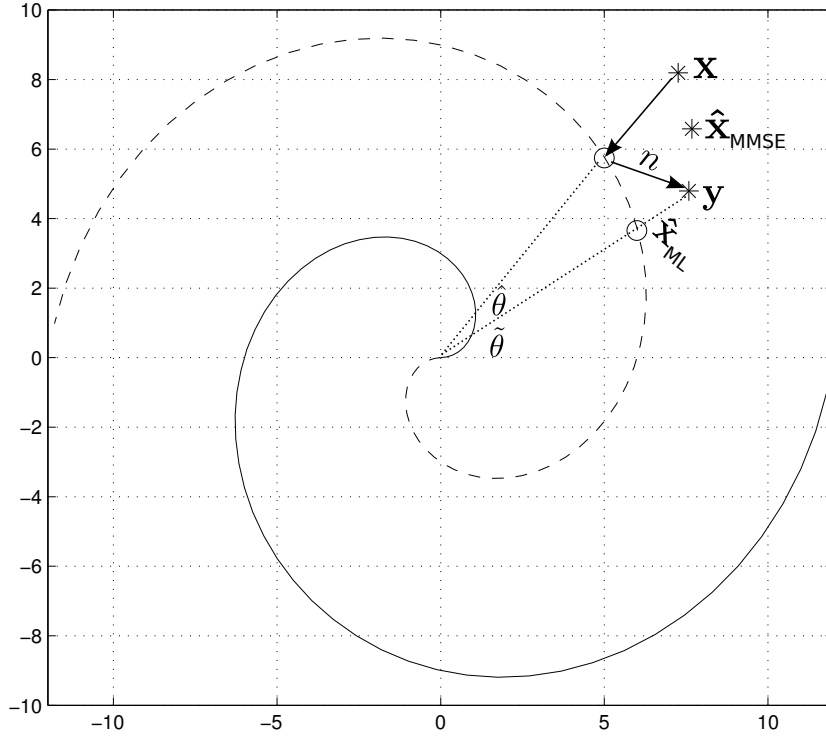


Figure 2.7: Example of ML and MMSE decoding for $N = 2$ and Archimedes' spiral.

Particularizing to the case $N = 2$, when the Archimedes' spiral is considered, the transmitted symbol is given by Equation (2.25). Therefore, ML decoding is equivalent to first applying the inverse function $T_\alpha^{-1}(\cdot)$ to the observation y after de-normalization and then find an estimate $\tilde{\theta}$ of the transmitted angle $\hat{\theta} = M_\delta(\mathbf{x})$, i.e.

$$\tilde{\theta} = T_\alpha^{-1}(\sqrt{\gamma}y) = \text{sign}(y)|\sqrt{\gamma}y|^{-\alpha}. \quad (2.29)$$

We finally obtain the point on the spiral corresponding to $\tilde{\theta}$ as $\hat{\mathbf{x}}_{\text{ML}} = (\hat{x}_1, \hat{x}_2) = \mathbf{z}_\delta(\tilde{\theta})$. Notice that the overall decoder complexity is extremely low since the two decoding steps previously described only involve simple mathematical operations. Analog JSCC over an AWGN channel with ML decoding is analyzed in [20, 50, 51], where it is shown that its performance is close to the OPTA limit for medium and high CSNRs but it significantly degrades when we consider low CSNR values given that the ML approximation becomes more inaccurate as the noise level increases.

Figure 2.7 shows an example where a received symbol is decoded following the MMSE or the ML criterion for the particular case of $N = 2$ and the Archimedes' spiral. The stretching step and its inverse operation are disregarded for clarity. The point \mathbf{x}_{MMSE} is a spatial representation of the value calculated according to the integral defined in Equation (2.27). As can be observed, this point does not belong to the Archimedes' spiral unlike in the ML case.

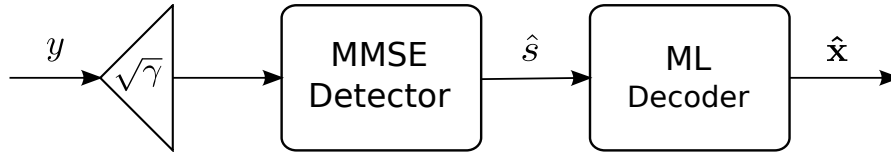


Figure 2.8: Block diagram of the proposed two-stage decoding scheme.

2.3.3 Proposed Decoding Method

In the previous section, we have studied two different approaches for decoding the received symbols. In summary, ML decoding provides a low complexity solution that achieves a good performance for high CSNR, but it tends to move away from the optimal limit as we decrease the CSNR value. On the other hand, MMSE decoding closely approaches the OPTA in the whole CSNR range but its complexity is considerably higher than that of ML and, therefore, this alternative goes against the philosophy of zero-delay and low complexity in which analog JSCC is supported. Obviously, the ideal option would be to find a low complexity and zero-delay decoding method whose performance always remains close to the theoretical limit for any CSNR value.

The reason why ML decoding performance degrades at low CSNRs is because it produces estimates of the source symbols directly from the received symbols. When the channel noise is high, the received symbols are severely distorted and shifted along the curve so the estimates produced by the ML decoder are far from the source symbols.

Intuitively, it should be possible to improve the ML estimates if the received symbols are previously filtered to reduce the distortion introduced by the channel into the transmitted symbols. For this reason, we propose a two-stage decoding approach in such a manner that an MMSE filter is placed prior to ML decoding with the aim of minimizing the MSE between the transmitted and filtered symbols. Figure 2.8 shows the block diagram of the proposed decoding scheme.

A similar idea has been discussed in [34] by Forney who showed that MMSE estimation is instrumental for achieving the capacity of AWGN channels but in the context of digital communications using lattice-type coding.

In the case of AWGN channels, the linear MMSE estimate of the transmitted symbol s is given by

$$\hat{s} = \frac{y}{1 + \sigma_n^2}, \quad (2.30)$$

where y is the received symbol and σ_n^2 is the noise variance. Thus, the received symbols are filtered employing the MMSE detector according to Equation (2.30) in a first stage. Next, ML decoding is applied to the linear filter output \hat{s} and an estimate of the transmitted source symbols is obtained. This two-step decoding strategy resembles the one used in coded-modulated digital systems that makes use of separate detection and decoding stages.

Notice that when transmitting over AWGN channels, the complexity of MMSE filtering is

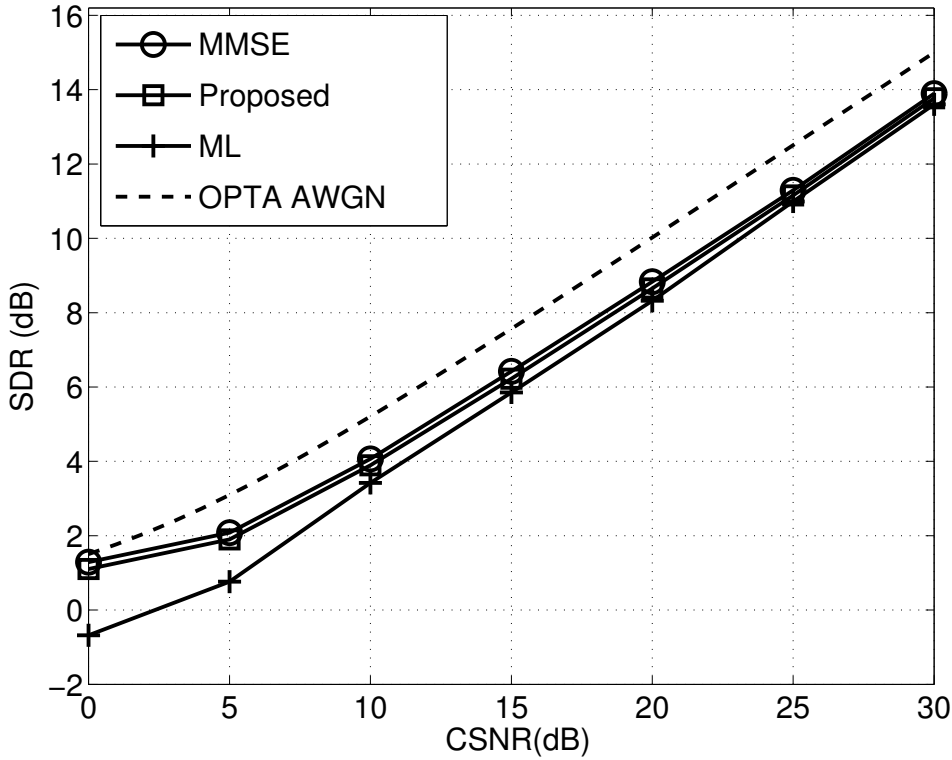


Figure 2.9: Performance of the 2:1 analog JSCC system when using the two-stage decoding for Gaussian sources.

minimum, since it simply consists on the multiplication of the received symbols and a number that depends on σ_n^2 . For high CSNRs, this number is close to one and the influence of the MMSE filter is small. However, for low CSNR values the impact of this filtering is significant.

Figures 2.9 and 2.10 show the performance of the analog JSCC system considering the two-stage decoding for the case of Gaussian and Laplacian sources, respectively. As observed, the performance curves corresponding to the proposed decoding scheme and the optimal MMSE decoding almost overlap in both cases with a constant gap (about 1.5 dB) with respect to the OPTA for all CSNR values. Also, the proposed solution outperforms ML decoding at low CSNR values (i.e. below 15 dB) with similar complexity. The OPTA bound is calculated according to Equation (2.15) and Equation (2.17) for Gaussian and Laplacian sources, respectively.

According to these results, it is possible to assert that we have devised a low complexity decoding method for analog JSCC which provides a performance very close to that of the optimal solution. This new approach not only represents an interesting contribution to design near-optimal analog JSCC schemes for the AWGN case, but also will be a fundamental strategy to preserve low complexity and low delay when the decoding operation is implemented on more complex transmission models, such as MIMO systems.

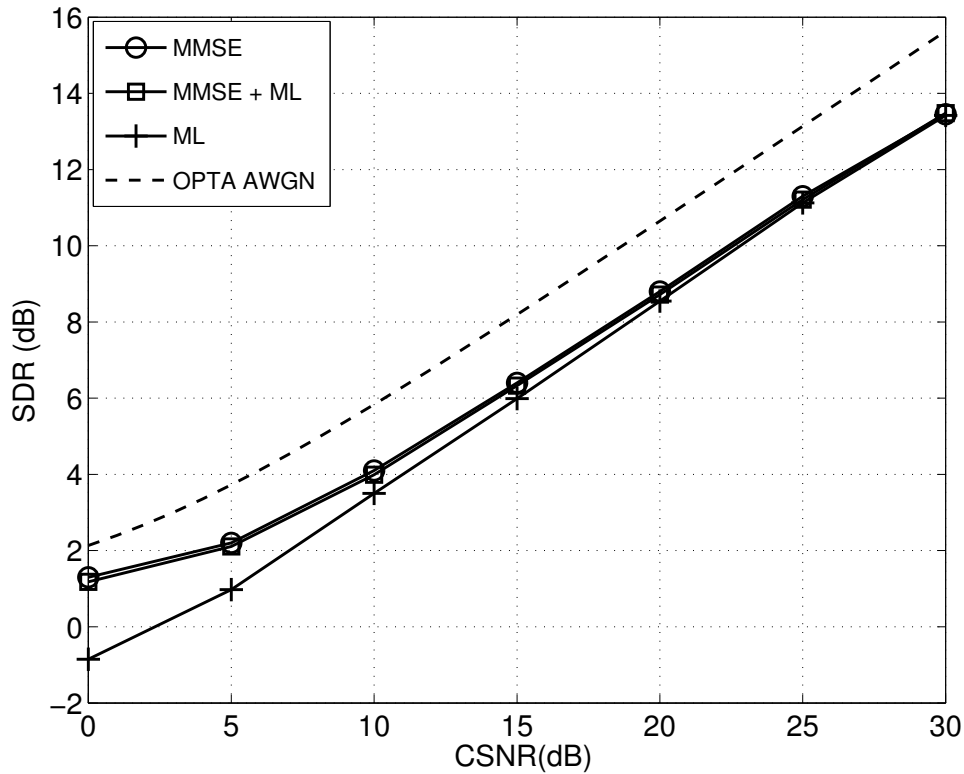


Figure 2.10: Performance of the 2:1 analog JSCC system when using the two-stage decoding for Laplacian sources.

2.3.4 Distortion Analysis and Parameter Optimization

At this point, we certainly know that the set of Archimedes' spirals is the ideal candidate for properly filling a 2-D space when we have source distributions whose most likely symbols are placed close to the plane origin, such as Gaussian and Laplacian sources. However, the specific shape of these spiral-like curves exclusively depends on the distance between two adjacent arms, namely, it is determined by the parameter δ . Logically, as δ is lower, the distance between neighbouring arms is smaller and the spiral becomes denser, reaching the limit point when $\delta \rightarrow 0$, where the 2-D space would be filled continuously. Conversely, as δ becomes larger, the spiral arms get further away and the spiral becomes more sparse.

At first sight, the 2-D source space is filled more efficiently by choosing the δ value as low as possible, minimizing the approximation error when the source points are projected onto the spiral. Unfortunately, as the separation between the spiral arms is made smaller, channel symbols corresponding to different spiral arms are closer on the channel space, so the probability of crossing to a neighbouring arm when they are corrupted by noise (threshold effect), is inevitably increased. Thus, as shown in Figure 2.11, there are two different contributions to the overall distortion of the received symbols:

- The approximation distortion, D_r , induced by the impossibility of finding a continuous representation of a 2-D space by a one-dimensional curve. This contribution is smaller as

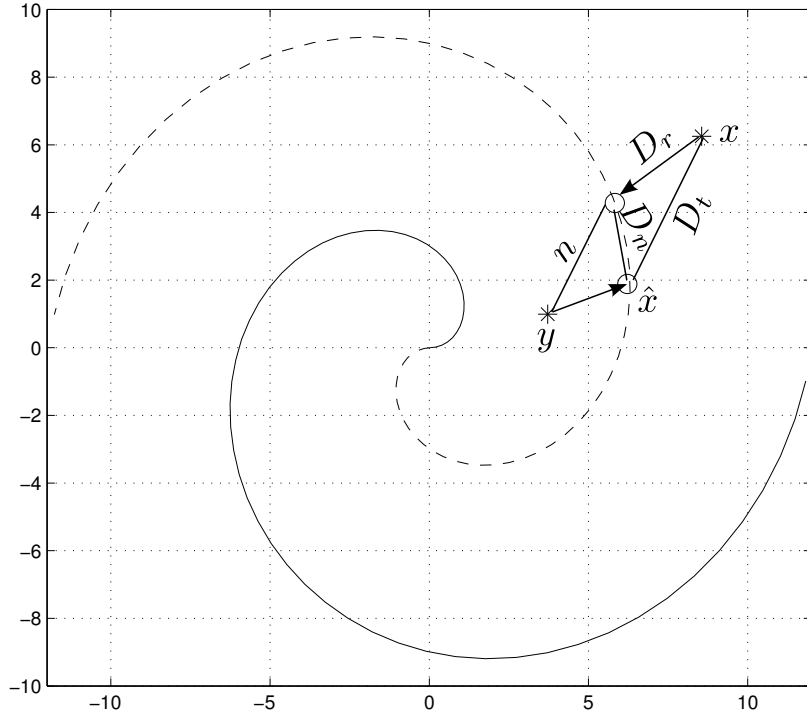


Figure 2.11: Distortion components when using the Archimedes' spiral and ML decoding.

we make the spiral denser.

- The noise distortion, D_n , caused by transmitting over a noisy channel that disturbs the symbols. The channel noise moves the transmitted symbol along the spiral but, if the noise reaches a level beyond a certain threshold value, the symbol can cross to a neighbouring arm. This effect becomes more probable as the spiral is denser.

Both distortion components need to be balanced in order to reduce the overall distortion between source and received symbols. Chung [20] and Hekland [50, 51] stated a minimization problem to find the δ value that minimizes the distortion as follows

$$\delta_{opt} = \arg \min_{\delta} [D_t(\delta)] \quad \text{s.t. } \mathbb{E}[|s|^2] \leq P_T, \quad (2.31)$$

where $D_t(\delta)$ is the overall distortion of the received symbols when using δ at the coding operation and $\mathbb{E}[|s|^2] \leq P_T$ is the power constraint. The distortion per source symbol after decoding the received symbols is defined as

$$D_t(\delta, \sigma_n) = D_r(\delta) + D_n(\delta, \sigma_n) = \frac{\mathbb{E}[\|\mathbf{x} - \hat{\mathbf{x}}\|^2]}{2},$$

where \mathbf{x} and $\hat{\mathbf{x}}$ are the source and decoded vectors, respectively. As long as it is assumed that the spiral is sufficiently dense at the origin, so that the average error on the projection step is approximately equal for the two source samples, the total distortion can be decomposed in two orthogonal components: a radial component (the approximation error), $D_r(\delta)$, and an

angular component (the noise distortion), $D_n(\delta, \sigma_n)$. Notice that this assumption only holds on the high CSNR region. In this situation, the approximation error can be approximated by the quantization error incurred by a standard scalar quantizer, i.e.

$$D_r(\delta) \approx \frac{1}{2} \frac{\delta^2}{12}.$$

$D_r(\delta)$ represents the approximation error per source symbol, so the quantization error must be divided by 2 since we actually project two source symbols.

On the other hand, the noise distortion is more complicated to calculate since it depends on the channel input distribution $f_s(\cdot)$ and the noise variance σ_n^2 . When the noise contribution is small (high CSNR) and employing ML decoding, the received symbols are given by

$$z(s+n) \approx z(s) + z'(s)n,$$

where z defines the points on the spiral in Equation (2.22), and the last term is the noise contribution to the overall distortion. Thus, the average noise distortion can be expressed [51] as

$$\epsilon^2 = \frac{\sigma_n^2}{2} \int_{S_z} \|z'(s)\|^2 f_s(s) ds. \quad (2.32)$$

Remember that the transmitted symbols are given by Equation (2.25) and, therefore, $f_s(\cdot)$ is a function of δ and α parameters. Again, assuming that the spiral is dense enough to cover the entire space (high CSNR) such that the approximation error can be disregarded, and assuming the stretching function as the square of the angle θ , the channel input distribution $f_s(\cdot)$ approaches a zero-mean Laplacian with variance

$$\sigma_s^2 = 2\left(2a \frac{\pi^2}{\delta^2} \sigma_x^2\right),$$

where σ_x^2 is the source variance. The noise distortion can be hence calculated according to Equation (2.32) as

$$D_n(\delta, \sigma_n) = \frac{1}{2} \left(\frac{\sigma_s^2}{P_T} \sigma_n^2 \right) = \frac{8(a\pi^2\sigma_x^2\sigma_n)^2}{2\delta^2 P_T},$$

and the overall distortion is given by

$$D_t(\delta, \sigma_n) = D_r(\delta) + D_n(\delta, \sigma_n) = \frac{\delta^2}{24} + \frac{8(a\pi^2\sigma_x^2\sigma_n)^2}{2\delta^2 P_t}. \quad (2.33)$$

Once the overall distortion is explicitly determined as a function of the parameter δ , we can obtain the optimal δ that minimizes the distortion between the source and the decoded symbols for different σ_n^2 and CSNRs values.

This approach has a series of inherent limitations because we actually calculate an approximation for the total distortion considering a set of assumptions that only hold for high CSNR, ML decoding and $\alpha = 2$. Otherwise, this approximation can be rather inaccurate.

2. Analog Joint Source Channel Coding

CSNR (dB)	0	1	2	3	4	5	6	7	8	9	10	11	12
δ	9.8	8.0	5.6	5.0	4.2	4.0	3.9	3.7	3.6	3.4	3.2	3.1	3.0
γ	0.1	0.11	0.12	0.14	0.16	0.2	0.6	1.2	1.9	2.5	3.0	3.3	3.5
CSNR (dB)	13	14	15	16	17	18	19	20	21	22	23	24	25
δ	2.9	2.7	2.5	2.3	2.2	2.1	2.0	1.8	1.7	1.5	1.4	1.3	1.2
γ	3.9	4.7	5.7	7.1	7.9	8.9	10.0	13.1	15.1	20.5	24.5	29.7	35.3
CSNR (dB)	26	27	28	29	30	31	32	33	34	35	36	37	38
δ	1.1	1.0	0.9	0.8	0.8	0.8	0.7	0.7	0.6	0.6	0.5	0.5	0.4
γ	45	56	74	99	99	99	140	140	209	209	333	333	588

Table 2.1: Optimal values for δ and γ for 2:1 analog JSCC and Gaussian sources.

CSNR (dB)	0	1	2	3	4	5	6	7	8	9	10	11	12
δ	12.0	11.0	10.2	9.5	8.6	6.5	5.8	4.7	4.2	3.7	3.2	3.1	3.0
γ	0.08	0.1	0.14	0.16	0.23	0.5	0.7	1.26	1.7	2.4	3.5	3.8	4.13
CSNR (dB)	13	14	15	16	17	18	19	20	21	22	23	24	25
δ	2.9	2.7	2.5	2.3	2.1	1.9	1.7	1.5	1.5	1.4	1.3	1.2	1.2
γ	4.5	5.4	6.55	8.1	10.2	13.1	17.3	23.6	23.6	28.2	34	41.6	41.6
CSNR (dB)	26	27	28	29	30	31	32	33	34	35	36	37	38
δ	1.1	1.0	0.9	0.8	0.8	0.8	0.7	0.7	0.6	0.6	0.5	0.5	0.4
γ	51.9	66	86.4	116	116	116	164	164	244	244	387	387	674

Table 2.2: Optimal values for δ and γ for 2:1 analog JSCC and Laplacian sources.

In addition, as shown in Section 2.3.2, MMSE decoding involves numerical integration in Equation (2.27), making it cumbersome to analytically derive a closed-form expression for the distortion function with respect to δ . Therefore, the only feasible alternative is to numerically find the tuple (δ, α) that optimizes the system performance by simulation as shown in [55].

We have empirically determined through off-line computer simulations that using $\alpha = 1.3$ provides a good performance over AWGN channels and a wide range of CSNR and δ values. Thus, optimal α values are always around 1.3 for the range of evaluated CSNRs [0-40 dB] and small variations on such a value slightly impact on the overall system performance. For this reason, we have decided to select $\alpha = 1.3$, and hence the optimization procedure can be restricted to find the optimal value for δ parameter, whose influence on the performance is more critical. The second row of Tables (2.1) and (2.2) corresponds to the best values of the

parameter δ for Gaussian and Laplacian sources, respectively. These values were found via computer simulations for a 2:1 compression rate, $\alpha = 1.3$ and for a range of CSNR values between 0 and 40 dB. Concretely, optimum δ values were determined by exhaustive search over the range $0 < \delta < 12$ using a 0.1 step-size.

Another important issue regarding the optimization of the analog JSCC scheme is the normalization of the channel symbols. The normalization factor, γ , actually corresponds to the mean square value of the symbols at the output of the analog encoder, i.e. $\gamma = \mathbb{E}[|\tilde{s}|^2]$. However, the statistical description of \tilde{s} is extremely difficult to characterize and strongly depends on the source distribution and the encoder parameter δ . We can overcome this limitation if the mean square value of \tilde{s} for a given source distribution and a set of δ values is also determined off-line, via computer simulations. The third row of Tables (2.1) and (2.2) shows the values of γ obtained for Gaussian and Laplacian sources, respectively, and for the corresponding δ values resulting from the aforementioned encoding optimization.

2.4 Conclusions

In this chapter, we have reviewed the transmission of discrete-time continuous-amplitude samples over AWGN channels using analog JSCC. The use of this strategy allows to drastically reduce the complexity and the delay of the capacity-achieving digital SSCC systems by optimizing the source and channel encoders jointly in one single step. In addition, analog JSCC has been recently shown to approach the theoretical limits when employing for bandwidth compression.

We have described the different components of the considered analog JSCC system along this chapter. On one hand, the encoding operation at the transmitter consists in a non-linear continuous mapping based on the use of space-filling curves (Shannon-Kotel'nikov mappings), namely we focus on the doubly intertwined Archimedes' spiral for the case of a 2:1 compression. On the other hand, the decoding operation is carried out at the receiver in order to recover the transmitted source samples corrupted by channel noise. After evaluating the decoding methods considered for analog JSCC until now in the literature, we have designed an alternative two-stage receiver structure based on the splitting between the detection and decoding operations. This strategy has been shown to achieve a near-optimal performance while preserving low complexity. For that reason, the proposed two-stage decoding scheme constitutes an important contribution to the design of efficient analog JSCC systems and also represents a fundamental strategy to preserve low complexity and delay when the decoding operation is implemented on more complex transmission models such as, for example, MIMO schemes.

The performance of the analog communication systems is directly related to the distortion

2. Analog Joint Source Channel Coding

between the source and decoded symbols. As seen, such a distortion is caused by the compression operation and the channel noise and it can be mathematically determined under certain assumptions. However, we also show that the overall performance of the analog JSCC system can be improved if such assumptions are disregarded and the optimal values for the encoder parameters are calculated by computer simulations.

Chapter 3

Comparison between Analog JSCC and Digital Systems

In previous chapters, analog Joint Source Channel Coding (JSCC) has been presented as an appealing alternative to conventional digital systems under certain circumstances such as high transmission rate requirements, delay/complexity constraints (real time systems) or time-varying environments (wireless channels). However, if we want to consider analog JSCC as a real alternative in the aforementioned scenarios, it is essential to compare the performance of this scheme with that of a purely digital one at the same transmission rate with similar complexity. We follow the traditional approach for the design of digital systems when the source information to be transmitted are analog data: quantization of the analog source, entropy coding devoted to remove the redundant information and channel coding to protect the binary symbols against the channel noise. Thereby, according to the complexity, delay and transmission rate restrictions, we design an optimal low complexity digital system where each step is individually optimized following the separation principle stated by Shannon. Finally, the performance of both approaches are compared to each other and with respect to the optimal bounds for the transmission of analog sources –modeled as Gaussian or Laplacian distributions– over an Additive White Gaussian Noise (AWGN) channel.

3.1 Digital BICM Systems

Trellis Coded Modulation (TCM) [127] and Bit Interleaved Coded Modulation (BICM) [16, 141] are the two most prominent examples of digital transmission schemes using coded modulation. TCM combines encoding and modulation in a single operation in such a manner that the coded bits are mapped into a single constellation with the aim of maximizing the Euclidean distance between any two different signals of the constellation. On the other hand, the design of BICM systems is based on the individual optimization of an encoder and a

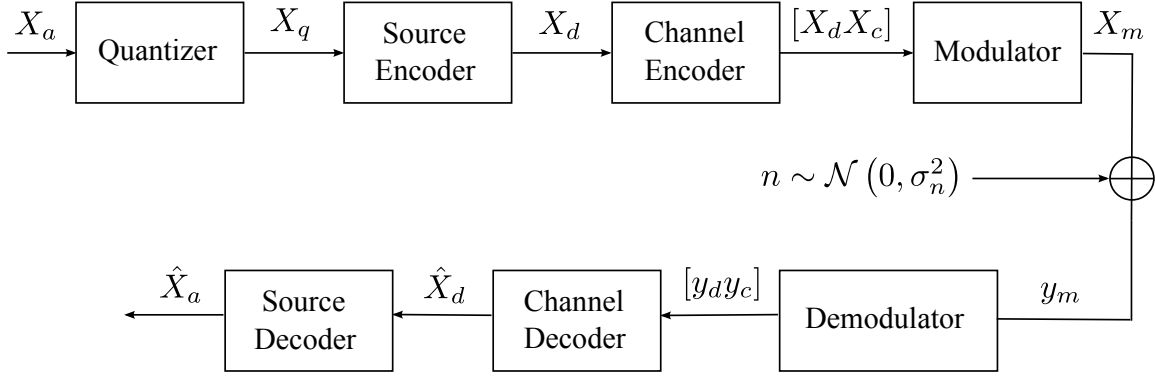


Figure 3.1: Block diagram of Bit Interleaved Coded Modulation (BICM) systems over AWGN channels.

modulator, separated by a bit interleaver. Both models are capable of approaching the Shannon capacity limit over an AWGN channel. However, in this thesis, we have chosen BICM as the representative capacity-approaching digital transmission scheme because of its simplicity and lower complexity.

Figure 3.1 shows the block diagram of the BICM digital system that we will use to compare with the analog system described in Chapter 2. We assume a discrete-time source that produces Gaussian or Laplacian independent and identically distributed (i.i.d.) real-valued symbols X_a . These continuous symbols are first mapped to a discrete set of values using an optimum N -level scalar quantizer, $Q^{(N)}$. Both the quantization levels and the partition regions can be obtained using the well-known Lloyd-Max algorithm [75, 81]. Although better performance could be obtained if Vector Quantization (VQ) is considered, we discarded this possibility to preserve the overall quantization complexity at a low level.

Next, the discrete-time discrete-amplitude symbols at the quantizer output are converted into a binary representation using a suitable source encoder. Again, among the many existing source encoding methods, we decided to use Huffman encoding because it is a simple algorithm that approaches the source entropy. The input alphabet to the Huffman encoder is made up of the Q -levels of the scalar quantizer, i.e. no grouping is performed prior to the encoding. The average length of the Huffman codewords used to represent each source sample will be denoted by L_m .

The output bit sequence is encoded with a capacity-approaching channel encoder prior to transmission. The rate of the channel encoder will be denoted by R_c and, as explained later, its value must be selected to ensure that the transmission rate of the digital system is equal to the rate achieved when employing the analog JSCC scheme. Notice that this value will also depend on the average length of the source codewords and on the number of bits per transmitted symbol used for signaling. Due to their low encoding and decoding complexity, we decided to use Irregular Repeat Accumulate (IRA) codes [60]. In order to approach the channel capacity, IRA codes have to be properly optimized for each specific rate, R_c . In our case, the optimization operation was carried out by EXtrinsic Information Transfer (EXIT) analysis [123].

Finally, the channel coded bits are modulated using a real-valued M -Pulse Amplitude Modulation (PAM) constellation. Notice that an interleaver between the channel encoder and the modulator is not strictly necessary since we are transmitting over an AWGN channel. A one-dimensional PAM constellation has been chosen to keep the same signaling as the analog system in Chapter 2 where real-valued analog coded symbols are transmitted. The constellation size M limits the maximum attainable data rate over the channel. We chose the value $M = 256$ which allows the transmission of a maximum of 8 bits per channel use, a transmission rate high enough for the comparison with the analog system. Higher values of M could be used but they yield to extremely complex PAM constellations that are not feasible in practice.

At the receiver, an optimum detector calculates the Log-Likelihood Ratio (LLR) values of the transmitted bits and passes them to the sum-product IRA decoding algorithm. After a maximum number of decoding iterations, the resulting bits are hard-decoded and dequantized to the corresponding levels.

In the following sections we will explain in detail the main components of the BICM digital system presented in this section: scalar quantizer, source encoder, channel encoder and M -PAM modulator.

3.1.1 Scalar Quantization

An analog signal is usually represented by a continuous function, $x(t)$, which describes the behavior of a physical phenomenon on the domain t , usually the time domain. The function domain and the amplitude range of $x(t)$ is continuous and, therefore, the information carried by an analog signal is actually infinite. Nevertheless, the digital systems only can convey a certain finite amount of binary information. Thus, we inevitably need to discretize both the domain and range of the function $x(t)$ in order to obtain a discrete-time discrete-amplitude version of the analog signal as input to the digital system.

A discrete-time version $x(n)$ is obtained from the continuous original signal by a sampling operation. As mentioned in Chapter 2, assuming Nyquist sampling and an ideal Nyquist channel, it is possible to represent an analog signal by a finite number of discrete samples, in such a manner that the original signal can be perfectly reconstructed from the discrete version. Thus, the sampling operation does not entail any sort of error or distortion. Hence, we omit this step and directly focus on the transmission of continuous-amplitude samples.

Prior to generating the digital representation of the analog signal, the amplitude range must be also discretized by the quantization operation. In general, a quantizer maps an infinite set of input amplitudes to a finite subset of output values suitable to be digitalized. Unfortunately, the quantization operation removes certain amount of relevant information in the input signal, making its recovering impossible. The distortion between the original and reconstructed signals is referred to as quantization error.

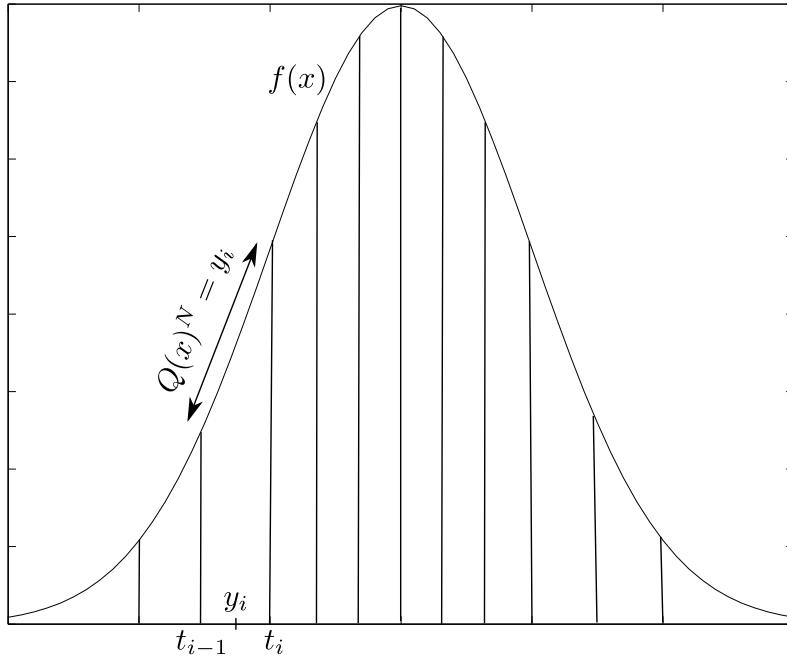


Figure 3.2: Example of non uniform scalar quantization of a Gaussian source.

If the source generates a sequence of continuous samples, $\mathbf{x} = \{x_1, x_2, \dots, x_i\}$, the quantizer must produce a sequence with the corresponding discrete values, $\mathbf{y} = \{y_1, y_2, \dots, y_i\}$. There exists two main approaches to perform the corresponding mapping operation. Firstly, each input sample is independently mapped to one output value, i.e., $Q : X \rightarrow Y$. In this case, Q is called scalar quantizer since one single sample of the source signal is quantized at each time. The second alternative is to consider a N -vector quantizer [46, 74], where a vector of N input samples is mapped to an output vector of M components, i.e., $Q : X^N \rightarrow Y^M$, $N > M$. Thus, a vector quantizer encodes N -component vectors from a continuous multidimensional space into a finite set of representative M -component vectors (codebooks) from a discrete subspace of lower dimension.

Remember that we are interested in designing an optimal low complexity digital system in order to fairly compare it to the analog JSCC scheme proposed in Chapter 2. However, the complexity of the optimal vector quantizer significantly increases as N becomes larger, since a discretization of the N -dimensional space –defined by the probability density function (pdf) of the source– is required. Hence, its complexity is much higher than that of the scalar quantizer even for small values of N . According to complexity/delay constraints, we decided to rule out vector quantization and focus on the scalar case. Also, this decision is supported by the fact that vector quantization improves only slightly -in term of distortion- the performance of the scalar quantization for small values of N .

Let Q^N be an N -level scalar quantizer that defines a partition of the amplitude range of the source signal. Thus, the range of $x(n)$ is divided in N disjoint intervals (or bins), $T_i = (t_{i-1}, t_i]$, $i = 1, \dots, N$, each one represented by a single value, y_i , $i = 1, \dots, N$. Hence

Q^N maps the set of all input amplitudes falling into the same interval i to the same output value, y_i , which is the representative point of the interval, i.e.

$$Q^N(x) = y_i, \quad t_{i-1} < x \leq t_i. \quad (3.1)$$

In this case, the quantization error is determined by the the distortion between the original and quantized signals, measured commonly according to the Mean Square Error (MSE) metric, i.e

$$D(Q^N) = \mathbb{E} \left[|x - Q^N(x)|^2 \right] = \sum_{i=1}^N \int_{t_{i-1}}^{t_i} |x - y_i|^2 p(x) dx, \quad (3.2)$$

where $p(x)$ is the pdf of the source signal, $x(n)$.

At the receiver, a similar mapping has to be applied to reconstruct a discrete version of the original signal. Thus, each received sample z is remapped to the representative point of the interval in which the sample z fall into

$$\hat{x} = Q^N(z) = y_i, \quad t_{i-1} < z \leq t_i. \quad (3.3)$$

Logically, assuming error-free transmission, the distortion between the recovered and original signals will be equal to the quantization error. The quantization error is directly related to the interval sizes, $l_i = (t_i - t_{i-1})$, $i = 1, \dots, N$, and the probability distribution of the source, $p(x)$. If all bins have the same size, we have a simple uniform scalar quantizer. Otherwise, the quantizer is called non uniform, and the interval limits t_i and the representative points y_i for each interval must be determined in order to minimize the distortion between the original and quantized signals. For non uniform distributions, such as Gaussian and Laplacian sources, using an uniform scalar quantizer is not recommended since the quantization error is much lower, for the same N value, if we choose an optimal non uniform quantizer. Notice that a quantizer is optimal in the sense that no other one results in a lower distortion assuming the same number of levels.

Lloyd [75] and Max [81] independently proposed an algorithm, known in the literature as the LLOYD-Max's algorithm, to compute optimum scalar quantizers for a certain source distribution using MSE as distortion measure. Given a certain number of levels N , the LLOYD-Max's algorithm calculates the intervals and representative points of the quantizer that minimize the quantization error using the statistical properties of the input signal. LLOYD and Max proved that the optimum interval limits are the midpoints of the interval between two neighbouring representation points and, at the same time, the representation points are the centroid of the probability density function in the corresponding interval. Using these two simple conditions, an iterative algorithm can be formulated to jointly determine the interval limits and the representative points.

This algorithm is widely used in practice because it can be easily implemented. However, it usually converges slowly and, due to limitations in numerical precision, it may not converge.

Therefore, in real applications, Lloyd-Max's algorithm is interrupted once the partition is good enough. The convergence of this iterative algorithm has been widely studied in the literature [31, 86, 138] and, in general, it is closely related to the initial partition of the signal range so it is fundamental to select the initial intervals carefully.

We will focus on the quantization of Gaussian and Laplacian sources due to the importance of these distributions in real applications, such as image compression or speech transmission, beyond their theoretical significance. Max calculated the optimum quantizers for a Gaussian source with unit standard deviation and zero mean for different number of levels in [81]. In addition, the expected average distortion and the entropy of the quantized source is computed. For Laplacian sources, the optimum scalar quantizer for any number of levels can be easily obtained running the Lloyd-Max algorithm, and the distortion and the entropy can be calculated from Equations (3.2) and (2.1), respectively. Notice that the entropy equation must be particularized for discrete sources.

Logically, as the number of levels becomes larger, the distortion between the original and quantized signal lowers, since the input samples are more tightly represented by the representative point of the corresponding interval. Conversely, the entropy of the quantized source increases since a higher number of bits are required to represent the information at the quantizer output. Thus, there is a tradeoff between the resulting signal quality and the amount of data needed to represent each sample.

3.1.2 Source Coding

After the quantization operation, the analog source signal is represented by a finite sequence of discrete symbols. The next step in a digital system consists of obtaining the most efficient digital representation of such symbols. This task is carried out by the source encoder, which defines a reversible mapping of sequences of discrete source symbols into sequences of codewords. Source coding is also referred to as noiseless coding since it does not involve loss of information or entropy coding since, if the original signal contains certain statistical properties or dependencies, they can be exploited for data compression.

The source message at the encoder input, $s^{(L)} = \{s_0, \dots, s_{L-1}\}$, comprises L source symbols that belong to a discrete alphabet $A = \{a_0, \dots, a_{M-1}\}$. The encoder output is represented by a finite set of codewords, which are actually a sequence of binary symbols (bits) of the alphabet $B = \{0, 1\}$. Thus, the lossless coding transforms the source message $s^{(L)}$ into a sequence $b^{(K)} = \{b_0, \dots, b_{K-1}\}$ of K bits.

In practical coding algorithms, the input message $s^{(L)}$ is often split into blocks $s^{(N)} = \{s_n, \dots, s_{n+N-1}\}$ of N symbols, with $1 \leq N \leq L$, and a codeword $b^{(l)}(s^{(N)}) = \{b_0, \dots, b_{l-1}\}$ of l bits is assigned to each of these blocks $s^{(N)}$. The length l of a codeword $b^{(l)}(s^{(N)})$ depends on the symbol block $s^{(N)}$. The codeword sequence $b^{(K)}$ that represents the message $s^{(L)}$ is

obtained by concatenating the codewords $b^{(l)}(s^{(N)})$ associated to each symbol block $s^{(N)}$. Thus, a source encoder can be described by the following operation

$$b^{(l)} = \gamma(s^{(N)}),$$

which specifies a mapping from the set of finite length symbol blocks to the set of finite length binary codewords. The decoder mapping

$$s^{(N)} = \gamma^{-1}(b^{(l)}) = \gamma^{-1}(\gamma(s^{(N)}))$$

is the inverse of the encoder mapping γ .

Depending on whether the number N of symbols in the block $s^{(N)}$ and the number l of bits for the associated codewords are fixed or variable, the following types of encoders can be defined:

- Fixed-to-fixed coding: a fixed number of symbols, N , is mapped to fixed-length codewords of size l .
- Fixed-to-variable coding: a fixed number of symbols is mapped to variable-length codewords. A well-known method for designing fixed-to-variable mappings is the Huffman algorithm.
- Variable-to-fixed coding: a variable number of symbols is mapped to fixed-length codewords. Tunstall codes [103, 126] are a representative example of this type of source coding.
- Variable-to-variable coding: a variable number of symbols is mapped to variable-length codewords. Arithmetic coding is a typical example for this type of lossless source coding.

In this thesis, we will focus on the source encoders that assign a variable-length codeword to each symbol $s_i, i = 1, \dots, L - 1$ of an input message $s^{(L)}$. The symbols s_i obtained after the quantization operation are assumed to be characterized by the random variable S , which takes values of a finite symbol alphabet $A = \{a_0, \dots, a_{M-1}\}$ with a probability mass function $p(a_i) = P(S = a_i)$. The source code associates each symbol a_i of the alphabet A to a binary codeword $b_i = \{b_0^i, \dots, b_{l(a_i)-1}^i\}$ of length $l(a_i) \geq 1$. According to this statement, our purpose is to build a lossless source code that minimizes the average codeword length given by

$$L_m(S) = \mathbb{E}[l(S)] = \sum_{i=0}^{M-1} p(a_i)l(a_i), \quad (3.4)$$

while ensuring that each message $s^{(L)}$ can be uniquely decodable from its coded representation $b^{(K)}$. A code is said to be uniquely decodable if and only if each valid coded representation $b^{(K)}$

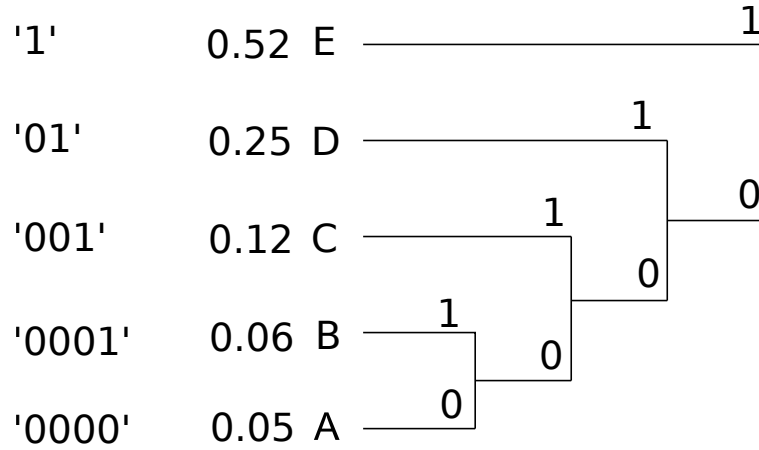


Figure 3.3: Example of a Huffman code for an input alphabet $S = \{A, B, C, D, E\}$ with probability mass function $p(S) = \{0.05, 0.06, 0.12, 0.25, 0.52\}$. The average length of the code is 1.82 and the entropy of the source is 1.8173.

of a finite number K of bits can be produced by only one possible sequence of source symbols $s^{(L)}$. A necessary condition for uniquely decodable codes is given by the Kraft inequality [68]

$$\sum_{i=0}^{M-1} 2^{-l(a_i)} \leq 1. \quad (3.5)$$

A code will be also instantaneously decodable if each output symbol can be rightly decoded after the bits of its corresponding codeword are received. Using the Kraft inequality and the expression for the average codeword length L_m given by Equation (3.4), it is straightforward to prove that

$$L_m \geq H(S), \quad (3.6)$$

where $H(S)$ is the entropy of the discrete source S . In addition, the redundancy of the code is given by the difference between the source entropy and the average length of such a code.

To design an optimal uniquely decodable code, i.e. a code that achieves the minimum average codeword length, it is necessary to consider the prefix codes. A code is said to be a prefix code if no codeword for an alphabet symbol represents the codeword or a prefix of the codeword for any other alphabet symbol. An optimal prefix code must have the following properties:

- For any symbol pair $a_i, a_j \in A$ with $p(a_i) > p(a_j)$, the associated codeword lengths satisfy $l(a_i) \leq l(a_j)$.
- There are always two codewords that have the maximum codeword length and differ only in the final bit.

Logically, both conditions are simultaneously fulfilled if the two codewords with the maximum length that differ only in the final bit are assigned to the two symbols a_i and a_j

with the smallest probabilities. Using this condition, an iterative algorithm was developed and shown to be optimal by Huffman in [56]. The Huffman algorithm is based on the construction of a binary code tree for a given alphabet A with a probability mass function $p(A)$ and can be summarized in the following steps:

- Select the two symbols a_i and a_j with the smallest probabilities and create a parent node for the nodes that represent these two symbols in the binary code tree.
- Replace the symbols a_i and a_j by a new symbol with an associated probability given by $p(a_i) + p(a_j)$.
- If more than one symbol remains, repeat the two previous steps.
- Convert the resulting binary code tree into a prefix code.

An example of a Huffman code built using this procedure is shown in Figure 3.3. It is known that scalar Huffman codes achieve the smallest average codeword length among all uniquely decodable codes that assign a separate codeword to each symbol of an alphabet. However, if the source is correlated, i.e., there are strong dependencies between the symbols, they can be very inefficient. In this case, Huffman codes can be extended to assign a codeword to a block of two or more successive symbols. They are referred to as block Huffman codes or vector Huffman codes. In this thesis, we employ optimal scalar Huffman codes for the source coding operation since the information transmitted by the digital system is assumed to be uncorrelated.

3.1.3 Channel Coding

The aim of channel coding is to achieve error-free transmission (or with a small probability of error) by protecting the source messages against the channel noise. On the transmitter side, a certain amount of redundancy is cleverly added to the bitstream generated by the source encoder so that the receiver can detect and correct the transmission errors. This operation hence guarantees a high reliability of the transmitted information. Furthermore, it is possible to cancel out the effect of the interference from external sources which could not be managed by simply increasing the transmit power.

In Chapter 2, we introduced the channel coding theorem stated by Shannon in 1948 [108]. According to this theorem, each channel can be numerically described by its capacity which determines the highest transmission rate at which the information can be sent over such a channel for achieving an error-free transmission. Thus, the channel properties do not restrict the quality of the transmission but only the throughput. By using a proper coding scheme, the channel capacity can be asymptotically achieved assuming infinite block length (large blocks in practice).

Channel coding can be formally defined as a mapping that converts an input message into a sequence of codewords that belongs to the channel alphabet. Notice that the message at the channel encoder input corresponds to the bitstream generated by the source encoder from the source information after quantization and compression operations. Depending on the way of generating the channel codewords from the input message, there are two main classes of channel codes:

- *Block codes* segment the source bitstream into blocks of K bits. Each block is then mapped into a codeword of N bits ($N > K$) on the vector subspace generated by code. The extra $N - K$ check bits provide the required error protection.
- *Convolutional Codes* are a particular type of codes with memory where a message is not coded block by block, but it is continuously processed by the encoder to generate the associated codeword. They use a memory register for generating the codeword at each time instant as function of the source message and the register state. The name of convolutional codes come from the fact that the output bitstreams are essentially the convolution of the input bitstream and the code coefficients.

Both types of codes can closely approach the theoretical limits given by the channel capacity as long as they are optimally designed but, as already mentioned in Section 3.1, in this chapter we will focus on block codes because of their larger simplicity and lower complexity.

A (N, K) block code defines a mapping between each K -bit block b_j of the source message, $b = \{b_1 b_2 \dots b_M\}$, and its corresponding N -length codeword, $c_j, j = 1, \dots, 2^K$. The number of possible codewords is 2^N whereas the number of different input blocks is given by $2^K, K < N$, so the number of useful codewords is also 2^K . That is, the set of all valid codewords forms a vector subspace inside the N -dimensional codeword space. This mapping is required to be

- unique and injective: two different information blocks are mapped to two different codewords;
- time-invariant: the assignment scheme does not change over a period of time;
- memoryless: each information block only influences one codeword, and each codeword is influenced by only one information block.

A linear block code can be precisely defined by a particular $K \times N$ matrix, called the generator matrix of the code, G . The codeword associated to an input message b_i is straightforwardly obtained using the generator matrix as $c_j = G^T b_j$. In addition, given that the columns of the matrix G generate a vector subspace of the N -dimensional space defined by the set of all possible codewords, there must exist other $(N - K) \times N$ matrix H whose right null space is equivalent to the subspace generated by the set of valid codewords. In other words,

for any codeword c_j , we have $Hc_j = 0$. Such matrix H is commonly known as the parity check matrix of the code and satisfies the condition $HG^T = 0$.

If the message b_i is placed in the first K bits of the associated codeword, G will have the form $[I|P]$ and essentially $N - K$ redundant bits are added to the message. These redundant bits are referred to as the parity check bits and the coding scheme is called systematic. Systematic codes are more convenient since after correcting the channel errors at the decoder, we can extract the source message directly from the decoded codeword. For non-systematic coding, we need an extra step to translate the corrected codeword to the actual message.

Assuming that the source encoder generates messages at an average bit rate of n_s bits per second and the channel encoder maps each K -bit message into a N -bit codeword, then the (N, K) code rate will be

$$n_c = \frac{N}{K}n_s = \frac{1}{R_c}n_s. \quad (3.7)$$

At the receiver, the channel decoder is the device responsible for the detection of bit errors on the received messages from the channel and (if possible) correcting those errors. There are two basic schemes of error-control coding which depend on the requirements of the tolerable end-to-end delay and whether a feedback channel is available:

- Automatic-Repeat-Request (ARQ): If the channel decoder performs error detection, errors can be detected and a feedback channel from the channel decoder to the channel encoder can be used to control the retransmission of the codeword until it is received without detectable errors.
- Forward Error Correction (FEC): If the channel decoder performs error correction then errors are not only detected but the incorrect bits can be also identified and corrected.

The main advantage of ARQ techniques is that error detection needs less redundancy. However, erroneous messages need to be transmitted repeatedly until they are received without errors and, therefore, the delay can become large. Thus, the throughput with the ARQ strategy basically depends on the quality of the channel. Since the analog JSCC strategy ensures a low delay transmission, we focus on FEC techniques using a particular class of block code: Irregular Repeat-Accumulate (IRA) codes.

3.1.3.1 A Historical Perspective

The beginning of channel coding theory dates back to 1948, when Shannon formulated his famous channel coding theorem [108]. From that moment, a long journey with the aim of designing capacity-achieving codes started and continues to the present. Shortly after Shannon's work, Richard Hamming and Marcel Golay independently proposed the first practical codes, known in the literature as Hamming codes [45, 48].

In 1955, convolutional codes were first introduced by Elias [25] as an alternative to block codes. Later, Wozencraft and Reiffen [137], Fano [27] and Massey [80] stated different sequential decoding algorithms for convolutional codes. Finally, in 1967, Viterbi [132] managed to design an efficient decoding algorithm to obtain a Maximum Likelihood (ML) estimate of the transmitted sequence. Such algorithm is relatively easy to implement for convolutional codes with short constraint length.

Other coding schemes, such as BCH (Bose-Chaudhuri-Hocquenghem) or Reed-Solomon, were also proposed but none of them were able to approach the theoretical limit with a reasonable encoding and decoding complexity. In 1993, Berrou et al. presented the Turbo codes [13] that completely revolutionized the coding theory. The basic principle of these codes is the iterative decoding of concatenated components that exchange information (called extrinsic information) based on soft decisions about the transmitted bits. This idea is referred to as the turbo principle.

The generalization of this idea led in 1995 to the rediscovery almost simultaneously of the Low Density Parity Check (LDPC) codes by Mackay [77, 78] and Spielman [111, 115]. These codes were first proposed in the 60s by Gallager [40] but both its coding scheme and its A Posteriori Probability (APP) decoding algorithm were largely forgotten for more than 30 years because they were too complex for the technology of that time.

LDPC codes are linear block codes with a sparse parity check matrix that outperform Turbo codes with a smaller decoding complexity. They can be represented by a Tanner graph or factor graph [118] where the relations between the variables and check nodes are graphically shown. The decoding operation is based on the Belief Propagation (BP) algorithm - or also Sum-Product Algorithm (SPA)- which is an iterative algorithm that efficiently computes the marginal distribution of a single variable from the joint distribution of multiple variables.

However, due to the fact that the generator matrix of general LDPC codes is not sparse, their encoding complexity can be rather high. Low Density Generator Matrix (LDGM) codes are a particular case of LDPC codes whose generator matrix is sparse, making a lower encoding complexity possible. However, except for the case of very high rate codes, they have a non-zero error probability that is independent of the code block length. More recently, IRA codes, consisting of the serial concatenation of a LDGM code and an accumulator, have been proposed [60, 123]. IRA codes are able to get close to the performance of LDPC codes with an encoding complexity similar to that of LDGM codes.

3.1.3.2 Irregular Repeat-Accumulate Codes

Repeat Accumulate (RA) codes consist of the serial concatenation of a repetition code, a bit interleaver and a set of parity checks (i.e. an LDGM code), and an accumulator. RA codes are usually systematic, so the parity accumulated bits are appended to the uncoded bits to obtain

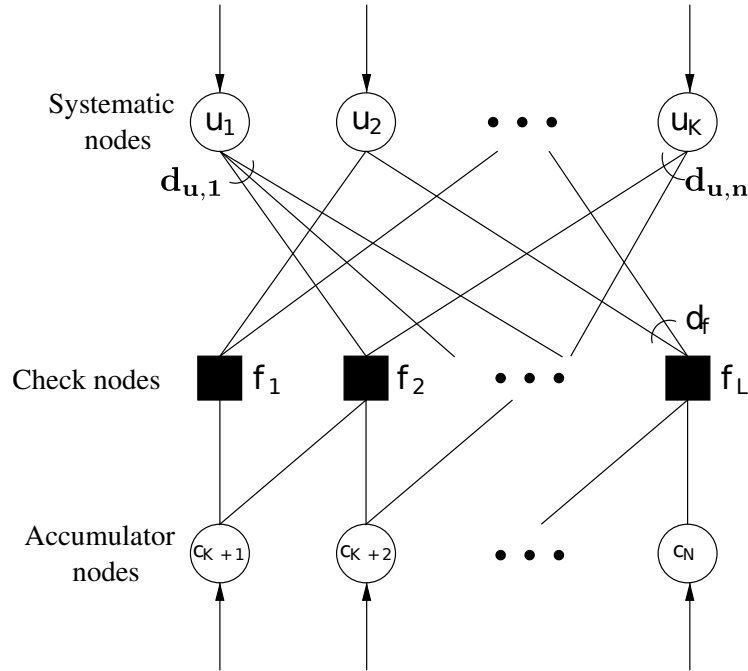


Figure 3.4: Example of factor graph for a systematic IRA code.

the final coded sequence. As occurs with LDPC and LDGM codes, we can use a factor graph [118] to represent RA codes and apply the BP algorithm to decode them. In case the graph is irregular, the code is usually named Irregular Repeat-Accumulate (IRA) code.

Figure 3.4 shows the factor graph for a (N, K) systematic IRA code with a degree profile given by the parameters $(d_{u,1}, \dots, d_{u,n}, d_f)$, where $d_{u,i} \geq 0$, $\sum_i d_{u,i} = 1$ and d_f is a positive integer. We can distinguish three kind of nodes in the factor graph: K systematic or information nodes, $N - K$ accumulator or parity nodes and L check nodes. Each check node is exactly connected to d_f information nodes whereas $d_{u,i}$ specifies the fraction of information nodes connected to i check nodes. The connection pattern is specifically determined by an interleaver. In general, the relation between check and parity nodes follows a zig-zag pattern as can be observed in Figure 3.4.

The particular structure of this type of linear codes simplifies the encoding operation since the modulo-2 sum of the values p_i corresponding to the parity nodes connected to a specific check node and such a node must be zero. Applying this condition, $N - K$ parity bits can be easily obtained by the recursive equation

$$\begin{aligned} c_{K+1} &= p_1 \\ c_{K+i} &= c_{K+i-1} + p_i, \end{aligned}$$

for $i = 2, \dots, N - K$. We can build the codeword simply by appending the obtained parity bits to the information bits, i.e. $c = [u_1 \dots u_K; c_{K+1} \dots c_{N-K}]$.

The decoding operation for IRA codes is carried out by using the SPA, which is an iterative procedure based on message passing between the different nodes of the factor graph. For codes

represented by factor graphs, the SPA can be interpreted as a particularization of the powerful BP algorithm proposed by Pearl [90] to efficiently compute the marginal distribution out of the joint distribution of multiple variables. Since the unknown variables are binary, the actual messages are initially calculated from the Log-Likelihood Ratio (LLR) of each coded bit c_i , defined as

$$L_{ch,i} = \log \frac{p(x|c_i = 1)}{p(x|c_i = 0)} \quad (3.8)$$

and then passed to the decoder. Next, an iterative decoding is started where the check and variables nodes exchange information (soft decisions) until they reach the stopping criterion.

In a similar way to LDPC codes, this class of codes also needs to be optimized in order to approach the theoretical limits. In this context, the optimization of IRA codes implies to obtain the degree profile that achieves the best performance for a particular channel. Two basic techniques have been proposed for the design of LDPC and IRA codes: Density Evolution (DE) [96] and EXtrinsic Information Transfer (EXIT) charts [122].

Density Evolution (DE) is an optimization method based on studying the variation of the pdf of the messages between variable and check nodes in the factor graph of a code. EXIT charts are based on tracking the extrinsic information exchanged between the components of an iterative decoder. Instead of tracking the probability density function (pdf) of the messages, a representative value is used to simplify the problem and effectively capture the most relevant information about the decoding process: the bitwise mutual information between the messages and the codeword [121]. Thus, EXIT charts provide a graphical representation of the code convergence.

3.2 Design of Digital BICM Systems

In the 2:1 analog JSCC transmission system described in Chapter 2, two source samples are encoded into one channel symbol and transmitted in each channel use. Logically, the digital system employed to perform the comparison with the analog scheme must be designed to transmit the same amount of information per channel use.

In the digital system, each source sample is quantized with an N -level scalar quantizer and represented by a codeword whose average length is L_m . Thus, $2L_m$ bits are used to represent the two source samples at the output of the source encoder. The digital system is designed in such a way that the information rate is less than the channel capacity so that no errors occur during the transmission. Thus, the Signal-to-Distortion Ratio (SDR) is just determined by the quantization error that is directly related to the number of quantization levels, N .

When transmitting over an AWGN channel, the Channel Signal-to-Noise Ratio (CSNR) should be high enough in order to ensure that the channel capacity is higher than the information rate. Two different expressions of the AWGN channel capacity will be conveniently used:

the unconstrained channel capacity that assumes Gaussian input symbols and the constrained channel capacity that takes into account that the channel symbols are modulated with a PAM constellation. Thus, we have to calculate the minimum CSNR necessary to achieve an error-free transmission according to the unconstrained and constrained capacity limits, which are well-known for the AWGN channel. Notice that the minimum CSNR necessary to achieve the constrained channel capacity is slightly higher than that of the unconstrained one because we use a PAM constellation whereas the mutual information over an AWGN channel is actually maximized when the input is Gaussian.

If the digital system uses a $M = 256$ PAM constellation, 8 bits per channel use can be employed to transmit the two source symbols. Hence, if $2L_m < 8$, an error-free transmission of the uncoded bits over an AWGN channel is possible as long as the CSNR is high enough. Moreover, there is room enough to introduce redundant channel bits that are essential to achieve the channel capacity. In order to preserve the same number of channel uses as in the analog JSCC scheme, the information rate must satisfy the constraint $2L_m/R_c = 8$. According to this condition, the design of the digital system can be summarized in the following steps:

- We select the number of levels for the scalar quantizer and calculate the average length of the associated Huffman code, L_m .
- From L_m we can straightforwardly determine the channel code rate as $R_c = L_m/4$. Next, a channel encoder, with rate R_c , capable of approaching the capacity of an AWGN channel should be designed. Such a channel encoder can be optimized using EXIT analysis. In particular, we have optimized IRA codes for certain rates and obtained their threshold values, i.e., the minimum CSNR necessary for the IRA codes to correct all channel errors. These threshold values are slightly higher than those obtained from the channel capacity because practical IRA codes always incur in some performance losses.
- We can finally determine the expected SDR for the corresponding CSNR value at which the IRA code designed in the previous step is able to correct all transmission errors. The SDR values depend on the distortion between the source and decoded signals, which is given by the quantization error or, equivalently, by the number of levels employed at the scalar quantizer.

This design procedure implies that in the digital transmission system a different channel encoder should be used each time the target SDR is changed. For example, if we need to attain a higher SDR (lower distortion), the number of quantization levels N must be increased in order to minimize the distortion (error quantization) and, as consequence, the channel code rate R_c will be larger and, logically, the CSNR that guarantees an error-free transmission will be also higher.

3. Comparison between Analog JSCC and Digital Systems

Q	SDR (dB)	Entropy	L_m	Code Rate	Unconstrained	Constrained	IRA
					Capacity (dB)	Capacity (dB)	Threshold
2	4.397	1.000	1.000	0.250	11.76	12.51	13.01
3	7.208	1.536	1.541	0.385	18.49	19.65	
4	9.300	1.911	1.980	0.495	23.82	25.15	25.78
5	10.972	2.203	2.213	0.553	26.63	28.01	
6	12.367	2.443	2.477	0.619	29.82	31.28	32.65
7	13.565	2.647	2.688	0.672	32.36	33.82	
8	14.617	2.825	2.880	0.721	34.69	36.17	
9	15.552	2.983	3.033	0.758	36.52	38.02	
10	16.396	3.125	3.166	0.792	38.13	39.63	40.40
11	17.162	3.253	3.282	0.821	39.53	41.04	
12	17.867	3.372	3.391	0.848	40.83	42.36	
13	18.520	3.481	3.508	0.877	42.25	43.76	
14	19.090	3.582	3.622	0.905	43.62	45.14	
15	19.694	3.677	3.722	0.931	44.82	46.39	46.81
16	20.224	3.765	3.805	0.951	45.76	47.53	
17	20.725	3.849	3.895	0.974	46.90	49.03	
18	21.199	3.928	3.977	0.994	47.89	51.36	

Table 3.1: Parameters of a 2:1 digital BICM system with Gaussian sources, scalar quantization, Huffman source coding, IRA channel coding and 256-PAM modulation.

Tables 3.1 and 3.2 show the parameters of the resulting BICM digital transmission systems designed for Gaussian and Laplacian sources, respectively. The first column of Tables 3.1 and 3.2 contains the number of scalar quantization levels, Q . The second column is the expected SDR provided by the optimum MSE Lloyd-Max scalar quantizer, calculated as the inverse of the quantization error. The third column shows the average length values obtained when the sources are Huffman encoded while the fourth column is the channel encoder rate allowed by the 256-PAM modulator. The fifth and sixth columns are the minimum CSNR necessary to achieve the unconstrained and constrained channel capacity, respectively. Finally, the seventh column shows the threshold values obtained when using a practical IRA code.

Other BICM digital transmission systems could be designed with different modulation levels and channel code rates, specially for the case of low number of quantization levels, Q . For instance, if a $M = 64$ PAM constellation is used, information transfer is feasible as long as

Q	SDR (dB)	Entropy	L_m	Code Rate	Unconstrained	Constrained	IRA
					Capacity (dB)	Capacity (dB)	Threshold
2	3.010	1.000	1.000	0.250	11.76	12.51	13.01
3	5.780	1.317	1.368	0.342	16.37	17.42	
4	7.540	1.728	1.805	0.451	21.71	22.97	
5	9.215	1.946	1.996	0.499	24.02	25.31	26.29
6	10.464	2.207	2.291	0.573	27.58	28.97	
7	11.669	2.374	2.427	0.607	29.22	30.67	
8	12.638	2.565	2.607	0.652	31.39	32.86	33.02
9	13.581	2.701	2.749	0.687	33.01	34.56	
10	14.372	2.852	2.882	0.721	34.70	36.18	
11	15.145	2.966	3.017	0.754	36.33	37.81	
12	15.815	3.091	3.142	0.785	37.83	39.35	
13	16.471	3.189	3.221	0.805	38.79	40.30	41.04
14	17.051	3.295	3.349	0.837	40.33	41.84	
15	17.621	3.382	3.431	0.858	41.31	42.84	
16	18.132	3.474	3.512	0.878	42.29	43.81	
17	18.636	3.552	3.578	0.894	43.08	44.61	
18	19.093	3.634	3.666	0.916	44.15	45.68	
19	19.545	3.704	3.736	0.934	44.99	46.54	
20	19.959	3.777	3.804	0.951	45.80	47.50	48.41

Table 3.2: Parameters of a 2:1 digital BICM system with Laplacian sources, scalar quantization, Huffman source coding, IRA channel coding and 256-PAM modulation.

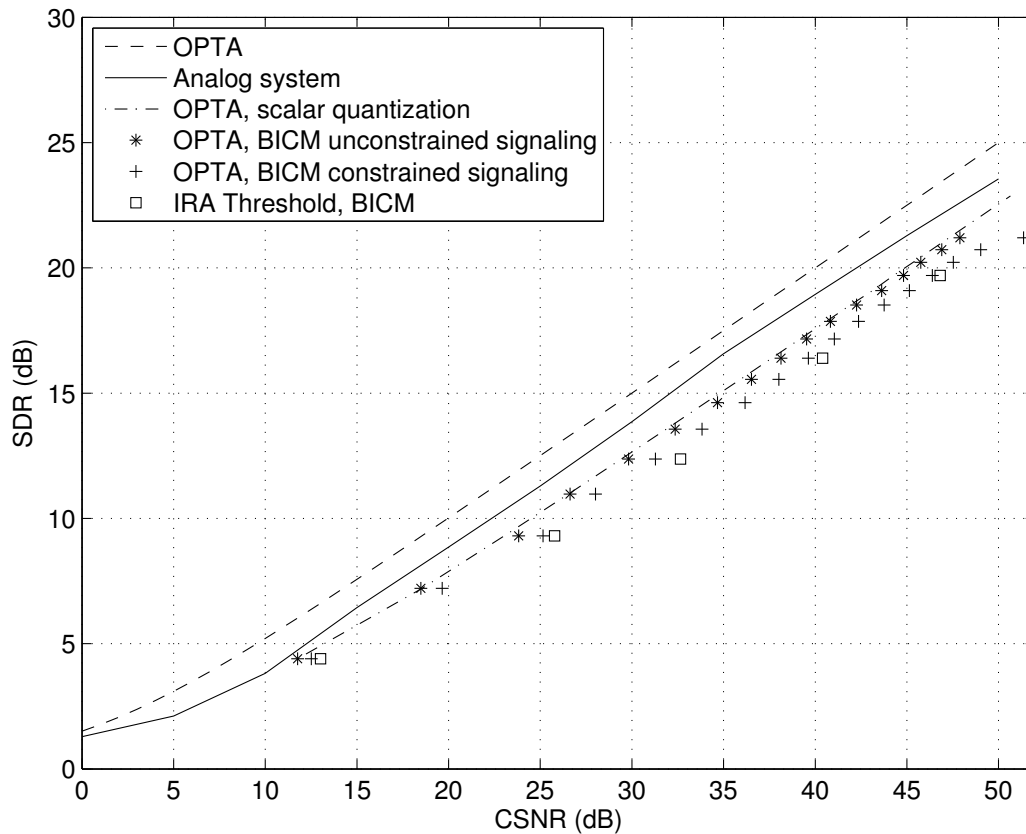


Figure 3.5: Performance comparison of 2:1 analog JSCC and digital 256-PAM schemes for Gaussian sources.

$2L_m < 6$. This channel information rate limit forces the maximum achievable SDR value to be 14.617 dB ($Q = 8$) for Gaussian sources and 14.372 dB ($Q = 10$) for Laplacian sources. In addition, the rate of the channel encoder should be changed now to $R_c = L_m/3$. Nevertheless, since the constrained capacities for 64 and 256 PAM are very similar in the low CSNR regime, the results are almost identical to those in Tables 3.1 and 3.2. The same is true for $M = 16$ PAM. On the other hand, higher values of Q would lead to better performance only for very high CSNR, but not for the CSNR range considered for the comparison with the analog JSCC scheme.

3.3 System Comparison

Figures 3.5 and 3.6 show the SDR versus CSNR performance points that were obtained for the analog JSCC scheme and the digital system described in the previous sections. Figure 3.5 is for the case of Gaussian distributed sources while Figure 3.6 is for the Laplacian case. The different points represent the performance of the analog system, the theoretical limit of a digital system that utilizes scalar quantization and has the same number of channel uses as the analog system (i.e., the ultimate limit with scalar quantization using perfect source and channel

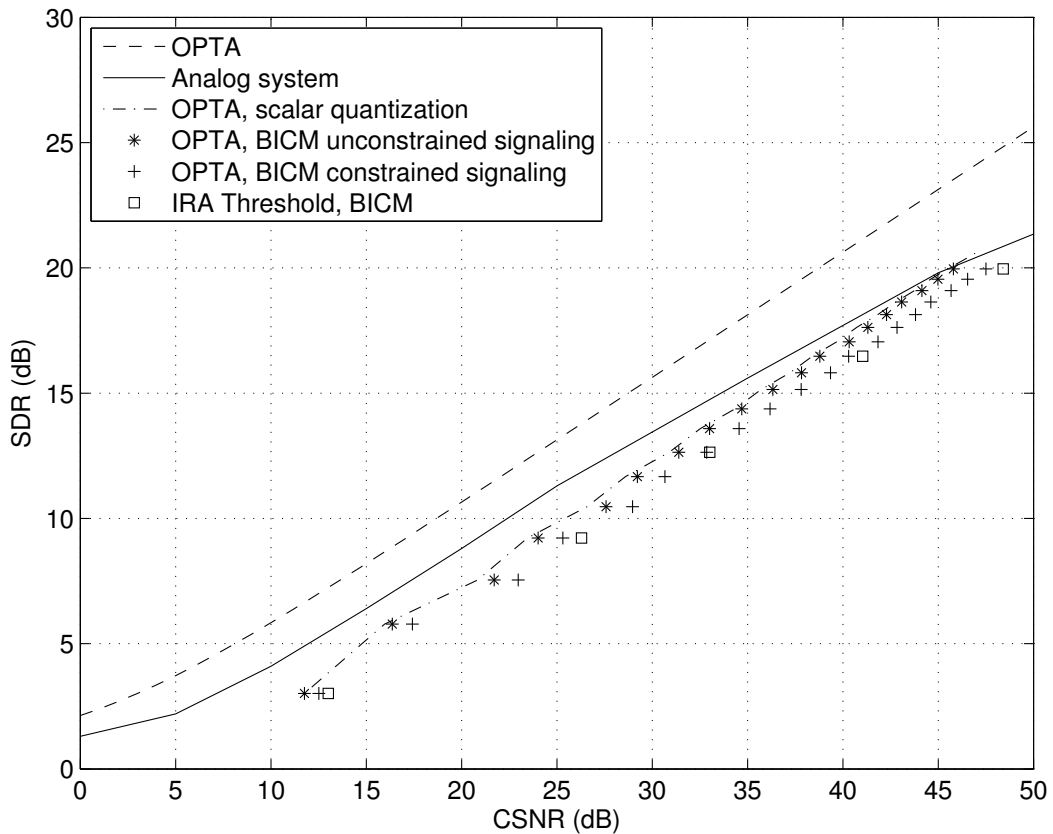


Figure 3.6: Performance comparison of 2:1 analog JSCC and digital 256-PAM schemes for Laplacian sources.

coding and optimal signaling), and the performance of a BICM digital system that utilizes scalar quantization and has the same number of channel uses as the analog system when i) Huffman coding and Gaussian signaling are employed, ii) Huffman coding and PAM signaling are used, and iii) the most realistic scenario in which a Huffman code, a PAM constellation and a practical IRA channel encoder are utilized. The performance curves corresponding to the analog JSCC scheme are calculated according to the system design explained in Chapter 2, including the proposed low complexity two-step receiver and an appropriate optimization of the encoder parameters. The OPTA curves have also been included as a benchmark.

From Figures 3.5 and 3.6, it is clear that the performance of the analog JSCC system is significantly better than that of the digital BICM systems, even when optimal (Gaussian) signaling is used. For Gaussian sources, the difference in performance is about 5 dB when considering 256-PAM constellations (3 dB when using Gaussian modulations) for CSNR values above 20 dB. For Laplacian sources, differences are particularly remarkable in the low CSNR regime where the analog JSCC outperforms the BICM digital system about 6 dB for PAM and 5 dB for Gaussian modulations. Differences are smaller at high CSNR values although still important (2 – 3 dB for the more realistic case of using PAM).

It is worth to notice that the superior performance of the analog JSCC system is achieved

with extremely low complexity (the encoding and decoding is carried out at symbol level) that is independent of the target SDR and/or the CSNR. Furthermore, not only is the resulting complexity of the digital BICM systems higher, but also the digital design must change radically when the operating conditions vary. Vector quantization can be considered in order to improve the performance of the digital BICM system but this would be only accomplished at the cost of an even greater increase in complexity.

3.4 Conclusions

For analog JSCC can be actually considered a practical alternative to conventional digital systems, it is important to assess the performance of both approaches under similar transmission conditions. In this chapter, we have carried out a fair comparison between the analog JSCC system described in Chapter 2 and a digital SSCC scheme that is conveniently designed to achieve the same transmission rate as that of the analog system. In particular, Bit-Interleaved Coded Modulation (BICM) systems has been selected because of its simplicity and lower complexity with respect to other digital approaches. Such a scheme consists of an optimum scalar quantizer, a Huffman source encoder, an optimized IRA channel encoder and a 256-PAM modulator.

The results of the computer simulations show that the analog JSCC system outperforms the considered digital systems for the whole SNR region with a significantly lower encoding and decoding complexity. Thereby, we have validated that analog JSCC is an adequate strategy for the transmission of analog sources when it is necessary to achieve high transmission rates while preserving low complexity and delay. On the other hand, the analog JSCC scheme can be constantly adapted to the channel conditions in a time-varying scenario by optimizing the encoder parameters whereas the digital BICM system should be completely redesigned whenever the channel varies in order to update its different components to the new conditions.

Chapter 4

Experimental Evaluation of Analog JSCC in Indoor Environments

As shown in Chapter 2, analog Joint Source Channel Coding (JSCC) has been proved to closely approach the Optimum Performance Theoretically Attainable (OPTA) for the transmission of analog sources over Additive White Gaussian Noise (AWGN) channels on simulated scenarios. Moreover, this coding strategy represents a better solution than the traditional design of the digital systems on such scenarios and under certain premises, as seen in Chapter 3. However, the behavior of analog schemes designed according to this approach has not been deeply studied yet on more complex and realistic environments, such as wireless systems.

The GTEC research group at the University of A Coruña has developed a hardware testbed that provides a useful tool to experimentally evaluate the performance of wireless communication systems in realistic scenarios at a reasonable effort. We have employed it with the aim of evaluating the feasibility of analog JSCC schemes on real wireless environments and corroborating the promising results obtained over simulated AWGN channels. In this chapter, we describe the software-defined radio implementation of a practical wireless communication system using analog JSCC and will measure its performance in a representative indoor scenario. In addition, such performance is compared to the results obtained for the simulated AWGN case and to the OPTA limit.

When carrying measurements over the software-defined radio testbed, we have addressed some problems that analog compression schemes pose in practice. First, the Peak-to-Average Power Ratio (PAPR) of the transmitted signal can be very high, so careful normalization of the transmitted samples is required to prevent performance degradation due to Digital-to-Analog Converter (DAC)/Analog-to-Digital Converter (ADC) limited resolution. Second, the analog mappings used to encode the source samples are parametrized depending on the Channel Signal-to-Noise Ratio (CSNR) value, so it was necessary to implement a closed-loop system. Although an open-loop system would be much simpler to implement, it would limit the

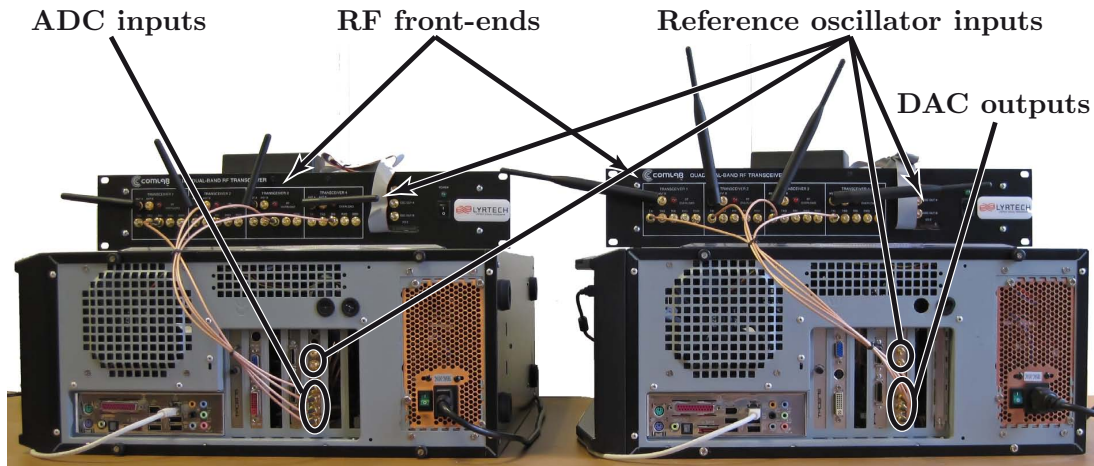


Figure 4.1: Picture of the GTEC MIMO Testbed.

attainable performance.

4.1 Testbed Description

In this section, we introduce a brief hardware description of the testbed (see figure Figure 4.1) developed by research members of the Grupo de Tecnología Electrónica y Comunicaciones (GTEC) at the University of A Coruña, named GTEC MIMO testbed.

In this context, a testbed can be defined as a hardware implementation for wireless communication systems, offering real-time transmission capabilities while the data is usually generated and post-processed off-line. The general idea of a testbed is to implement in real-time only those operations needed to transmit the signals through the wireless channel and acquire them for off-line evaluation or signal processing later using some type of additional software (in a high level programming language such as MATLAB). Hence, a testbed allows us to experimentally evaluate the performance of wireless communication systems on realistic scenarios with an affordable complexity and effort.

Figure 4.2 shows the block diagram of the main hardware components of a traditional testbed. As observed, the connection between the hardware and software parts is established by a main bus that allows the data to be transferred from the host -where additional software is running- to the testbed hardware and vice-versa. Thus, it is possible to send samples coming directly from the main bus, process them in baseband by using the DSPs and FPGAs, convert them into the analog domain using the DACs and, finally, up convert them to the desired carrier RF using the RF front-ends. At the receiver side, the signals are down converted by the RF front-ends, converted to the digital domain by the ADCs and sent to the host through the main bus.

In our particular case, the GTEC MIMO testbed basically consists of several transmit and receive nodes, externally controlled by standard Transmission Control Protocol (TCP) socket

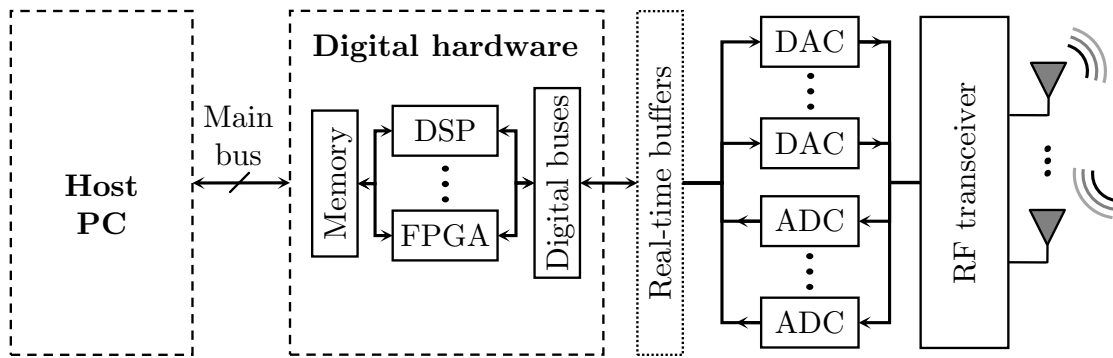


Figure 4.2: Block diagram of the testbed hardware components

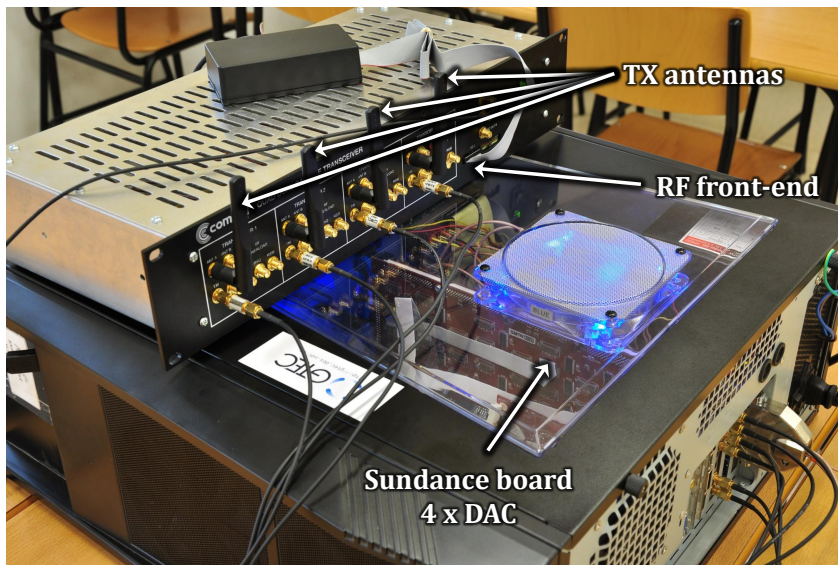


Figure 4.3: Picture of a transmit node of the GTEC MIMO Testbed.

connections. Both transmit and receive testbed nodes are equipped with a Quad Dual-Band front-end from Lyrtech, Inc [2](see Figure 4.3). The Radio Frequency (RF) front-end is equipped with up to eight antennas that are connected to four direct conversion transceivers by means of an antenna switch. The front-end is based on Maxim [3] MAX2829 chip (also found in front-ends like Ettus [1] XCVR2450 or Sundance [4] SMT911). It supports both up and down conversion operations from either a 2.4 to 2.5 GHz band or a 4.9 to 5.875 GHz band. The front-end also incorporates a programmable variable attenuator to control the transmit power. The attenuation ranges from 0 to 31 dB in 1 dB steps, while the maximum transmit power declared by Lyrtech is 25 dBm per transceiver.

The baseband hardware of all testbed nodes is based on Commercial Off-The-Shelf (COTS) components from Sundance Multiprocessor [4] (see Figure 4.3). More specifically, each transmit node is based on the SMT8036E kit, containing four DACs that generate Intermediate Frequency (IF) signals that fed the RF front-end only through the I branch. Given that an IF signal is provided to a direct conversion front-end, we obtain at the output of the front-end the desired signal plus an undesired replica which is removed at the receiver by shifting the RF

carrier frequency and by adequate filtering in the digital domain.

Both transmit and receive nodes are supplied with real-time buffers where the signals to be sent to the DACs as well as the signals acquired by the ADCs are stored. The use of such buffers is crucial since it makes the transmission and acquisition of the signals in real-time possible, while the signal generation and processing can be accomplished off-line by the host PC.

Additionally, the baseband hardware and RF front-ends of all nodes need to be synchronized both in time and in frequency. This critical operation is carried out by means of two mechanisms ensuring a right synchronization both at the transmitter and receiver:

- At the transmitter side, a hardware trigger is attached to each one of the DACs and real-time buffers. Prior to beginning the data transmission, this trigger is activated (this action can be started by the user from the high-level Application Program Interface (API) in MATLAB) in such a manner that all buffers and DACs are notified and the node starts to transmit simultaneously.
- Similarly, when the receiver node is triggered -simultaneously with the transmitters or in a different step- all ADCs start to acquire the data from real-time buffers at the same time.
- For the frequency synchronization, the same common external 40 MHz reference oscillator is utilized by all nodes. At each node, a three-way splitter is used to provide the clock signal to the DACs (or the ADCs) and the RF front-end. This scheme guarantees the frequency synchronization of all nodes except for the frequency shift between the transmit RF front-ends and the receive RF front-end.

The hardware of the testbed is also complemented with a distributed multilayer software architecture based on the software defined radio concept [83, 97], and specifically designed to simplify the interaction of the users with the testbed hardware [30, 41, 42].

4.2 General Procedure for Data Transmission

Once the hardware module of the testbed has been described, we will explain in this section the set of operations needed for transmitting a sequence of samples from a transmit node to a receive node by using the hardware platform GTEC MIMO testbed. Figures 4.4 and 4.5 show the block diagram of one transmit node and one receive node, respectively, including the software and hardware elements utilized for data transmission.

Once the discrete-time complex-valued sequences to be transmitted have been generated, the resulting symbols are processed as follows (see Figure 4.4):

- Each data frame is constructed from a sequence of source symbols. In the case of analog JSCC, the symbols to be transmitted by the testbed are the coded samples at the analog encoder output and, therefore, no other coding operation is required.

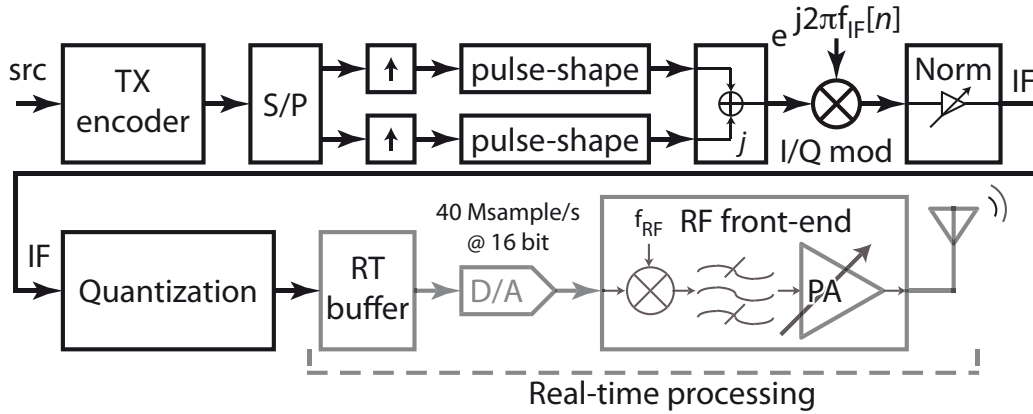


Figure 4.4: Block diagram of hardware and software elements at the transmitter.

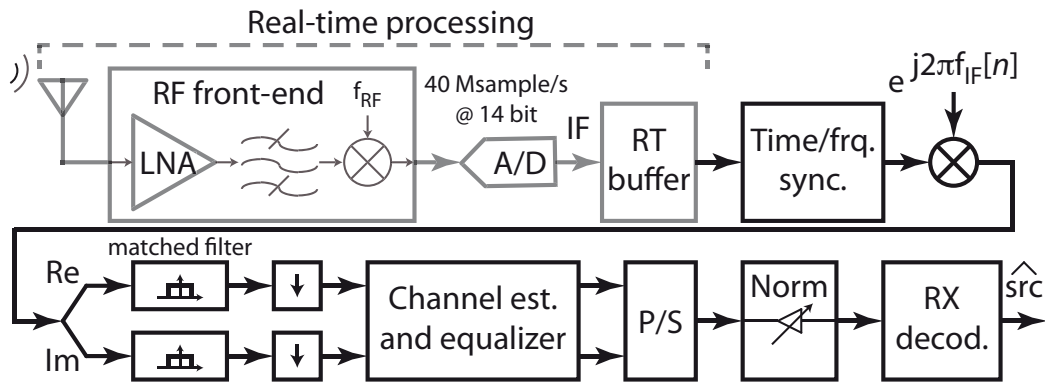


Figure 4.5: Block diagram of hardware and software elements at the receiver.

- A Pseudo-Noise (PN) sequence is added to the data frame as a preamble for synchronization together with a silence that will be used at the receiver to estimate the noise power spectral density. The complete frame structure is plotted in Figure 4.6.
- The symbol sequence is then up-sampled by a factor of T_s . For analog JSCC transmissions, we considered a specific factor $T_s = 20$, so that each analog coded symbol is represented by 20 samples.
- The next step consists of a pulse-shape filtering using a squared root-raised cosine filter with 20% roll-off. Consequently, given that the sampling frequency of the DACs is set to 40 MHz, the resulting signal bandwidth is 2.24 MHz, which leads –according to our tests– to a frequency-flat channel response. Note that the DACs implement an internal interpolating filter that improves the signal quality at the output, resulting in an actual sample rate of 160 Msamples/s.
- The resulting signals are I/Q modulated to obtain a passband signal at a carrier frequency of f_{IF} MHz (in our setup this frequency is $f_{IF} = 5$ MHz).
- In order to satisfy the transmit power constraint, the I/Q signals generated in the previous step must be properly normalized.

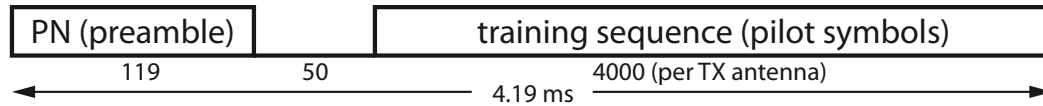


Figure 4.6: Frame structure used to transmit the source symbols.

- Since the resolution of the DACs is 16 bits, the signals are properly quantized to obtain 16-bit integer values for each sample.
- The resulting data is stored off-line in the buffers available at the transmit nodes of the testbed.
- Once all symbols are stored in the real-time buffers, all transmitters switch on the trigger used for synchronization at the same time and then all buffers are read simultaneously, cyclically, and in real-time by the corresponding DACs which generate a signal at the IF.
- The resulting analog signals are sent to the RF front-end to be transmitted at the desired RF center frequency. In our measurements for the experimental evaluation of the analog JSCC scheme, we specifically employed the center frequency of 5.605 GHz.

After the transmit node is triggered, the corresponding RF signals -generated by the RF front-end- are sent in real-time by the active transmit antennas through the real wireless channel between the transmit and receive nodes. Once the receive nodes are also triggered, the following steps are carried out to recover the sequence of transmitted samples (see Figure 4.5):

- Initially, the RF front-end acquires the signals received by the selected antennas (up to four) and down-converts them to the baseband, generating the corresponding analog passband signals.
- Such IF signals are then digitized by the ADCs by sampling at 40 MHz, and they are stored in the real-time buffers available at the receive nodes. Given that the signals are transmitted cyclically and, in order to guarantee that a whole frame is received, twice the length of the transmit frame is acquired and stored.
- The signals are properly scaled according to the 14 bits ADC resolution. Notice that this factor is constant during the whole measurement, hence not affecting the properties of the channel.
- Next, the acquired signals are filtered using a custom-designed passband filter that eliminates all undesired replicas of the signals induced by the up-conversion to RF.
- Afterwards, time and frequency synchronization are carried out making use of the known preamble inserted into the data frames by the transmitter.

- Once the acquired frames are correctly synchronized, the resulting signals are I/Q demodulated and filtered again (matched filter) and, as a result, discrete-time, complex-valued observations with T_s samples per symbol are obtained. After filtering, the signals are decimated.
- Instantaneous receive power as well as instantaneous power spectral density of the noise are estimated making use of the silence inserted in the transmitted frame.
- Finally, the frame is properly disassembled, and the corresponding observations are then sent to the channel estimator and the channel equalizer.
- The raw acquired signals, the discrete-time complex-valued observations (including those observed during the silence) as well as the estimated channel coefficients are then stored for subsequent evaluation.

4.3 Experimental Measurements

As mentioned at the beginning of this chapter, the GTEC MIMO testbed can be employed to evaluate the actual performance of the analog JSCC transmission scheme in a realistic scenario, namely an indoor environment (an office). For that purpose, we consider the transmission of sequences of discrete-time continuous-amplitude source symbols, which are first compressed using the $N:K$ analog encoder based on the Archimedes' spiral described in Chapter 2 and then sent over a real wireless channel following the procedure explained in Section 4.2. Finally, the distortion between the original source samples and the recovered symbols from the received sequence is computed.

Thus, the mean performance in terms of Signal-to-Distortion Ratio (SDR) with respect to CSNR of the analog JSCC system is experimentally measured in the aforementioned scenario using the testbed. The measured results are compared to both the OPTA and the results attained from simulations over the AWGN channel, shown in Section 2.3.3. Remember that three different methods can be employed to decode the received symbols: Maximum Likelihood (ML), Minimum Mean Square Error (MMSE) and our two-step approach (MMSE linear filtering + ML decoding). Nevertheless, since the two-step decoding strategy provides a virtually equal performance to that of MMSE decoder and similar complexity to ML, it will be the only considered method.

In addition, three different compression rates are evaluated: 2:1, 10:6 and 10:9. In the case of rates different to 2:1, it is possible to consider two schemes: one where the transmit power is not optimally redistributed between coded and uncoded symbols, and another one where the power allocation module -described in Section 2.3.1.1- is used to allocate the appropriate amount of power for both coded and uncoded symbols.

4.3.1 Closed-Loop Setup

The experimental measurements have been carried out for a narrowband single-antenna configuration for simplicity reasons. An interesting feature of our experimental setup is that all signal processing operations were implemented in MATLAB. According to the philosophy of experimental measurements with testbeds, the data to be transmitted is generated off-line, sent in real-time over a real wireless channel and the received signals are stored in the buffers available at the receiver. The obtained measurement data is then transferred to the host for later off-line evaluation and processing. Unrealistic results would be obtained if the real-time channel is replaced with a simulated channel whose coefficients were obtained from a channel sounder, since the possible hardware impairments could not be detected.

Given the specific properties of the signals obtained after the analog JSCC (e.g. the high PAPR) it is very important to carry out experiments over the hardware testbed to take into account the effects of the ADCs, DACs and transmit amplifier. In addition, it is also important to determine the range of values at the analog encoder output in order to avoid clipping caused by the DAC while, at the same time, the whole available dynamic range is used.

Another particular feature of the analog JSCC scheme is the importance of selecting an optimum value for the encoder parameter δ , which depends on the actual CSNR and the input distribution. Wireless channels suffer from fading caused by multipath propagation which makes the received CSNR fluctuate continuously over time and, therefore, the δ value must be continuously adapted. Therefore, it is necessary to implement a feedback channel from the receiver to the transmitter, constructing a closed-loop setup. Thus, the CSNR is estimated at the receiver side and sent through a feedback channel to the transmitter to select the optimum δ value using Table 2.1 for the case of Gaussian sources. In this case, we implemented such feedback channel by means of an Ethernet network connection.

4.3.2 A Typical Indoor Environment

Figure 4.7 shows the indoor scenario employed to experimentally measure the performance of the analog JSCC system. As observed, the plan corresponds to an office inside an university building. The transmit antennas are placed on a table adjacent to a WiFi access point of the public wireless network at the University of A Coruña. The receive antennas are placed on a table used by one of the employees in the office, thus emulating the actual position that a desktop or laptop computer would occupy. The transmit and receive antennas are at a distance of approximately 9 m with direct line-of-sight.

In order to incorporate more realism into the measurements, we use standard rod antennas (see 4.1) with a gain of 3 dBi. These antennas are similar to those employed in WiFi access points that operate at 5 GHz.

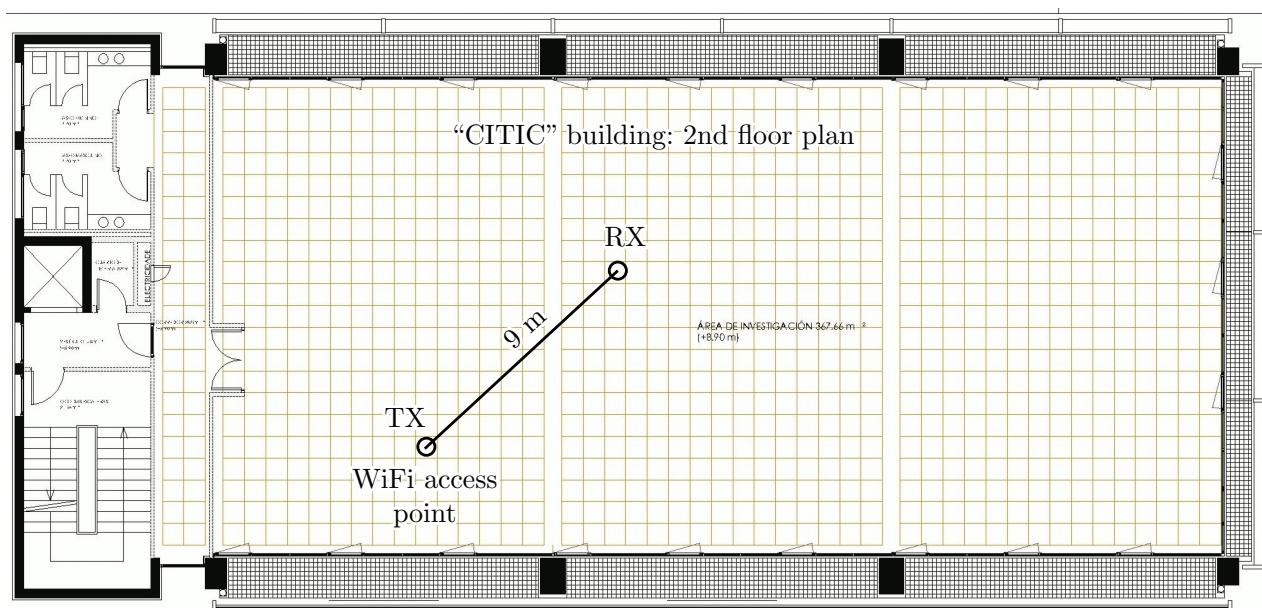


Figure 4.7: Plan of the second floor of the CITIC building and localization of the transmit and receive nodes.

4.3.3 Quantization of the Transmitted Signals

As explained in Section 4.3.1, one of the main hindrances of the analog JSCC systems implemented on the software-defined radio testbed is the potentially high PAPR that the transmitted signals can attain. We need to ensure that every generated sequence has the same mean power value with the aim of avoiding accuracy loss in the measurements. This constraint is guaranteed by means of the following procedures:

- The channel symbols obtained at the output of the analog encoder are normalized to ensure that the whole sequence –including the uncoded symbols– always has a mean power equal to one. This is done independently of the rate and the utilized power allocation scheme.
- After the channel symbols are converted to discrete IF signals, they have to be quantized according to the 16 bits resolution of the DAC. Given the high PAPR of the resulting signals, we have determined by computer simulations the maximum absolute value that a channel symbol can reach for all possible compression rates and power allocation schemes considered. In particular, we have observed that the largest PAPR value is approximately equal to 8.8 for Gaussian sources. Once we know this value, it is easy to compute the maximum scale factor for every generated sequence, ensuring that no clipping effects are introduced and, at the same time, the whole available dynamic range is used.

4.3.4 Measurement Procedure

The source samples are transmitted over the wireless channel according to the following steps:

- Prior to beginning the data transmission, the current CSNR is estimated at the receiver – using the previous transmitted frame – and sent to the transmitter through the feedback channel implemented in the closed-loop setup.
- The analog encoder selects the optimum δ value for the estimated CSNR by using a look-up table (see Table 2.1) previously stored at the transmitter. Such value is then used to encode two Gaussian samples into the corresponding channel symbol. The wireless channel is described by complex-valued coefficients so it is necessary to perform a complex interleaving where two real-valued channel symbols are merged into one complex-valued symbol. Thus, each pair of real-valued channel symbols is mapped into a complex I/Q symbol.
- Each sequence of complex-valued channel symbols is normalized to ensure a transmit power value equal to one. This normalization factor must be available at the receiver to perform the inverse operation before decoding.
- Next, the resulting sequence is pulse-shape filtered, scaled and I/Q modulated.
- The transmit frame is assembled. In addition to the encoded signal, a preamble and a training sequence (pilots) is included. They are needed for time and frequency synchronization, and to equalize the channel at the receiver, respectively.
- The assembled frame is then transmitted over the wireless channel.
- The received frame is disassembled and the channel is estimated from the training sequence using a simple Least Squares (LS) algorithm. Then, the CSNR is also estimated and fed back to the transmitter. In order to guarantee the accuracy of the CSNR estimation, the receiver actually estimates the noise power spectral density during the time intervals when no signals are transmitted.
- Finally, the operations executed at the transmitter are inverted and the observed sequence is stored for subsequent evaluation. In particular, the calculation of the distortion between the original and received symbols is performed.

All transmitted frames share the same structure: a Pseudo Noise (PN) sequence comprising 100 symbols (preamble), 16 pilot symbols, and 7200 source symbols that are encoded according to one of the possible rates considered, i.e. 2:1, 10:6, or 10:9. This frame structure resembles the one shown in Figure 4.6 but is adapted to the particular case of analog JSCC in an indoor scenario.

Rate	Source symbols	Coded symbols	Uncoded symbols	Total I/Q symbols	Frame duration (ms)	Transfer rate (symbol/s)
2:1	7200	3600	0	1800	0.9	$8 \cdot 10^6$
10:6	7200	2880	1440	2160	1.1	$6.55 \cdot 10^6$
10:9	7200	720	5760	3240	1.6	$4.5 \cdot 10^6$

Table 4.1: Transfer rates according to the code rate. Frame overheads are not included.

As mentioned in Section 4.2, we use a symbol period of $T_s = 20$ samples per symbol, with the sampling frequency of both the DAC and the ADC fixed to 40 MSPS (Megasamples per second). The symbols are pulse-shape filtered using a squared root raised cosine filter with 20 % of roll-off, hence resulting in an occupied bandwidth of 2.4 MHz at the carrier frequency of 5.605 GHz. Table 4.1 shows the corresponding transfer rate for the three different compression rates (i.e. 2:1, 10:6 and 10:9) and the number of coded and uncoded symbols (i.e. the channel symbols) obtained when 7200 source symbols are used. Additionally, the number of I/Q symbols that compose the transmit frame and the frame duration are indicated. Notice that Table 4.1 does not include the overheads due to preamble and pilot symbols.

4.4 Results

In this section, we focus on the transmission of discrete-time Gaussian samples over the indoor wireless channel described in Section 4.3.2 by using the GTEC MIMO testbed. The results obtained after the experimental measurement are presented and compared with respect to the performance attained for the analog JSCC system on the simulated AWGN case, and to the theoretical limit (OPTA). In both scenarios –simulated AWGN channel and real wireless channel–, the analog JSCC scheme uses the $N:K$ analog encoder based on the Archimedes’ spiral (Section 2.3.1.1) and the two-stage method proposed for decoding the received symbols (Section 2.3.3). Three different compression rates are assessed: 2:1, 10:6 and 10:9. In turn, for the 10:6 and the 10:9 cases, two different schemes are considered. The first one transmits the whole sequence –i.e. coded and uncoded symbols– with the same mean power value, while the second one uses the power allocation module. In total, five different schemes are measured. In order to get smooth curves of SDR, each scheme is measured at different transmit power values to obtain different CSNR values. We repeated the experiments 100 times, which resulted in approximately 6000 different realizations.

Notice that, in order to achieve low CSNR values (≈ 5 dB) while keeping the complexity of the synchronization tasks in reasonable terms, we boost the preamble such that the mean power

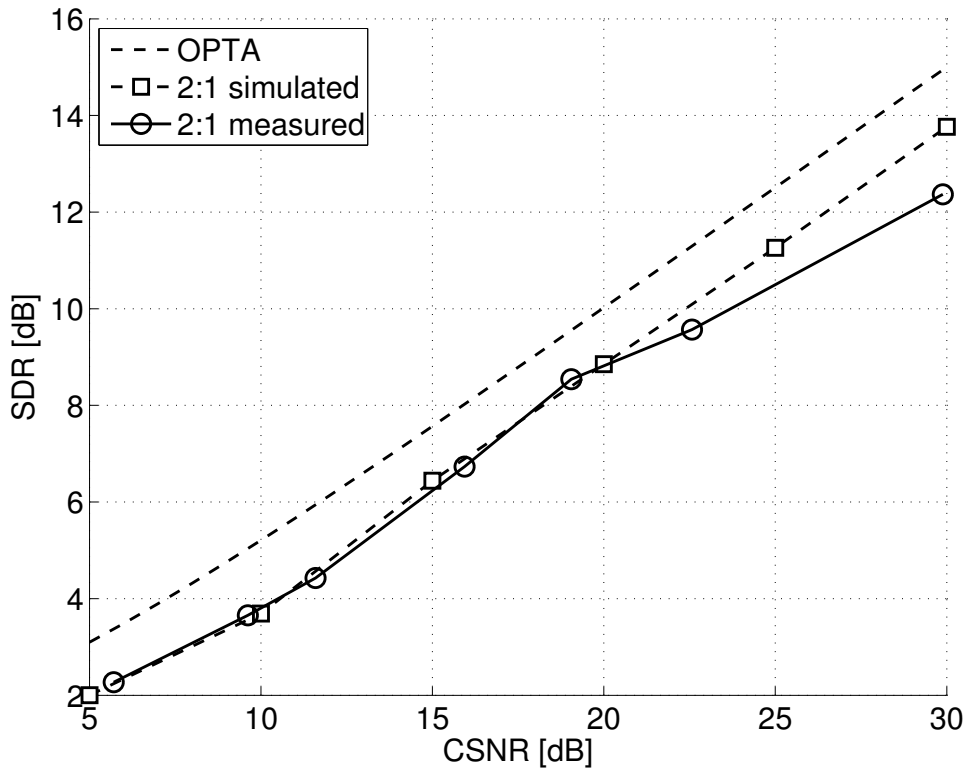


Figure 4.8: Performance of the 2:1 analog JSCC scheme over the simulated AWGN channel and on the real indoor scenario.

of the acquired preamble is significantly larger than that of the rest of the frame.

Figures 4.8–4.10 show the results obtained for the compression rates 2:1, 10:6, and 10:9, respectively. The abscissas and the ordinates axes correspond to the CSNR and the SDR values expressed in decibels (dB), respectively. In the 2:1 case there is no possibility of including a power allocation scheme because all transmitted symbols are actually coded symbols.

Figures 4.8–4.10 clearly show that the measurement curves perfectly match the simulated ones for CSNR values below 20 dB. When the CSNR is greater than 20 dB, the SDR curves exhibit saturation effects. Such effects are mainly caused by the limited number of resolution bits of the DAC (16 bits in this case) and also by the high PAPR of the transmitted signals. Looking at Table 4.1, and at the graphs mentioned above, it is interesting to see how the SDR increases as the transfer rate decreases.

4.5 Conclusions

In this chapter we have described a software-defined radio implementation of a practical wireless communication system that uses analog JSCC. As shown in Chapter 3, the performance of a digital system is below that of an analog JSCC scheme with lower complexity and negligible delay for compression rates beyond 1:1 and AWGN channel. However, these

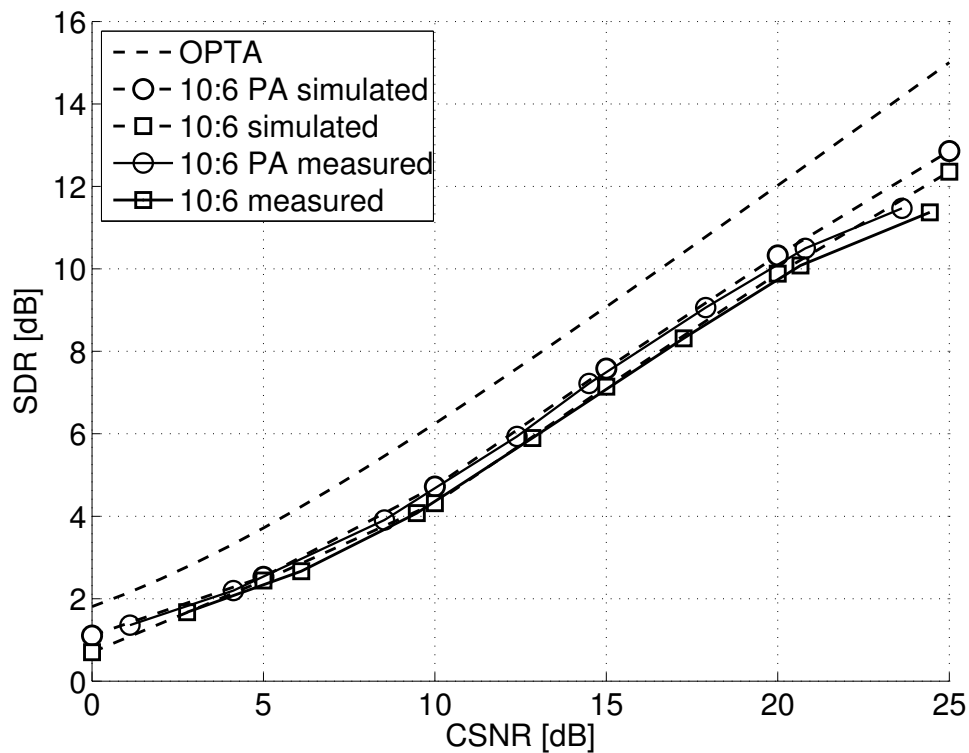


Figure 4.9: Performance of the 10:6 analog JSCC scheme: simulated SDR with and without power allocation (PA), and measured SDR with and without power allocation (PA).

results were obtained using computer simulations and no feasibility studies of the analog JSCC on realistic scenarios (e.g. real wireless channels) have been undertaken so far. We consider essential to address the experimental evaluation of analog JSCC transmission schemes on real environments and, for that reason, we have carried out closed-loop narrowband single-antenna measurements in a typical and very realistic indoor scenario, which has forced us to deal with some practical problems of analog JSCC that are not encountered in simulation scenarios (e.g. high PAPR of the resulting signals or feedback channel implementation).

Fortunately, the performance measured using the GTEC MIMO testbed for the three evaluated compression rates confirms the results previously obtained by simulation over the AWGN channel. Both SDR curves -on simulated and real scenario- perfectly match for CSNR values below 20 dB and hence the feasibility of this type of analog compression schemes in real environments is clearly demonstrated. Thus, the results shown along this chapter, together with the conclusions derived by the comparison study in Chapter 3, lay solid foundations for our further research and the application of analog JSCC techniques on wireless communications.

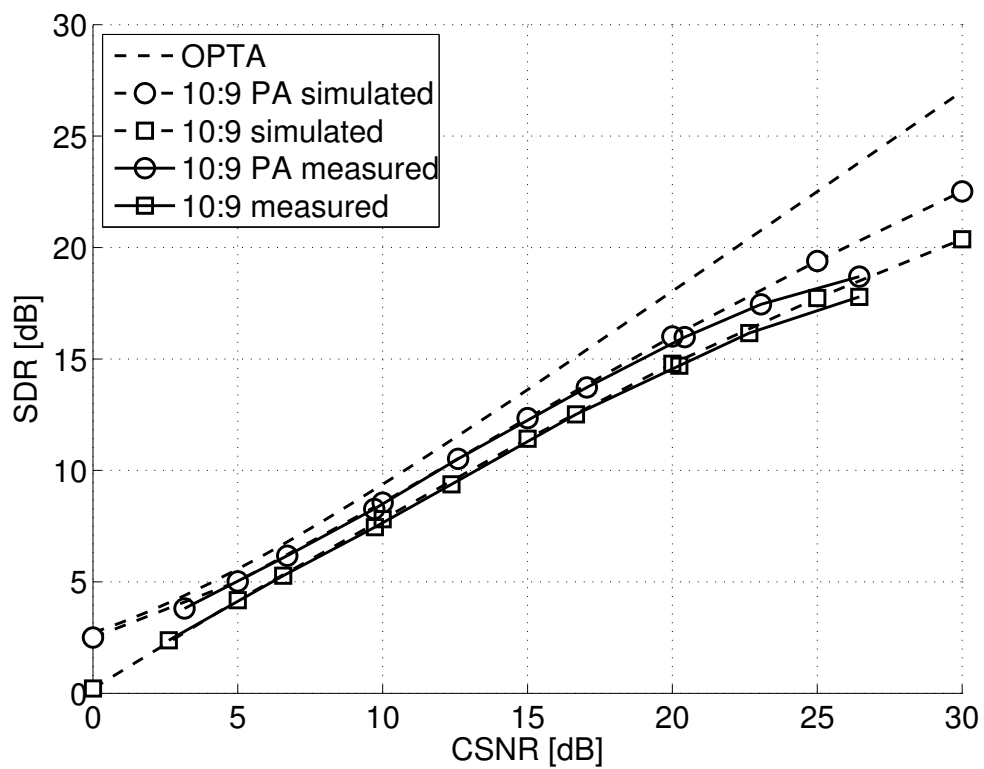


Figure 4.10: Performance of the 10:9 analog JSCC scheme: simulated SDR with and without power allocation (PA), and measured SDR with and without power allocation (PA).

Chapter 5

Analog JSCC over MIMO Channels

Over the last two decades, the demand of reliable high-speed transmissions over wireless channels has exponentially grown in order to support a wide range of applications like voice, images or video. In the context of wireless communications, unlike other communication models, a transmitted radio signal usually propagates through several different paths before it reaches the receiver (multipath propagation). As a result, a superposition of multiple attenuated copies of the transmitted signal with different delays and phase shifts is received incurring a severe performance degradation. This is commonly referred to as fading. In addition, the available bandwidth is often a scarce resource which must be efficiently allotted with the aim of providing a high spectral efficiency.

At the end of the 1990s, pioneering works in Bell Labs [35, 36, 119, 120] first showed that the use of multiple antennas at both link ends of a communication system leads to a substantial increase in the channel capacities, which immediately translates to higher data throughput without any extra bandwidth or transmission power requirements. Systems employing multiple antennas at both transmission and reception are referred to as Multiple Input Multiple Output (MIMO) systems in the literature and they have been also proved to achieve a considerably larger capacity than that of conventional single-antenna systems [120].

MIMO systems are also able to combat the harmful effects of the channel fading by combining the multiple realizations of the signal received through different paths. Indeed, this strategy exploits the independent fading experienced by the signal paths corresponding to the different antennas at the receiver (diversity) to provide a significant improvement of the system performance, known as diversity gain.

These appealing properties have motivated the MIMO strategy to be adopted as the transmission scheme by the last generation of wireless communication standards such as IEEE 802.11 (Wi-Fi), IEEE 802.16 (WiMAX) or 3rd Generation Partnership Project (3GPP). For all those reasons, we consider interesting to assess the performance of analog Joint Source Channel Coding (JSCC) schemes over MIMO scenarios, since the characteristics of this technique -high

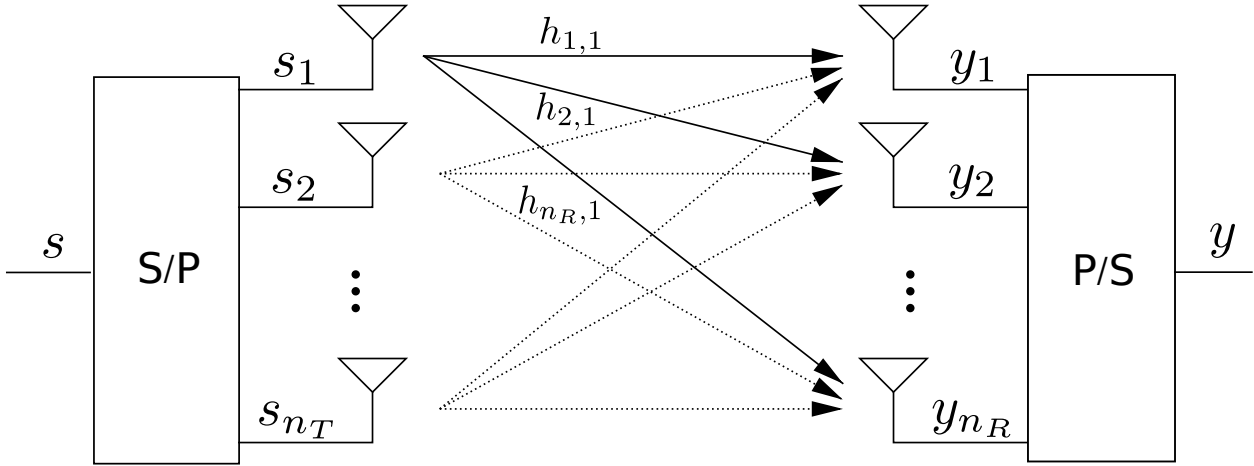


Figure 5.1: Block diagram of a MIMO system with n_T transmit and n_R receive antennas.

transmission rate, low complexity, negligible delay- makes it specially suitable to support the increasing requirements of the current wireless services.

In this chapter, we study the feasibility of analog JSCC MIMO transmissions over fading channels. First, a review of the Optimum Performance Theoretically Attainable (OPTA) limit is required to define the optimal performance for the considered communication model. We then extend the low complexity two-stage receiver structure stated in Chapter 2, in such manner that a linear detector is first used to transform the MIMO channel into several parallel Single Input Single Output (SISO) channels. Then, a bank of conventional Maximum Likelihood (ML) SISO decoders is employed to recover the transmitted source samples. We also examine the performance of a Decision Feedback (DF) MIMO detector [84, 100] as the first stage of our receiver. Finally, we explore the case where the channel is perfectly known at the transmitter suggesting the use of linear Minimum Mean Square Error (MMSE) precoding techniques in order to improve the overall performance of the analog JSCC MIMO systems.

5.1 Description of a MIMO Communication System

We focus on a single-user communication model and consider a point-to-point transmission scheme where the transmitter is equipped with n_T antennas and the receiver with n_R antennas. Figure 5.1 shows the block diagram of such MIMO system. We assume that the bandwidth of the transmitted signal is small enough so that we can disregard the InterSymbol Interference (ISI). This narrowband model results in a frequency-flat channel and, therefore, each signal path can be represented by a complex-valued gain coefficient. If the channel is frequency-selective, Orthogonal Frequency-Division Multiplexing (OFDM) modulation can be employed to transform the MIMO channel into a set of parallel frequency-flat MIMO channels, as we will see in the ensuing chapter.

In this model, a set of n_T complex-valued signals $\{s_1, \dots, s_{n_T}\}$ is spatially multiplexed over

the n_T transmit antennas and sent over a wireless channel. If h_{ij} represents the complex-valued fading coefficient corresponding to the path between the transmit antenna j and the receive antenna i , the received signal at antenna i can be expressed as

$$y_i = \sum_{j=1}^{n_T} h_{ij}s_j + n_i,$$

where n_i is the additive spatially white thermal noise. This linear relation can be rewritten in matrix notation as

$$\mathbf{y} = \mathbf{H}\mathbf{s} + \mathbf{n}, \quad (5.1)$$

with $\mathbf{y} = [y_1, \dots, y_{n_R}]^T$, $\mathbf{s} = [s_1, \dots, s_{n_T}]^T$, $\mathbf{n} = [n_1, \dots, n_{n_R}]^T$ and

$$\mathbf{H} = \begin{bmatrix} h_{11} & h_{12} & \cdots & h_{1n_T} \\ h_{21} & h_{22} & \cdots & h_{2n_T} \\ \vdots & \vdots & \ddots & \vdots \\ h_{n_R1} & h_{n_R2} & \cdots & h_{n_Rn_T} \end{bmatrix}$$

Notice that $\mathbf{y} \in \mathbb{C}^{n_R}$ is a vector comprising the received values, $\mathbf{s} \in \mathbb{C}^{n_T}$ is a vector containing the transmitted values, $\mathbf{n} \in \mathbb{C}^{n_R}$ represents the noise vector and $\mathbf{H} \in \mathbb{C}^{n_R \times n_T}$ is the channel response matrix. Along this chapter, the h_{ij} coefficients are assumed to be statistically independent. In practice, the channel coefficients h_{ij} are usually correlated because of the propagation environment, the polarization of the antenna elements and the spacing between them.

The symbols to be transmitted, \mathbf{s} , are normalized in order to satisfy the transmit power constraint, i.e. $\text{tr}(\mathbf{C}_s) \leq P_T$, where \mathbf{C}_s is the covariance matrix of the transmitted symbols, P_T is the total power available at the transmitter and $\text{tr}(\cdot)$ represents the trace operator. Initially, we address the case where the Channel State Information (CSI) is not available at the transmitter side, i.e. the channel \mathbf{H} is unknown prior to transmission. In this case, it makes sense to distribute the available power uniformly among the transmit antennas so that the radiated power at each antenna will be P_T/n_T . If the symbols are assumed to be also spatially white, the covariance matrix \mathbf{C}_s can be expressed as

$$\mathbf{C}_s = \mathbb{E}[\mathbf{s}\mathbf{s}^H] = \frac{P_T}{n_T} \mathbf{I}_{n_T}, \quad (5.2)$$

where $\mathbb{E}[\cdot]$ represents the statistical expectation, the super index H is the Hermitian operator and \mathbf{I}_{n_T} is the n_T -dimensional identity matrix. On the other hand, the thermal noise is modeled as a complex-valued zero-mean circularly-symmetric Gaussian random variable, i.e. $n \sim \mathcal{N}_{\mathbb{C}}(0, \sigma_n^2 \mathbf{I})$. Hence, the noise covariance matrix is given by

$$\mathbf{C}_n = \mathbb{E}[\mathbf{n}\mathbf{n}^H] = \sigma_n^2 \mathbf{I}_{n_R}, \quad (5.3)$$

where \mathbf{I}_{n_R} is the n_R -dimensional identity matrix.

5.2 OPTA for Analog MIMO Systems

In Chapter 2 we derived a theoretical performance upper bound, referred to as OPTA, for the transmission of discrete-time analog symbols over a point-to-point communication system in a single-antenna scenario. This limit was calculated equating the rate distortion function of a given source and the capacity of the memoryless channel over which the source signals are transmitted. In the case of MIMO schemes, the OPTA can be similarly obtained by simply replacing the Additive White Gaussian Noise (AWGN) channel capacity with the proper expression for the MIMO capacity.

5.2.1 Channel Known at the Receiver

We consider the MIMO transmission model described in the previous section by Equation (5.1) with perfect CSI at the receiver. This situation is the classical case analyzed in the literature, where the channel \mathbf{H} is assumed to be perfectly estimated at the receiver and unknown at the transmitter. The channel knowledge can be acquired by using some type of estimation method like training and tracking [95], blind estimation [85, 124] or any other technique, although an accurate channel estimation can be difficult in time-varying environments.

The capacity of the MIMO channel is defined equivalently to the AWGN case (see Equation (2.6)), i.e.

$$C = \max_{p(\mathbf{s})} I(\mathbf{s}; \mathbf{y}). \quad (5.4)$$

Remember that the mutual information between two random variables can be rewritten in terms of the entropy as

$$I(\mathbf{s}; \mathbf{y}) = H(\mathbf{y}) - H(\mathbf{y}|\mathbf{s}), \quad (5.5)$$

where $H(\mathbf{y})$ is the entropy of the received information and $H(\mathbf{y}|\mathbf{s})$ denotes the conditional entropy of \mathbf{y} with respect to \mathbf{s} . Because \mathbf{y} is linearly determined by the MIMO transmission model, we can express the second term as $H(\mathbf{y}|\mathbf{s}) = H(\mathbf{n}|\mathbf{s})$. Moreover, the noise \mathbf{n} and the transmit vector \mathbf{s} are assumed to be statistically independent, so we can further write

$$H(\mathbf{y}|\mathbf{s}) = H(\mathbf{n}|\mathbf{s}) = H(\mathbf{n})$$

and, therefore, Equation (5.5) is given by

$$I(\mathbf{s}; \mathbf{y}) = H(\mathbf{y}) - H(\mathbf{n}). \quad (5.6)$$

Telatar [120] showed that, when the noise is described by a zero-mean circularly-symmetric complex-valued Gaussian random variable, the mutual information given by Equation (5.6) is maximized if \mathbf{y} is also a zero-mean circularly-symmetric complex-valued Gaussian. In such a case, the entropies $H(\mathbf{y})$ and $H(\mathbf{n})$ can be evaluated [21] as

$$I(\mathbf{s}; \mathbf{y}) = \log [\det (\pi e \mathbf{C}_{\mathbf{y}})] - \log [\det (\pi e \mathbf{C}_{\mathbf{n}})], \quad (5.7)$$

where \mathbf{C}_y and \mathbf{C}_n represent the covariance matrix of the received signal, \mathbf{y} , and the noise, \mathbf{n} , respectively. The covariance matrix \mathbf{C}_y is defined as

$$\mathbf{C}_y = \mathbb{E}[\mathbf{y}\mathbf{y}^H] = \mathbf{H}\mathbb{E}[\mathbf{s}\mathbf{s}^H]\mathbf{H}^H + \mathbb{E}[\mathbf{n}\mathbf{n}^H] = \mathbf{H}\mathbf{C}_s\mathbf{H}^H + \mathbf{C}_n. \quad (5.8)$$

Hence, substituting Equation (5.8) into Equation (5.7), the mutual information results in

$$\begin{aligned} I(\mathbf{s}; \mathbf{y}) &= \log[\det(\pi e \mathbf{C}_y)] - \log[\det(\pi e \mathbf{C}_n)] \\ &= \log[\det(\pi e \mathbf{H}\mathbf{C}_s\mathbf{H}^H + \mathbf{C}_n)] - \log[\det(\pi e \mathbf{C}_n)] \\ &= \log[\det((\mathbf{H}\mathbf{C}_s\mathbf{H}^H + \mathbf{C}_n)(\mathbf{C}_n)^{-1})] \\ &= \log[\det(\mathbf{H}\mathbf{C}_s\mathbf{H}^H(\mathbf{C}_n)^{-1} + \mathbf{I}_{n_R})]. \end{aligned} \quad (5.9)$$

Remember that \mathbf{C}_s and \mathbf{C}_n are given by Equation (5.2) and Equation (5.3), respectively, so the expression for MIMO capacity finally becomes

$$C(\mathbf{H}, \text{CSNR}) = \max_{p(\mathbf{s})} I(\mathbf{s}; \mathbf{y}) = \max_{p(\mathbf{s})} \log \left[\det \left(\mathbf{I}_{n_R} + \frac{\text{CSNR}}{n_T} \mathbf{H}\mathbf{H}^H \right) \right], \quad (5.10)$$

where $\text{CSNR} = P_T/\sigma_n^2$ is the Channel Signal-to-Noise Ratio. For a fading channel, the matrix \mathbf{H} is random and, therefore, the corresponding channel capacity C is also a random variable. However, if we assume that the channel realizations are described by a Wide Sense Stationary (WSS) stochastic process, we can calculate the associated ergodic capacity as the expectation over all realizations of the random variable \mathbf{H} , i.e.

$$C_E(\text{CSNR}) = \mathbb{E}_{\mathbf{H}} \left[\log \det \left(\mathbf{I}_{n_R} + \frac{\text{CSNR}}{n_T} \mathbf{H}\mathbf{H}^H \right) \right]. \quad (5.11)$$

Once the MIMO capacity is known, we can easily calculate the OPTA of an analog MIMO transmission system using the following equality

$$2Nn_T R(D) = KC_E(\text{CSNR}), \quad (5.12)$$

where $R(D)$ is the rate distortion function of the analog source while N and K represent the bandwidth of the source and the channel, respectively. Like the case of single-antenna systems, this equation comes from equating the rate distortion function and the channel capacity but now the number of real-valued source symbols transmitted per channel use is actually $(2n_T N)/K$. For the particular case of Gaussian sources and Mean Square Error (MSE) as distortion metric, the rate distortion function is given by Equation (2.10) and, therefore, the OPTA of a generic analog MIMO $n_T \times n_R$ system can be obtained from

$$2Nn_T \frac{1}{2} \log(\text{SDR}_{\text{opt}}) = KC_E(\text{CSNR}), \quad (5.13)$$

computing the optimal Signal-to-Distortion Ratio (SDR) as a function of the CSNR, i.e.

$$\text{OPTA} = \text{SDR}_{\text{opt}} = \exp\left(\frac{K}{Nn_T} C_E(\text{CSNR})\right) \quad (5.14)$$

Equivalently, the OPTA for Laplacian sources can be obtained using the lower bound given by Equation (2.13) for the rate distortion function, $R(D)$, i.e.

$$\text{OPTA} = \text{SDR}_{\text{opt}} \leq \frac{\pi}{e} \exp\left(\frac{K}{Nn_T} C_E(\text{CSNR})\right) \quad (5.15)$$

5.2.2 Channel Known at the Transmitter and Receiver

Let us now obtain the OPTA bound for analog JSCC MIMO systems when CSI is also available at the transmitter. In this case, the transmission system must be supplied with a feedback channel which through the channel estimation is sent from the receiver to the transmitter. Notice that this situation is practically feasible as long as the coherence time of the channel is larger than the feedback channel rate or, equivalently, if the wireless channel varies slowly enough in time.

For digital MIMO systems, the channel information at the transmitter can be exploited to optimally allocate the available power among the transmit antennas using the well-known water-filling algorithm [21]. This strategy has been shown to be optimal for this type of communications because it maximizes the system capacity. In our case, given that the performance of analog JSCC systems is measured in terms of distortion between the source and the received symbols, we propose to use the channel knowledge for designing an optimal linear precoder according to the MMSE criterion [53, 61], as we will see in Section 5.3.3. The OPTA for an analog JSCC MIMO system with a linear MMSE precoder \mathbf{P} can be calculated according to Equation (5.12) using the capacity of the equivalent channel $\mathbf{H}\mathbf{P}$ given by

$$C_E(\text{CSNR}) = \mathbb{E}_{\mathbf{H}} \left[\log \det \left(\mathbf{I}_{n_R} + \frac{\text{CSNR}}{n_T} \mathbf{H}\mathbf{P}\mathbf{P}^H \mathbf{H}^H \right) \right]. \quad (5.16)$$

The use of a linear precoder not only allows to exploit the channel knowledge at the transmitter, but also makes the separation of the data streams corresponding to different transmit antennas at the receiver possible when $n_T > n_R$. In this case, since the actual number of channel symbols transmitted per channel use is now limited by the number of receive antennas, n_R , the equality in Equation (5.12) becomes

$$2Nn_R R(D) = K C_E(\text{CSNR}). \quad (5.17)$$

5.3 Analog JSCC over MIMO Channels

In this section we focus on the design of analog JSCC schemes for MIMO wireless channels with n_T transmit and n_R receive antennas. The source symbols are first spatially multiplexed

over the n_T transmit antennas. At each transmit antenna i , $i = 1, \dots, n_T$, a vector \mathbf{x}_i of N analog source symbols is then encoded into one channel symbol s_i using the $N:1$ analog encoder described in Chapter 2. Notice that bandwidth reduction in this system setup is equal to Nn_T and, therefore, significant bandwidth reductions can be achieved when using multiple transmit antennas.

Initially, we assume that the channel is perfectly known at the receiver but unknown at the transmitter. Hence, the available power P_T is uniformly distributed among the n_T transmit antennas, so the radiated power at each antenna is P_T/n_T . The resulting channel symbols must be normalized to satisfy the power constraint using a factor γ_i , which can be different at each transmit antenna i . Then, the normalized symbols are sent over a frequency-flat MIMO fading channel. Thus, the observed symbols at the MIMO channel output are given by

$$\mathbf{y} = \mathbf{H}\mathbf{s} + \mathbf{n}, \quad (5.18)$$

where \mathbf{s} , \mathbf{y} and \mathbf{n} are the vectors that represent the analog channel symbols, the received symbols and the additive thermal noise, respectively.

As already commented, the performance of analog systems increases as the MSE between the source and decoded symbols decreases, hence the optimum receiver is the known MMSE receiver [55], which for this particular channel model is given by

$$\begin{aligned} \hat{\mathbf{x}}_{\text{MMSE}} &= \mathbb{E}[\mathbf{x}|\mathbf{y}] = \int \mathbf{x} p(\mathbf{x}|\mathbf{y}) d\mathbf{x} \\ &= \frac{1}{p(\mathbf{y})} \int \mathbf{x} p(\mathbf{y}|\mathbf{x}) p(\mathbf{x}) d\mathbf{x}, \end{aligned} \quad (5.19)$$

where \mathbf{x} represents the vector with the Nn_T source samples. Like in the single-antenna case, the conditional probability $p(\mathbf{y}|\mathbf{x})$ depends on the mapping function $M_\delta(\cdot)$. Hence, the integral in Equation (5.19) can only be calculated numerically because $M_\delta(\cdot)$ is discontinuous and highly non-linear. The complexity of the MMSE detector could become extremely high even for a small number of antennas, since it would involve the discretization of an Nn_T dimensional space.

As an alternative, we can extend the two-stage receiver described for SISO channels (see Section 2.3.3) to the MIMO case. Instead of directly calculating an MMSE estimate of the source symbols, we first obtain an estimate of the channel symbols transmitted from each antenna using a conventional MIMO detector, and then proceed to the ML decoding of the estimated channel symbols. In this work we will study two MIMO detectors: the MMSE linear detector and the MMSE Decision Feedback (DF) detector with ordering. The basic premise of these two detectors is to perform a spatial filtering of the observations to cancel the spatial interferences transforming the MIMO channel into n_T parallel SISO channels. Thereby, the analog JSCC encoding and decoding procedures can be applied straightforwardly.

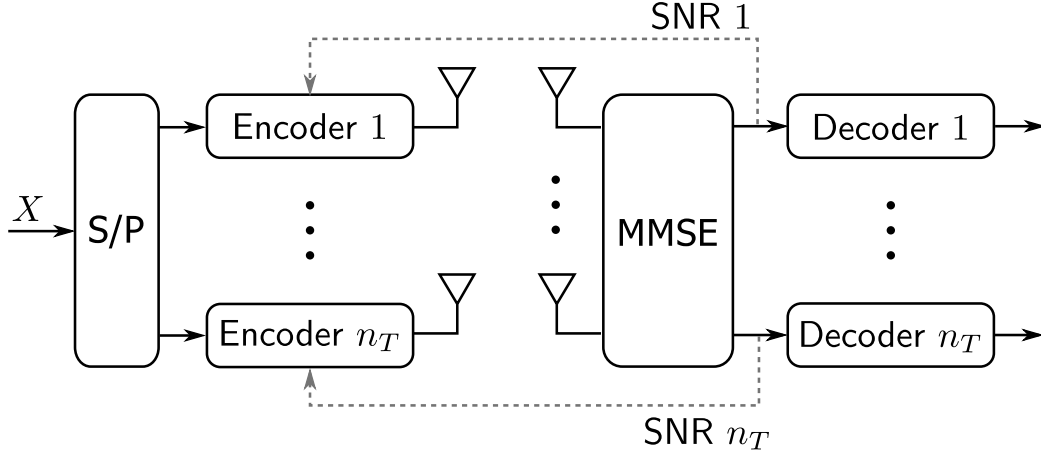


Figure 5.2: Analog MIMO JSCC system with MMSE linear detection.

Another important issue regarding the design of analog JSCC schemes is the optimization of the parameter δ at the MIMO transmitter. It is important to note that, like the normalization factors γ_i , the value of the parameter δ can be different at each transmit antenna i . As explained in Section 2.3.4, the overall performance of the analog scheme can be substantially improved if the δ_i values are properly optimized depending on the actual CSNR. In a MIMO transmission system, the CSNR at reception can be generally computed as

$$\text{CSNR}(\mathbf{H}) = \frac{\text{tr}(\mathbf{H}\mathbf{C}_s\mathbf{H}^H)}{\text{tr}(\mathbf{C}_n)} = \frac{P_T \text{tr}(\mathbf{H}\mathbf{H}^H)}{n_T n_R \sigma_n^2}.$$

If the MIMO fading channels are normalized so that $E_{\mathbf{H}}[\text{tr}(\mathbf{H}\mathbf{H}^H)] = n_T n_R$, the average CSNR is P_T/σ_n^2 . Unfortunately, the instantaneous CSNR continuously fluctuates over time when we are transmitting over fading channels. In that case, the optimal cost-distortion tradeoff can be closely approached if the parameters δ_i are continuously adapted to the channel variations by using the proper CSNR values to select the optimal analog encoders in the look-up Tables 2.1 or 2.2. Given that we assume that the channel is unknown at the transmitter side, it is necessary to estimate the actual CSNR value at the receiver and send it to the transmitter over a feedback channel. Notice that in such a case the coherence time of the channel must be larger than the feedback delay.

5.3.1 MIMO Decoding with MMSE Linear Detection

Figure 5.2 shows the block diagram of an analog JSCC MIMO transmission system with linear MMSE detection. The MMSE filter that minimizes the MSE between the channel symbol vector \mathbf{s} and the estimated symbol vector $\hat{\mathbf{s}} = \mathbf{W}\mathbf{y}$ is given by

$$\mathbf{W}_{\text{MMSE}} = (\mathbf{H}^H\mathbf{H} + \rho\mathbf{I}_{n_T})^{-1} \mathbf{H}^H, \quad (5.20)$$

where $\rho = (n_T\sigma_n^2)/P_T$. The filter \mathbf{W}_{MMSE} does not completely cancel the spatial interference of the MIMO channel, i.e. at \hat{s}_i the desired symbol s_i is corrupted by thermal noise and a residual

spatial interference from symbols transmitted over other antennas. Considering this residual spatial interference as Gaussian noise that adds to the thermal noise, it is shown in [133] that the equivalent CSNR at each output of the linear MMSE receiver can be computed as

$$\text{CSNR}_i = \frac{\mu_i^2}{\mu_i - \mu_i^2} = \frac{\mu_i}{1 - \mu_i}, \quad i = 1, \dots, n_T, \quad (5.21)$$

where $\mu_i = (\mathbf{W}_{\text{MMSE}}\mathbf{H})_{ii}$. Thus, the equivalent channel that comprises the concatenation of the MIMO channel and the linear MMSE receiver can be interpreted as a set of SISO parallel channels, each with an equivalent CSNR given by Equation (5.21). Each entry of the estimated symbol vector can be decoded independently using the analog JSCC decoding approach explained in Section 2.3.3.

It should be noticed that linear MMSE detection is optimum only when the channel symbols are Gaussian [64], which is not the case. Indeed, even when the sources are Gaussian, the analog JSCC mapping consists in a non-linear transformation that produces non-Gaussian channel symbols. It is possible to formulate the optimum non-linear MMSE detector, but this requires knowledge of the channel symbols probability $p(\mathbf{s})$ and the calculation of an integral similar to that in Equation (5.19). Notice the extraordinary complexity of the optimum non-linear MMSE detector. Firstly, $p(\mathbf{s})$ has to be discretized and estimated using Monte Carlo methods since it is not possible, in general, to find an analytical expression for $p(\mathbf{s})$. When considering fading channels, knowledge of $p(\mathbf{s})$ is particularly difficult since it depends on the analog JSCC parameters which in turn change with the CSNR. Moreover, the non-linear MMSE detection integral has to be computed numerically which requires a refined discretization of $p(\mathbf{s})$ to approach optimality. In the ensuing subsection we investigate the utilization of a non-linear receiving structure for analog JSCC over MIMO channels that, although suboptimal, outperforms linear MMSE detection while keeping complexity at a low level.

5.3.2 MIMO Decoding with Decision Feedback Detection

Figure 5.3 plots the block diagram of an analog JSCC MIMO transmission system with a Decision Feedback (DF) receiver. Both the Feed Forward (FF) and the Feed Backward (FB) filters are optimized according to the MMSE criterion. The FF filter is obtained from the Cholesky factorization of

$$\mathbf{H}^H\mathbf{H} + \rho\mathbf{I}_{n_T} = \mathbf{L}^H\mathbf{\Delta}\mathbf{L},$$

where \mathbf{L} is an $n_T \times n_T$ lower triangular matrix and $\mathbf{\Delta}$ is an $n_T \times n_T$ diagonal matrix. If we define the whitening filter $\mathbf{B}^H = \mathbf{\Delta}^{-1}\mathbf{L}^{-H}$, the FF filter is the product of the matched and whitening filters, i.e. $\mathbf{W}_{\text{MMSE}}^{\text{DF}} = \mathbf{B}^H\mathbf{H}^H$. Hence the overall response of the FF filter and the channel is

$$\mathbf{W}_{\text{MMSE}}^{\text{DF}}\mathbf{H} = \mathbf{L} - \rho\mathbf{\Delta}^{-1}\mathbf{L}^{-H}. \quad (5.22)$$

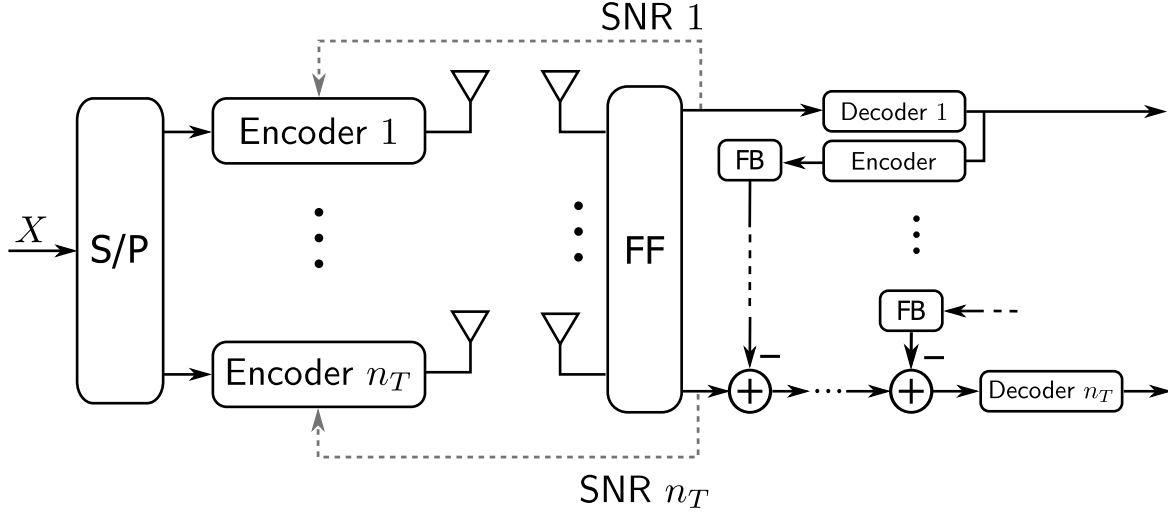


Figure 5.3: Analog MIMO JSCC system with Decision Feedback detection.

In order to simplify the derivation of the DF receiver, we will assume that there are no decoding errors. Under this assumption, the spatially causal component of the interference in Equation (5.22) can be successively removed with the FB filter $(\mathbf{L} - \mathbf{I}_{n_T})$ without altering the noise statistics at the decoder inputs. An advantage of analog JSCC is that there is no delay in the encoding and re-encoding steps which significantly simplifies the implementation of DF MIMO receivers.

Similarly to the case of linear detection, we assume the instantaneous CSNR at the filter output is known at the transmitter thanks to the existence of a feedback channel (see Figure 5.3). This allows the continuous update of the δ_i parameter according to the look-up Tables 2.1 or 2.2. It can be shown (see Appendix A) that Equation (5.21) is also valid in this case to calculate the CSNR value of each equivalent SISO channel with

$$\begin{aligned} \mu_i &= (\mathbf{B}^H \mathbf{H}^H \mathbf{H} - \mathbf{L} + \mathbf{I}_{n_T})_{ii} \\ &= (\mathbf{I}_{n_T} - \rho \mathbf{\Delta}^{-1} \mathbf{L}^{-H})_{ii}. \end{aligned} \quad (5.23)$$

Notice that decoding ordering is important and significantly impacts on the performance of DF MIMO receivers [37]. Ordering can be interpreted as a permutation of the columns of the MIMO channel matrix, i.e. $\bar{\mathbf{H}} = \mathbf{H}\mathbf{P}$, where \mathbf{P} is a permutation matrix. Conversely to [37], the optimum ordering in our case is the one that minimizes the MSE at the decoder inputs, i.e.

$$\begin{aligned} \text{MSE} &= \rho \text{tr} (\mathbf{\Delta}^{-1} (\mathbf{I}_{n_T} - \rho \mathbf{L}^{-H} \mathbf{L}^{-1} \mathbf{\Delta}^{-1})) \\ &\approx \rho \text{tr} (\mathbf{\Delta}^{-1}), \end{aligned} \quad (5.24)$$

where the approximation holds when $\sigma_n^2 \ll 1$. Thus, the optimum ordering is given by

$$\mathbf{P}_{\text{opt}} = \arg \min_{\mathbf{P}} \rho \text{tr} (\bar{\mathbf{\Delta}}^{-1}), \quad (5.25)$$

where $\bar{\Delta}$ results from the Cholesky factorization of $\bar{\mathbf{H}}^H \bar{\mathbf{H}} + \rho \mathbf{I}_{n_T}$. This optimization problem can be readily solved by searching over the $n_T!$ possible permutation matrices and selecting the one that minimizes the MSE cost function given by Equation (5.24). This ordering procedure is specially adequate for high CSNRs ($\sigma_n^2 \ll 1$) but, in practice, computer simulations have shown that, in the medium and low CSNR regime, the same ordering results are obtained when considering either the exact or the approximate expression in Equation (5.24).

5.3.3 Linear MMSE Precoding

If CSI is assumed to be also available at transmission, further performance improvements can be attained if channel symbols are precoded prior to their transmission over the MIMO channel. In conventional digital systems, it is well-known that the water-filling algorithm [21] optimally distributes the available power among the transmit antennas in order to maximize the data throughput. As previously mentioned, the water-filling solution is not necessarily the optimal strategy for power allocation in analog JSCC systems since the objective is to minimize the signal distortion. For that reason, we propose to jointly calculate the linear transmit and receive filters that optimize the system performance [52, 88, 104]. Specifically, we opt to design the linear precoder and its corresponding detector following the MMSE criterion and according to a transmit power constraint, as shown in [53, 105]. Notice that this approach is more suitable for our analog JSCC MIMO model since the overall performance is directly determined from the MSE between the source and decoded symbols.

Let \mathbf{P} be the linear precoder and \mathbf{W} the linear detector, respectively. The channel symbol estimates obtained at the detector output are given by

$$\hat{\mathbf{s}} = \mathbf{W}(\mathbf{H}\mathbf{P}\mathbf{s} + \mathbf{n})$$

and, thus, the error vector between the estimated and transmitted symbols can be computed as

$$\mathbf{e} = \|\mathbf{s} - \hat{\mathbf{s}}\| = \|\mathbf{s} - \mathbf{W}(\mathbf{H}\mathbf{P}\mathbf{s} + \mathbf{n})\|. \quad (5.26)$$

The linear MMSE precoder and detector are obtained after solving the following constrained optimization problem

$$\arg \min_{\mathbf{P}, \mathbf{W}} \mathbb{E}[\text{tr}(\mathbf{e}\mathbf{e}^H)] \quad \text{s.t.} \quad \text{tr}(\mathbf{P}\mathbf{P}^H) \leq P_T, \quad (5.27)$$

where P_T is the total power available at the transmitter. Substituting the error expression given by Equation (5.26) into Equation (5.27), we obtain the following expression for the MSE

$$\begin{aligned} \xi &= \mathbb{E}[\text{tr}(\mathbf{e}\mathbf{e}^H)] = \mathbb{E}[\text{tr}\{(\mathbf{s} - \mathbf{W}[\mathbf{H}\mathbf{P}\mathbf{s} + \mathbf{n}])(\mathbf{s} - \mathbf{W}[\mathbf{H}\mathbf{P}\mathbf{s} + \mathbf{n}])^H\}] \\ &= \mathbb{E}[\text{tr}\{(\mathbf{s}\mathbf{s}^H) - (\mathbf{W}\mathbf{H}\mathbf{P}\mathbf{s}\mathbf{s}^H) - (\mathbf{W}\mathbf{n}\mathbf{s}^H) - (\mathbf{s}\mathbf{s}^H\mathbf{P}^H\mathbf{H}^H\mathbf{W}^H) + \\ &\quad + (\mathbf{W}\mathbf{H}\mathbf{P}\mathbf{s}\mathbf{s}^H\mathbf{P}^H\mathbf{H}^H\mathbf{W}^H) + (\mathbf{W}\mathbf{n}\mathbf{n}^H\mathbf{W}^H)\}]. \end{aligned}$$

Due to the linear nature of the expectation operator, we can split the previous expression in its individual terms. In addition, the resulting equation can be simplified given that the transmitted symbols and the noise are assumed to be uncorrelated, i.e. $\mathbb{E}[\mathbf{sn}^H] = \mathbb{E}[\mathbf{n}^H \mathbf{s}] = \mathbf{0}$, while the autocovariance matrices must now satisfy $\mathbb{E}[\mathbf{ss}^H] = \mathbf{I}_{n_T}$ and $\mathbb{E}[\mathbf{nn}^H] = \sigma_n^2 \mathbf{I}_{n_R}$. Thus, the quadratic error expression is given by

$$\xi = \mathbb{E} \left[\text{tr} \left\{ \mathbf{I}_{n_T} - (\mathbf{WHP}) - (\mathbf{P}^H \mathbf{H}^H \mathbf{W}^H) + (\mathbf{WHPP}^H \mathbf{H}^H \mathbf{W}^H) + (\sigma_n^2 \mathbf{W} \mathbf{W}^H) \right\} \right].$$

In order to determine the linear precoder \mathbf{P} and the corresponding detector \mathbf{W} that minimize the MSE, the error expression is differentiated with respect to \mathbf{P}^H and \mathbf{W}^H and then equated to 0. Also, the well-know Karush-Kuhn-Tucker (KKT) conditions [70, 136] are used to guarantee the power constraint is satisfied, obtaining the following equations

$$\begin{aligned} \frac{d\xi}{d\mathbf{P}^H} &= -\mathbf{H}^H \mathbf{W}^H + \mathbf{H}^H \mathbf{W}^H \mathbf{WHP} + \lambda \mathbf{P} = 0, \\ \frac{d\xi}{d\mathbf{W}^H} &= -\mathbf{P}^H \mathbf{H}^H + \mathbf{WHPP}^H \mathbf{H}^H + \sigma_n^2 \mathbf{W} = 0, \end{aligned} \quad (5.28)$$

where $\lambda \geq 0$ is the Lagrange multiplier [26] that ensures the total transmit power is equal to P_T . Solving these equation with respect to \mathbf{P} and \mathbf{W} , respectively, the optimal linear MMSE filters are given by

$$\mathbf{P} = (\lambda \mathbf{I}_{n_T} + \mathbf{H}^H \mathbf{W}^H \mathbf{WH})^{-1} (\mathbf{H}^H \mathbf{W}^H), \quad (5.29)$$

$$\mathbf{W} = (\mathbf{P}^H \mathbf{H}^H) (\sigma_n^2 \mathbf{I}_{n_R} + \mathbf{HPP}^H \mathbf{H}^H)^{-1}. \quad (5.30)$$

At first sight, since both equations depend on each other we can use the idea of alternating optimization [14] to state an iterative algorithm that calculates both filters jointly. Thus, we start assuming an initial precoder equal to the identity matrix and, at each iteration, both the detector and the precoder are sequentially updated using Equations (5.29) and (5.30). Notice that the Lagrange multiplier λ should be recalculated at each iteration –using for example the Newton’s method– to ensure that the transmit power constraint is still satisfied. Although the convergence of this algorithm has not been mathematically analyzed, it has been shown to converge after a few iterations in practice for the whole range of CSNRs.

Alternatively, an explicit solution for Equations (5.29) and (5.30) can be directly computed by assuming a Single Value Decomposition (SVD) of the MIMO channel, \mathbf{H} . The procedure used to jointly calculate the two linear filters for the proposed analog MIMO scheme is detailed in Appendix B. The precoder and detector obtained according to the explicit solution have been shown to achieve a identical performance than that of the iterative case. In addition, the complexity and delay introduced by the explicit solution are practically negligible with respect to the iterative procedure which introduces a certain latency until the algorithm converges.

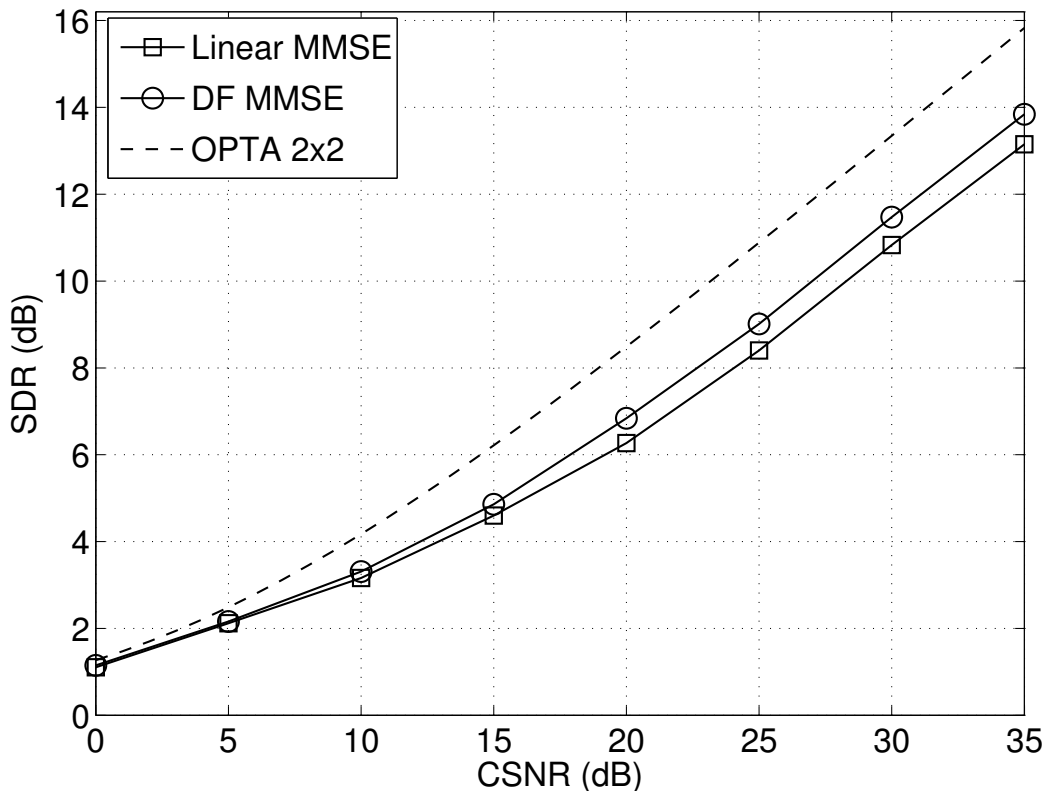


Figure 5.4: Performance of 2:1 analog JSCC over 2×2 MIMO Rayleigh channels: Gaussian source.

5.4 Experimental Results

In this section we present the results of several computer experiments carried out to assess the performance of analog JSCC transmissions over MIMO flat-fading channels in different situations. We first consider the general model described in Section 5.3, where the analog JSCC MIMO system performs a 2:1 bandwidth compression of the source samples and employs either MMSE linear detection or DF detection at the receiver. Initially, we focus on the symmetrical case, i.e. $n_T = n_R$, and assume that CSI is not available at the transmitter.

Some modifications on this basic configuration of the analog MIMO scheme are later addressed in subsequent sections: different compression rate, unequal number of transmit and receive antennas (asymmetrical case) and, finally, the use of real fading channels which were obtained after a measurement campaign carried out in a multiuser indoor scenario.

5.4.1 Symmetrical MIMO Rayleigh Channels

In this subsection we focus on the case of symmetrical MIMO transmission systems. Specifically, we consider $n_T = n_R = 2$ and $n_T = n_R = 4$ transmit and receive antennas. Two types of source distributions are evaluated: Gaussian and Laplacian. These distributions are typically encountered in practical applications such as image transmission or Compressive Sensing [54].

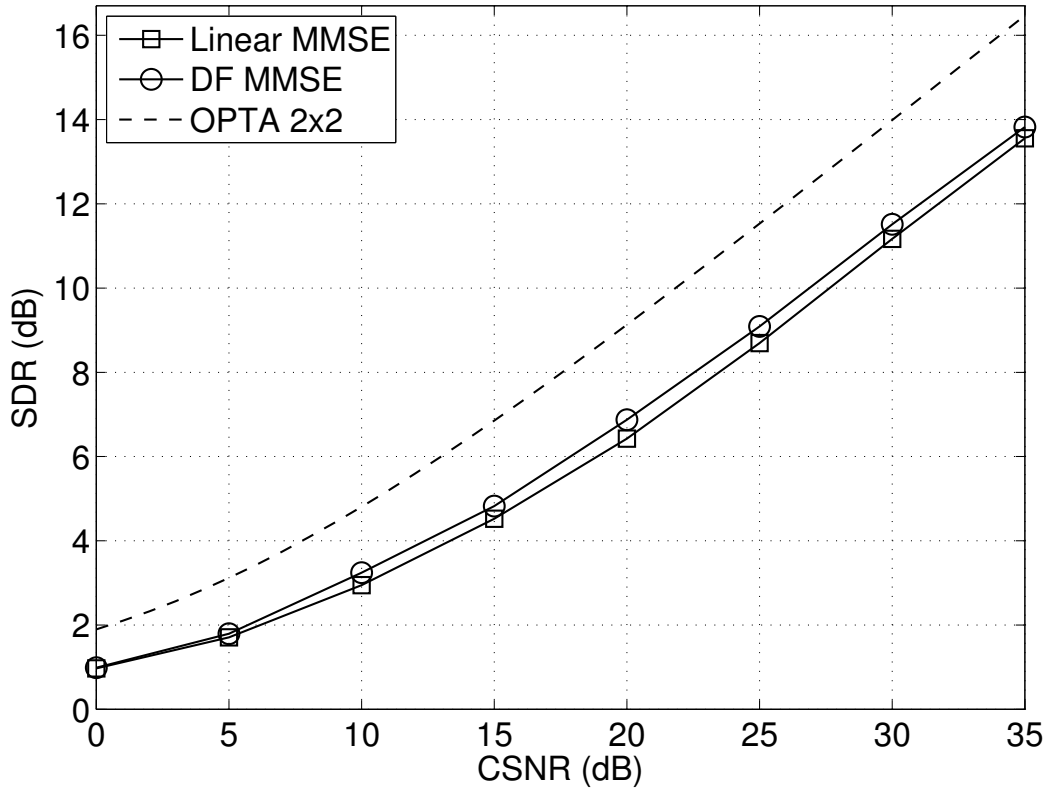


Figure 5.5: Performance of 2:1 analog JSCC over 2×2 MIMO Rayleigh channels: Laplacian source.

The MIMO channels are synthetically generated with random numbers obtained from a computer program. In particular, we emulate ergodic spatially white MIMO Rayleigh fading channels whose entries h_{ij} are realizations of complex-valued zero-mean circularly-symmetric Gaussian independent and identically distributed (i.i.d.) random variables.

Figures 5.4 and 5.5 show the performance results obtained for a 2:1 bandwidth reduction analog JSCC system over 2×2 MIMO Rayleigh channels with Gaussian and Laplacian source symbols, respectively. The SDR versus CSNR performance curves for the two analog JSCC MIMO receivers described in Section 5.3, together with the OPTA, are plotted in each figure. It can be seen that, for Gaussian sources, the SDR obtained with DF MIMO receivers is 2 dB below the OPTA, while the SDR obtained with linear MMSE MIMO receivers is 3 dB below the OPTA, thus DF MIMO receivers produce a distortion that is 1 dB better than that obtained with linear MIMO receivers. For Laplacian sources, DF MIMO receivers perform only slightly better than linear MIMO receivers. The SDR distance to the OPTA is about 2.5 dB in both cases.

Figures 5.6 and 5.7 show the performance results obtained for a 2:1 compression analog JSCC system over 4×4 MIMO Rayleigh channels with Gaussian and Laplacian source symbols, respectively. Notice the similarity between the OPTA curves in Figures 5.4 - 5.5 (MIMO 2×2) and Figures 5.6 - 5.7 (MIMO 4×4) caused by the normalization of the MIMO fading channels, i.e. $\mathbb{E}_{\mathbf{H}} [\text{tr}(\mathbf{H}\mathbf{H}^H)] = n_T n_R$, as well as by the normalization of the channel symbols

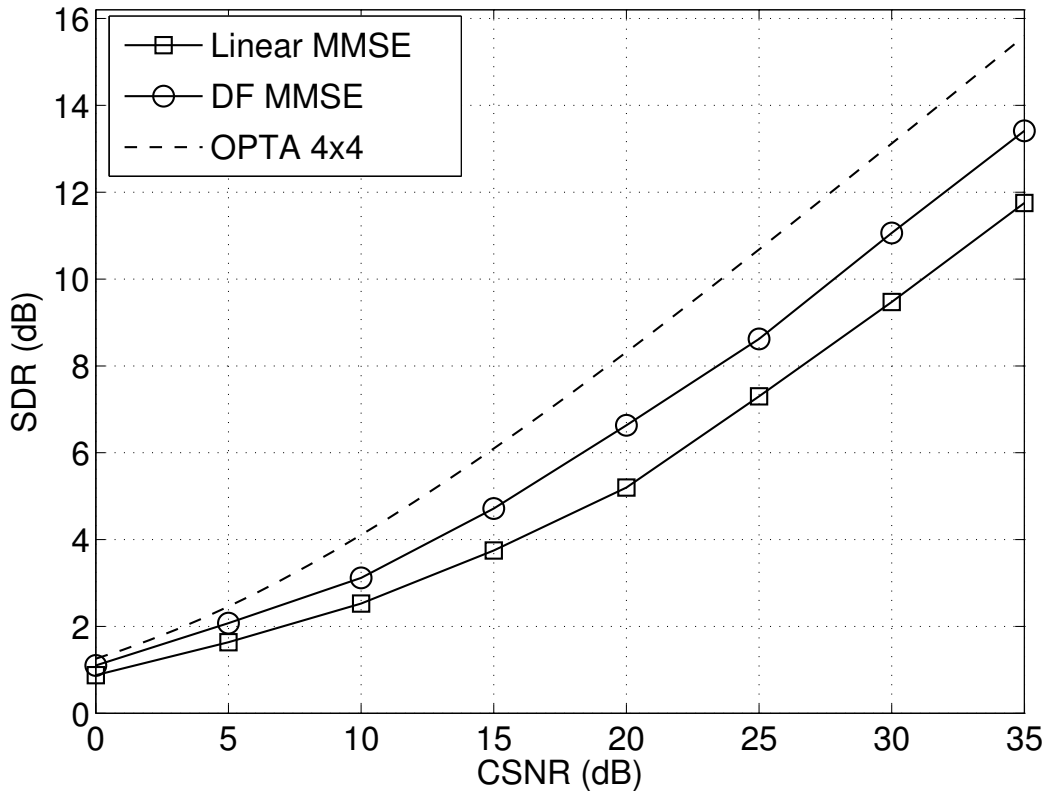


Figure 5.6: Performance of 2:1 analog JSCC over 4×4 MIMO Rayleigh channels: Gaussian source.

covariance matrix given by Equation (5.2).

As expected, performance differences between DF and linear MIMO receivers are significantly larger as the number of transmit and receive antennas increases. This gain is due to the higher impact of both the non-linear transformations carried out in the DF detection and the ordering procedure as the number of antennas is larger. It can be seen that, for Gaussian sources, the SDR obtained with DF MIMO receivers is 2 dB below the OPTA while this difference is 4 dB for linear receivers, i.e. DF MIMO receivers produce a distortion that is 2 dB better than that obtained with linear MIMO receivers. For Laplacian sources, the performance of the proposed MIMO receivers is slightly worse than in the case of Gaussian sources: the distortion obtained with DF and linear MIMO receivers is 3 dB and 4.2 below the OPTA, respectively. Yet, DF MIMO receivers clearly outperform linear MIMO receivers yielding a 1.2 dB better SDR.

5.4.2 Compression Rate 3:2

In this subsection, we assess the performance of the analog MIMO system using the same configuration as in the previous section although, in this case, the bandwidth compression rate is set to 3:2. Thus, we consider a symmetrical MIMO system transmitting analog source samples over synthetically generated Rayleigh fading channels. The source samples are assumed to be Gaussian distributed and they are encoded according to the specified rate 3:2. This rate can

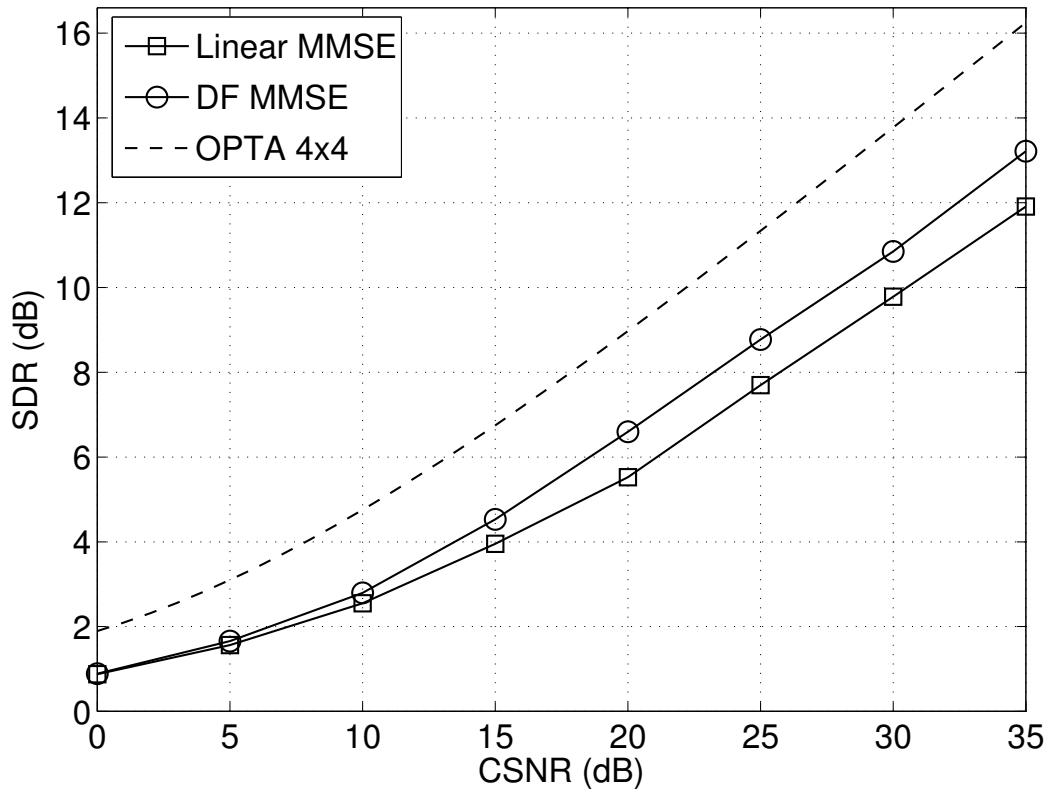


Figure 5.7: Performance of 2:1 analog JSCC over 4×4 MIMO Rayleigh channels: Laplacian source.

be easily achieved if two source samples are compressed using an 2:1 analog encoder whereas other source sample is directly transmitted. The available power must be properly distributed with a power allocation module (see 2.3.1.1).

Simulation results are presented in Figures 5.8 and 5.9 for 2×2 and 4×4 MIMO systems, respectively. The performance curves of the two proposed MIMO receivers – linear MMSE and DF detector –, together with the corresponding OPTA, are plotted again in each figure. Notice that the OPTA of analog JSCC MIMO systems when the compression rate is 3:2 is logically larger than that of the 2:1 case, because the compression rate is lower and, therefore, we can achieve a lower distortion level if the information is transmitted at the same data rate (in terms of symbols per channel use). As observed, the attained results with a 3:2 compression rate reinforce the conclusions drawn in the previous section for a 2:1 rate. The DF performance remains about 1 dB above with respect to that of the linear MIMO receiver for the 2×2 MIMO case, whereas the gap between both performance curves rises up to more than 2 dB for 4×4 MIMO. Thus, performance differences between DF and linear MIMO receivers are larger again as the number of transmit and receive antennas increases.

However, the two performance curves are significantly further from the OPTA limit in both considered cases. The performance degradation can be motivated by the fact that the power distribution at the transmitter is individually performed at each antenna using the power allocation module optimally designed for a SISO system. The utilization of this allocation

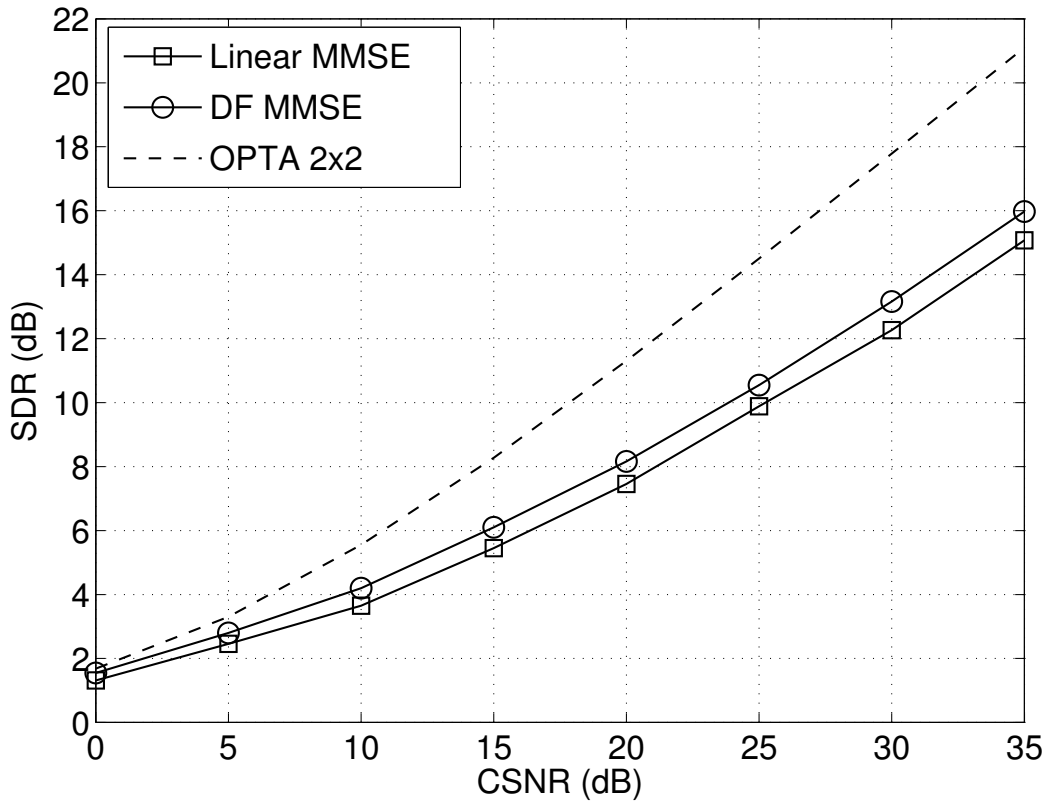


Figure 5.8: Performance of 3:2 analog JSCC over 2×2 MIMO Rayleigh channels with Gaussian sources.

strategy is chosen because its simplicity and low complexity with respect to other alternatives such as, for example, the derivation of the specific expression for the optimal joint power allocation module for the analog MIMO system. Unfortunately, this mathematical development implies non-linear transformations over several variables that can be only solved by numerical methods and, in addition, the allocation module should be readjusted whenever the CSNR varies. Logically, the computational cost of this method is significantly higher and the resulting latency is not acceptable for analog JSCC communications. Indeed, the proposed analog MIMO scheme has been designed to be decoupled into a set of parallel SISO channels by channel equalization using the linear MMSE or DF detector.

The results obtained for Laplacian sources are not included in this section given that they are quite similar to the Gaussian case, so we think the performance of the analog JSCC MIMO system is conveniently illustrated for a 3:2 compression rate in Figures 5.8 and 5.9.

5.4.3 Asymmetrical MIMO Systems

So far, analog JSCC has been shown to achieve good results over symmetrical MIMO channels. However, we are also interested in assessing the performance of this transmission technique when the number of transmit and receive antennas is different. In this subsection we consider the transmission of analog samples over asymmetrical MIMO channels with $n_T \neq n_R$. Specifically,

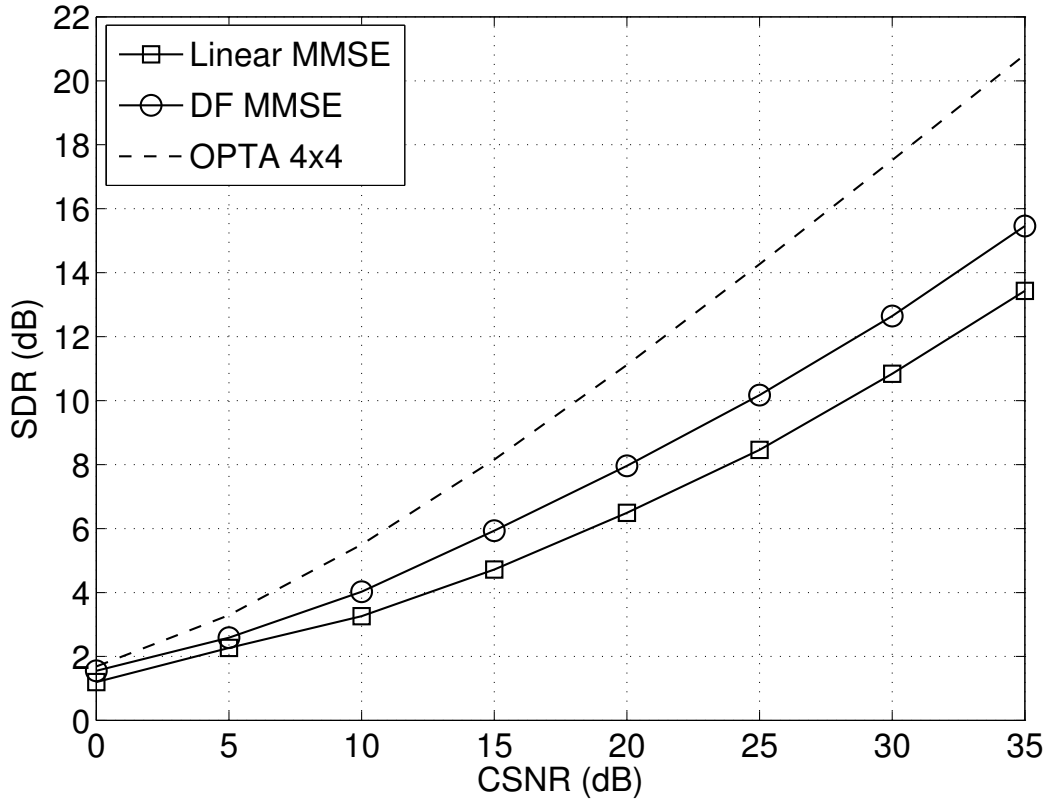


Figure 5.9: Performance of 3:2 analog JSCC over 4×4 MIMO Rayleigh channels with Gaussian sources.

we will focus on the case that the number of transmit antennas is larger than the number of receive antennas, i.e. $n_T > n_R$. The opposite case, $n_T < n_R$, is not addressed in this thesis since a simple combination of the received signals (for example using the Maximal-Ratio Combining (MRC) method) allows us to exploit the spatial diversity of the MIMO channel, reaching a good system performance with low complexity.

However, when $n_T > n_R$, the transmission model implementation is not immediate. We need to combine the n_T channel symbols in some way with the aim of recovering them later at the receiver in spite of the fading introduced by the channel. An interesting solution is to extend the general analog JSCC MIMO scheme to add a precoder at the transmitter, which cleverly combines the channel symbols while exploiting the channel information. As explained in Section 5.3.3, a linear MMSE precoder –and its corresponding detector– can be calculated for the proposed analog MIMO model if the CSI is also available at the transmitter. Hence, we now need to feedback not only the CSNR information but the complete CSI.

The source samples are first generated from a Gaussian distribution and then compressed with the 2:1 analog encoder. The resulting channel symbols are now combined by using a linear MMSE precoder and sent then over synthetical randomly-generated fading channels. At the receiver, a linear MMSE filter is employed to recover the transmitted channel symbols which are used by the ML decoder to produce the estimates of the source samples.

Figures 5.10 and 5.11 show the obtained results for 4×1 and 4×2 MIMO systems,

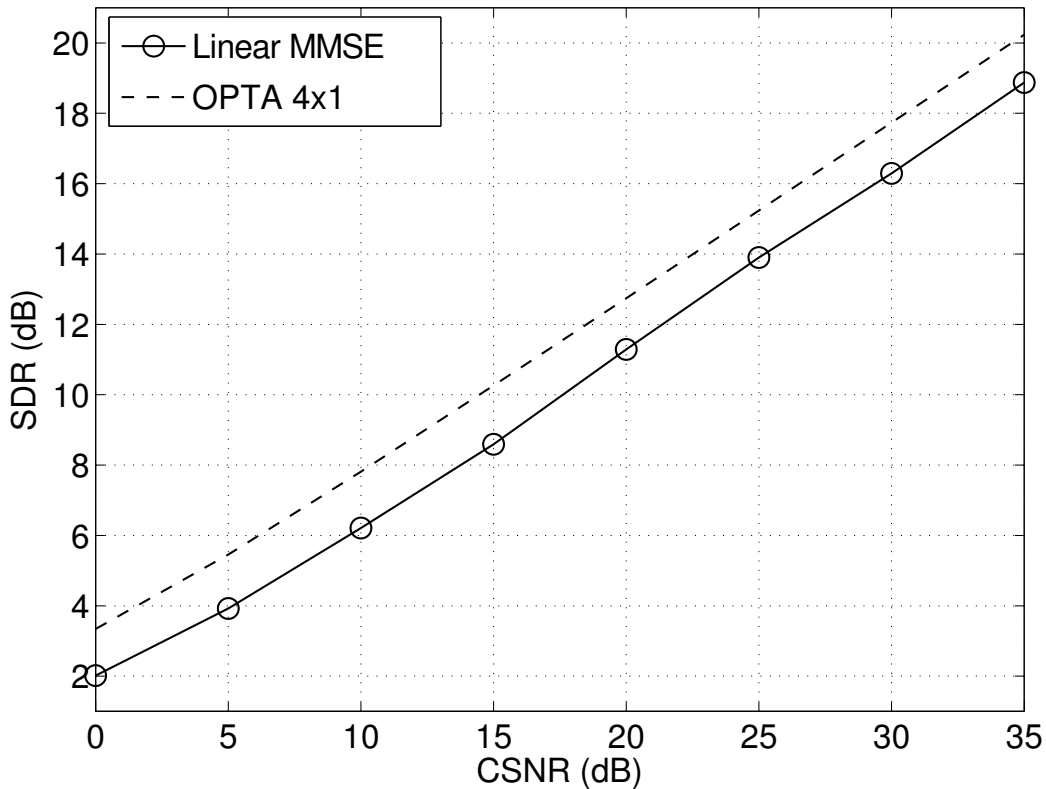


Figure 5.10: Performance of 2:1 analog JSCC over 4×1 MIMO Rayleigh channels.

respectively. In this case, one single performance curve –corresponding to the joint linear MMSE precoder and detector– is presented in the figures. The other alternative consists in designing the optimal non-linear precoder for the DF detector. Nevertheless, the design of the non-linear precoder and the DF detector must be jointly addressed so that it is not clear the feasibility of this model in practical JSCC systems because of its huge complexity.

The OPTA bound for the analog MIMO system with linear precoding is recalculated according to Equation (5.16) and plotted in each figure. As observed, the OPTA in asymmetrical systems is considerably higher than that of the symmetrical 4×4 case. The explanation of this fact is easy and intuitive: the capacity of a MIMO channel is clearly larger if the channel is known at the transmitter so, consequently, the OPTA will be also larger. On the other hand, the transmission rate is given by the factor $\max[n_T, n_R]$, which actually determines the number of channel symbols transmitted per channel use. In 4×4 MIMO systems, 4 channel symbols are transmitted per channel use whereas this number is smaller for an asymmetrical system with $n_R < 4$ receive antennas. The source information is hence transmitted at a lower rate and, therefore, the distortion of the received symbols will be lower.

In addition, both the 4×1 system and the 4×2 MIMO system exhibit a better performance than that of the symmetrical case due in part to the same reason. It is also worth noting that the distance between the performance curve and the OPTA bound significantly decreases to even less than 1 dB for asymmetrical systems. This improvement is motivated by the use of the channel

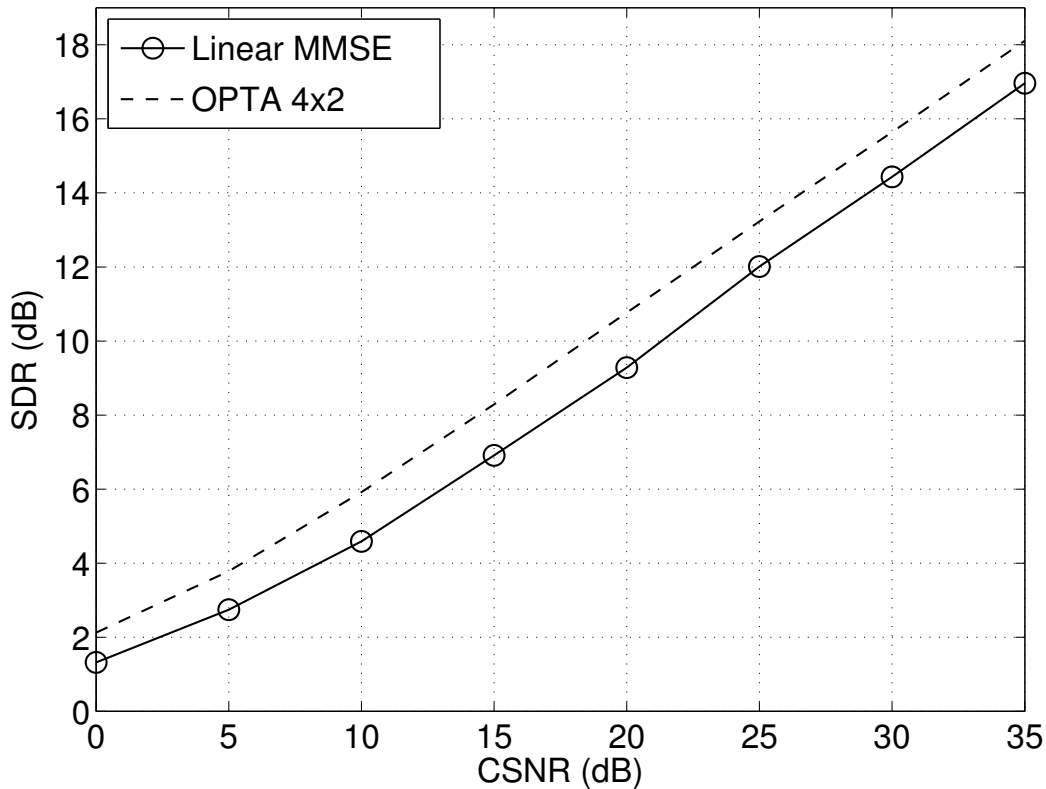


Figure 5.11: Performance of 2:1 analog JSCC over 4×2 MIMO Rayleigh channels.

knowledge at the transmitter to combine the transmitted symbols in order to exploit the diversity provided by the channel at reception. Thus, the proposed analog JSCC MIMO scheme using the optimal linear MMSE filters closely approaches the theoretical bounds for asymmetrical systems, and more sophisticated and huge complexity strategies (such as non-linear precoder and DF detector) can barely outperform this approach.

5.4.4 Real Indoor Channels

In order to get a more complete assessment of the analog JSCC MIMO scheme presented in this chapter, we carried out a series of computer experiments considering real wireless channels instead of the synthetically-generated Rayleigh channels employed so far. These real channels were measured from an indoor scenario by using the GTEC MIMO testbed described in Chapter 4. Figure 5.12 shows a picture of the setup where the location of the different transmitters and receivers is clearly appreciated. As observed, the testbed consists of three transmit and three receive nodes each equipped with MIMO capabilities. A number of 5844 2×2 MIMO channel realizations were obtained after the measurement campaign. These data are freely available to the research community and can be downloaded from the COMONSENS project web page [93]. In this same web address there is a detailed description of the setup and the measurement campaign from which the real channels were obtained.

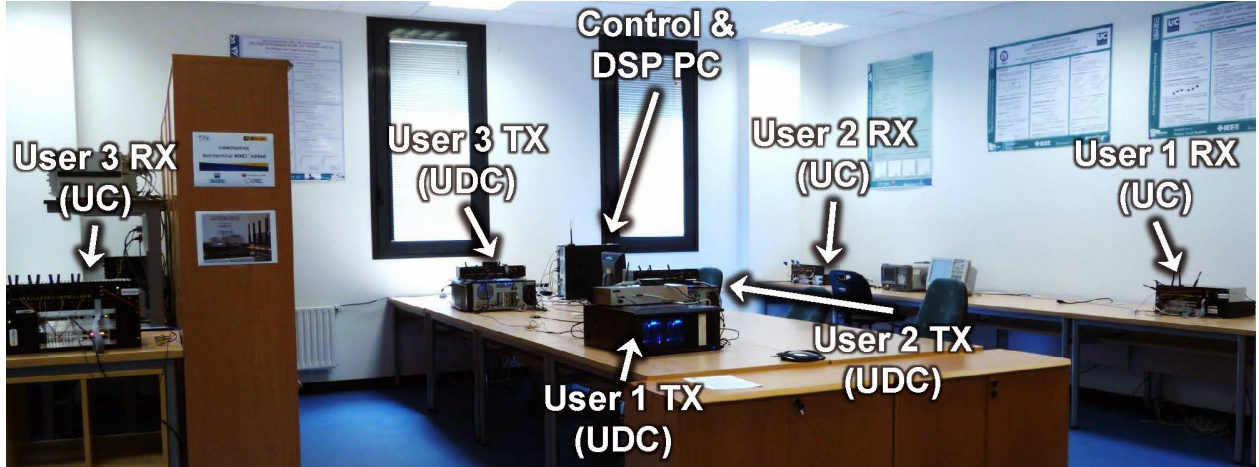


Figure 5.12: Picture of the real indoor scenario setup during measurement campaign.

Figures 5.13 and 5.14 plot the performance results for the proposed scheme when transmission is performed over real measured indoor 2×2 MIMO channels with Gaussian sources and Laplacian sources, respectively. The resulting distortion when using DF detection is within 1 dB from the OPTA for Gaussian sources, and within 2 dB for Laplacian sources. Contrarily to the synthetic case, a significant improvement in performance (2 dB) is obtained when using DF MIMO detection rather than linear MIMO detection for both Gaussian and Laplacian sources.

5.5 Conclusions

The feasibility of analog JSCC transmissions over MIMO fading channels has been evaluated in this chapter. In particular, an analog JSCC MIMO system has been designed for the transmission of discrete-time analog samples over wireless channels. At the transmitter, the source symbols are spatially multiplexed over n_T transmit antennas and then encoded at each antenna using the analog encoder based on the Archimedes' spiral. At the receiver, the analog MIMO scheme extends the design of the low complexity two-stage receiver presented for AWGN channels in Chapter 2 to the case of MIMO transmissions. Specifically, we consider two different types of filters in the first stage of the receiver structure: linear MMSE detection and Decision Feedback (DF).

Like in the case of SISO channels, we must first determine the OPTA for analog MIMO communications in order to establish an upper bound for the system performance. Next, we have evaluated the proposed analog JSCC schemes in different situations depending on the number of transmit and receive antennas or the compression rate. For asymmetrical MIMO systems where the number of transmit antennas is larger than the number of receive antennas, we have calculated the optimal linear precoder and its corresponding detector that minimize the distortion of the received signal. The utilization of linear MMSE filters is supported by

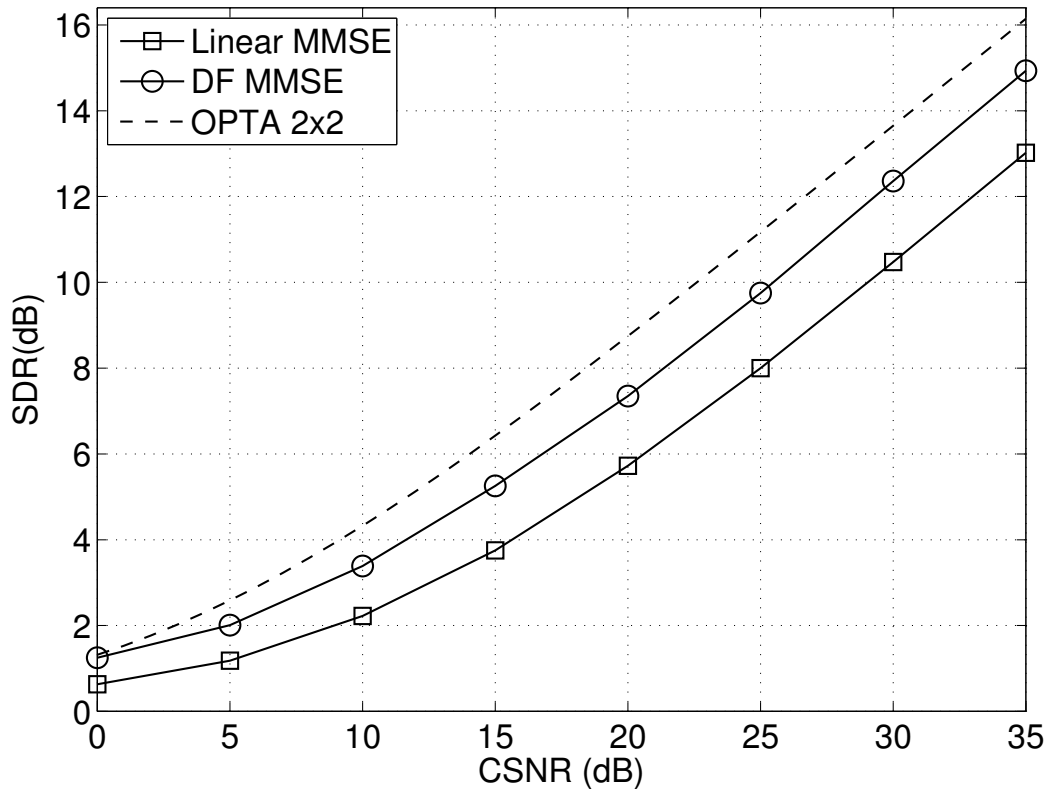


Figure 5.13: Performance of 2:1 analog JSCC over indoor measured 2×2 MIMO channels: Gaussian source.

the fact that the performance of analog JSCC systems is improved as the MSE between the source and the decoded symbols is minimized. Finally, a series of computer experiments have also carried out to assess the practical utility of analog JSCC MIMO transmissions over real wireless channels measured from an indoor scenario.

The promising results of the computer simulations support the use of analog JSCC for the MIMO transmission of analog sources over fading channels. In particular, DF MMSE MIMO receiver provides a better overall performance than that of the linear MMSE detector in the different evaluated scenarios. This performance improvement is more perceptible as the number of antennas increases as well as when considering real indoor channels. Both receivers approach the OPTA limit specially for the case of a 2:1 compression whereas the system performance seems to degrade for lower transmission rates (e.g. 3:2) due to the use of a suboptimal low complexity power allocation strategy. On the other hand, asymmetrical MIMO schemes requires a linear precoder at the transmitter which is designed according to the MMSE criterion. The proposed scheme exhibits an excellent performance that is only about 1 dB below the OPTA curve.

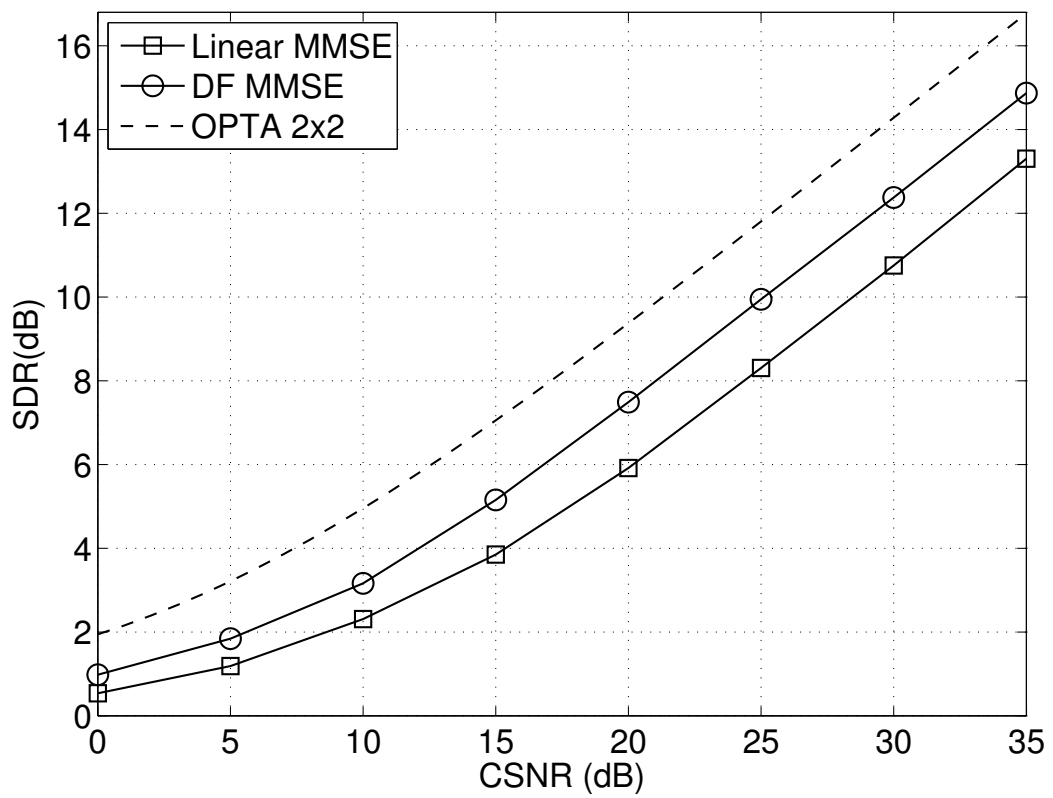


Figure 5.14: Performance of 2:1 analog JSCC over indoor measured 2×2 MIMO channels: Laplacian source.

Chapter 6

Analog JSCC for OFDM Systems

In the previous chapter, we considered analog Joint Source Channel Coding (JSCC) techniques over sufficiently narrowband channels in such a manner that the multipath delay spread only occurs during one symbol period and, hence, the InterSymbol Interference (ISI) can be disregarded. In general, this model is not very realistic since the users of the current wireless applications demand increasingly high data rates so that the symbols period has to be shortened and the narrowband assumption no longer holds. In this case, the ISI caused by multipath propagation can cause a severe degradation of the system performance.

When considering single-carrier transmission schemes, the wideband wireless applications demand time-domain equalization at the receiver to combat the delay spread effects. However, the number of taps required for an equalizer to ensure a good performance in a high data rate transmission is typically large. Thus, these equalizers are quite complex and can introduce large delay. In order to overcome these drawbacks, a different paradigm of communication based on multi-carrier modulation arises as alternative to the traditional single-carrier transmission.

In this chapter, we analyze the performance of analog JSCC transmissions over frequency-selective channels using an Orthogonal Frequency-Division Multiplexing (OFDM) modulation. OFDM is a multi-carrier transmission scheme that splits a wideband channel into a set of non-interfering orthogonal narrowband subchannels. Thus, a multipath channel is transformed into multiple parallel flat-fading subchannels where the received symbols will not be affected by ISI and channel equalization is potentially simpler. The number of subcarriers must be chosen to ensure that each subchannel has a bandwidth smaller than the channel coherence bandwidth.

OFDM-based systems that communicate over wideband channels were first used in military radios in the late 1950s and early 1960s. In the literature, Chang [17] first introduced the idea of using parallel data transmission by means of Frequency Division Multiplexing (FDM) with overlapping subcarriers. Soon after, different studies about this new transmission scheme were carried out in a short time [18, 99], where the performance of several communication systems using OFDM was assessed. Since the 1990s, the use of OFDM has been extended

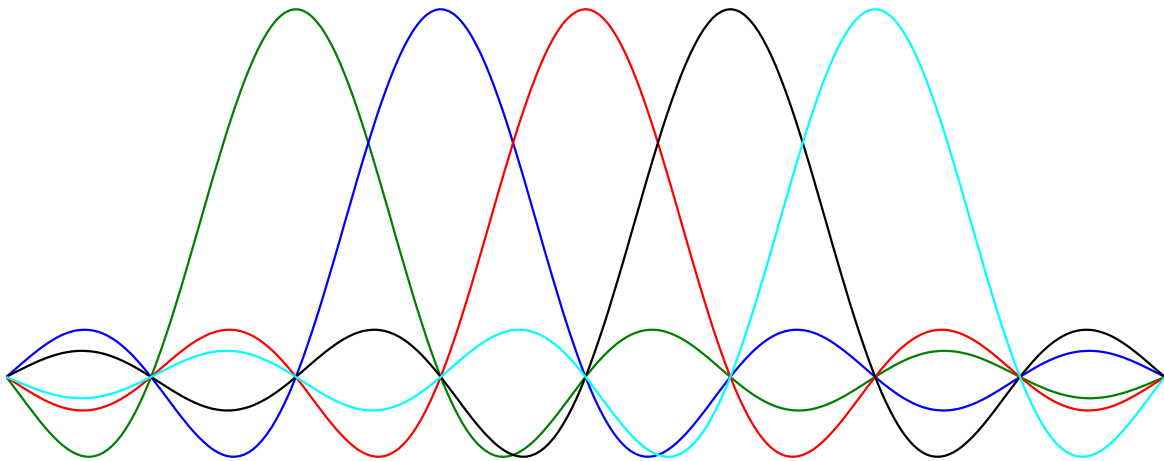


Figure 6.1: Example of the frequency spectrum of the orthogonal subcarriers.

to diverse wideband communications like Digital Audio Broadcasting (DAB), Digital Video Broadcasting (DVB) [102] as well as Wireless Local Network Areas (LANs) [5, 6].

Over the past years, OFDM has been widely shown to be a very promising strategy to enhance data rate, capacity and quality for broadband wireless systems over frequency-selective fading channels [117]. We can also combine an OFDM scheme with the use of multiple transmit and receive antennas (i.e. Multiple Input Multiple Output (MIMO) systems), resulting in a signaling method referred to as MIMO-OFDM. This transmission method has been adopted by the last generation of broadband wireless communication standards [7, 8] due to its ability to achieve large spectral efficiencies while enabling low complexity equalization of frequency-selective channels.

In this Chapter, the transmission of analog JSCC symbols using OFDM over MIMO frequency-selective fading channels is studied. First, we will briefly review the main characteristics of the OFDM modulation and present its strengths and impairments. We then propose a specific design for the analog MIMO-OFDM JSCC scheme and address certain important issues regarding the system optimization in order to improve the overall performance. Assuming channel knowledge at the receiver and/or at the transmitter, we can adapt the analog encoder parameters to the channel conditions or use optimal linear transmit and receive filters specifically designed for the MIMO-OFDM case. Finally, the results obtained for the different evaluated configurations of analog MIMO-OFDM systems are presented.

6.1 Description of OFDM Modulation

As previously introduced, OFDM is a multi-carrier scheme that effectively decomposes a wideband frequency-selective channel into a set of non-interfering parallel flat-fading

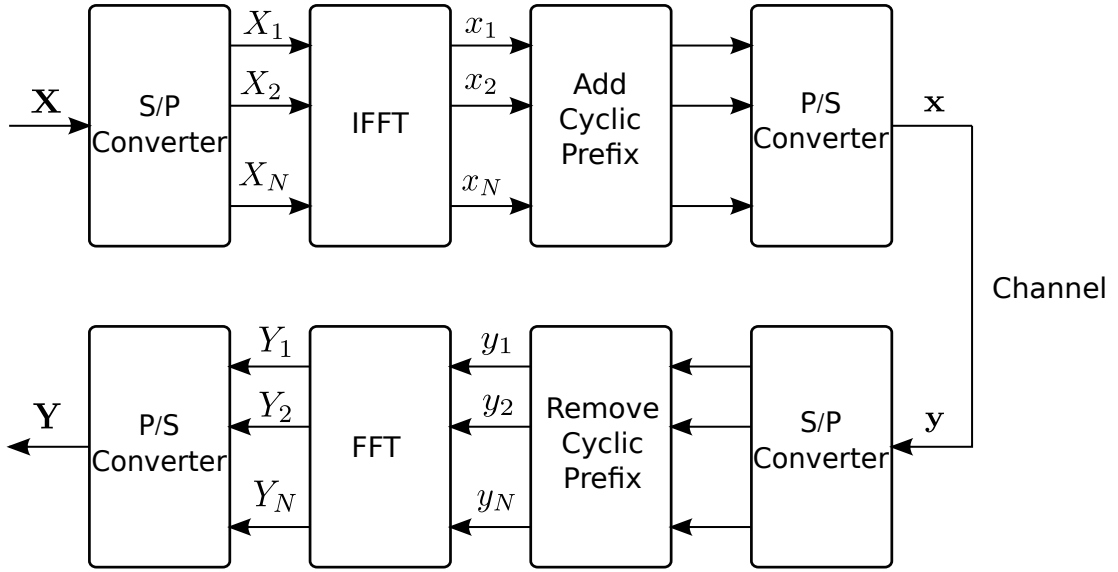


Figure 6.2: Practical implementation of OFDM modulation using FFT/IFFT and the cyclic prefix.

subchannels. This modulation splits the available spectrum into K orthogonal subcarriers in the frequency-domain (see Figure 6.1), which can be hence separated by the demodulator at the receiver.

Consequently, the data stream has to be transformed into K parallel substreams, each of which is modulated into one subcarrier at a low data rate and sent over the corresponding narrowband subchannel. Notice that an overall high spectral efficiency is achieved since the use of overlapped subcarriers allows us to simultaneously transmit the K substreams in the same OFDM symbol. The symbol period is enlarged by K times with respect to the single-carrier transmission and, thus, the ISI effects are substantially reduced.

Figure 6.2 shows the general block diagram of a system using OFDM modulation. Let f_s be the available bandwidth to transmit an OFDM symbol and, therefore, $T_s = 1/f_s$ is the symbol period. The subcarrier k is centered at the frequency

$$f_k = f_0 + k\Delta f,$$

where f_0 is the initial frequency and $\Delta f = 1/KT_s$ is the frequency separation between two contiguous subcarriers. If s_k , $k = 1, \dots, K$ represents the k -th input sequence, the corresponding OFDM signal can be generated as

$$s(t) = \frac{1}{\sqrt{T_s}} \sum_{k=1}^K s_k \exp(j2\pi f_k t) \quad 0 < t < T_s, \quad (6.1)$$

when using shifted rectangular pulses in the time-domain. In practice, the hardware effort of adjusting multiple local oscillators at the desirable frequencies f_k , $k = 1, \dots, K$, is very high. Moreover, small deviations on the subcarrier frequency offset can completely break down the orthogonality between subcarriers resulting in InterCarrier Interference (ICI). In order to

overcome this impairment, Weinstein and Ebert [134] proposed a practical implementation of OFDM using the Inverse Discrete Fourier Transform (IDFT) and the Discrete Fourier Transform (DFT) to perform baseband modulation at the transmitter and demodulation at the receiver, respectively. The IDFT operation preserves the orthogonality between the output sequences and avoids the use of multiple local oscillators. Also, the OFDM implementation is significantly simplified if the number of subcarriers K is a power of 2, since the highly efficient Inverse Fast Fourier Transform (IFFT) and Fast Fourier Transform (FFT) algorithms can be employed for modulation and demodulation, respectively.

Another key aspect of the OFDM implementation is the use of a guard interval to mitigate the effect of the delay spread. This guard interval –whose length should ideally exceed the maximum expected delay of the multipath channel –is added at the beginning of the OFDM symbol and it allows delayed versions of the previous symbols to die away before the useful information from the current symbol is recovered, hence completely removing the ISI. A large guard interval implies more robustness against the multipath, but it leads to an increase of the data overhead and, therefore, a lower spectral efficiency.

There exists other impairments that can cause the undesirable effect of ICI when OFDM is employed on wireless communications and frequency-selective fading channels. Among them, Doppler shifts, frequency offsets or timing synchronization errors can severely threaten the orthogonality of the OFDM subcarriers. Peled and Ruiz [91] solved these problems substituting the conventional null guard interval by a cyclic extension, more commonly referred to as Cyclic Prefix (CP). Thanks to the CP, the effect of the time-dispersive multipath channel becomes equivalent to a cyclic convolution of the transmitted OFDM symbol and the channel impulse response. The CP ensures the orthogonality over a time-dispersive channel and eliminates ISI completely between subcarriers as long as the guard period remains longer than the impulse response of the channel.

Other well-known problem of OFDM systems is the potential high Peak-to-Average Power Ratio (PAPR) of the modulated signals that linearly increases with the number of subcarriers. Additionally, a high PAPR requires high resolution for the Analog-to-Digital Converters (ADCs) and Digital-to-Analog Converters (DACs) since the dynamic range of the signals is much larger. In practice, this usually causes non-linear effects in the amplified OFDM signals due to the saturation of the amplifiers. There are several ways to reduce or tolerate the PAPR of the modulated symbols such as clipping of the OFDM signal above some threshold, peak cancellation with a complementary signal or correction of the non-linear distortion introduced by the amplifier.

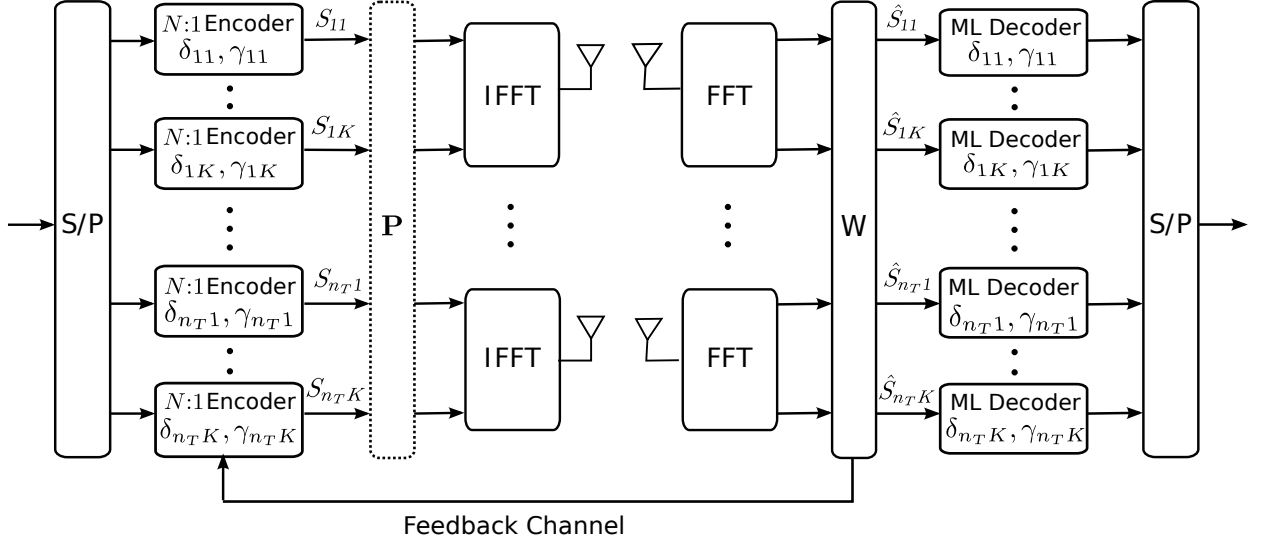


Figure 6.3: Block diagram of the analog JSCC MIMO-OFDM system.

6.2 Analog JSCC in MIMO-OFDM

In this section we present the general structure of the analog JSCC systems designed for the transmission of analog data over frequency-selective MIMO channels using OFDM. Figure 6.3 shows the block diagram of the proposed analog MIMO-OFDM scheme. As observed, discrete-time continuous-amplitude symbols are considered to be transmitted over a frequency-selective MIMO channel with n_T transmit antennas and n_R receive antennas using an OFDM modulation with K subcarriers. We also assume that the total available power to transmit the source symbols is P_T .

Source symbols are first spatially multiplexed over the n_T transmit antennas. At each transmit antenna, a set of KN source symbols is encoded into K channel symbols using the $N:1$ analog encoder explained in Chapter 2. Let $\tilde{S}_{i,k}$, $i = 1, \dots, n_T$; $k = 1, \dots, K$, denote the unnormalized encoded symbols transmitted over antenna i and subcarrier k . The corresponding normalized symbols will be represented by $S_{i,k} = \tilde{S}_{i,k}/\sqrt{\gamma_{i,k}}$. In a general setting, both the encoder parameter $\delta_{i,k}$ and the normalization factor $\gamma_{i,k}$ may be different at each transmit antenna i and/or subcarrier k . Next, blocks of K normalized channel symbols are put together to be transmitted as OFDM symbols. Let $\mathcal{S}_i = [S_{i,1}, \dots, S_{i,K}]^T$, $i = 1, \dots, n_T$ be the channel symbols that constitute the OFDM symbol transmitted over antenna i . We can also define the spatial vector $\mathbf{S}_k = [S_{1,k}, \dots, S_{n_T,k}]^T$, $k = 1, \dots, K$ to represent the MIMO symbols transmitted over subcarrier k .

We assume a block-fading channel that remains constant at least during the transmission of one OFDM symbol. In the time-domain, the block-fading MIMO channel is represented by a sequence of $n_R \times n_T$ matrices $\mathbf{H}[l]$ for $l = 0, \dots, L - 1$, where L is the length of the channel impulse response. For Rayleigh fading MIMO channels, the entries to $\mathbf{H}[l]$ are complex-valued zero-mean circularly-symmetric Gaussian random variables. In the frequency-domain,

the MIMO channel response matrices can be expressed as [76]

$$\mathbf{H}_k = \sum_{l=0}^{L-1} \mathbf{R}[l]^{1/2} \mathbf{H}[l] \mathbf{T}[l]^{1/2} \exp\left(\frac{-j2\pi lk}{K}\right), \quad (6.2)$$

where \mathbf{H}_k is the frequency-domain $n_R \times n_T$ MIMO channel matrix corresponding to the k -th subcarrier, $k = 1, \dots, K$, whereas $\mathbf{R}[l]$ and $\mathbf{T}[l]$ represent the receive and transmit spatial-correlation matrices, respectively.

In order to eliminate the channel ISI, the IFFT is applied to the vector of channel symbols \mathcal{S}_i , $i = 1, \dots, n_T$ and a CP larger than the channel impulse response is appended at the beginning. These two stages produce the discrete-time representation of the OFDM symbols to be transmitted over the MIMO channel. At reception, the inverse operations, i.e. the FFT transformation and CP removal, are applied to the received symbol vector. Elaborating the signal model, the received observations \mathbf{Y}_k at subcarrier k are given by

$$\mathbf{Y}_k = \mathbf{H}_k \mathbf{S}_k + \mathbf{N}_k, \quad k = 1, \dots, K \quad (6.3)$$

where \mathbf{N}_k is an i.i.d. circularly-symmetric complex-valued Gaussian random vector that represents the additive spatially and temporally white channel noise, i.e. $\mathbf{N}_k \sim \mathcal{N}_{\mathbb{C}}(0, \sigma_n^2 \mathbf{I})$. Thus, the analog JSCC system over a frequency-selective fading channel can be interpreted as a set of K parallel MIMO subsystems transmitting over flat-fading channels.

At the receiver, MMSE estimation of the source symbols is the optimal decoding strategy for analog JSCC as seen in Chapter 2. When considering an analog JSCC MIMO-OFDM system, optimal decoding consists in the calculation, at each subcarrier k , of the MMSE estimate of the Nn_T transmitted source symbols $\mathbf{x}_k = [x_{1,1}, \dots, x_{N,1}, \dots, x_{1,n_T}, \dots, x_{N,n_T}]^T$ from the received symbol vector \mathbf{Y}_k , i.e.

$$\begin{aligned} \hat{\mathbf{x}}_{k,\text{MMSE}} &= \mathbb{E}[\mathbf{x}_k | \mathbf{Y}_k] = \int \mathbf{x}_k p(\mathbf{x}_k | \mathbf{Y}_k) d\mathbf{x}_k \\ &= \frac{1}{p(\mathbf{Y}_k)} \int \mathbf{x}_k p(\mathbf{Y}_k | \mathbf{x}_k) p(\mathbf{x}_k) d\mathbf{x}_k, \end{aligned} \quad (6.4)$$

where $\mathbb{E}[\cdot]$ denotes the expectation operator. Since the conditional probability, $p(\mathbf{Y}_k | \mathbf{x}_k)$, involves the mapping function $M_\delta(\cdot)$, which is discontinuous and highly non-linear, the integral in Equation (6.4) can only be calculated numerically. As occurs for analog MIMO systems, the discretization of the set of all possible source values, \mathbf{x}_k , is required. If L discrete-points are selected per source dimension, we would have to calculate L^{Nn_T} values for $p(\mathbf{Y}_k | \mathbf{x}_k)$ and $p(\mathbf{x}_k)$, and then compute the integral in Equation (6.4). This is unfeasible in MIMO-OFDM even for a small number of transmit antennas and subcarriers.

Alternatively, the two-stage receiver presented in Section 2.3.3 for analog JSCC decoding in Single Input Single Output (SISO) channels can also be applied to MIMO-OFDM channels. In this case, we first perform an estimation of the OFDM symbols transmitted from each

antenna using a conventional linear Minimum Mean Square Error (MMSE) filter. From the filtered OFDM symbols, we obtain an estimate of the analog channel symbols that is in turn used to calculate an estimate of the transmitted source symbols by Maximum Likelihood (ML) decoding.

Assuming \mathbf{H}_k is perfectly known at the receiver, the linear filter \mathbf{W}_k that minimizes the MSE between the channel symbol vector \mathbf{S}_k and the corresponding estimated symbol vector $\hat{\mathbf{S}}_k = \mathbf{W}_k \mathbf{Y}_k$ is given by

$$\mathbf{W}_k = (\mathbf{H}_k^H \mathbf{H}_k + \rho \mathbf{I}_{n_T})^{-1} \mathbf{H}_k^H, \quad (6.5)$$

where $\rho = (n_T \sigma_n^2) / P_T$ and the super-index H represents conjugate transposition. Then, the set of estimated symbols $\hat{\mathbf{S}}_k = [\hat{S}_{1,k}, \dots, \hat{S}_{n_T,k}]^T$ can be denormalized and input to a bank of ML decoders to calculate an estimate $\hat{\mathbf{x}}_{i,k}$, $i = 1, \dots, n_T$, of the source symbols transmitted over antenna i and subcarrier k . In the particular case of a 2:1 compression using the Archimedes' spiral, these estimates are obtained from

$$\hat{\mathbf{x}}_{i,k} = \mathbf{z}_\delta(\tilde{\theta}_{i,k}) \quad (6.6)$$

where

$$\tilde{\theta}_{i,k} = T_\alpha^{-1}(\sqrt{\gamma} \hat{S}_{i,k}) = \text{sign}(\hat{S}_{i,k}) |\sqrt{\gamma} \hat{S}_{i,k}|^{-\alpha}. \quad (6.7)$$

6.3 Adaptive Analog JSCC

As explained in Chapter 2, the optimal encoders have to be used for analog JSCC systems to closely approach the optimal distortion-cost tradeoff (see Section 2.3.4). Remember that the optimal value for the δ parameter depends on the actual Channel Signal-to-Noise Ratio (CSNR) at each channel realization (fading channel). In the case of MIMO-OFDM systems, symbols transmitted over different antennas and subcarriers generally experience different CSNR. For that reason, the impact of the system optimization on the analog JSCC performance is more critical in this case and, therefore, it is specially important to employ the proper values $\delta_{i,k}$ to encode the source symbols.

If no information about the channel is available at the transmitter, the same δ value should be used to encode all analog source symbols. In this case, it is sensible to use the δ value that corresponds to the average expected CSNR. This fixed approach will perform adequately in frequency-flat and quasi-static channels where the CSNR remains approximately the same at all antennas and all subcarriers during the transmission of several OFDM symbols. However, it can lead to a severe performance degradation in practical MIMO-OFDM channels where each subcarrier is expected to have a different time-varying CSNR.

Better performance is obtained when we follow an adaptive coding strategy where the optimal $\delta_{i,k}$ values are used according to the instantaneous CSNR at each subcarrier and transmit

antenna, $\eta_{i,k}$. In a practical setting, this implies that the system must be equipped with a feedback channel that regularly sends the $\eta_{i,k}$ values to the transmitter.

As mentioned in Chapter 5, the MMSE filter \mathbf{W}_k does not completely cancel the spatial interference of the MIMO channel. In this case, the CSNR at each antenna and subcarrier can be estimated using Equation (5.21) extended to the MIMO-OFDM model as

$$\eta_{i,k} = \frac{\mu_{i,k}}{1 - \mu_{i,k}}, \quad (6.8)$$

where $\mu_{i,k} = (\mathbf{W}_k \mathbf{H}_k)_{ii}$ is the i -th diagonal entry of the equivalent MIMO channel $\mathbf{W}_k \mathbf{H}_k$.

In summary, the MMSE detector transforms the MIMO-OFDM channel into a set of n_T SISO-OFDM parallel channels, each one with an equivalent CSNR per subcarrier given by Equation (6.8). At the transmitter, we encode the symbols to be transmitted through each antenna and subcarrier using the appropriate $\delta_{i,k}$ parameter. This parameter is selected from the fed-back $\eta_{i,k}$ values using Table 2.1 (Gaussian sources) or Table 2.2 (Laplacian sources), which are assumed to be stored at the transmitter and at the receiver.

Another important issue regarding the optimization of an adaptive analog JSCC MIMO-OFDM system is the normalization of the transmitted symbols $S_{i,k}$. In a non-adaptive system, all subcarriers in the OFDM symbol transmitted over the i -th antenna can be normalized using the same factor γ_i , $i = 1, \dots, n_T$ per antenna. However, when considering adaptive coding, source symbols are encoded with different $\delta_{i,k}$ values and, therefore, the normalization factors $\gamma_{i,k}$ will be also different. Such factors can be also selected according to $\eta_{i,k}$ values provided by the feedback channel using the third row of Tables 2.1 and 2.2.

6.3.1 Adaptive Analog JSCC with Linear Precoding

If the feedback channel is able to provide the transmitter with information from the MIMO channel matrices, \mathbf{H}_k , $k = 1, \dots, K$ (and not just with the $\eta_{i,k}$ values), further performance improvements can be obtained if the channel symbols are precoded prior to their transmission. Following the same approach presented for analog MIMO systems (see Section 5.3.3), we will use the MMSE criterion to jointly design the optimal linear precoder and its corresponding detector for the proposed analog JSCC scheme in MIMO-OFDM.

Let us assume the output encoder symbols are linearly precoded with a rectangular $n_T \times n_R$ matrix \mathbf{P}_k at each subcarrier. Thus the transmitted symbols are $\mathbf{P}_k \mathbf{S}_k$. As in Section 6.2, \mathbf{W}_k represents the MIMO linear detector per subcarrier. Hence, the channel symbol estimates obtained at the detector output are given by

$$\hat{\mathbf{S}}_k = \mathbf{W}_k (\mathbf{H}_k \mathbf{P}_k \mathbf{S}_k + \mathbf{n}_k), \quad (6.9)$$

and the error between the estimated and transmitted symbols per subcarrier is

$$\mathbf{e}_k = \mathbf{S}_k - \hat{\mathbf{S}}_k = \mathbf{S}_k - \mathbf{W}_k (\mathbf{H}_k \mathbf{P}_k \mathbf{S}_k + \mathbf{n}_k). \quad (6.10)$$

The MMSE linear precoder and detector are obtained after solving the following constrained optimization problem

$$\arg \min_{\mathbf{P}_k, \mathbf{W}_k} \sum_{k=1}^K \mathbb{E}[\text{tr}(\mathbf{e}_k \mathbf{e}_k^H)] \quad \text{s.t.} \quad \sum_{k=1}^K \text{tr}(\mathbf{P}_k \mathbf{P}_k^H) \leq P_T, \quad (6.11)$$

where P_T represents the total power available at the transmitter.

Equivalently to the MIMO case, we substitute the error expression (6.10) into (6.11). Differentiating with respect to \mathbf{P}_k^H and \mathbf{W}_k^H , and using the Karush-Kuhn-Tucker (KKT) conditions, we arrive at the following equations

$$\mathbf{P}_k = (\lambda \mathbf{I}_{n_T} + \mathbf{H}_k^H \mathbf{W}_k^H \mathbf{W}_k \mathbf{H}_k)^{-1} (\mathbf{H}_k^H \mathbf{W}_k^H), \quad (6.12)$$

$$\mathbf{W}_k = (\mathbf{P}_k^H \mathbf{H}_k^H) (\sigma_n^2 \mathbf{I}_{n_R} + \mathbf{H}_k \mathbf{P}_k \mathbf{P}_k^H \mathbf{H}_k^H)^{-1}, \quad (6.13)$$

where $\lambda \geq 0$ is the Lagrange multiplier that ensures the total transmit power is equal to P_T . As in the MIMO model, two alternatives are available to determine the linear MMSE precoder and the associated detector. On one hand, we can implement an iterative procedure that sequentially updates the precoder and the detector using Equations (6.12) and (6.13), respectively. On the other hand, we can extend the explicit solution developed for the MIMO case in Appendix B. Again, the performance of both approaches is quite similar although the complexity and delay introduced by the explicit solution are practically negligible compared to those of the iterative procedure.

It is important to notice that linear precoder changes the CSNR of the equivalent channel that corresponds to the symbols transmitted over antenna i and subcarrier k . As a consequence, the encoder parameter $\delta_{i,k}$ should be adapted accordingly. The CSNR values $\eta_{i,k}$ when linear precoding is used can be obtained if we take into account that linear precoders simply transform the MIMO channel \mathbf{H}_k into another one given by $\mathbf{H}_k \mathbf{P}_k$. Hence, the transmitter can calculate the corresponding $\eta_{i,k}$ values using equation Equation (6.8) and then choose $\delta_{i,k}$ according to Tables 2.1 and 2.2.

6.4 Experimental Results

Computer simulations were carried out to assess the performance of the analog JSCC MIMO-OFDM systems considered in previous sections. Three different configurations were evaluated: non-adaptive coding, adaptive coding and adaptive coding with linear precoding.

The performance attained in each case is compared with respect to the optimal distortion-cost tradeoff given by the Optimum Performance Theoretically Attainable (OPTA) corresponding to the analog JSCC MIMO-OFDM model. For Gaussian sources and $N:1$ compression over a generic stochastic $n_R \times n_T$ channel matrix \mathbf{H}_k , and assuming that the

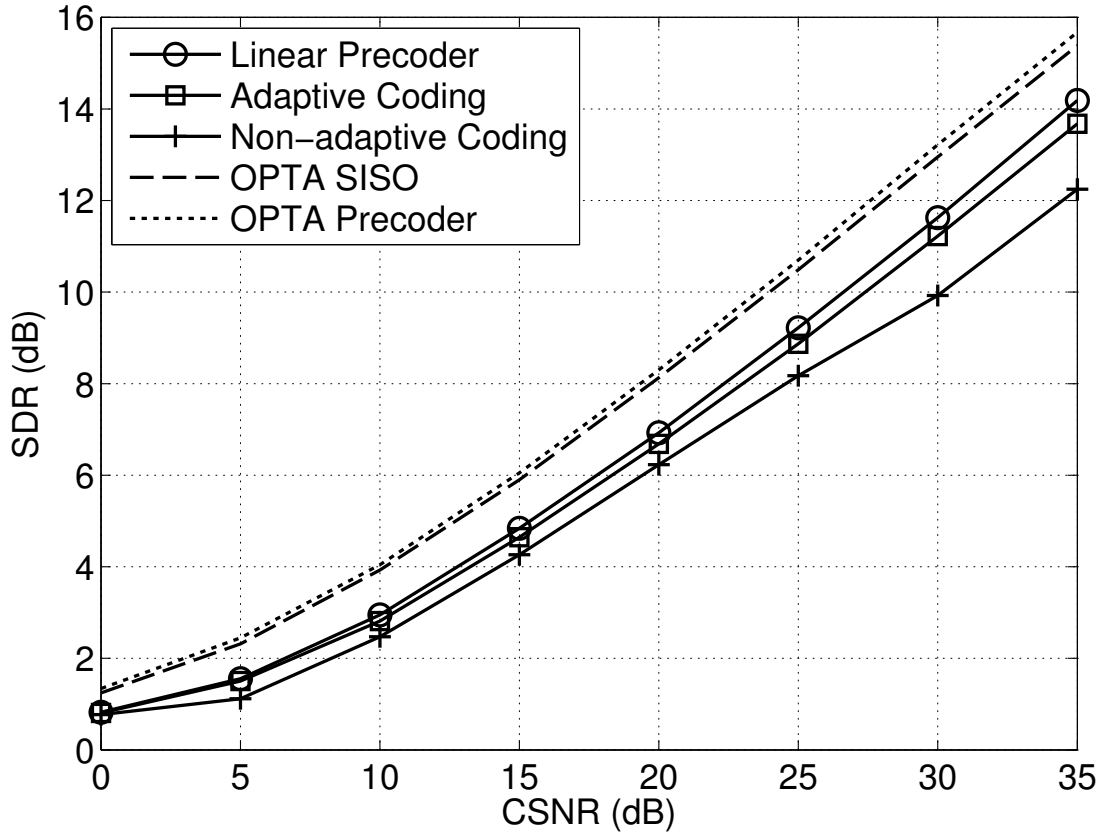


Figure 6.4: Performance of 2:1 analog JSCC SISO-OFDM systems over Rayleigh fading channels.

channel is not known at the transmitter, the OPTA can be calculated using the equality (5.12) and the proper capacity for the MIMO-OFDM channel given by

$$C_E(\text{CSNR}) = \mathbb{E}_{\mathbf{H}_k} \left[\log \det \left(\mathbf{I}_{n_R} + \frac{\text{CSNR}}{n_T} \mathbf{H}_k \mathbf{H}_k^H \right) \right]. \quad (6.14)$$

As already mentioned in Chapter 5, if the channel is known at the transmitter, the capacity of a digital system is maximized by the water-filling solution at each channel realization. In our case, however, channel knowledge at transmission is not exploited to maximize capacity but to precode the transmitted symbols with the linear MMSE precoding matrices \mathbf{P}_k , $k = 1, \dots, K$. In that case (full CSI), the OPTA can be calculated by replacing the channel matrices \mathbf{H}_k with the equivalent matrices $\mathbf{H}_k \mathbf{P}_k$ in Equation (6.14).

Let us start by considering the case $n_T = n_R = 1$, i.e. SISO-OFDM. We assume that the source samples are generated from i.i.d. normalized Gaussian random variables and encoded using the 2:1 analog mapping based on the Archimedes' spiral. In addition, the number of subcarriers in each OFDM symbol is $K = 64$. In a first computer experiment we considered a Rayleigh fading channel with $L = 10$ and a flat delay power profile. Block-fading was assumed, i.e. the channel remains constant during the transmission of a block of T OFDM symbols but changes independently from one block to another.

Figure 6.4 plots the obtained results for this case. It can be seen that the three proposed

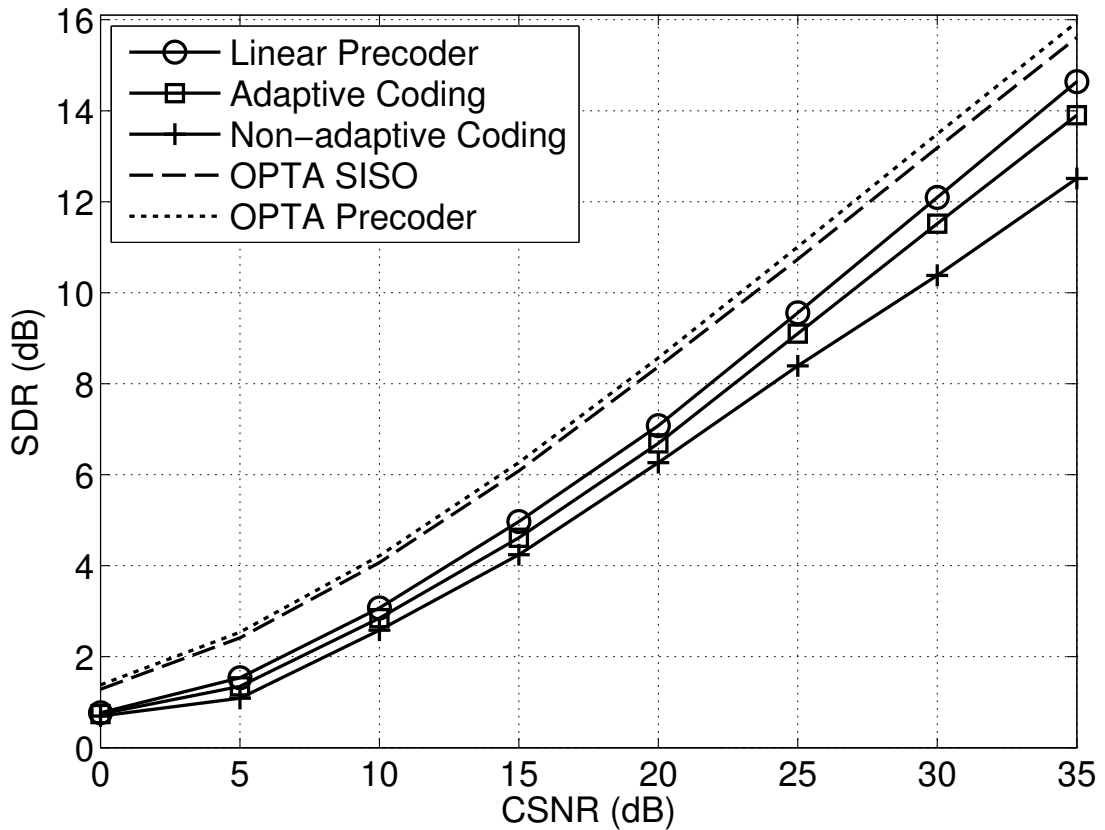


Figure 6.5: Performance of 2:1 analog JSCC SISO-OFDM systems over fading channels simulated according to the ITU-Pedestrian B specifications.

analog JSCC techniques approach the OPTA in the whole CSNR region. As expected, the worst performance is obtained when no CSI is available at the transmitter (i.e. non-adaptive coding and no precoding), specially when the CSNR is high, in which case the performance is 3.0 dB below the OPTA. The system performance is significantly improved (about 1.8 dB at high CSNR) when adaptive coding is considered. Further improvement are obtained if MMSE linear precoding is utilized. This latter improvement, however, is marginal (only a fraction of dB) since we are in a SISO scenario and not much performance gain should be expected from linear precoding.

In a second computer experiment, we considered the ITU-Pedestrian B model. For a complete description of the delay and Doppler power profiles of such a model, see reference [59]. Doppler shift is assumed low enough so that the channel remains unchanged during the transmission of an OFDM symbol and no ICI arises. In the ITU-Pedestrian B channel model this condition is met for a reasonable large number of practical situations. Nevertheless, the channel changes from one OFDM symbol to another according to the Doppler profile of the model. Figure 6.5 shows the obtained results, which are similar to those obtained for Rayleigh channels although the performance gains when considering adaptive coding and linear precoding are slightly higher.

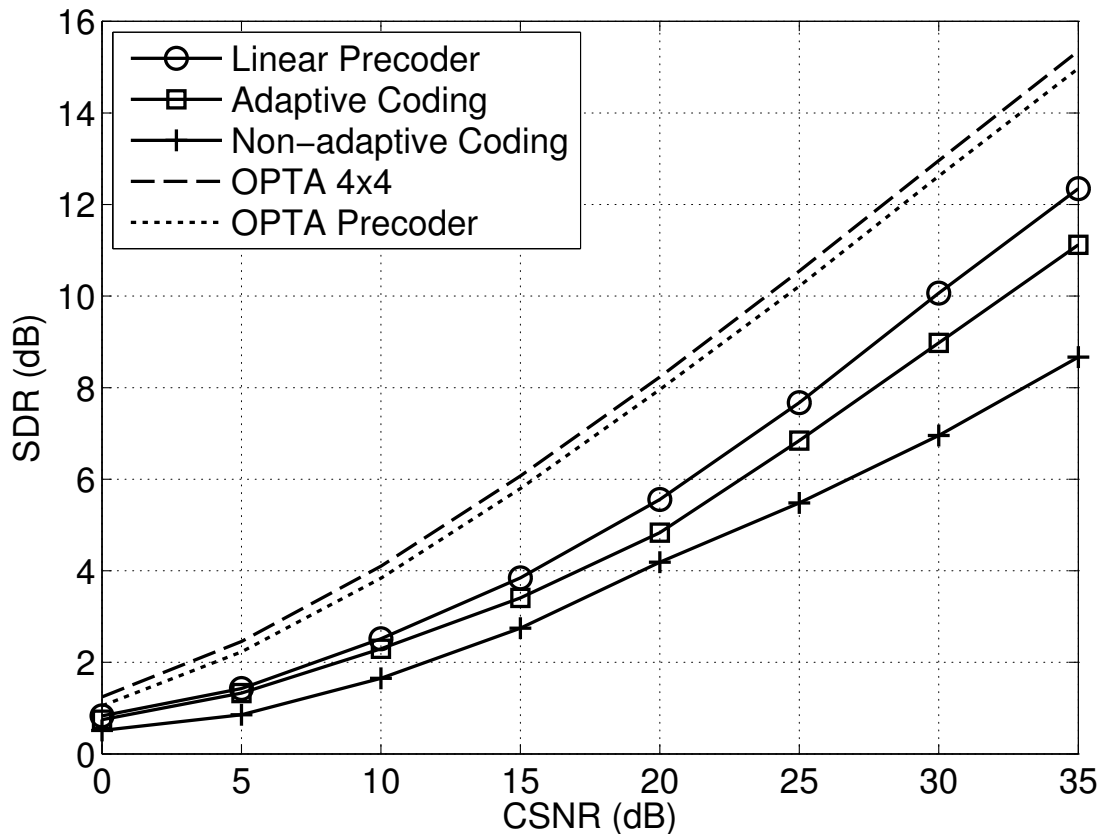


Figure 6.6: Performance of analog JSCC 4×4 MIMO-OFDM systems over Rayleigh channels.

We now shift our focus to MIMO-OFDM channels. Let us start by considering a spatially and temporally white MIMO-OFDM Rayleigh fading channel with $n_T = n_R = 4$, $K = 64$ and $L = 10$. According to Equation (6.2), this corresponds to the case where $\mathbf{R}[l]$ and $\mathbf{T}[l]$ are identity matrices and the entries of $\mathbf{H}[l]$ are i.i.d. complex-valued circularly-symmetric zero-mean Gaussian random variables. Block-fading was again assumed in such manner that the channel does not change during the transmission of a block of T OFDM symbols but varies independently from one block to another.

The performance curves corresponding to the three optimization alternatives for the proposed analog JSCC MIMO-OFDM scheme are plotted in Figure 6.6. The non-adaptive coding strategy exhibits the worst performance. It is about 6.0 dB below the OPTA at high CSNR values. A significant improvement in performance is obtained (2.5 dB at high CSNR) when considering adaptive coding. Contrarily to the SISO case, performance also improves significantly (1.2 dB at high CSNR) when incorporating linear MMSE precoding. It is interesting to note from Figure 6.6 that the OPTA with precoding is actually lower than that without precoding. This is because the precoder has been designed to minimize the MSE and not to maximize the channel capacity. Nevertheless, the actual performance of the precoded system is better than that of the system without precoding.

We also carried out computer experiments considering a standard model such as the

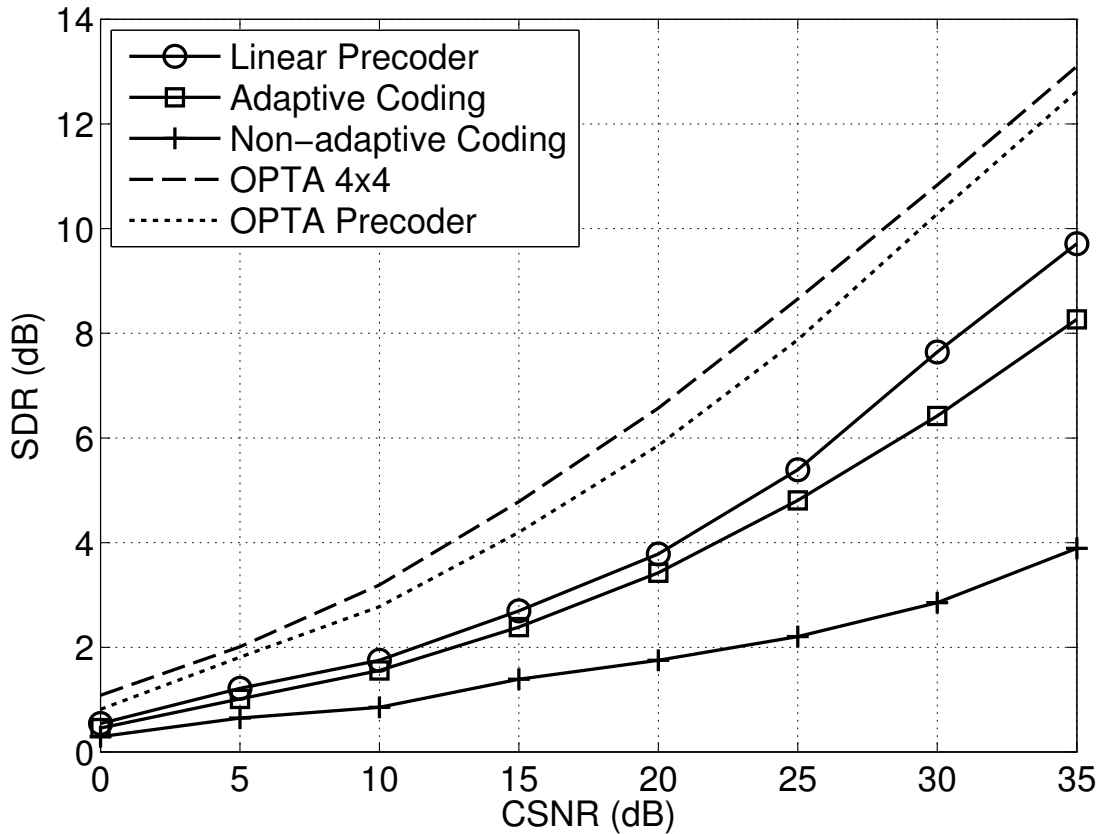


Figure 6.7: Performance of analog JSCC 4×4 MIMO-OFDM systems over an IMETRA-D channel.

Intelligent Multi-element Transmit and Receive Antennas case D (IMETRA-D) channel model described in [58]. The IMETRA-D model only specifies the spatial correlation of a MIMO channel, i.e. the matrices $\mathbf{R}[l]$ and $\mathbf{T}[l]$ in Equation (6.2). For the delay and Doppler power profile we chose the same parameters as in the ITU-pedestrian B model [59]. Figure 6.7 plots the obtained results, which highlight the importance of using adaptive coding strategies. Indeed, without adapting the analog encoder parameters, the system performance is very far away from the OPTA (9.0 dB at high CSNR). With adaptive coding the gap to the OPTA reduces significantly (5.0 dB at high CSNR) while the distance to the OPTA is even less (2.5 dB at high CSNR) when adaptive coding with linear precoding is utilized.

6.5 Conclusions

In this chapter we have studied the use of analog JSCC techniques over frequency-selective MIMO fading channels. OFDM is employed to transform the transmission of the analog symbols over wideband channels into a orthogonal transmission over a set of non-interfering narrowband subchannels. Hence the received symbols are no longer affected by ISI and the the design of analog JSCC systems presented in the previous chapter for MIMO flat-fading channels can be now extended to this case. We have noticed that the symbol normalization and

the optimization of the encoder parameters are two operations particularly relevant to ensure that the proposed analog MIMO-OFDM system approaches the OPTA. In order to complete our analysis, besides synthetically-generated fading channels we have also considered wireless channel models described by the standards ITU-Pedestrian B and I-METRA D for SISO and MIMO, respectively.

Simulation results show that the proposed scheme exhibits a satisfactory performance in the whole CSNR region while preserving low complexity and delay. We have also assessed three different configurations for system optimization depending on whether only the receiver knows the channel, either partial CSI is also available at the transmitter or we have full CSI at both sides: non-adaptive coding, adaptive coding and adaptive coding with linear MMSE precoding. The obtained results show that the three analog JSCC transmission strategies approach the OPTA, although the best performance is attained when the adaptive coding with linear precoding method is employed. From such results, we can conclude the importance of using adaptive coding strategies for analog JSCC systems to closely approach the optimal performance in MIMO-OFDM scenarios, specially in the case of real wireless channels.

Chapter 7

Analog JSCC for Multiple Access Channels

In previous chapters, we focused on point-to-point wireless communications where a single user independently sends information to a single receiver. However, there exists a large number of scenarios that cannot be modeled as non-interfering point-to-point links between transmitters and receivers such as, for instance, cellular communications. In this type of systems, a large number of mobile units are accommodated over a long area within a limited frequency spectrum and hence the users need to share the available bandwidth to communicate with the base station.

In this chapter we turn our attention to the use of analog Joint Source Channel Coding (JSCC) in multiuser communications. Specifically, we focus on the transmission of analog data over a Multiple Access Channel (MAC). The transmission of information over a MAC is a fundamental problem in wireless communications that arises in many practical situations such as the uplink in a cellular system [125]. In a MAC scenario, multiple users simultaneously transmit their information over the same channel to a centralized receiver responsible for separating the data streams corresponding to each user. It is hence necessary to enable some mechanism to allow the users to share the MAC while ensuring a interference-free transmission of the information.

Frequency Division Multiple Access (FDMA) and Time Division Multiple Access (TDMA) are two well-known orthogonal channel access techniques employed in conventional mobile communications. FDMA assigns different subchannels to each user whereas TDMA divides the transmission time into separate time slots, and in each slot only one user is allowed to either transmit or receive. Both orthogonal strategies actually transform the multiuser scenario into several point-to-point channels and, therefore, the transmission techniques explained for the single-user case can be applied. In the previous generation of cellular communications, Code Division Multiple Access (CDMA) was adopted as the access method to the MAC. CDMA is another orthogonal access scheme based on the use of spreading codes [95] where

the available resources are allocated to all active users unlike FDMA and TDMA techniques. Thus, the advantage of CDMA with respect to other orthogonal access methods is that all users synchronously and simultaneously transmit over the MAC.

Orthogonal access schemes have been shown to achieve the sum-capacity of a MAC when the channel is assumed to be Gaussian [125]. Nevertheless, orthogonal strategies are strictly suboptimal for fading MAC. In the particular case of single-antenna fading MACs with Channel State Information (CSI) available at the transmitters, it can be shown [65] that the optimal channel access scheme consists in allocating all available power to the user with the strongest channel. This strategy is commonly referred to as Opportunistic Communication and it is optimal in the sense that maximizes the sum-rate of the MAC model. However, opportunistic access is no longer optimal when the users and the common receiver employ multiple antennas, i.e. for Multiple Input Multiple Output (MIMO) MAC systems. In that case, the capacity of digital Separate Source Channel Coding (SSCC) communication systems over a block-fading MAC can be achieved using a scheme based on superposition coding and successive interference cancellation at the receiver [129]. In such a scheme, it is possible to decode the information from one of the users without errors as long as its rate is below the capacity limit imposed by the Signal-to-Interference Noise Ratio (SINR) for such a user. Then, the information corresponding to that user is subtracted from the incoming signal before decoding the next user. Unfortunately, this strategy is unfeasible for analog JSCC since a certain level of distortion always remains after decoding the user information in such manner that the subtracting process does not completely remove the interference of each user causing an inevitable degradation of the successive cancellation procedure.

In this chapter we study the application of analog JSCC techniques for the transmission of analog sources over Gaussian and block-fading MACs. In the last years, the design of suitable JSCC techniques for multiuser communications has been investigated from different points of view. Some interesting examples are [10, 69], where the design of optimal non-parametrized analog mappings for Gaussian MAC is addressed. In [33] a particular hybrid JSCC scheme is proposed for the transmission of two correlated Gaussian sources over Gaussian MAC. This scheme is referred to as Scalar Quantizer Linear Coding (SQLC) because it consists of a scalar quantizer and a optimized linear analog mapping. It can be hence considered as an extension of the Nested Quantization digital technique [106]. Analog JSCC has been also applied to relay multiple access channels in [139] where an analog network coding mapping that combines the Archimedean spiral and a like-sawtooth mapping is proposed assuming orthogonal transmission of the information. Like in the case of point-to-point transmissions, most of those works focus on the case of Gaussian channels. An exception is [92] that introduces an JSCC scheme based on Channel Optimized Vector Quatization (COVQ) for the transmission of uncorrelated sources over MIMO broadcast channels. In this case, the mappings are not strictly analog because a discrete set of representation vectors is actually employed at the encoder.

In the MAC case, the design of the optimal analog JSCC mappings requires to solve complex optimization problems and, in general, the resulting mappings are not very practical. For that reason, instead of designing specific analog mappings for a given MAC scenario, we propose a distributed approach. On one hand, each user employs the 2:1 analog encoder based on the Archimedes' spiral at the transmitter and the two-stage receiver explained in Chapter 2 to separate and decode the signal corresponding to each user. On the other hand, the channel access scheme is specifically designed for the transmission of discrete-time analog samples over the MAC using analog JSCC. We show that this strategy not only simplifies the design of analog JSCC schemes for multiuser communications but also it is able to approach the optimal distortion-cost tradeoff using the traditional analog JSCC mappings for point-to-point communications.

At the beginning of this chapter, we focus on multiuser transmissions over Gaussian MAC. In this case, we choose CDMA as the channel access method because this orthogonal scheme achieves the sum-capacity and allows us to configure the individual data rates at which each user should transmit its information. Next, three different access methods are designed for the case of block-fading MAC: orthogonal CDMA, linear Minimum Mean Square Error (MMSE) codes and opportunistic access. If only the receiver knows the channel, CDMA guarantees an orthogonal and simultaneous transmission of the user information at the desired individual rates. When the Channel State Information (CSI) is also available at the transmitters, we can exploit this knowledge to determine the optimal linear MMSE access codes to be used instead of the orthogonal CDMA codes. It is important to note that such codes are designed to minimize the sum-Mean Square Error (MSE) between the transmitted and the filtered symbols. Finally, the opportunistic access is intended to maximize the sum-rate of the multiuser analog JSCC system regardless user rate/power constraints. Unfortunately, we show that the opportunistic strategy can lead to unfair distributions of the individual user powers and rates.

7.1 OPTA for Analog JSCC Systems over MAC

As seen for point-to-point communications, the optimal distortion-cost tradeoff curve defines the performance upper bound for the transmission of analog sources. This bound is referred to as Optimum Performance Theoretically Attainable (OPTA) and it is calculated by equating the rate distortion function of the source and the capacity of the channel. We can easily extend these ideas to the case of multiuser communications.

In the MAC scenario, several users simultaneously send their data to a common receiver over the same channel. Hence, the received signal corresponding to each user is affected by interferences caused by the rest of users. Thus, the MAC model can be actually interpreted as a set of interfering point-to-point links and we can focus on either the maximum data rate at

which each user can transmit over the MAC or the total sum-rate for the set of all users. In the former approach, we should calculate a different upper bound for each user in terms of the rate distortion function of the corresponding source and the maximum individual rate such a user can achieve. Conversely, in the second case we can calculate a single OPTA curve that describes the optimal performance of the overall MAC system.

Rather than minimizing the individual signal distortion corresponding to each user, we are interested in the overall distortion of the set of received signals. In such a case, the sum-distortion can be defined as

$$D_{\text{sum}} = \sum_{i=1}^N D_i \quad (7.1)$$

as long as we consider a linear distortion metric such as the MSE. The index N represents the number of the active users transmitting over the MAC and D_i is the distortion observed in the recovered signal for each user i . The performance of analog JSCC systems in MAC communications can be measured in terms of the average Signal-to-Distortion Ratio (SDR) given by

$$\overline{\text{SDR}} = \frac{\sigma_s^2}{(\sum_{i=1}^N D_i)/N} = \frac{\sigma_s^2}{D_{\text{sum}}/N},$$

where D_{sum}/N is the average distortion and the N sources are assumed to have the same variance σ_s^2 for simplicity. If the sources are also independent, the OPTA bound can be calculated similarly to the point-to-point case by equating the rate distortion function of the sources and the sum-capacity of the MAC, i.e.

$$M \sum_{i=1}^N R(D_i) = K R_{\text{sum}}, \quad (7.2)$$

where $R(D_i)$ is the rate distortion function of user i given a distortion target D_i , and R_{sum} is the sum-capacity of the MAC, i.e. the maximum sum transmission rate that the set of all users can achieve. The terms M and K represent the bandwidth of the sources and the channel, respectively and, therefore, such values determine the expansion/compression factor applied when the source symbols are mapped into the channel symbols at the transmitters.

Finally, if we assume that the N sources are also identically distributed, it is logical to consider that the individual contribution of each user to the sum-distortion is the same [71], thus $D_i = (D_{\text{sum}}/N) \forall i$. In such a case, the general expression for the OPTA given by Equation (7.2) can be simplified as follows

$$MNR(D) = KR_{\text{sum}}, \quad (7.3)$$

where $D = D_{\text{sum}}/N$ the individual distortion of each user. Notice that the product $MNR(D)$ specifies the total number of source symbols required to be transmitted by the set of N users along K channel uses to obtain the sum-distortion D_{sum} after decoding the received MAC signal.

In this chapter, we will focus on the transmission of i.i.d. complexed-valued Gaussian symbols with zero mean and variance σ_s^2 . If we consider the MSE as the distortion metric, the rate distortion function of a complexed-valued Gaussian source is given by [21]

$$R(D) = \max \left[0, \log \left(\frac{\sigma_s^2}{D} \right) \right].$$

By inserting the above expression into Equation (7.3), we obtain

$$MN \log \left(\frac{\sigma_s^2}{D_{\text{sum}}/N} \right) = KR_{\text{sum}}$$

or equivalently

$$MN \log (\overline{\text{SDR}}) = KR_{\text{sum}}. \quad (7.4)$$

The optimal performance of the a MAC system can be hence calculated by solving the average SDR from Equation (7.4) as

$$\overline{\text{SDR}} = \exp \left(\frac{K}{MN} R_{\text{sum}} \right). \quad (7.5)$$

Thus, the OPTA for the transmission of analog sources over the MAC can be calculated according to Equation (7.5) using the appropriate expression for the sum-rate of the considered MAC system.

7.2 Gaussian MAC

We start considering the Gaussian MAC model with N independent users sending their information simultaneously to a common receiver. In this case, the received signal can be expressed as

$$y = \sum_{i=1}^N \sqrt{P_i} z_i + w, \quad (7.6)$$

where P_i and z_i , $1 \leq i \leq N$, represents the power and the transmitted symbol corresponding to user i , respectively, while $w \sim \mathcal{N}(0, \sigma_n^2)$ is the Additive White Gaussian Noise (AWGN) at the receiver. The total available power P_T is assumed to be allocated among the users according to the sum-power constraint $\sum_{i=1}^N P_i = P_T$.

In this model, the data rate that each subset of users may individually achieve is restricted by the following set of $2^N - 1$ inequalities, one for each possible non-empty subset \mathcal{N} of users

$$\sum_{i \in \mathcal{N}} R_i \leq \frac{1}{2} \log(1 + \sum_{i \in \mathcal{N}} P_i) \quad (7.7)$$

for all $\mathcal{N} \subset \{1, 2, \dots, N\}$. The capacity region is hence given by an N -dimensional polyhedron where each of its edges corresponds to one inequality in Equation (7.7). The maximum sum-rate to be achieved in the Gaussian MAC is limited by the inequality where all users are in the subset \mathcal{N} , i.e.

$$R_{\text{sum}} = \sum_{i=1}^N R_i \leq \frac{1}{2} \log(1 + \sum_{i=1}^N P_i). \quad (7.8)$$

In order to simplify the previous equations we assumed without loss of generality that the noise variance is equal to one, i.e. $\sigma_n^2 = 1$. Notice that the OPTA for the transmission of analog sources over Gaussian MAC can be straightforwardly calculated from Equation (7.5) using the corresponding expression of the sum-capacity given by Equation (7.8).

7.2.1 Orthogonal CDMA Scheme

As mentioned in the introduction, a channel access scheme is required to allow multiple users to send their information to the centralized receiver over the MAC since the signal of one user interferes with the data transmitted by the rest of users. We propose to use an orthogonal like-CDMA scheme based on the use of spreading codes. Hence, the receiver can exploit the orthogonality of these codes to remove the Multiple Access Interference (MAI).

We propose to construct the spreading codes corresponding to each user from a unitary matrix such as the Hadamard matrix or the DFT matrix. Let $R_i = k_i/K$, $i = 1, \dots, N$, be the data rate at which user i aims to transmit. In such a case, we start with a $K \times K$ unitary matrix \mathbf{U} and assign k_i columns to user i such that $\sum_{i=1}^N k_i \leq K$. Thus, the code corresponding to user i , \mathbf{C}_i , will be a $K \times k_i$ matrix defined as follows

$$\mathbf{C}_i = \begin{bmatrix} \mathbf{c}_{i1} \\ \mathbf{c}_{i2} \\ \vdots \\ \mathbf{c}_{iK} \end{bmatrix} = \begin{bmatrix} c_{i1}(1) & c_{i1}(2) & \cdots & c_{i1}(k_i) \\ c_{i2}(1) & c_{i2}(2) & \cdots & c_{i2}(k_i) \\ \vdots & \vdots & \cdots & \vdots \\ c_{iK}(1) & c_{iK}(2) & \cdots & c_{iK}(k_i) \end{bmatrix} \quad (7.9)$$

This matrix \mathbf{C}_i will be used to combine k_i source symbols of user i , $\mathbf{x}_i = [x_{i1}, x_{i2}, \dots, x_{ik_i}]^T$, to produce a vector of K channel symbols, $\mathbf{z}_i = \mathbf{C}_i \mathbf{x}_i$. Notice that in order to ensure that $\mathbb{E}[|\mathbf{z}_i|^2] = P_i$ is satisfied, the columns of the matrix \mathbf{U} assigned to user i must be normalized by a factor $1/\sqrt{k_i}$ given that such a user actually sends a combination of k_i symbols at each time instant. Finally, the overall access code matrix utilized by all users in the MAC is $\mathbf{C}_K = [\mathbf{C}_1, \mathbf{C}_2, \dots, \mathbf{C}_N]$.

A remarkable property of the proposed CDMA scheme is its flexibility to achieve any distribution of the user data rates by appropriately selecting k_i and K . In addition, cooperation among users is not required and, therefore, the use of these orthogonal codes enables a simple mechanism to guarantee that all users achieve a certain individual rate.

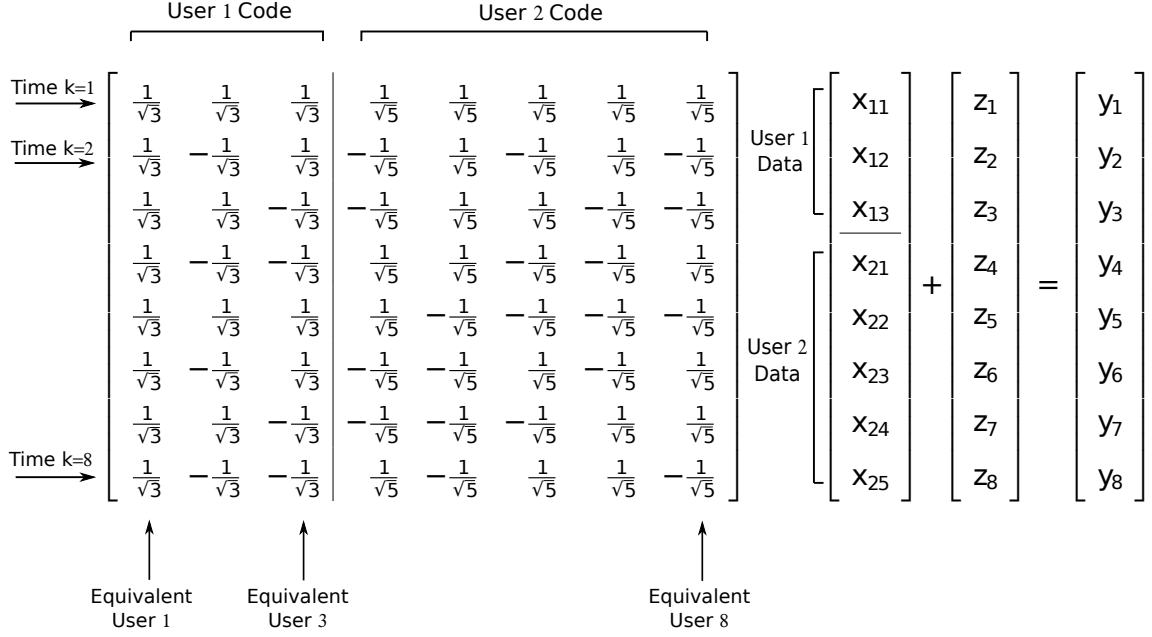


Figure 7.1: Example of orthogonal spreading codes for the proposed CDMA access scheme.

Figure 7.1 shows an example of orthogonal codes designed for a MAC scheme with two users whose individual data rates are $R_1 = 3/8$ and $R_2 = 5/8$, respectively. These codes are constructed from a Hadamard matrix of order 8. As observed, the three first columns of the Hadamard matrix are assigned to user 1 and the remaining five ones to user 2. Notice that the columns of the code matrix are normalized by the proper factor for each user.

At each time instant $k = 1, \dots, K$, each user i transmits the same vector of k_i source symbols multiplied times the code corresponding to that instant, \mathbf{c}_{ik} , to produce the transmitted symbol $z_i = \mathbf{c}_{ik}\mathbf{x}_i$. Hence, the received signal is

$$y_k = \sum_{i=1}^N \sqrt{P_i} \mathbf{c}_{ik} \mathbf{x}_i + w_k \quad 1 \leq k \leq K$$

where w_k is the AWGN at time k .

Given that the input source samples are assumed to be i.i.d., the proposed CDMA scheme can be interpreted as an equivalent model where K independent users transmit a single symbol along K time instants. In that case, the spreading code of each user is given by the corresponding column of the overall code matrix. On the other hand, the use of orthogonal codes ensures that the information transmitted by each user can be perfectly decoupled at the receiver by multiplying the received signal times the overall code matrix, since the product $\mathbf{C}_K \mathbf{C}_K^T$ results in a diagonal matrix. Thus, the proposed scheme transforms the Gaussian MAC model with CDMA into K orthogonal Single Input Single Output (SISO) channels and, therefore, its sum-capacity can be calculated as the sum of the individual capacities of those K Gaussian

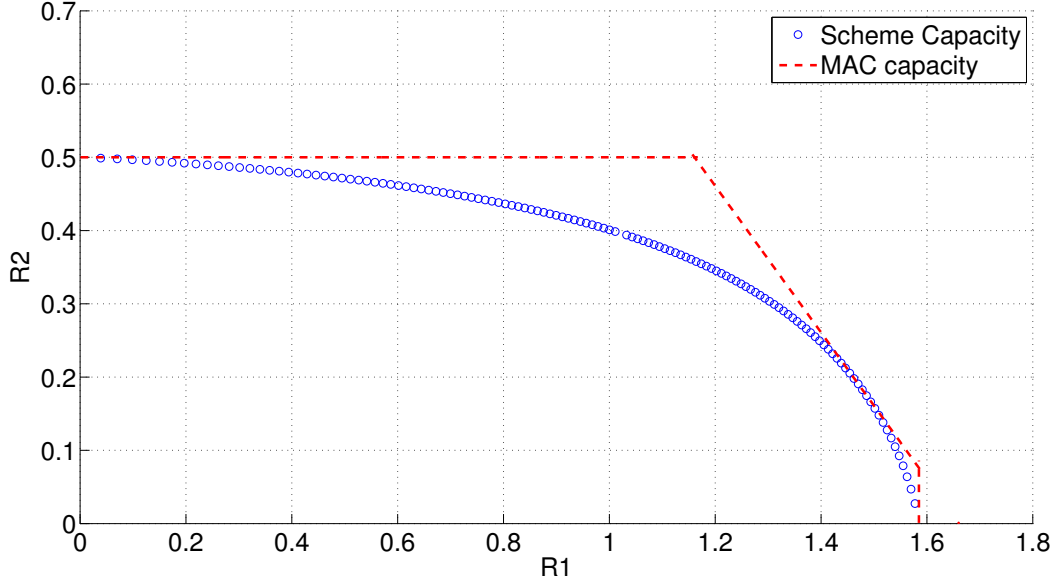


Figure 7.2: Capacity of the Gaussian MAC model and the proposed CDMA scheme for $P_1 = 8$, $P_2 = 1$ and a spreading factor $K = 64$.

SISO channels as follows

$$R_{\text{sum}}^{(\text{CDMA})} = \frac{1}{K} \left[\sum_{i=1}^N \sum_{j=1}^{k_i} \left(\frac{1}{2} \log \left(1 + \frac{K P_i}{k_i} \right) \right) \right]. \quad (7.10)$$

Given that R_{sum} is measured in terms of bits per channel use, the sum-capacity must be divided by the total number of times MAC is used, i.e. K . Notice that the factor $(K P_i)/k_i$ represents the fraction of power allocated to each source symbol of user i along the K intervals.

From Equation (7.8), the general expression of the maximum sum-rate for the Gaussian MAC can be rewritten as

$$R_{\text{sum}} = \frac{1}{2} \log \left(1 + \sum_{i=1}^N P_i \right) = \frac{1}{2} \log \left[1 + \sum_{i=1}^N \sum_{j=1}^{k_i} \left(\frac{P_i}{k_i} \right) \right]. \quad (7.11)$$

It can be easily shown that the sum-capacity of the proposed CDMA scheme, $R_{\text{sum}}^{(\text{CDMA})}$, and the Gaussian MAC capacity, R_{sum} , are equal if and only if

$$\frac{P_i}{k_i} = \frac{P_j}{k_j} \quad \forall j \neq i \text{ with } 1 \leq i, j \leq N. \quad (7.12)$$

The above condition hence defines the optimal allocation strategy for the user powers given a set of data rates, and viceversa. This result is not surprising since the CDMA scheme achieves the MAC capacity when all symbols of the equivalent system are transmitted with the same power.

Figure 7.2 shows the maximum rates achieved by each user for the two user case when $P_1 = 8$ and $P_2 = 1$, and the spreading factor is $K = 64$. The MAC capacity region, obtained

from Equation (7.8), is represented by the red line. The capacity region of the CDMA scheme is represented by the blue curve whose points have been calculated according to Equation (7.10) for different k_1 and k_2 values. As indicated in (7.12), there exists a point in the graph in which the proposed scheme achieves the MAC capacity. Such a point corresponds to the optimal values for k_1 and k_2 determined according to the previous equality.

7.3 Block-Fading MAC

Let us consider now a scenario where N users transmit independent information simultaneously to a common receiver over a block-fading MAC. Thus, the channel is assumed to remain static during the transmission of a packet of symbols but independently varies from one packet to another. We address the general MIMO case where each user is equipped with n_{T_i} , $i = 1, \dots, N$, transmit antennas and the centralized receiver with n_R antennas. Notice that the single-antenna MAC model is easily derived if n_{T_i} and n_R are set to 1. The signal at the MIMO MAC receiver is given by

$$\mathbf{y} = \sum_{i=1}^N \sqrt{\frac{P_i}{n_{T_i}}} \mathbf{H}_i \mathbf{z}_i + \mathbf{w}, \quad (7.13)$$

where P_i and \mathbf{z}_i are the power and the $n_{T_i} \times 1$ vector of complex-valued transmitted symbols corresponding to user i , respectively. \mathbf{H}_i is the $n_R \times n_{T_i}$ complex-valued MIMO fading channel matrix for user i and $\mathbf{w} \sim \mathcal{N}_{\mathbb{C}}(0, \sigma_n^2 \mathbf{I})$ represents the AWGN at the receiver. Without loss of generality, we assume that the variance of the entries in \mathbf{z}_i and \mathbf{H}_i are equal to one. We also impose the sum-power constraint $\sum_{i=1}^N P_i = P_T$.

If we assume that the channel coefficients are described by a stationary stochastic process, the individual rate users may achieve, R_i , $1 \leq i \leq N$, are restricted by the following set of $2^N - 1$ inequalities, one for each possible subset \mathcal{N} of users

$$\sum_{i \in \mathcal{N}} R_i \leq \mathbb{E}_{\{\mathbf{H}_i\}_{i \in \mathcal{N}}} \left[\log \det \left(\mathbf{I}_{n_R} + \frac{1}{\sigma_n^2} \mathbf{H}_i \mathbf{K}_i \mathbf{H}_i^H \right) \right], \quad (7.14)$$

for all $\mathcal{N} \subset \{1, 2, \dots, N\}$. The superindex H , $\mathbb{E}[\cdot]$ and $\text{tr}(\cdot)$ denote the Hermitian, expectation and trace operator, respectively, and \mathbf{K}_i represents the transmit covariance matrix of the i -th user for a specific channel realization \mathbf{H}_i . The maximum sum-rate to be achieved in the block-fading MIMO MAC is limited by the inequality where all users are in the subset \mathcal{N} , i.e.

$$R_{\text{sum}} = \sum_{i=1}^N R_i \leq \mathbb{E}_{\{\mathbf{H}_i\}_{i=1}^N} \left[\log \det \left(\mathbf{I}_{n_R} + \frac{1}{\sigma_n^2} \sum_{i=1}^N \mathbf{H}_i \mathbf{K}_i \mathbf{H}_i^H \right) \right]. \quad (7.15)$$

In the case of multiple transmit antennas, it is not feasible to find N covariances matrix \mathbf{K}_i that simultaneously maximizes the individual rates given by the inequalities in Equation (7.14) and the sum-rate in Equation (7.15) [125]. In general, the achievable rates are therefore defined by

the particular allocation strategy employed at the users to send the information over the MAC. For example, it can be shown that the achievable capacity region for digital multiuser systems is provided by dirty paper coding [131] but, unfortunately, this method can not be successfully applied to analog JSCC transmissions. For that reason, we will specifically consider the achievable sum-rates corresponding to the proposed access schemes to calculate the OPTA curves.

When sending information over a MAC, the channel access scheme can be designed according to diverse objectives as, e.g. minimizing the transmission power while ensuring a certain distribution of the user rates or maximizing the sum-rate. In the ensuing sections, we present three different access methods designed for the transmission of continuous sources over block-fading MACs using analog JSCC: Orthogonal CDMA, Linear MMSE Access Coding and Opportunistic Access.

7.3.1 Orthogonal CDMA Scheme

Let us first consider a MAC scenario where users transmit their data with a given constant rate and the CSI is only available at the receiver. In this situation, orthogonal CDMA based on the spreading codes explained in Section 7.2.1 is a viable access method for the block-fading MAC. Remember that the advantage of CDMA with respect to other orthogonal access methods like TDMA or FDMA is that all users synchronously and simultaneously transmit over the same bandwidth while the receiver exploits the orthogonality of the spreading codes to remove the MAI. In addition, the flexible design of the proposed CDMA scheme guarantees that all users achieve the target rate.

In MIMO MAC, the spatial diversity provided by the deployment of multiple antennas at transmission and reception can be exploited to increase either the transmission rate or the communication reliability. As already seen, analog JSCC is able to provide high transmission rates with zero-delay and minimum decoding complexity. For that reason, it is more helpful to exploit the MIMO spatial diversity to improve reliability.

Let $R_i = k_i/K$, $i = 1, \dots, N$, be the target rate at which each user i should transmit the data to the receiver. Figure 7.3 shows the block diagram of the proposed orthogonal CDMA access scheme for the transmission of analog symbols over the block-fading MIMO MAC. As observed, the i -th user encodes the same vector \mathbf{x}_i of k_i symbols at each transmit antenna using the spreading codes obtained according to the procedure described in Section 7.2.1. The resulting vectors of K coded symbols, $\mathbf{z}_i^q = \mathbf{C}_i^q \mathbf{x}_i = [z_{ik}^q, \dots, z_{iK}^q]$, $q = 1, \dots, n_{T_i}$, are then sent sequentially over the MAC into K channel uses. Finally, the receiver utilizes the sequences of K symbols received through the n_R antennas to recover the information corresponding to each user by using a proper filter.

Alternatively, we can construct an overall MAC access code for each user by stacking the set

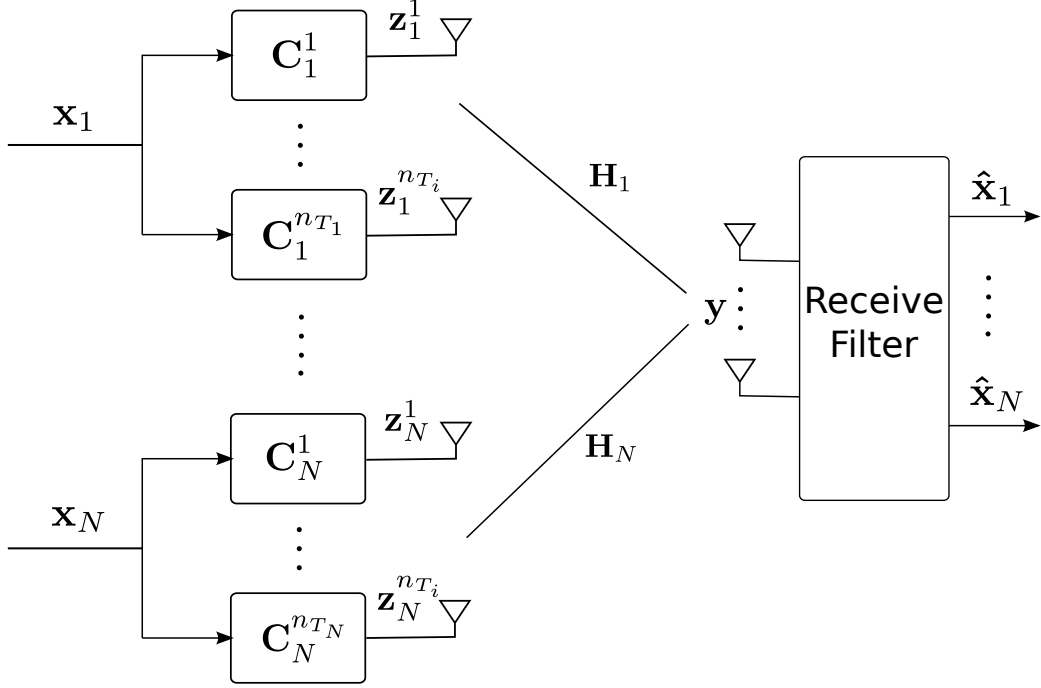


Figure 7.3: Block diagram of the orthogonal CDMA access scheme proposed for the block-fading MIMO MAC.

of n_{T_i} orthogonal codes employed at each antenna. Thus, $\tilde{\mathbf{C}}_i = [\mathbf{C}_i^1; \dots; \mathbf{C}_i^{n_{T_i}}]$ is a $n_{T_i}K \times k_i$ matrix that represents the MAC access code for the i -th user. If $\mathbf{x}_i = [x_{i1}, x_{i2}, \dots, x_{ik_i}]^T$ is the vector of source symbols corresponding to user i , the vector of $n_{T_i}K$ coded symbols can be hence obtained as $\mathbf{z}_i = \tilde{\mathbf{C}}_i \mathbf{x}_i$. These coded symbols are first spatially multiplexed over the n_{T_i} transmit antennas and then sent over the block-fading MIMO MAC along K time instants. Therefore, the received signal vector at time k is given by

$$\mathbf{y}_k = \sum_{i=1}^N \sqrt{\frac{P_i}{n_{T_i}}} \mathbf{H}_i \mathbf{z}_{ik} + \mathbf{w}_k \quad 1 \leq k \leq K. \quad (7.16)$$

where \mathbf{z}_{ik} and \mathbf{w}_k are the n_{T_i} transmitted symbol vector of the user i and the noise at time k , respectively. Since the channel is unknown at the transmitters, the user power P_i is uniformly distributed among the n_{T_i} antennas.

The MIMO MAC system model given by Equation (7.16) can be reformulated to an equivalent model. Indeed, let us define

$$\mathbf{A}_{pq} = \left[\sqrt{\frac{P_1}{n_{T_1}}} (\mathbf{H}_1)_{p,q} \mathbf{C}_1^q, \dots, \sqrt{\frac{P_N}{n_{T_N}}} (\mathbf{H}_N)_{p,q} \mathbf{C}_N^q \right],$$

where $(\mathbf{H}_i)_{p,q}$ is the (p, q) entry of \mathbf{H}_i that represents the channel gain between the antennas q and p of user i with $p = 1, \dots, n_R$ and $q = 1, \dots, n_{T_i}$. We now build the matrix $\tilde{\mathbf{H}}$ stacking the

matrices \mathbf{A}_{pq} as follows

$$\tilde{\mathbf{H}} = \left[\sum_{i=1}^{n_T} \mathbf{A}_{1i} ; \sum_{i=1}^{n_T} \mathbf{A}_{2i} ; \dots ; \sum_{i=1}^{n_T} \mathbf{A}_{n_R i} \right].$$

If we now stack the source symbols from the N users into one single vector $\mathbf{x} = [\mathbf{x}_1^T, \mathbf{x}_2^T, \dots, \mathbf{x}_N^T]^T$, Equation (7.16) can be rewritten as

$$\mathbf{y} = \tilde{\mathbf{H}}\mathbf{x} + \mathbf{w}, \quad (7.17)$$

where the vector \mathbf{y} comprises the symbols received through the n_R antennas along K intervals, $\tilde{\mathbf{H}}$ is the equivalent channel matrix obtained from the orthogonal codes and the channel paths, and $\mathbf{w} = [w_1, w_2, \dots, w_K]^T$ is the AWGN vector.

We now assume that a linear filter \mathbf{G} is employed at the MAC receiver to produce estimates of the transmitted symbols from the vector of received symbols \mathbf{y} , i.e. $\hat{\mathbf{x}} = \mathbf{G}\mathbf{y}$. Given that the source symbols are transmitted using analog JSCC, we consider the linear MMSE filter given by

$$\mathbf{G} = \left(\tilde{\mathbf{H}}^H \tilde{\mathbf{H}} + \rho \mathbf{I}_K \right)^{-1} \tilde{\mathbf{H}}^H, \quad (7.18)$$

where $\rho = (\sum_i n_{T_i} \sigma_n^2) / P_T$. The linear filter \mathbf{G} is able to separate the information corresponding to each user because of the orthogonal properties of the spreading codes. Hence ML decoding can be then applied to the resulting symbols at the filter output to obtain the corresponding estimate of the analog source symbols transmitted by each user.

7.3.2 Linear MMSE Access Coding

We now assume that the block-fading channel for each user, \mathbf{H}_i , is also known at the corresponding transmitter. In this case, CSI can be exploited by the users to calculate the optimal access codes for the considered MAC model. Since the objective of analog JSCC communications is to minimize the sum-MSE between the source and received signals, we design these access codes according to the MMSE criterion.

The system design quite resembles the scheme shown in Figure 7.3 for CDMA, but the orthogonal codes employed at the transmitters are now substituted by the optimal linear MMSE codes. We continue to assume that the i -th user transmits at the fixed rate $R_i = k_i/K, i = 1, \dots, N$, i.e. user i transmits k_i symbols along K channel uses. Unlike the orthogonal case, the access codes can be separately designed for each user and, therefore, we can express the received MAC signal as

$$\mathbf{y} = \sum_{i=1}^N \frac{1}{\sqrt{n_{T_i}}} \tilde{\mathbf{H}}_i \mathbf{F}_i \mathbf{x}_i + \mathbf{w}, \quad (7.19)$$

where \mathbf{F}_i is an $(n_T K \times k_i)$ matrix that represents the non-orthogonal access code for user i and $\tilde{\mathbf{H}}_i$ is a $(n_R K \times n_T K)$ block-diagonal matrix where the i -th element of the diagonal

corresponds to the MIMO channel of user i , \mathbf{H}_i . Since the transmitted symbols are assumed to be normalized, the access codes \mathbf{F}_i must satisfy the transmit sum-power constraint, i.e. $\sum_{i=1}^N \|\mathbf{F}_i\|_F^2 = P_T$.

Similarly to the previous section, we can further elaborate the signal model of the proposed MIMO MAC system. If the source symbols of all users are compacted into a single vector $\mathbf{x} = [\mathbf{x}_1^T, \dots, \mathbf{x}_N^T]^T$, and if we define the matrices $\tilde{\mathbf{H}} = [\frac{1}{\sqrt{n_{T1}}}\tilde{\mathbf{H}}_1, \dots, \frac{1}{\sqrt{n_{TN}}}\tilde{\mathbf{H}}_N]$ and $\mathbf{F} = \text{blockdiag}\{\mathbf{F}_i\}_{i=1}^N$, Equation (7.19) can be rewritten as

$$\mathbf{y} = \tilde{\mathbf{H}}\mathbf{F}\mathbf{x} + \mathbf{w}. \quad (7.20)$$

At the receiver, a linear filter \mathbf{G} is also employed to obtain an estimate of the transmitted symbols from vector \mathbf{y} , i.e. $\hat{\mathbf{x}} = \mathbf{G}\mathbf{y}$. According to this model, the optimal linear codes \mathbf{F}_i and the corresponding receiver filter \mathbf{G} that minimize the sum-MSE can be determined solving the following constrained minimization problem:

$$\arg \min_{\mathbf{F}, \mathbf{G}} \mathbb{E} [\text{tr}(\mathbf{e}\mathbf{e}^H)] \quad \text{s.t.} \quad \|\mathbf{F}\|_F^2 = P_T, \quad (7.21)$$

where $\mathbf{e} = \mathbf{x} - \hat{\mathbf{x}}$ represents the error vector. Given that the estimated symbol vector $\hat{\mathbf{x}}$ is calculated as

$$\hat{\mathbf{x}} = \mathbf{G}\mathbf{y} = \mathbf{G}\tilde{\mathbf{H}}\mathbf{F}\mathbf{x} + \mathbf{G}\mathbf{w},$$

the error vector is hence given by

$$\hat{\mathbf{e}} = \mathbf{x} - [\mathbf{G}\tilde{\mathbf{H}}\mathbf{F}\mathbf{x} + \mathbf{G}\mathbf{w}]. \quad (7.22)$$

In the literature, the sum-MSE minimization for a MAC system using linear filters has been specifically addressed in several works [57, 62, 116]. As an example, [116] uses the idea of alternating optimization to pose an iterative algorithm where the linear MMSE filters are updated in an alternating fashion. Rather than this option, we consider the approach described in [57], where a projected gradient algorithm is employed to improve the convergence speed at high SNRs.

The expected sum-MSE at the output of the receiver filter can be directly computed from Equation (7.22) as

$$\begin{aligned} \epsilon &= \text{tr}(\mathbf{e}\mathbf{e}^H) = \sum_{i=1}^N k_i - \text{tr} \left[\mathbf{G}\tilde{\mathbf{H}}\mathbf{F} + \mathbf{F}^H\tilde{\mathbf{H}}^H\mathbf{G}^H \right] \\ &+ \text{tr} \left[\mathbf{G}\tilde{\mathbf{H}}\mathbf{F}\mathbf{F}^H\tilde{\mathbf{H}}^H\mathbf{G}^H + \sigma_n^2\mathbf{G}\mathbf{G}^H \right]. \end{aligned} \quad (7.23)$$

Notice that the linear receive filter \mathbf{G} is calculated from the overall code matrix \mathbf{F} and the equivalent channel matrix $\tilde{\mathbf{H}}$ as

$$\mathbf{G} = \mathbf{F}^H\tilde{\mathbf{H}}^H(\sigma_n^2\mathbf{I}_{n_{RK}} + \tilde{\mathbf{H}}\mathbf{F}\mathbf{F}^H\tilde{\mathbf{H}}^H)^{-1}.$$

If we define the auxiliary matrix $\mathbf{X} = \sigma_n^2 \mathbf{I}_{n_R K} + \tilde{\mathbf{H}} \mathbf{F} \mathbf{F}^H \tilde{\mathbf{H}}^H$, the expression for the receive filter can be rewritten as $\mathbf{G} = \mathbf{F}^H \tilde{\mathbf{H}}^H \mathbf{X}^{-1}$, and the calculation of the sum-MSE in Equation (7.23) simplifies as follows

$$\epsilon = \sum_{i=1}^N k_i - N + \sigma_n^2 \text{tr} [\mathbf{X}^{-1}]. \quad (7.24)$$

We can now state an iterative gradient algorithm to update the linear codes (and implicitly the receive filter), with the following iteration step

$$\mathbf{F}^{(l+1)} = \left[\mathbf{F}^{(l)} - \frac{\lambda^{(l)}}{s^{(l)}} \nabla^* \epsilon(\mathbf{F}^{(l)}) \right], \quad (7.25)$$

where $s^{(l)}$ is the step size and $\nabla^*(\cdot)$ is the conjugate nabla operator that generates all conjugate Jacobi matrices. Such operator is computed as

$$\nabla^* \epsilon(\mathbf{F}^{(l)}) = \frac{\partial \epsilon(\mathbf{F}^{(l)})}{\partial \mathbf{F}^H} = -\sigma_n^2 \tilde{\mathbf{H}}^H \mathbf{X}^{-2} \tilde{\mathbf{H}} \mathbf{F}^{(l)}.$$

The factor $\lambda^{(l)}$ in Equation (7.25) is intended to speed up the algorithm convergence at the high SNR region where the sum-MSE cost function is almost flat and the norm of the Jacobi matrices is hence small. At each iteration, l , a normalization of $\mathbf{F}^{(l)}$ is also required in order to satisfy the imposed sum-power constraint. Such a normalization actually consists in the orthogonal projection of the linear codes obtained at each iteration into the subspace defined by the set of feasible solutions that satisfy the sum-power constraint.

Notice that the access codes \mathbf{F}_i can be actually interpreted as a type of spatio-temporal precoders where the data symbols are combined at the spatial and temporal domain to produce the whole set of coded symbols. Applying the projected gradient algorithm above, the optimal access codes and the linear receive filter that minimize the sum-MSE are obtained.

The achievable sum-rate of the analog JSCC system with linear MMSE access can be directly computed from the general expression for the sum-capacity of the MIMO MAC given by Equation (7.15) by replacing the covariance matrices with the corresponding optimal codes \mathbf{F}_i , i.e.

$$R_{\text{sum}} \leq \mathbb{E}_{\{\mathbf{H}_i\}_{i=1}^N} \left[\log \det \left(\mathbf{I}_{n_R} + \frac{1}{\sigma_n^2} \sum_{i=1}^N \mathbf{H}_i \mathbf{F}_i \mathbf{H}_i^H \right) \right]. \quad (7.26)$$

The implementation of this MAC access method requires perfect CSI available at both sides. Thus, we assume that the receiver is able to correctly estimate the channels of all users and then feedback the information of each transmitter to the corresponding user.

7.3.3 Opportunistic Access

Finally, we consider a MAC scenario where there is perfect CSI at the receiver and the transmitters, and the constraints imposed on the individual user rates are eliminated. Thus,

the user rates can be dynamically adapted according to the channel conditions. We first address the particular case where each user transmits with a single antenna. It has been shown in [65] that the access scheme that maximizes the sum-capacity of a block-fading SISO MAC consists in allocating the available transmit power P_T to the user with the highest channel gain at each time block. Such a scheme is usually referred to as Opportunistic Communication.

In this context, opportunistic access actually transforms the MAC problem into a point-to-point transmission where only the user with the best channel transmits at each time instant and, therefore, the received signal is not affected by MAI and can be expressed as

$$y = \sqrt{P_T} h_i z_i + w, \quad (7.27)$$

where z_i and h_i are the transmitted symbol and the channel gain corresponding to the user that experiences the best channel realization.

Like in previous schemes, the received symbols must be filtered before proceeding to the decoding of the source information in order to reduce the impact of the channel noise. Since only one user transmits at each instant, we can directly use the two-stage receiver proposed for single-user analog JSCC transmissions. Thus, an MMSE estimate of the transmitted symbol z_i is first computed as

$$\hat{z}_i = \left(\frac{\sqrt{P_T} h_i^*}{P_T |h_i|^2 + \sigma_n^2} \right) y$$

and then ML decoding is applied to the resulting filtered symbol \hat{z}_i .

As already mentioned, opportunistic access has been proved to achieve the ergodic sum-capacity of a block-fading SISO MAC when perfect CSI is available at both sides [125], which is given by

$$R_{\text{sum}} \leq \mathbb{E}_{\{h_i\}_{i=1}^N} \left[\log \left(1 + P_T \max_i |h_i|^2 \right) \right]. \quad (7.28)$$

As observed, Equation (7.28) corresponds to the capacity of a point-to-point communication system where the block-fading gain h_i is given by the strongest channel at each time block and the power used to transmit is the total available power P_T .

In the case of MIMO MAC, the allocation of the available power to the user with the best channel is no longer the optimal strategy when the objective is to maximize the sum-capacity [130, 140]. In that case, the spatial diversity provided by the use of multiple antennas can be employed to allow multiple users to transmit simultaneously over the block-fading MIMO MAC. As explained in Section 7.3.1, it is however preferable to exploit the spatial diversity to improve the reliability of analog JSCC transmissions rather than increasing the sum-rate of the system. For that reason, opportunistic access is also a suitable scheme for the transmission of analog samples over the MIMO MAC using analog JSCC. Thus, only the user i with the best channel at each time block transmits its information over the n_{T_i} antennas using the total available power.

Like in the single-antenna case, the MIMO MAC model with opportunistic access is transformed into a point-to-point MIMO communication and, therefore, the received symbols are given by

$$\mathbf{y} = \sqrt{\frac{P_T}{n_{T_i}}} \bar{\mathbf{H}} \mathbf{z}_i + \mathbf{w}, \quad (7.29)$$

where \mathbf{z}_i is the symbol vector transmitted by the best user and $\bar{\mathbf{H}}$ represents the response of the strongest MIMO channel at each block time that is determined as follows

$$\bar{\mathbf{H}} = \{\mathbf{H}_i \mid \max_i [C_E(\mathbf{H}_i)], \quad i = 1, \dots, N\}. \quad (7.30)$$

The term $C_E(\mathbf{H}_i)$ corresponds to the ergodic capacity of the MIMO channel for the i -th user considering the interferences caused by the rest of users.

At the receiver, a linear filter is also used to obtain an estimate of the transmitted symbols from the vector of n_R received symbols as $\hat{\mathbf{z}}_i = \mathbf{G} \mathbf{y}$. We consider a conventional linear MMSE filter for MIMO systems, i.e.

$$\mathbf{G} = \left(\bar{\mathbf{H}}^H \bar{\mathbf{H}} + \rho \mathbf{I}_{n_{T_i}} \right)^{-1} \bar{\mathbf{H}}^H,$$

where $\rho = (n_{T_i} \sigma_n^2) / P_T$. The achievable sum-rate of the MIMO MAC system with opportunistic access actually corresponds to the single-user MIMO capacity when the channel response is always given by the strongest channel at each time block and the power used to transmit is the total available power P_T . Thus,

$$R_{\text{sum}} = \mathbb{E}_{\mathbf{H}} \left[\log \det \left(\mathbf{I}_{n_R} + \frac{P_T}{n_{T_i} \sigma_n^2} \bar{\mathbf{H}} \bar{\mathbf{H}}^H \right) \right]. \quad (7.31)$$

It is important to note that the practical implementation of an opportunistic access scheme is difficult because it requires that either all transmitters know all the pair-wise MAC channel responses or that the transmissions be coordinated by the MAC receiver. In addition, a feedback channel is required for the receiver to send all the CSI to all users or indicate which is the user allowed to transmit at each channel realization.

Another remarkable disadvantage of the opportunistic strategy with respect to the previous proposed access schemes is that it can lead to unfair situations in terms of rate distribution and power consumption because one user may experience a better channel during a large number of channel realizations. Such user is consequently forced to consume more power although it also achieves a higher rate. There are many practical situations where this unfair behaviour of opportunistic access is unacceptable.

7.4 Results

In this section, the results of several computer simulations are presented to illustrate the performance of the different access schemes designed for the transmission of analog data over

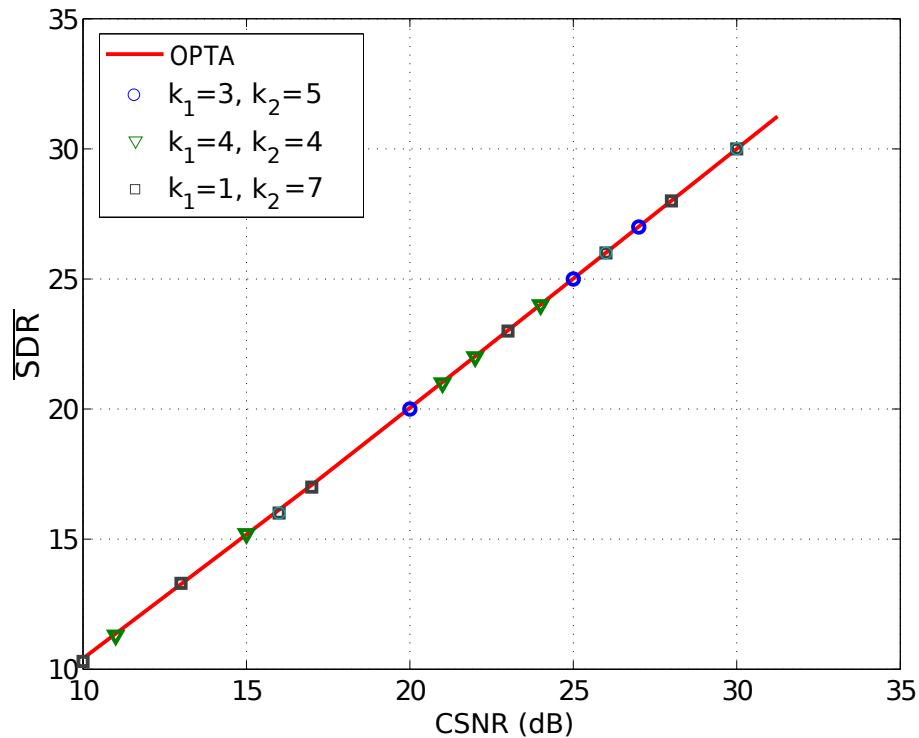


Figure 7.4: Performance of the orthogonal CDMA scheme for the transmission of uncoded samples over the Gaussian MAC.

a MAC. Specifically, we assume that the discrete-time continuous symbols to be transmitted by the users are generated from N i.i.d. Gaussian sources with zero mean and variance σ_s^2 .

We first evaluate a scenario where two users send independent data over a Gaussian MAC using the proposed orthogonal CDMA method with a spreading factor of $K = 8$. In such a scenario, the analog source symbols are first mapped into the channel symbols using an analog JSCC scheme and then encoded with the corresponding spreading codes. In order to show that the proposed method achieves the theoretical limits, we consider two particular analog JSCC strategies: uncoded transmission, i.e. ($M = 1$), and a 2:1 compression scheme based on the Archimedes' spiral, i.e. ($M = 2$).

Figures 7.4 and 7.5 show the system performance in term of average SDR with respect to CSNR for uncoded transmission and 2:1 compression of the source symbols, respectively. Each point in the graphs corresponds to the average SDR attained for a given pair of user rates (R_1, R_2) defined by the corresponding values for k_1 and k_2 . It is important to note that the power used for each user to transmit is optimally determined according to the allocation policy defined by Equation (7.12). In both figures, we also plot the OPTA bound calculated according to Equation (7.5) and using the proper expression of the sum-capacity for Gaussian MAC given by Equation (7.8).

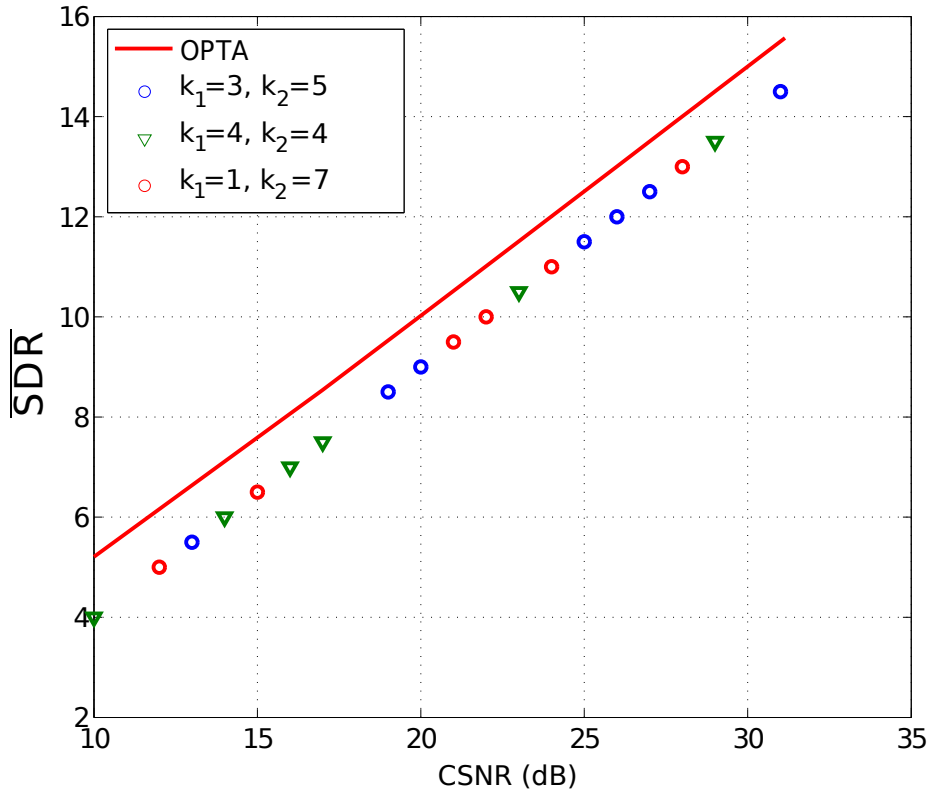


Figure 7.5: Performance of the orthogonal CDMA scheme for the transmission of 2:1 compressed samples over the Gaussian MAC.

As observed in Figure 7.4, the system achieves the optimal performance when the source symbols are directly transmitted using the orthogonal CDMA approach. This result is not surprising because, as already mentioned, the proposed scheme actually transforms the MAC model into a set of orthogonal SISO Gaussian channels and the uncoded transmission of Gaussian samples over Gaussian channels has been shown to be optimal when both source and channel have the same bandwidth [44]. In the case of 2:1 compression (Figure 7.5), the system performance is about 1 dB below the OPTA, regardless of the k_1 and k_2 values. This gap with respect to the optimal performance is motivated by the lossy compression operation carried out at each transmitter.

In the second part of this section, we present the results obtained for the block-fading MAC with the three proposed access methods: Orthogonal CDMA, Linear MMSE Coding and Opportunistic Access. We first focus on a SISO scenario where each user and the receiver are equipped with a single antenna. We consider again two independent users sending analog Gaussian symbols to a common receiver over the block-fading MAC. In this case, we focus on the 2:1 compression of the source symbols. Thus, at each transmitter, the source information is first encoded using the analog mapping based on the Archimedes' spiral and then input to the considered access scheme. We also assume constant user rates $R_1 = 3/8$ and $R_2 = 5/8$

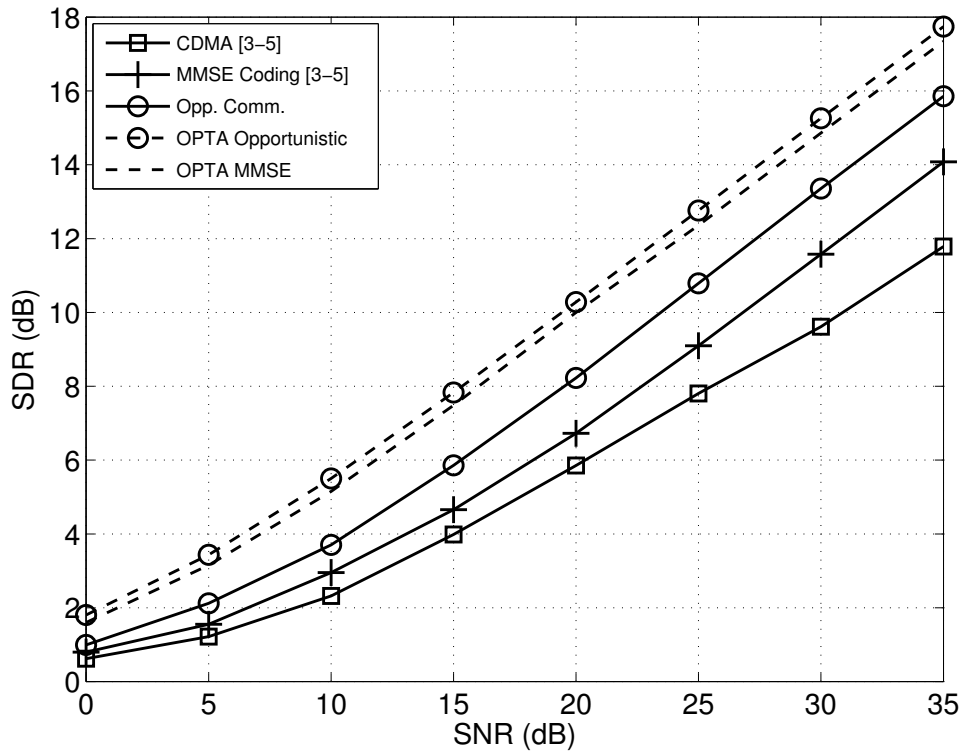


Figure 7.6: Performance of the three proposed access scheme for the transmission of Gaussian samples over a SISO MAC using a 2:1 analog JSCC scheme.

for CDMA and MMSE coding whereas the user rates are dynamically adapted in opportunistic access.

Figure 7.6 shows the system performance for the three employed MAC access methods. The OPTA curves for the MAC system with linear MMSE coding and with opportunist access are also plotted. Both curves are calculated according to Equation (7.5) using the proper expression for the achievable sum-rates given by Equation (7.26) and Equation (7.28), respectively. Recall that the theoretical optimal performance when CSI is also available at the transmitters in the single-antenna case is determined by the achievable sum-rate of the MAC system with opportunistic access given that such a strategy maximizes the sum-capacity.

As observed, the overall performance of the analog system is substantially improved when the CSI at the transmitters is exploited to design the optimal linear access codes and optimize the encoder parameters δ and α . The average SDR curve corresponding to CDMA remains about 2 dB below the performance curve of the linear MMSE access for medium and high CSNRs. As also shown in Figure 7.6, opportunistic access provides the best results and significantly improves the system performance, specially at the high CSNR region. However, it is important to remember that such a strategy does not allow us to guarantee the target data rates to be achieved by the MAC users during the transmission. These rates are optimally allocated according to the channel conditions of the users and it can lead to unfair distribution of both the user rates and power consumption.

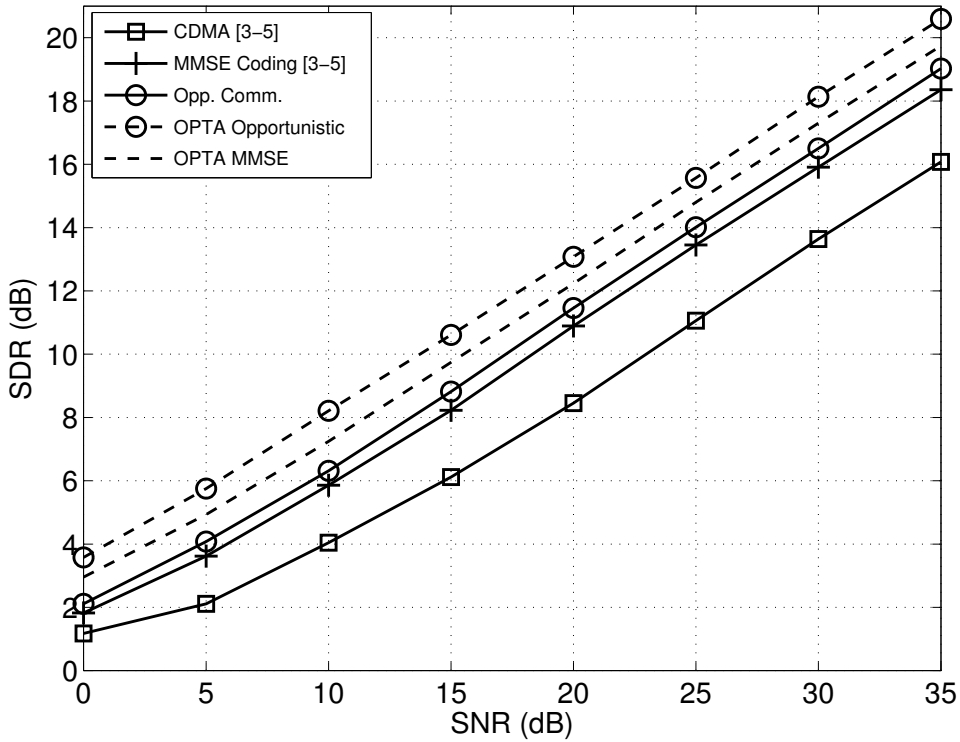


Figure 7.7: Performance of the three proposed access scheme for the transmission of Gaussian samples over a block-fading 2×2 MIMO MAC using a 2:1 analog JSCC scheme.

We finally consider a MIMO MAC scenario where two users send their data using $n_{T_i} = 2 \forall i$ antennas to the centralized receiver equipped with $n_R = 2$ antennas. The users are assumed to transmit at the same rate as in the SISO case, thus $R_1 = 3/8$ and $R_2 = 5/8$ for CDMA and MMSE coding whereas such rates and the available power are dynamically allocated in opportunistic access.

Figure 7.7 shows the performance of the analog JSCC system for the three considered MAC access methods when the source symbols are compressed with rate 2:1. In the figure, we also include the OPTA curves corresponding to the MIMO MAC model with linear MMSE coding and when the opportunistic method is employed to access to the block-fading MAC. As observed, the obtained results are similar to that of the SISO scenario. The use of optimal MMSE access codes allows us to significantly improve the overall performance of the analog system and the gap with respect to the performance upper bound is reduced down to less than 2 dB. In addition, we can appreciate that the performance difference between the linear MMSE coding and the opportunistic access is reduced to a large degree with respect to the SISO case and both performance curves are quite close to each other. Nevertheless, the opportunistic method continues to provide the best average SDR for the whole CSNR range and closely approaches the theoretical limits.

7.5 Conclusions

In this chapter, the application of analog JSCC techniques to multiuser communications has been studied. In particular, we have addressed the transmission of independent analog data over two types of MAC models: Gaussian MAC and block-fading MAC. At each transmitter, the source information is first encoded using analog JSCC and then input to the MAC access scheme. We have proposed three suitable channel access methods for analog JSCC transmissions: Orthogonal CDMA, Linear MMSE Coding and Opportunistic Access. CDMA is employed when the channel information is only available at the receiver whereas the other two alternatives exploit the channel knowledge at the transmitters to improve the overall system performance. Hence, the use of MMSE coding and opportunistic strategies makes only sense in the case of block-fading MAC. On the other hand, CDMA and linear MMSE coding are specially appropriate for MAC systems with specific per-user rate constraints since they provide a flexible framework to obtain any distribution of the individual user rates.

The results of computer simulations carried out to evaluate the Gaussian MAC model confirm that the proposed CDMA method achieves the optimal performance (OPTA) as long as the power for each user is distributed according to the optimal allocation policy and the source symbols are directly input to the MAC access scheme. When the information to be transmitted is first compressed using analog JSCC, the system no longer achieves the optimal performance although it remains only 1 dB below the OPTA. This performance loss is motivated by the compression operation at the analog encoders.

In the case of block-fading MAC, computer simulations show that the performance of the proposed CDMA scheme is relatively apart from the OPTA because orthogonal strategies are actually suboptimal for fading channels. As shown, the MAC performance can be significantly improved if the optimal linear MMSE access codes are employed instead of the orthogonal CDMA ones. Finally, the opportunistic access provides the best results in terms of sum-distortion but it may lead to an unfair distribution of both the user rates and power consumption.

Chapter 8

Conclusions and Future Work

8.1 Conclusions

The main purpose of this thesis is to assess the feasibility of analog Joint Source Channel Coding (JSCC) transmissions in wireless communications. Analog JSCC is an alternative strategy to encode and transmit discrete-time analog symbols capable of achieving high transmission rates with very low complexity and almost zero delay. Most of previous works in the literature focused on the transmission of continuous sources using analog JSCC over Additive White Gaussian Noise (AWGN) channels. For that reason, we consider very interesting to extend this approach to wireless environments, since it constitutes an promising strategy to satisfy the high speed and low latency requirements demanded by the users of current wireless applications.

As suggested by Shannon, we start reviewing the main concepts of analog JSCC in Chapter 2 according to a geometrical interpretation of the transmission problem. We focused on the case of point-to-point communications, memoryless channels and 2:1 bandwidth compression of the source information. Under these conditions, it is well-know that the analog mapping consisting in a doubly intertwined Archimedes' spiral closely approaches the optimal cost-distortion tradeoff given by the Optimum Performance Theoretically Attainable (OPTA). In order to improve the performance of analog JSCC systems based on Archimedes' spiral, certain optimization issues are further addressed at the end of Chapter 2. On one hand, the optimal cost-distortion tradeoff can be only achieved if the optimal values for the encoder parameters are employed. On the other hand, the power constraint inevitably imposes a normalization of the coded symbols at the transmitter. The optimal values of the parameters and the normalization factors that satisfy the transmit power constraint have been determined off-line for a wide range of Channel Signal-to-Noise Ratios (CSNRs).

After evaluating the decoding operation, we proposed a two-stage receiver structure to deal with the impairments of the existing decoding methods: Maximum Likelihood (ML) and Minimum Mean Square Error (MMSE). As seen, the proposed approach achieves near-optimal

performance of the MMSE decoding while maintaining the receiver complexity at low level. This contribution not only allows us to overcome the limitations of ML and MMSE decoding but it is also essential to preserve the low complexity and low delay at the receiver when analog JSCC is implemented on more complex transmission models. In such systems, the use of the optimal MMSE approach is unfeasible since its complexity is prohibitive.

In Chapter 3, the performance of the proposed analog JSCC scheme and that of a digital Bit Interleaved Coded Modulation (BICM) system is compared. For a fair comparison, the digital system has been designed to transmit at the same rate as the analog scheme (high throughput). In this context, the attained results show that the analog system outperforms the considered practical digital systems with a significantly lower encoding and decoding complexity. In fact, its performance is even above the theoretical limit for digital systems employing the same number of channel uses. According to these results, we conclude that analog JSCC is an appealing alternative to the traditional design of digital systems for applications with strong requirements on delay and/or complexity and where a high transmission rate is required.

At this point, the potential virtues of analog JSCC have been already corroborated on ideal conditions (by simulation), although its actual performance has not been assessed yet on realistic environments, such as wireless communications. No experimental evaluation of the practical feasibility of this scheme has been performed to date. In Chapter 4, we describe a software-defined radio implementation of a system that uses analog JSCC to send analog data over real wireless channels. Specifically, we have carried out closed-loop narrowband single-antenna measurements in a typical and realistic indoor scenario (an office). This experimental evaluation shows that the obtained performance curves almost perfectly match the ones reported by simulations in AWGN channels for CSNR values below 20 dB. Thus, the feasibility of the proposed analog JSCC scheme on wireless communications and real environments is clearly demonstrated.

During the past years, the increasingly demand of reliable high-speed transmissions over wireless channels has lead to devise new communication paradigms in order to satisfy such high throughput requirements while making efficiently use of the scarce available resources and exploiting the diversity gain provided by fading channels. These techniques are generally based on the utilization of multiple antennas at both the transmitter and the receiver. In Chapter 5, we design an analog JSCC Multiple Input Multiple Output (MIMO) system that performs a 2:1 compression at each transmit antenna and employs the proposed two-step decoding strategy at the receiver, since the optimal MMSE decoding is unfeasible even for a small number of antennas. Along Chapter 5, the performance of this analog MIMO scheme is evaluated for several scenarios, including different compression rates, asymmetrical system configurations, perfect Channel State Information (CSI) at the receiver and/or the transmitter. For these experiments we considered two different types of channels: randomly-generated synthetic and real wireless channels. From this detailed study, we conclude that the proposed analog

MIMO scheme approaches the theoretical limits (OPTA), specially for the case of Decision Feedback (DF) detection and 2:1 compression rate.

The transmission of analog JSCC samples over frequency-selective fading channels is addressed in Chapter 6. In order to avoid the harmful effects of multipath propagation, the analog channel symbols are modulated using the well-know multicarrier scheme Orthogonal Frequency-Division Multiplexing (OFDM), prior to be transmitted over the wideband channels. This OFDM scheme is further combined with the use of multiple antennas at both the transmitter and the receiver. In this case, a appropriate optimization of analog JSCC MIMO-OFDM systems is specially important because the symbols transmitted over different antennas and subcarriers experience different fading. For that reason, several alternatives are considered for the optimization procedure depending on whether partial/full CSI or no CSI is available at the transmitter. The performance of analog MIMO-OFDM systems is assessed in two scenarios: synthetic channels and channels generated according to the specifications of standards for mobile communications. The obtained results show that the proposed analog MIMO-OFDM scheme exhibits good performance, specially when adaptive coding is employed together with linear precoding in order to exploit the channel information at the transmitter.

Finally, we have evaluated the use of analog JSCC for the transmission of continuous-amplitude symbols over Multiple Access Channels (MACs) in Chapter 7. In this communication model, it is essential to design a channel access scheme that allows the users to transmit their information simultaneously over the same channel while the receiver is able to decouple the data streams corresponding to each user. Rather than designing particular analog mappings for each MAC scenario, we propose to employ the analog mappings and the receiver structure considered for point-to-point communications, and focus on the design of suitable access methods for analog JSCC. Specifically, three different channel access schemes have been presented: Orthogonal CDMA, Linear MMSE Coding and Opportunistic Access. The obtained results show that this strategy is able to approach the theoretical optimal performance of the considered MAC systems. Thus, we can confirm that the application of analog JSCC techniques can be actually considered an appealing alternative to the conventional Separate Source Channel Coding (SSCC) systems in several multiuser scenarios, such as cellular communications or sensor networks, where there usually exist severe constraints on delay and/or power consumption and the information must be transmitted at high data rates.

In summary, the promising results of analog JSCC in the area of wireless communications confirm the potential advantages of using this novel strategy in future wireless applications. This strategy seems specially suitable to satisfy the high transmission rate and low-delay requirements of the real-time applications. Moreover, under these premises, analog JSCC has been shown as a better solution than traditional digital systems. Along this thesis, several wireless transmission schemes using analog JSCC have been proposed to deal with the hindrances of fading channels and exploit the different types of diversity gain provided by

such channels. This study has not been exclusively restricted to simulated environments, but we have also considered various situations on realistic scenarios and real wireless channels together with their corresponding implementation problems.

8.2 Future Work

When we started investigating the utilization of analog JSCC over fading channels, our main concern was to prove its feasibility in the context of wireless communications. Hence, we decided to address the 2:1 compression of analog sources on a point-to-point scenario under some practical assumptions, such as channel perfectly known at the receiver (i.e. regardless of the error introduced by the channel estimation), noiseless feedback channel, uncorrelated sources or memoryless channels –although spatially correlated MIMO channels and slow-fading time correlated channels are actually considered in Chapter 6–. For the future, the communication models based on analog JSCC can be further enhanced by including these pending issues, i.e. the channel estimation, the impact of a noisy feedback channel, the use of correlated sources or other types of fading channels. In addition, due to the particular properties of analog JSCC, there exists multiple scenarios where the application of this strategy can be also very interesting.

8.2.1 Analog JSCC for Bandwidth Expansion

Along this thesis, we focused on the particular case of a 2:1 compression using a doubly intertwined Archimedes' spiral. This decision comes because Shannon-Kotel'nikov mappings have been shown to approach the theoretical limit as long as they are designed for bandwidth compression of analog sources. Specifically, mappings based on the Archimedes' spiral provide a near-optimal performance for a 2:1 compression rate. Nevertheless, the design of analog mappings that approach the OPTA for bandwidth expansion still constitutes an important challenge on current analog JSCC research. This fact significantly limits the application of this strategy to those models where a high transmission rate is not specially critical but it is more convenient to ensure a data transmission with good quality. For the future, an interesting work area is the design of optimal analog mappings for expansion coding in order to achieve similar results to the compression case.

8.2.2 Correlated Sources

A memoryless source generating identically and independent distributed (i.i.d.) samples is a traditional assumption on signal processing. Nevertheless, this premise is not adequate for modeling multitude of practical situations where the information to be transmitted is correlated

in some way. Additional research would be required in the future to adapt the proposed analog JSCC systems if the source is no longer memoryless. For the case of correlated sources, a more convenient approach could be the design of optimal analog mappings according to the correlation level between the source samples.

8.2.3 Imperfect CSI in Fading Channels

In this work, we decided to disregard the stage corresponding to the estimation of the time-varying fading channels. Thus, the channel is assumed to be perfectly known (estimated) at the receiver and, as long as necessary, we consider that this information is sent error-free to the transmitter through a feedback channel. However, small errors introduced by the estimation procedure can induce significant distortions after the filtering operation and, as consequence, a severe degradation of the system performance. At present, there exist several estimation methods –such as, for example, training and tracking methods or blind estimation– that generally provide accurate information of the channel. The study of the impact of the CSI estimation errors on the overall performance of the proposed analog scheme represents an interesting complement to the work carried out in this thesis.

In a similar way, another possibility is to consider a noisy feedback channel which introduces a certain level of distortion on the channel information. In this situation, the information used by the transmitter either to select the optimal parameters or precode the channel symbols (full CSI) may not be sufficiently accurate. We can combine this scenario together with the former approach and evaluate the joint effect on the system performance.

8.2.4 Analog JSCC in Feedback Channels

Related to the feedback channel, it is only possible to assume that the CSI is available at the transmitter if the coherence time of the fading channel is guaranteed to be larger than the time required to feedback the information. When the fading channel varies quickly –for example in the context of vehicular communications– its coherence time is short and, therefore, the receiver needs to send the channel estimation through the feedback link at high rate. Thus, in this case of fast fading environments, the part corresponding to the feedback operation must be equipped with some transmission mechanism that tolerates these high rate requirements.

At this point, a compression scheme based on analog JSCC immediately arises as a possible solution instead of more complex and slower digital approaches. In such digital schemes, the information has to be first quantized and then encoded using a channel code in order to recover the quantized information with a low error probability at the transmitter. In the literature, analog transmission [79, 101] and hybrid analog-digital schemes [107] have been already applied to this problem and promising results have been obtained. Our intention is to design a purely

analog solution, based on Shannon-Kotel'nikov mappings, that sends the channel information at very high rates in fast fading environments.

8.2.5 Broadcast Channel

The application of analog JSCC mappings to multiuser communications has been studied in the particular case of MACs. The MAC dual model is the broadcast channel where one single transmitter simultaneously sends information to many receivers sharing the same bandwidth. Hence the transmitter needs to employ some communication scheme that allows each user to recover only the data intended to it in spite of the interferences caused by the signals corresponding to the other users. Examples of such transmission model are broadcast television systems or the downlink in cellular communications. In the future we plan to extend the ideas presented for the MAC case to the design of analog JSCC systems that reliably transmit analog data over broadcast channels. In this case, we also expect to obtain good results since the problem of the sum-Mean Square Error (MSE) minimization in the broadcast channel can be reformulated from the point of view of the MAC due to the duality properties between both models [57].

Appendix A

Estimation of Channel SNR in MIMO Systems with Decision Feedback Receivers

Let us consider a $n_T \times n_R$ MIMO transmission scheme that employs a Decision Feedback (DF) filter designed according to the MMSE criterion at the receiver. The channel is assumed to be unknown at the transmitter so that the total power P_T is uniformly distributed among the n_T antennas.

Theorem 1 *The CSNR of the equivalent Single Input Single Output (SISO) channels can be calculated at the output of the MMSE DF filter as*

$$CSNR_i = \frac{\mu_i^2}{\mu_i - \mu_i^2} = \frac{\mu_i}{1 - \mu_i}, \quad i = 1, \dots, n_T, \quad (\text{A.1})$$

where μ_i represents the diagonal elements of the matrix $\mathbf{I}_{n_T} - \frac{n_T \sigma_n^2}{P_T} \mathbf{\Delta}^{-1} \mathbf{L}^{-H}$.

Proof: We start considering the transmission of a vector \mathbf{s} , that comprises n_T analog coded symbols, over a MIMO channel whose response is represented by the matrix \mathbf{H} . In the proposed model, the vector of received symbols can be determined as

$$\mathbf{x} = \mathbf{H}\mathbf{s} + \mathbf{n}.$$

At the receiver, an MMSE DF filter is employed to cancel the spatial interference introduced by the MIMO channel. The DF detector consists of a Feed Forward (FF) filter and a Feed Backward (FB) filter whose expressions are respectively given by

$$\text{FF}_{\text{DF}} = \mathbf{B}^H \mathbf{H}^H = \mathbf{\Delta}^{-1} \mathbf{L}^{-H} \mathbf{H}^H, \quad (\text{A.2})$$

$$\text{FB}_{\text{DF}} = \mathbf{L} - \mathbf{I}_{n_T}, \quad (\text{A.3})$$

where the lower triangular matrix \mathbf{L} and the diagonal matrix $\mathbf{\Delta}$ are obtained from the following Cholesky decomposition

$$\mathbf{H}^H \mathbf{H} + \rho \mathbf{I}_{n_T} = \mathbf{L}^{-H} \mathbf{\Delta} \mathbf{L},$$

where $\rho = (n_T \sigma_n^2)/P_T$. Hence, the response of the channel alongside the matched filter, \mathbf{H}^H , can be straightforwardly computed from the above equation as

$$\mathbf{H}^H \mathbf{H} = \mathbf{L}^{-H} \Delta \mathbf{L} - \rho \mathbf{I}_{n_T}. \quad (\text{A.4})$$

In the detection stage, the FF filter is first applied to the vector \mathbf{x} of the symbols observed at the DF detector input, i.e

$$\mathbf{y} = \mathbf{B}^H \mathbf{H}^H \mathbf{H} \mathbf{s} + \mathbf{B}^H \mathbf{H}^H \mathbf{n},$$

and the FB filter is then employed to remove the channel interferences successively. Thus, the resulting symbols after the filtering operations are defined by the expression

$$\mathbf{z} = \mathbf{y} - (\mathbf{L} - \mathbf{I}_{n_T}) \mathbf{s} = \mathbf{B}^H \mathbf{H}^H \mathbf{H} \mathbf{s} + \mathbf{B}^H \mathbf{H}^H \mathbf{n} - \mathbf{L} \mathbf{s} + \mathbf{s}. \quad (\text{A.5})$$

Substituting the term $\mathbf{H}^H \mathbf{H}$ in Equation (A.5) by its corresponding expression in Equation (A.4) and simplifying some terms, we finally obtain the following expression for the vector of filtered symbols:

$$\mathbf{z} = (\mathbf{I}_{n_T} - \rho \Delta^{-1} \mathbf{L}^{-H}) \mathbf{s} + \mathbf{B}^H \mathbf{H}^H \mathbf{n}. \quad (\text{A.6})$$

In order to further simplify the ensuing calculations, we define the auxiliary matrices \mathbf{G} and \mathbf{Q}^H as

$$\begin{aligned} \mathbf{G} &= \mathbf{B}^H \mathbf{H}^H \mathbf{H} - \mathbf{L} + \mathbf{I}_{n_T} = \mathbf{I}_{n_T} - \rho \Delta^{-1} \mathbf{L}^{-H}, \\ \mathbf{Q}^H &= \mathbf{B}^H \mathbf{H}^H = \Delta^{-1} \mathbf{L}^{-H} \mathbf{H}^H. \end{aligned}$$

According to this notation, Equation (A.6) can be more compactly rewritten as

$$\mathbf{z} = \mathbf{G} \mathbf{s} + \mathbf{Q}^H \mathbf{n}.$$

Now, we can obtain the signal power at the output of the DF filter by computing the autocovariance matrix of vector \mathbf{z} , i.e.

$$C_z = \mathbb{E}[\mathbf{z} \mathbf{z}^H] = \mathbf{G} C_s \mathbf{G}^H + \mathbf{Q}^H C_n \mathbf{Q},$$

where C_s and C_n are the autocovariance matrix of the transmitted signal and the noise, respectively. Remember that $C_s = \frac{P_T}{n_T} \mathbf{I}_{n_T}$ and $C_n = \sigma_n^2 \mathbf{I}_{n_R}$ and, therefore, the covariance matrix C_z can be expressed as

$$C_z = \mathbb{E}[\mathbf{z} \mathbf{z}^H] = \frac{P_T}{n_T} \mathbf{G} \mathbf{G}^H + \sigma_n^2 \mathbf{Q}^H \mathbf{Q}. \quad (\text{A.7})$$

In order to determine the equivalent CSNRs at the output of the MMSE DF filter, the ratio between the fraction of the total power (given by Equation (A.7)) corresponding to the signal and noise components is now computed by

$$\text{CSNR}_i = \frac{\frac{P_T}{n_T} |g_{ii}|^2}{\frac{P_T}{n_T} [\mathbf{G} \mathbf{G}^H + \rho \mathbf{Q}^H \mathbf{Q}]_{ii} - \frac{P_T}{n_T} |g_{ii}|^2}. \quad (\text{A.8})$$

Substituting \mathbf{G} and \mathbf{H}^H by their expressions in terms of $\mathbf{\Delta}$ and \mathbf{L} matrices, we can further develop the term corresponding to the total power that appears at the denominator in the above expression, i.e.

$$\begin{aligned} \mathbf{G}\mathbf{G}^H + \rho\mathbf{Q}^H\mathbf{Q} &= (\mathbf{I}_{n_T} - \rho\mathbf{\Delta}^{-1}\mathbf{L}^{-H}) (\mathbf{I}_{n_T} - \rho\mathbf{L}^{-1}\mathbf{\Delta}^{-1}) + \\ &+ \rho(\mathbf{\Delta}^{-1} - \rho\mathbf{\Delta}^{-1}\mathbf{L}^{-H}\mathbf{L}^{-1}\mathbf{\Delta}^{-1}). \end{aligned}$$

Making the product and extracting the common factor ρ , we finally obtain

$$\begin{aligned} \mathbf{G}\mathbf{G}^H + \sigma_n^2\mathbf{Q}^H\mathbf{Q} &= \mathbf{I}_{n_T} - \rho\mathbf{\Delta}^{-1}\mathbf{L}^{-H} - \rho\mathbf{L}^{-1}\mathbf{\Delta}^{-1} + \rho\mathbf{\Delta}^{-1} \\ &= \mathbf{G} - \rho(\mathbf{L}^{-1}\mathbf{\Delta}^{-1} - \mathbf{\Delta}^{-1}). \end{aligned}$$

The diagonal elements of the resulting matrix can be easily simplified taking into account that \mathbf{L} is lower triangular and $\mathbf{\Delta}$ is diagonal. Hence,

$$(\mathbf{G})_{ii} - \rho(\mathbf{L}^{-1}\mathbf{\Delta}^{-1} - \mathbf{\Delta}^{-1})_{ii} = g_{ii} - \rho(\delta_{ii}^{-1} - \delta_{ii}^{-1}) = g_{ii},$$

where $(\mathbf{G})_{ii} = g_{ii}$ is the i -th element of the diagonal of the matrix \mathbf{G} and δ_{ii} represents the components of the diagonal matrix $\mathbf{\Delta} = \{\delta_{11}, \dots, \delta_{n_T n_T}\}$. Thereby, it is proved that the CSNR at the output of the DF MIMO filter is given by

$$\text{CSNR}_i = \frac{\frac{P_T}{n_T}|g_{ii}|^2}{\frac{P_T}{n_T}g_{ii} - \frac{P_T}{n_T}|g_{ii}|^2} = \frac{|g_{ii}|^2}{g_{ii} - |g_{ii}|^2}, \quad i = 1, \dots, n_T \quad (\text{A.9})$$

Appendix B

Explicit Solution for the Design of MMSE MIMO Transceivers

Let us consider a $n_T \times n_R$ MIMO system where the linear transmit and receive filters are jointly designed according to the MMSE criterion. As shown in Chapter 5, the general expressions for the optimal MMSE linear precoder and equalizer under a transmit power constraint are respectively given by

$$\mathbf{P} = (\lambda \mathbf{I}_{n_T} + \mathbf{H}^H \mathbf{W}^H \mathbf{W} \mathbf{H})^{-1} (\mathbf{H}^H \mathbf{W}^H), \quad (\text{B.1})$$

$$\mathbf{W} = (\mathbf{P}^H \mathbf{H}^H) (\sigma_n^2 \mathbf{I}_{n_R} + \mathbf{H} \mathbf{P} \mathbf{P}^H \mathbf{H}^H)^{-1}, \quad (\text{B.2})$$

where $\mathbf{H} \in \mathbb{C}^{n_R \times n_T}$ represents the MIMO channel matrix, $\mathbf{P} \in \mathbb{C}^{n_T \times L}$ the precoding matrix and $\mathbf{W} \in \mathbb{C}^{L \times n_R}$ the receive equalizer. In addition, L represents the rank of the MIMO channel matrix and $\lambda \geq 0$ is the Lagrange multiplier that ensures the total transmit power does not exceed P_T .

At first sight, the above equations depend on each other and, therefore, an iterative procedure arises as a feasible option to compute \mathbf{P} and \mathbf{W} . Nevertheless, a solution for the optimal MMSE MIMO transceiver can be explicitly calculated from Equations (B.1) and (B.2) by assuming a Single Value Decomposition (SVD) of the MIMO channel.

We start exposing the particular decomposition of the optimal linear precoder and equalizer by the two following lemmas

Lemma 1 *The optimal linear MMSE precoder for the MIMO transmission $\mathbf{y} = \mathbf{H}\mathbf{s} + \mathbf{n}$ is of the form $\mathbf{P} = \mathbf{V}\mathbf{T}$, where $\mathbf{T} = \text{diag}\{t_1, t_2, \dots, t_L\} \in \mathbb{R}^{n_T \times L}$ and $\mathbf{V} \in \mathbb{C}^{n_T \times n_T}$ is a unitary matrix from the channel SVD, i.e. $\mathbf{H} = \mathbf{U}\mathbf{\Sigma}\mathbf{V}^H$.*

Proof: As shown in [120], applying the Hadamard inequality [21], the linear precoder $\mathbf{P} = \mathbf{V}\mathbf{T}$ maximizes the mutual information along the MIMO channel when the input symbols are

Gaussian, i.e.,

$$I(\mathbf{s}, \mathbf{y}) = \log_2 \det \left(\mathbf{I}_{n_R} + \frac{1}{\sigma_n^2} \mathbf{H} \mathbf{C}_s \mathbf{H}^H \right), \quad (\text{B.3})$$

where $\mathbf{C}_s = E\{\mathbf{s}\mathbf{s}^H\}$ is the input signal covariance matrix. Notice that Equation (B.3) is straightforwardly obtained by particularizing the general expression of the mutual information for MIMO systems, given by Equation (5.9). The corresponding derivation of such a expression can be reviewed in Section 5.2.1. On the other hand, due to the existing relation between the mutual information and the MMSE [47], and taking account that the mutual information for MIMO channels is a logarithmic function, the choice of the optimal precoder that maximizes the mutual information in turn leads to the minimization of the MMSE.

Lemma 2 *The optimal linear MMSE equalizer is of the form $\mathbf{W}_{\text{MMSE}} = \mathbf{D}\mathbf{U}^H$ where $\mathbf{D} = \text{diag}\{d_1, d_2, \dots, d_L\} \in \mathbb{R}^{L \times n_R}$ and $\mathbf{U} \in \mathbb{C}^{n_R \times n_R}$ is a unitary matrix that comes from the channel SVD $\mathbf{H} = \mathbf{U}\mathbf{\Sigma}\mathbf{V}^H$.*

Proof: Substituting $\mathbf{P} = \mathbf{V}\mathbf{T}$ in (B.2) we obtain

$$\mathbf{W}_{\text{MMSE}} = \mathbf{T}\mathbf{\Sigma}^T [\mathbf{\Sigma}\mathbf{T}\mathbf{T}\mathbf{\Sigma}^T + \sigma_n^2 \mathbf{I}_{n_R}]^{-1} \mathbf{U}^H = \mathbf{D}\mathbf{U}^H \quad (\text{B.4})$$

and the lemma is proved.

From Lemmas 1 and 2, an estimate of the transmitted symbol vector \mathbf{s} at the equalizer output is hence calculated as

$$\hat{\mathbf{s}} = \mathbf{W}\mathbf{H}\mathbf{P}\mathbf{s} + \mathbf{W}\mathbf{n} = \mathbf{D}\mathbf{\Sigma}\mathbf{T}\mathbf{s} + \mathbf{D}\mathbf{v}, \quad (\text{B.5})$$

where $\mathbf{\Sigma} = \text{diag}\{\sigma_1, \sigma_2, \dots\} \in \mathbb{R}^{n_R \times n_T}$ is also a real diagonal matrix and $\mathbf{v} = \mathbf{U}^H \mathbf{n}$ is the additive Gaussian noise. Notice that $\mathbf{v} \sim \mathcal{N}_{\mathbb{C}}(0, \sigma_n^2 \mathbf{I})$, since \mathbf{U} is a unitary matrix and hence does not change the noise distribution. Since \mathbf{D} , $\mathbf{\Sigma}$ and \mathbf{T} are diagonal matrices, equation (B.5) can be rewritten component-wise as follows

$$\hat{s}_i = d_i \sigma_i t_i s_i + d_i v_i, \quad i = 1, \dots, L. \quad (\text{B.6})$$

Our next step is to determine the MMSE diagonal precoder \mathbf{T} and equalizer \mathbf{D} . Defining the error vector as $\mathbf{e} = \mathbf{s} - \hat{\mathbf{s}}$, the MSE is given by

$$\text{MSE} = \sum_{i=1}^L |s_i - \hat{s}_i|^2 = \sum_{i=1}^L (1 - d_i \sigma_i t_i)^2 + \sigma_n^2 d_i^2. \quad (\text{B.7})$$

This cost function should be minimized under the power constraint $\sum_{i=1}^L t_i^2 \leq P_T$. Thereby, an explicit expression for the precoder \mathbf{P} and the detector \mathbf{W} can be explicitly computed once the diagonal matrices \mathbf{T} and \mathbf{D} are obtained solving this minimization problem. The ensuing theorem provides the solution to this constrained optimization problem.

Theorem 2 The diagonal precoders $\{t_i\}_{i=1}^L$ and equalizers $\{d_i\}_{i=1}^L$ that minimize the MSE cost function (B.7) under the power constraint $\sum_{i=1}^L t_i^2 \leq P_T$ are calculated from the following equations:

$$d_i = \frac{1}{\sqrt{\sigma_n^2}} \sqrt{A_i [1 - A_i]^+} \quad (\text{B.8})$$

$$t_i = \frac{\sqrt{\sigma_n^2}}{\sigma_i} \sqrt{\left[\frac{1}{A_i} - 1 \right]^+} \quad (\text{B.9})$$

where

$$A_i = \frac{\frac{1}{\sigma_i} \sum_{k=1}^{L^*} \frac{1}{\sigma_k}}{\eta + \sum_{k=1}^{L^*} \frac{1}{\sigma_k^2}}. \quad (\text{B.10})$$

The operator $[\cdot]^+$ takes only the positive arguments and sets negative arguments to zero. The number $L^* \leq L$ refers to the number of singular values whose corresponding expressions for d_i or t_i are non-zero. Finally, $\eta = P_T/\sigma_n^2$ is the transmit Signal-to-Noise Ratio (SNR).

Proof: We start defining the Lagrangian cost function

$$\mathcal{L} = \sum_{i=1}^L (d_i \sigma_i t_i - 1)^2 + \sigma_n^2 d_i^2 + \lambda \left(\sum_{i=1}^L t_i^2 - P_T \right), \quad (\text{B.11})$$

where λ is the Lagrange multiplier. Equating to zero the derivative of \mathcal{L} with respect to d_i and t_i we obtain

$$\frac{\partial \mathcal{L}}{\partial d_i} = 0 \Rightarrow d_i = \frac{t_i \sigma_i}{\sigma_i^2 t_i^2 + \sigma_n^2}, \quad (\text{B.12})$$

$$\frac{\partial \mathcal{L}}{\partial t_i} = 0 \Rightarrow t_i = \frac{d_i \sigma_i}{\sigma_i^2 d_i^2 + \lambda}. \quad (\text{B.13})$$

Substituting one expression into the other leads to a quadratic form in d_i^2 :

$$\sigma_i^2 \left(\frac{d_i \sigma_i}{\sigma_i^2 d_i^2 + \lambda} \right)^2 + \sigma_n^2 = \frac{\sigma_i^2}{\sigma_i^2 d_i^2 + \lambda}. \quad (\text{B.14})$$

Solving for d_i^2 , we obtain a solution in terms of λ

$$d_i^2 = \frac{1}{\sigma_i^2} \left[\sqrt{\frac{\sigma_i^2 \lambda}{\sigma_n^2}} - \lambda \right]^+ \quad (\text{B.15})$$

and by substitution also a solution for t_i^2 in λ

$$t_i^2 = \frac{1}{\sigma_i^2} \left[\sqrt{\frac{\sigma_i^2 \sigma_n^2}{\lambda}} - \sigma_n^2 \right]^+. \quad (\text{B.16})$$

It is important to notice that the positivity conditions in (B.15) and (B.16) are equivalent and also equivalent to requirement $A_i < 1$ in (B.10). The next step is to determine the λ value that satisfies the power constraint $\sum_{i=1}^{L^*} t_i^2 = P_T$. Substituting (B.15) and (B.16) into the power constraint, the following value is obtained

$$\lambda = \frac{1}{\sigma_n^2} \left(\frac{\sum_{k=1}^{L^*} \frac{1}{\sigma_k}}{\eta + \sum_{k=1}^{L^*} \frac{1}{\sigma_k^2}} \right)^2 \quad (\text{B.17})$$

which is indeed a constant. Substituting λ into (B.15) and (B.16) we find the explicit solutions provided in the theorem.

The diagonal precoders and equalizers can be determined from (B.8), (B.9) and (B.10) with a waterfilling-like algorithm. Assuming the SVD of \mathbf{H} is available, the complexity of this algorithm is linear in L , i.e. $\mathcal{O}(L)$. Indeed, let us order the singular values from smallest to largest, i.e. $\sigma_{\min} = \sigma_1 \leq \sigma_2 \dots \leq \sigma_L = \sigma_{\max}$. Next, let us compute the sums $S_1(L) = \sum_{k=1}^L \sigma_k^{-1}$ and $S_2(L) = \eta + \sum_{k=1}^L \sigma_k^{-2}$. This complexity is linear in L . If $\sigma_1^{-1} S_1(L) / S_2(L) > 1$, then decrease L and reduce the terms S_1 and S_2 by their σ_1 contribution. Then, continue with the next singular value until the condition is not satisfied. The remaining $L = L^*$ and all remaining terms satisfy $A_i < 1$. The maximal number of such iterations is $L - 1$. It is interesting to note that this solution relates to the well-known waterfilling result [21] in the sense that it provides an optimal way (in the MMSE sense) to distribute the transmit power among the different data streams.

Appendix C

List of Acronyms

3GPP 3rd Group Partnership Project

ADC Analog-to-Digital Converter

API Application Program Interface

APP A Posteriori Probability

ARQ Automatic-Repeat-Request

AWGN Additive White Gaussian Noise

BICM Bit Interleaved Coded Modulation

BP Belief Propagation

CDMA Code Division Multiple Access

COTS Commercial Off-The-Shelf

COVQ Channel Optimized Vector Quantizer

CP Cyclic Prefix

CSI Channel State Information

CSNR Channel Signal-to-Noise Ratio

DAB Digital Audio Broadcasting

DAC Digital-to-Analog Converter

DF Decision Feedback

DFT	Discrete Fourier Transform
DSP	Digital Signal Processor
DVB	Digital Video Broadcasting
EXIT	EXtrinsic Information Transfer
FB	Feed Backward
FEC	Forward Error Correction
FF	Feed Forward
FFT	Fast Fourier Transform
FDM	Frequency Division Multiplexing
FDMA	Frequency Division Multiple Access
FPGA	Field Programmable Gate Array
ICI	InterCarrier Interference
IDFT	Inverse Discrete Fourier Transform
IF	Intermediate Frequency
IFFT	Inverse Fast Fourier Transform
IRA	Irregular Repeat Accumulate
ISI	InterSymbol Interference
JSCC	Joint Source Channel Coding
LAN	Local Network Area
LDGM	Low Density Generator Matrix
LDPC	Low Density Parity Check
LLR	Log-Likelihood Ratio
LS	Least Squares
MAC	Multiple Access Channel
MAI	Multiple Access Interference

MIMO	Multiple Input Multiple Output
ML	Maximum Likelihood
MMSE	Minimum Mean Square Error
MSE	Mean Square Error
MRC	Maximal-Ratio Combining
OFDM	Orthogonal Frequency-Division Multiplexing
OPTA	Optimum Performance Theoretically Attainable
PAM	Pulse Amplitude Modulation
PAPR	Peak-to-Average Power Ratio
PCCOVQ	Power Constrained Channel Optimized Vector Quantizer
PDF	Probability Density Function
PN	Pseudo-Noise
SDR	Signal-to-Distortion Ratio
SINR	Signal-to-Interference Noise Ratio
SISO	Single Input Single Output
SNR	Signal-to-Noise Ratio
SPA	Sum-Product Algorithm
SSCC	Separate Source Channel Coding
SVD	Single Value Decomposition
RA	Repeat Accumulate
RF	Radio Frequency
TDMA	Time Division Multiple Access
TCM	Trellis Coded Modulation
VQ	Vector Quantization
WSS	Wide Sense Stationary

Bibliography

- [1] “Ettus Research, LLC,” <http://www.ettus.com>, 2011.
- [2] “Lyrtech, Inc.” <http://www.lyrtech.com>, 2011.
- [3] “Maxim Integrated Products, Inc.” <http://www.maxim-ic.com>, 2011.
- [4] “Sundance Multiprocessor, Ltd.” <http://www.sundance.com>, 2011.
- [5] “High-speed physical layer in the 5 ghz band,” 1999.
- [6] “Further higher-speed physical layer extension in the 2.4 ghz band,” 2003.
- [7] “IEEE recommended practice for local and metropolitan area networks,” 2001.
- [8] “IEEE approves standard for mobile broadband wireless access (mbwa),” 2008.
- [9] E. Akyol, K. Rose, and T. Ramstad, “Optimal mappings for joint source channel coding,” in *Proc. of Information Theory Workshop (ITW)*, 2010.
- [10] ———, “Optimized analog mappings for distributed source-channel coding,” in *Proc. of IEEE Data Compression Conference*, 2010.
- [11] S. Arimoto, “An algorithm for computing the capacity of arbitrary discrete memoryless channels,” *IEEE Trans. Information Theory*, vol. 18, pp. 14–20, 1972.
- [12] T. Berger, *Rate Distortion Theory: A Mathematical Basis for Data Compression*. Englewood Cliffs, 1971.
- [13] C. Berrou, A. Glavieux, and P. Thitimajshima, “Near Shannon limit error-correcting coding and decoding: Turbo codes,” in *Proc. of Int. Conf. Commun. (ICC), Geneva, Switzerland*, May 1993, pp. 1064–1070.
- [14] J. C. Bezdek and R. J. Hathaway, “Convergence of alternating optimization,” *Neural, Parallel and Scientific Computation*, vol. 11, no. 4, pp. 351–368, 2003.
- [15] R. Blahut, “Computation of channel capacity and rate-distortion functions,” *IEEE Trans. Information Theory*, vol. 18, pp. 460–473, 1972.
- [16] G. Caire, G. Taricco, and E. Biglieri, “Bit-interleaved coded modulation,” in *Proc. of Int. Conf. Comm. (ICC)*, 1997, pp. 1463–1467.
- [17] R. W. Chang, “Synthesis of bandlimited orthogonal signals for multichannel data transmission,” *Bell Sys. Tech. Journal*, vol. 45, pp. 1775–1796, Dec 1966.
- [18] R. W. Chang and R. Gibby, “Theoretical study of performance of an orthogonal multiplexing data

- transmission scheme,” *IEEE Trans. on Communications*, vol. 16, pp. 529–540, Aug 1968.
- [19] B. Chen and G. W. Wornell, “Analog error-correcting codes based on chaotic dynamical systems,” *IEEE Trans. on Communications*, vol. 46, no. 7, pp. 881–890, Jul 1998.
- [20] S. Y. Chung, “On the construction of some capacity-approaching coding schemes,” *Ph.D. dissertation, Dept. EECS, MIT*, 2000.
- [21] T. Cover and J. Thomas, *Elements of Information Theory*. Wiley, 1991.
- [22] H. Coward and T. A. Ramstad, “Quantizer optimization in hybrid digitalanalog transmission of analog source signals,” in *Proc. of IEEE Int. Conf. Acoustics, Speech and Signal Processing (ICASSP), Istanbul, Turkey*, Jun 2000.
- [23] G. de Oliveira Brante, R. Souza, and J. Garcia-Frias, “Analog joint source-channel coding in rayleigh fading channels,” in *Proc. ICASSP*, May 2011, pp. 3148–3151.
- [24] J. G. Dunham and R. M. Gray, “Joint source and noisy channel trellis encoding,” *IEEE Trans. on Information Theory*, vol. 27, pp. 516–519, Jul 1981.
- [25] P. Ellias, “Coding for noisy channels,” in *IRE Conv. Rec.*, 1955, pp. 37 – 46.
- [26] H. Everett, “Generalized lagrange multiplier method for solving problems of optimum allocation of resources,” *Operations Research*, vol. 11, no. 3, pp. 399–417, 1963.
- [27] R. Fano, “A heuristic discussion of probabilistic coding,” *IEEE Trans. on Information Theory*, vol. IT-9, pp. 64 – 74, Apr. 1963.
- [28] N. Farvardin, “A study of vector quantization for noisy channels,” *IEEE Trans. on Information Theory*, vol. 36, no. 4, pp. 799–809, 1990.
- [29] N. Farvardin and V. Vaishampayan, “Optimal quantizer design for noisy channels: An approach to combined source-channel coding,” *IEEE Trans. on Information Theory*, vol. 33, no. 6, pp. 827–838, Nov 1987.
- [30] T. M. Fernández-Caramés, J. A. García-Naya, M. González-Lopez, and L. Castedo, “MIMO testbed middleware for transmission automation,” in *Proc. of 50th ELMAR*, Zadar, Croatia, Sep. 2008, pp. 215–218.
- [31] P. Fleischer, “Sufficient conditions for achieving minimum distortion in a quantizer,” *IEEE Int. Convention Record*, pp. 104– 111, 1964.
- [32] P. A. Floor and T. A. Ramstad, “Dimension reducing mappings in joint source-channel coding,” in *Proc. NORSIG*, Jun 2006.
- [33] P. A. Floor, A. N. Kim, N. Wernersson, T. A. Ramstad, M. Skoglund, and I. Balasingham, “Zero-delay joint source-channel coding for a bivariate gaussian on a gaussian MAC,” *IEEE Trans. on Communications*, vol. 60, no. 10, pp. 3091–3102, Oct 2012.
- [34] G. D. Forney, “On the role of MMSE estimation in approaching the information-theoretic limits of linear gaussian channels: Shannon meets wiener,” in *41st Allerton Conference on Communication, Control, and Computing, Monticello*, Oct 2003.
- [35] G. J. Foschini, “Layered space-time architecture for wireless communication in a fading

- environment when using multi-element antennas,” *Bell Labs Technical Journal*, vol. 1, no. 2, pp. 41–59, 1996.
- [36] G. J. Foschini and M. J. Gans, “On limits of wireless communications in a fading environment when using multiple antennas,” *Wireless Personal Communications*, vol. 6, no. 3, pp. 311–335, 1998.
- [37] G. Foschini, G. Golden, R. Valenzuela, and P. Wolniansky, “Simplified processing for high spectral efficiency wireless communication employing multi-element arrays,” *IEEE Journal on Selected Areas in Communications*, vol. 17, no. 11, pp. 1841–1852, Nov 1999.
- [38] A. Fuldseth, “A robust subband video compression for noisy channels with multilevel signaling,” *Ph.D. Thesis, Norwegian University of Science and Engineering (NTNU)*, 1997.
- [39] A. Fuldseth and T. A. Ramstad, “Bandwidth compression for continuous amplitude channels based on vector approximation to a continuous subset of the source signal space,” in *IEEE Int. Conf. Acoustics, Speech, Signal Process. (ICASSP)*, no. 1, Mar 1997, pp. 114–128.
- [40] R. G. Gallager, “Low-density parity-check codes,” *MIT Press*, 1963.
- [41] J. A. García-Naya, H. J. Perez-Iglesias, T. M. Fernández-Caramés, M. González-López, and L. Castedo, “A distributed multilayer architecture enabling end-user access to MIMO testbeds,” in *Proc. of IEEE 19th PIMRC*, Cannes, France, Sep. 2008, pp. 1–5, doi: 10.1109/PIMRC.2008.4699692.
- [42] J. A. García-Naya, M. González-López, and L. Castedo, *Radio Communications*. INTECH, Apr 2010, ch. A Distributed Multilayer Software Architecture for MIMO Testbeds, ISBN: 978-953-307-091-9.
- [43] M. Gastpar, B. Rimoldi, and M. Vetterli, “To code, or not to code: Lossy source channel communication revisited,” *IEEE Trans. on Information Theory*, vol. 49, no. 5, pp. 1147 – 1158, May 2003.
- [44] T. J. Goblick, “Theoretical limitations on the transmission of data from analog sources,” *IEEE Trans. on Information Theory*, vol. 11, no. 4, pp. 558–567, Oct 1965.
- [45] M. J. E. Golay, “Notes on digital coding,” in *Proc. IRE*, 1949.
- [46] R. M. Gray, “Vector quantization,” *Acoust., Speech, Signal Processing Magazine*, vol. 1, pp. 4–29, Apr 1984.
- [47] D. Guo, S. Shamai, and S. Verdú, “Mutual information and minimum mean-square error in gaussian channels,” *IEEE Trans. on Information Theory*, vol. 51, no. 4, pp. 1261–1282, Apr 2005.
- [48] R. W. Hamming, “Error-detecting and error-correcting codes,” *Bell System Technical Journal*, vol. 29, pp. 147 – 160, 1950.
- [49] F. Hekland, “On the design and analysis of Shannon-Kotelnikov mappings for joint source-channel coding,” *Ph.D. dissertation, Norwegian University of Science and Technology*, 2007.
- [50] F. Hekland, G. E. Oien, and T. A. Ramstad, “Using 2:1 Shannon mapping for joint source-channel coding,” in *Proc. of DCC’05*, Mar 2005.

-
- [51] F. Hekland, P. Floor, and T. A. Ramstad, "Shannon-Kotel'nikov mappings in joint source-channel coding," *IEEE Trans. on Communications*, vol. 57, no. 1, pp. 94–105, Jan 2009.
- [52] H. Sampath and A. Paulraj, "Joint transmit and receive optimization for high data rate wireless communications using multiple antennas," in *Proc. of 33rd Asilomar Conf. Signals, Syst. Comput., Pacific Grove, CA*, Oct 1999.
- [53] H. Sampath, P. Stoica, and A. Paulraj, "Generalized linear precoder and decoder design for MIMO channels using the weighted MMSE criterion," *IEEE Trans. on Communications*, vol. 49, no. 12, Dec 2001.
- [54] Y. Hu, Z. Wang, J. Garcia-Frias, and G. R. Arce, "Non-linear coding for improved performance in compressive sensing," in *Proc. of CISS09*, Mar 2009.
- [55] Y. Hu, J. Garcia-Frias, and M. Lamarca, "Analog joint source-channel coding using non-linear curves and MMSE decoding," *IEEE Trans. on Communications*, vol. 59, no. 11, pp. 3016–3026, Nov 2011.
- [56] D. A. Huffman, "A method for the construction of minimum redundancy codes," in *Proc. IRE*, pp. 1098 – 1101, Sep 1952.
- [57] R. Hunger, M. Joham, and W. Utschick, "On the mse-duality of the broadcast channel and the multiple access channel," *IEEE Trans. Signal Processing*, vol. 57, no. 2, pp. 698–713, Feb 2009.
- [58] <http://www.ist-imetra.org>.
- [59] "Guidelines for evaluation of radio transmission technologies for IMT-2000," <http://www.itu.int/rec/R-REC-M.1225/en>, 1997.
- [60] H. Jin, A. Khandekar, and R. McEliece, "Irregular repeat-accumulate codes," in *Proc. of 2nd Int. Symp. Turbo Codes and Related Topics*, Sep 2000.
- [61] M. Joham, W. Utschick, and J. Nossek, "Linear transmit processing in MIMO communications systems," *IEEE Trans. on Signal Processing*, vol. 53, no. 8, pp. 2700–2712, Aug 2005.
- [62] E. Jorswieck and H. Boche, "Transmission strategies for the MIMO MAC with MMSE receiver: Average MSE optimization and achievable individual MSE region," *IEEE Trans. Signal Processing*, vol. 51, no. 11, pp. 2872–2881, Nov 2003.
- [63] K. Kansanen, A. Kim, R. Thobaben, and J. Karlsson, "Low complexity bandwidth compression mappings sensor networks," in *Proc. of ISCCSP*, Mar 2010.
- [64] S. M. Kay, *Fundamentals of Statistical Signal Processing: Estimation Theory*. Prentice-Hall, 1993.
- [65] R. Knopp and P. A. Humblet, "Information capacity and power control in single-cell multiuser communications," in *Proc. of IEEE ICC*, Jun 1995.
- [66] V. Kotel'nikov, *The theory of optimum noise immunity*. New York: McGraw-Hill, 1959.
- [67] I. Kozintsev and K. Ramchandran, "Hybrid compressed uncompressed framework for wireless image transmission," in *Proc. of IEEE Int. Conf. Communications (ICC), Montreal, QC, Canada*, Jun 1997.
-

-
- [68] L. G. Kraft, "A device for quantizing, grouping and coding amplitude modulated pulses," *Masters thesis, Department of Electrical Engineering, MIT, Cambridge, MA*, 1949.
- [69] J. Kron, F. Alajaji, and M. Skoglund, "Low-delay joint source-channel mappings for the Gaussian MAC," *IEEE Communications Letters*, vol. 18, no. 2, pp. 249–252, Feb 2014.
- [70] H. W. Kuhn and A. W. Tucker, "Nonlinear programming," in *Proc. of 2nd Berkeley Symposium. Berkeley: University of California Press*, 1951, pp. 481–492.
- [71] A. Lapidoth and S. Tinguely, "Sending a bivariate gaussian over a gaussian MAC," *IEEE Trans. on Information Theory*, vol. 56, no. 6, pp. 2714–2752, 2010.
- [72] K. H. Lee and D. P. Petersen, "Optimal linear coding for vector channels," *IEEE Trans. on Communications*, vol. COM-24, no. 12, pp. 1283–1290, Dec 1976.
- [73] J. M. Lervik, "Subband image communication over digital transparent and analog wave-form channels." *Ph.D. thesis, NTNU*, 1996.
- [74] Y. Linde, A. Buzo, and R. M. Gray, "An algorithm for vector quantizer design," *IEEE Trans. on Communications*, vol. 28, pp. 84–95, Jan 1980.
- [75] S. Lloyd, "Least squares quantization in PCM," *IEEE Trans. on Information Theory*, vol. IT-28, no. 2, pp. 129 – 137, Mar 1982.
- [76] B. Lu, G. Yue, and X. Wang, "Performance analysis and design optimization of LDPC-coded MIMO OFDM systems," *IEEE Trans. on Signal Processing*, vol. 52, no. 2, Feb 2004.
- [77] D. J. C. MacKay and R. M. Neal, "Good codes based on very sparse matrices," in *Proc. of Cryptography Coding, 5th IMA Conf., Berlin, Germany*, 1995, pp. 100–111.
- [78] —, "Near Shannon limit performance of low-density parity-check codes," *Electronic Letters*, vol. 32, pp. 1645 – 1646, Aug 1996.
- [79] T. L. Marzetta and B. M. Hochwald, "Fast transfer of channel state information in wireless systems," *IEEE Trans. on Signal Processing*, vol. 54, no. 4, pp. 1268–1278, Apr 2006.
- [80] J. Massey, "Threshold decoding," *Cambridge, MA, USA: MIT Press*, 1963.
- [81] J. Max, "Quantizing for minimum distortion," *IEEE Trans. on Information Theory*, vol. IT-6, pp. 7 – 12, 1960.
- [82] M. Gatspar, "Uncoded transmission is exactly optimal for a simple gaussian sensor network," *IEEE Trans. on Information Theory*, vol. 54, no. 11, pp. 5247–5251, Nov 2008.
- [83] J. Mitola, "The software radio architecture," *IEEE Communications Magazine*, vol. 33, no. 5, pp. 26–38, May 1995.
- [84] P. Monsen, "Feedback equalization for fading dispersive channels," *IEEE Trans. Information Theory*, vol. 17, no. 1, pp. 56–64, Jan 1971.
- [85] E. Moulines, P. Duhamel, J. Cardoso, and S. Mayrargue, "Subspace methods for the blind identification of multichannel FIR filters," *IEEE Trans. on Signal Processing*, vol. 43, pp. 516–525, Feb 1995.
- [86] S. Na and D. L. Neuhoff, "On the support of quantizers - Part I: Conditions for asymptotic
-

- optimality,” *IEEE Trans. on Information Theory*, 1999.
- [87] H. Nyquist, “Certain topics in telegraph transmission theory,” *Trans. on AIEE*, vol. 47, pp. 617–644, Apr 1928.
- [88] D. Palomar, J. M. Cioffi, and M. A. Lagunas, “Joint Tx-Rx beamforming design for multicarrier MIMO channels: A unified framework for convex optimization,” *IEEE Trans. on Signal Processing*, vol. 51, no. 9, pp. 2381–2401, Sep 2003.
- [89] T. W. Parsons, *Voice and speech processing*. McGraw-Hill, 1987.
- [90] J. Pearl, *Probabilistic Reasoning in Intelligent Systems*. San Francisco, CA: Kaufmann, 1988.
- [91] A. Peled and A. Ruiz, “Frequency domain data transmission using reduced computational complexity algorithms,” in *Proc. of IEEE Int. Conf. on Acoustics, Speech, and Signal Processing (ICASSP)*, vol. 5, pp. 964–967, Apr 1980.
- [92] D. Persson, J. Kron, M. Skoglund, and E. G. Larsson, “Joint source-channel coding for the MIMO broadcast channel,” *IEEE Trans. on Signal Processing*, vol. 60, no. 4, pp. 2085–2090, Apr 2012.
- [93] <http://www.comonsens.org/>.
- [94] T. A. Ramstad, “Shannon mappings for robust communication,” *Teletronikk*, vol. 98, no. 1, pp. 114–128, 2002.
- [95] T. Rappaport, *Wireless Communications Principles and Practice*. Prentice Hall, 1996.
- [96] T. J. Richardson, M. A. Shokrollahi, and R. L. Urbanke, “Design of capacity-approaching irregular low-density parity-check codes,” *IEEE Trans. on Information Theory*, vol. 47, no. 2, pp. 619 – 637, 2001.
- [97] T. J. Rouhpael, *RF and Digital Signal Processing for Software-Defined Radio. A Multi-Standard Multi-Mode Approach*. USA: Elsevier, 2009. ISBN: 978-0-7506-8210-7.
- [98] M. Rungeler and P. Vary, “Hybrid digital analog transform coding,” in *Proc. of IEEE Int. Conf. Acoustics, Speech and Signal Processing (ICASSP)*, Vancouver, Canada, May 2013.
- [99] B. R. Saltzberg, “Performance of efficient parallel data transmission,” *IEEE Trans. on Communications*, vol. 15, pp. 805–811, Dec 1967.
- [100] J. Salz, “Optimum mean-square decision feedback equalization,” *Bell System Technical Journal*, vol. 52, no. 8, pp. 1341–1373, Oct 1973.
- [101] D. Samardzija and N. Mandayam, “Unquantized and uncoded channel state information feedback in multiple-antenna multiuser systems,” *IEEE Trans. on Communications*, vol. 54, no. 7, pp. 1335–1345, Jul 2006.
- [102] H. Sari, G. Karam, and I. Jeanclaude, “Transmission techniques for digital terrestrial TV broadcasting,” *IEEE Communications Magazine*, pp. 100–109, Feb 1995.
- [103] S. A. Savari and R. G. Gallager, “Generalized Tunstall codes for sources with memory,” *IEEE Trans. on Information Theory*, vol. 43, no. 2, pp. 658 – 668, Mar 1997.
- [104] A. Scaglione, G. B. Giannakis, and S. Barbarossa, “Redundant filterbank precoders and equalizers part I: Unification and optimal designs,” *IEEE Trans. on Signal Processing*, vol. 47, pp. 1988–

- 2006, Jul 1999.
- [105] A. Scaglione, P. Stoica, S. Barbarossa, G. B. Giannakis, and H. Sampath, “Optimal designs for space-time linear precoders and decoders,” *IEEE Trans. on Signal Processing*, vol. 50, no. 5, pp. 1051 – 1064, May 2002.
- [106] S. Servetto, “Lattice quantization with side information, codes, asymptotics, and applications in sensor networks,” *IEEE Trans. on Information Theory*, vol. 53, no. 2, pp. 714 – 731, 2007.
- [107] M. M. Shanechi, R. Porat, and U. Erez, “Comparison of practical feedback algorithms for multiuser MIMO,” *IEEE Trans. on Communications*, vol. 58, pp. 2436–2446, Aug 2010.
- [108] C. E. Shannon, “A mathematical theory of communication,” *The Bell System Technical Journal*, vol. 7, pp. 379–423, 1948.
- [109] —, “Communication in the presence of noise,” *Proceedings of the IRE*, vol. 37, no. 1, pp. 20–21, 1949.
- [110] —, “Coding theorems for a discrete source with a fidelity criterion,” *IRE Nat. Conv. Rec.*, pp. 142–163, Mar 1959.
- [111] M. Sipser and D. A. Spielman, “Expander codes,” *IEEE Trans. on Information Theory*, vol. 42, no. 11, pp. 1710 – 1722, Nov 1996.
- [112] M. Skoglund, “On channel-constrained vector quantization and index assignment for discrete memoryless channels,” *IEEE Trans. on Information Theory*, vol. 45, no. 7, pp. 2615–2622, 1999.
- [113] M. Skoglund, N. Phamdo, and F. Alajaji, “Design and performance of VQ-based hybrid digital-analog joint source-channel codes,” *IEEE Trans. on Information Theory*, vol. 48, no. 3, pp. 708–720, Mar 2002.
- [114] —, “Hybrid digital analog source channel coding for bandwidth compression/expansion,” *IEEE Trans. on Information Theory*, vol. 52, no. 8, pp. 3757–3763, Aug 2006.
- [115] D. A. Spielman, “Linear-time encodable and decodable error-correcting codes,” *IEEE Trans. on Information Theory*, vol. 42, pp. 1723 – 1732, Nov 1996.
- [116] S. Serbetli and A. Yener, “Transceiver optimization for multiuser mimo systems,” *IEEE Trans. on Signal Processing*, vol. 52, no. 1, pp. 214–226, Jan 2004.
- [117] G. L. Stuber, J. R. Barry, S. W. McLaughlin, Y. Li, M. A. Ingram, and T. Pratt, “Broadband MIMO-OFDM wireless communications,” in *Proc. of the IEEE*, vol. 92, pp. 271–294, Feb 2004.
- [118] R. M. Tanner, “A recursive approach to low complexity codes,” *IEEE Trans. on Information Theory*, vol. IT-27, no. 9, pp. 533 – 547, Sep 1981.
- [119] I. E. Telatar, “Capacity of multi-antenna gaussian channels,” *Bell Labs Technical Memorandum*, Jun 1995.
- [120] —, “Capacity of multi-antenna gaussian channels,” *European Trans. on Telecommunications*, vol. 10, no. 6, pp. 585–595, Nov 1999.
- [121] S. ten Brink, “Convergence behavior of iteratively decoded parallel concatenated codes,” *IEEE Trans. on Communications*, vol. 49, no. 10, pp. 1727 – 1737, Oct 2001.

- [122] ———, “Convergence of iterative decoding,” *Electronic Letters*, vol. 35, no. 10, pp. 806 – 808, May 1999.
- [123] S. ten Brink and G. Kramer, “Design of repeat-accumulate codes for iterative detection and decoding,” *IEEE Trans. on Signal Processing*, vol. 51, no. 11, pp. 2764 – 2772, Nov 2003.
- [124] L. Tong, G. Xu, and T. Kailath, “A new approach to blind identification and equalization of multipath channels,” *IEEE Trans. on Information Theory*, vol. IT-40, pp. 340–349, Mar 1994.
- [125] D. Tse and P. Viswanath, *Fundamentals of Wireless Communication*. Cambridge University Press, 2005.
- [126] B. P. Tunstall, “Synthesis of noiseless compression codes,” *Ph.D. dissertation, Georgia Inst. Technol.*, 1967.
- [127] G. Ungerboeck, “Channel coding with multilevel/phase signals,” *IEEE Trans. on Information Theory*, vol. IT-28, pp. 56–67, Jan 1982.
- [128] V. A. Vaishampayan and S. I. R. Costa, “Curves on a sphere, shift-map dynamics, and error control for continuous alphabet sources,” *IEEE Trans. on Information Theory*, vol. 49, no. 7, pp. 1658–1672, Jul 2003.
- [129] S. Verdu, *Multiuser Detection*. Cambridge Univ, 1998.
- [130] P. Viswanath, D. N. Tse, and V. Anantharam, “Asymptotically optimal water-filling in vector multiple-access channels,” *IEEE Trans. on Information Theory*, vol. 47, no. 1, pp. 241 – 267, Jan 2001.
- [131] P. Viswanath, N. Jindal, and A. Goldsmith, “Duality, achievable rates, and sum-rate capacity of Gaussian MIMO broadcast channels,” *IEEE Trans. on Information Theory*, vol. 49, no. 10, pp. 2658 – 2668, Oct 2003.
- [132] A. Viterbi, “Error bounds for convolutional codes and an asymptotically optimum decoding algorithm,” *IEEE Trans. on Information Theory*, vol. IT-13, pp. 260 – 269, Apr. 1967.
- [133] X. Wang and H. V. Poor, “Iterative (turbo) soft interference cancellation and decoding for coded CDMA,” *IEEE Trans. on Communications*, vol. 47, no. 7, pp. 1046–1061, Jul 1999.
- [134] S. B. Weinstein and P. M. Ebert, “Data transmission by frequency division multiplexing using discrete fourier transform,” *IEEE Trans. on Communications*, vol. 19, pp. 628–634, Oct 1971.
- [135] N. Wernersson, M. Skoglund, and T. A. Ramstad, “Polynomial based analog source-channel codes,” *IEEE Trans. on Communications*, vol. 57, no. 9, pp. 2600–2606, Sep 2009.
- [136] W. Karush, “Minima of functions of several variables with inequalities as side constraints,” *M.Sc. Dissertation, Dept. of Mathematics, Univ. of Chicago, Chicago, Illinois.*, 1939.
- [137] J. M. Wozencraft and B. Reiffen, “Sequential decoding,” *Cambridge, Mass: MIT Press*, 1961.
- [138] X. Wu, “On convergence of Lloyd’s method I,” *IEEE Trans. on Information Theory*, vol. 38, no. 1, pp. 171–174, Jan 1992.
- [139] S. Yao and M. Skoglund, “Analog network coding mappings in Gaussian multiple-access relay channels,” *IEEE Trans. on Communications*, vol. 58, no. 7, pp. 1973–1983, Jul 2010.

- [140] W. Yu, W. Rhee, and J. M. Cioffi, "Optimal power control in multiple access fading channels with multiple antennas," in *Proc. of International Conference on Communications (ICC), Helsinki*, 2001.
- [141] E. Zehavi, "8-PSK trellis codes for a Rayleigh channel," *IEEE Trans. on Communications*, vol. 40, pp. 873–884, May 1992.